NASA CR-159409
FR-10299

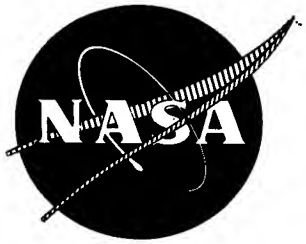

EVALUATION OF THE CYCLIC BEHAVIOR OF AIRCRAFT TURBINE DISK ALLOYS

By B. A. Cowles, D. L. Sims, and J. R. Warren

Pratt & Whitney Aircraft Group
Government Products Division

Prepared for
National Aeronautics and Space Administration

NASA Lewis Research Center
Contract NAS3-20367

FOREWORD

An evaluation of the cyclic behavior of five nickel-based superalloy turbine disk materials for aircraft gas turbine engine applications was performed from July 1976 through June 1978. The authors wish to express their gratitude to several Pratt & Whitney Aircraft employees who made significant contributions to the program effort. These include G. Scott, D. P. Shoemaker, E. J. Burke, C. K. Kraft, and J. M. Lieske II, who performed the majority of the materials tests. Special thanks are extended to Dr. G. T. Sha. Dr. Sha performed the elastic-plastic finite element analysis to determine first cycle stress-strain response and elastic stress fields for the disk analysis.

This program was conducted under the cognizance of M. C. VanWanderham, General Supervisor of the Mechanics of Materials and Structures section of the Materials and Mechanics Technology Department, at the Pratt & Whitney Aircraft Government Products Division.

TABLE OF CONTENTS

LIST OF ILLUSTRATIONS

LIST OF ILLUSTRATIONS (Continued)

LIST OF ILLUSTRATIONS (Continued)

LIST OF ILLUSTRATIONS (Continued)

LIST OF ILLUSTRATIONS (Continued)

LIST OF ILLUSTRATIONS (Continued)

LIST OF TABLES

LIST OF TABLES (Continued)

SUMMARY

Five nickel-base aircraft turbine disk superalloys representing various strengths and processing histories were evaluated at 650°C to determine if recent strength advances in powder metallurgy have resulted in corresponding increases in low-cycle fatigue (LCF) capability.

Controlled strain LCF tests and controlled load crack propagation tests were performed. Results were used for direct material comparisons and in the analysis of an advanced aircraft turbine disk having a fixed design and operating cycle.

Generally, crack initiation lives were found to increase with increasing tensile strength, while resistance to fatigue crack propagation generally decreased with increasing tensile strength.

INTRODUCTION

Recent strength advances in wrought powder-metallurgy superalloys offer the potential for increasing the performance and reducing the weight of gas turbine aircraft engines. Coupled with lower cost processing methods, such as hot isostatic pressing (HIP), the net result could be substantially reduced system life-cycle costs. After an alloy has been developed, critical evaluations must be conducted to define its capability and to enable utilization of that capability in the design, manufacture, and service of components. The cyclic behavior and capability of the new powder-metallurgy alloys become extremely important when they are considered for turbine disk applications. In many engine designs, these disks are often low cycle fatigue (LCF) limited.

Before these powder-metallurgy alloys can be incorporated into engine turbine disk designs a comparison of their cyclic fatigue behavior must be made with reference to an alloy in current use. Then an objective assessment of total-crack initiation plus crack propagation-fatigue life can be made to determine if the strength advances in wrought powder-metallurgy superalloys have resulted in corresponding increases in LCF capability, and if HIP processed alloys have cyclic lives substantially the same as their wrought powder counterparts.

Five nickel-base alloys were evaluated, all in the form of fully heat-treated disk shapes. The alloys are Waspaloy, Astroloy, NASA IIB-7, HIP-formed Astroloy, and GATORIZED® IN 100. These alloys represent a current and widely used turbine disk alloy produced from ingot (Waspaloy), and four advanced alloys produced from prealloyed powder. The four powder-metallurgy alloys exhibit a range of tensile strengths, increasing from HIP Astroloy, which is approximately equivalent to Waspaloy, to wrought Astroloy, GATORIZED IN 100, and NASA IIB-7.

The cyclic behavior of the alloys was evaluated from two aspects: crack initiation and crack propagation. The test vehicles to establish this behavior were axially-loaded strain-controlled LCF tests for initiation and load-controlled cyclic crack growth rate fracture mechanics tests for propagation. To more realistically simulate engine turbine disk operating conditions, these tests were conducted under both cyclic and cyclic/dwell conditions.

Upon completion of the materials tests, a total LCF life analysis was performed for an advanced turbine disk design to provide a relative comparison of four of the alloys.

MATERIALS TESTING AND DISK LIFE ANALYSIS

Material Procurement and Qualification

Five nickel-base superalloys for aircraft gas turbine engine disks were evaluated for resistance to cyclic crack initiation and propagation in tests which utilize long tensile hold times to simulate disk operating conditions. The alloys were selected to allow comparisons of an alloy currently used for turbine disks (alloy 1) with an advanced powder metallurgy alloy in both wrought (alloy 2) and hot-isostatically pressed (HIP) (alloy 4) forms, an advanced isothermally forged alloy (alloy 5), and a very advanced high strength wrought powder-metallurgy alloy (alloy 3). The five alloys selected for this program were:

Alloy 1 — Wrought Waspaloy produced from ingot: This is a turbine disk alloy with wide current usage in engines such as the JT8D, JT9D, TF30, FT4, and GG4 engines. It is also used as a compressor disk material in the JT11 and F100 engines.

Alloy 2 — Wrought Astroloy produced from prealloyed powder. This "next generation" alloy is forged from a HIP consolidated powder billet. It has been used as a turbine disk material in the TF30 engine.

Alloy 3 — Wrought NASA IIB-7 produced from prealloyed powder. This is an advanced high-strength experimental alloy developed by Cyclops Corporation under NASA Contract. (Reference 1.)

Alloy 4 — Astroloy produced as a HIP form from prealloyed powder.

Alloy 5 — GATORIZED IN 100 produced from prealloyed powder. This is an advanced high-strength turbine disk alloy currently being used in the F100 engine.

Nominal chemical composition and heat treatment of these alloys are listed in table I.

Alloy 1, Waspaloy, was procured in the form of a JT9D 3rd-stage turbine disk forging taken from a production run of this part. This disk was produced by the Ladish Company and is representative of the material in current usage. Representative microstructures of the disk are shown in figure 1. Comparison to other disks of this configuration indicates this structure is typical of wrought Waspaloy. The microstructure is relatively uniform within the flat portion of the disk, with grain size predominantly ASTM 4-5. Within the integral arm section some duplexing occurs, and for this reason, the LCF and crack propagation specimens were machined from the flat portion of the disk as shown in figure 2. This is the area of the disk that normally encompasses the LCF critical areas. To avoid possible surface microstructural discontinuities, no specimen surface was closer than 2 mm to the forging surface. At least this much surface is removed in machining the forging to a final disk configuration.

Material for alloy 2, wrought Astroloy, was procured as a TF30 1st-stage turbine disk forged by Ladish from a HIP processed powder billet. The powder which went into this disk came from Special Metals Blend 75025; the preform was HIP'd at Kawecki-Berylco.

Material for alloy 3, NASA IIB-7, consisted of a HIP processed powder billet which was cross rolled to a flat pancake configuration measuring approximately 35.5 cm (14 in.) in diameter and 4.5-cm (1.75-in.) thick by Universal Cyclops Corporation.

Alloy 4, HIP Astroloy, was obtained in the form of a JT8D-17 1st-stage turbine disk section. The Astroloy powder was produced by Udimet Division, Special Metals Corporation and the disk was HIP'd by KBI Industries, Inc. The HIP conditions were 3 hr at 1190°C (2175°F) and 103.4 MN/m^2 (15,000 psi) pressure.

Material for alloy 5, GATORIZED IN 100, was procured in the form of a pancake forging segment. The pancake was GATORIZED by the Pratt & Whitney Aircraft Group Government Products Division (P&WA/Florida) using Homogenous Metals billet stock (heat H45).

Mechanical property qualification results and chemical compositions determined for the forgings are presented in tables II through VI. Forging cut-up schematics showing test specimen locations and orientations are presented in figures 2 through 5. The test specimens consisted primarily of axial strain controlled LCF specimens and modified compact tension specimens for crack growth rate as shown in figure 6. The LCF specimens were oriented tangentially in the forgings; the modified compact tension specimens were oriented so that crack growth direction would be approximately radial to the disk forgings.

In addition to the required qualification tests, two elevated temperature tensile tests were performed on each alloy at 650°C (1200°F). Results of the tensile tests are presented in table VII.

Optical and electron micrographs representing the microstructure for each of the alloys are shown in figures 7 through 11.

Experimental Program

Introduction

Fully reversed ($\bar{\epsilon}=0$) strain-controlled LCF tests and load-controlled crack growth tests were conducted to characterize the cyclic behavior of all five alloys under both cyclic and cyclic-hold conditions. All tests were performed under isothermal conditions at 650°C (1200°F), a typical operating temperature for the fracture critical areas of an advanced engine turbine disk. The cyclic tests were performed at a frequency of 0.33 Hz (20 cpm). Hold time per cycle for the cyclic-dwell tests was 900-sec (15-min) at maximum tensile strain for the LCF tests and at maximum tensile load for the crack growth tests. In addition, crack growth rate tests were conducted at other frequencies and hold times for several alloys. Frequency and hold time models were developed for these alloys based on the hyperbolic sine model.

The experimental results were then used to directly compare the cyclic behavior of the five alloys.

Strain-Controlled LCF Testing

Currently, there are no industry-wide accepted ASTM procedures for strain-controlled or other LCF testing at elevated temperatures. The techniques for data generation and analysis used in this program are discussed below.

Specimen

The specimen used in this program is shown in figure 12 and conforms to FML 95716C (figure 13). Four basic requirements guided specimen design and development. These were that: (1) strain distribution be known over the gage section; (2) axial strain be accurately measurable; (3) there be minimum strain concentrations; and (4) failure location be in the gage section.

Additional requirements were that the specimen lend itself easily to installation and that calculations necessary for establishing machine-operating parameters be simple.

The specimen configuration, which incorporates integral machined extensometer collars, was determined experimentally using photoelastic and elastic-plastic strain analyses. A calibration procedure was established to relate the maximum strain to collar deflection during both the elastic and the plastic portions of the strain cycle. Subsequently, the specimen design and calibration procedures were analytically verified using finite-element and mathematical model analyses. (Reference 2.)

All test specimens were visually examined prior to testing in normal light and with fluorescent penetrant to screen for machining anomalies or surface discontinuities. Additional specimens were randomly selected for thorough dimensional inspection to ensure conformance to print requirements.

Testing Procedures

All testing machines were controlled under a system of calibration and preventative maintenance schedules. System accuracies are within 2%. Approved calibration procedures, records, and National Bureau of Standards (NBS) traceability were retained for all test equipment from which data were obtained.

Isothermal strain-controlled LCF characteristics were determined for this program using servohydraulic, closed-loop-on-axial strain, LCF testing machines designed and built at P&WA/Florida. A typical test machine with controls and readout instrumentation is shown in figure 14.

Specimen axial strain was measured and controlled by means of a proximity probe extensometer. Split extensometer heads were attached to the specimen by mating the grooves in the heads with the integral collars on the specimen and bolting the assembly together. Collar deflection is measured and controlled via proximity probes attached to the open ends of the extensometer tubes (the extensometer rod ends move relative to the probes as the specimen collars deflect, figures 15 and 16). Load measurement is obtained by a commerical tension-compression load cell.

An x-y recorder was used for recording load vs strain plots at predetermined cyclic intervals during testing. The recorder was calibrated with the extensometer so that the ratio of specimen collar deflection to x-y recorder pen movement in the "x" direction was known. The "y" axis of the x-y recorder was calibrated with the load cell so the ratio of specimen load to x-y recorder "y" axis pen movement was known.

The strain-controlled LCF tests were conducted at constant total strain ranges to establish cycles to failure in the 10^3 to 10^5 cyclic life range.

The cyclic LCF tests were performed using a sawtooth strain vs time waveform at a frequency of 0.33 Hz (20 cpm). The strain cycle was fully reversed (mean strain equal to zero, R = minimum strain/maximum strain = −1.0). A typical cyclic LCF test waveform and hysteresis loop are shown in figure 17.

The cyclic/dwell LCF tests were similar to the cyclic tests; however, the dwell tests incorporate a 900-sec (15-min) hold time applied at the maximum tensile strain of the cycle. The ramp rate for the remainder of the cycle corresponds to a 0.33 Hz (20 cpm) frequency. These tests also have a completely reversed strain cycle (mean strain equal to zero). A typical cyclic/dwell LCF test waveform and hysteresis loop are shown in figure 18.

All specimens were cycled to failure in the strain-controlled test mode with load-strain hysteresis plots obtained at intervals throughout the life of the specimen.

The number of cycles to complete specimen separation (N_f), and the number of cycles to produce a 5% drop in the cyclic load range (N_5) were determined for each test. The change in specimen compliance causing the drop in cyclic load range was used as an indicator for crack initiation. The 5% load range drop corresponded to a crack size of 0.25 to 0.76 mm, or 0.010 to 0.030 in. which is detectable by current fluorescent penetrant inspection methods.

The total strain and the elastic, inelastic, and creep strain components were determined at the specimen half-life ($N_f/_2$) from the hysteresis plots taken during each test. The strain components are described and presented in figures 17 and 18.

All tests were conducted in air at 650°C (1200°F). Temperature was controlled uniformly over the specimen gage section using calibrated thermocouple and temperature readout and control instrumentation.

Low Cycle Fatigue Test Results

A minimum of six cyclic tests and four cyclic/dwell tests were performed on each of five turbine disk alloys. All of the strain control LCF test results are presented in tables VIII through XII.

Stress range vs cycles for each test were determined from hysteresis plots generated periodically during the test. The data were analyzed by computer to estimate cycles to 5% stress range drop (N_5 life) and the results plotted. Stress range vs cycle plots for both cyclic and cyclic/dwell testing of each alloy are presented in figures 19 through 28. The 5% stress range drop occurred approximately within the last 15% of the total cyclic life for the majority of the tests.

Typical stress-strain hysteresis loops at the specimen half-life ($N_f/_2$) for all tests are presented in figures 29 through 38.

Mean stress information, as presented in the tables and shown in the hysteresis loops, indicates that nearly every test exhibited a slightly negative mean stress (engineering), and the deviation from zero stress was generally less than 2% of the total stress range.

Total strain range vs cycles to 5% stress range drop (N_5 life) and cycles to complete separation (N_f) for each alloy are presented in figures 39 through 48. Included in each figure is a strain range vs mean life regression curve.

The regression model used for the cyclic (0.33 Hz, 20 cpm) tests is a composite exponential function of the form $Y = AN^B + CN^D + E$, which relates total strain range (Y) to cyclic life (N). The inelastic strain component in this model is the AN^B term, and the elastic strain component is comprised of the $CN^D + E$ terms. The inelastic strain was statistically regressed as a log-linear (straight line on log-log paper) function ($Y_I = AN^B$). The elastic strain had the best statistically regressed curve fit as a nonlinear log (curved line on log-log paper) function ($Y_E = CN^D + E$). The total strain mean life equations for the cyclic tests are given in table XIII.

The regression model used for the dwell (900-sec hold at max tensile strain) tests is a composite exponential function of the form $Y = AN^B + CN^D$, which relates total strain (Y) to cyclic life (N). The inelastic strain component in this model is the AB^N term, and the elastic strain component is the CN^D term. The inelastic strain was statistically regressed as a log-linear function ($Y_I = AB^N$). The elastic strain was also statistically regressed as a log-linear function ($Y_E = CN^D$) due to the limited quantity of dwell LCF test data.

The total strain-mean life equations for the dwell LCF tests are given in table XIV.

Inelastic strain range data for all alloys has been adjusted to conform to the following reporting system:

If measured $\Delta\epsilon_i$ was:	Then reported $\Delta\epsilon_i$ was:
$\Delta\epsilon_i < 0.00005$	<0.0001
$0.00005 \leq \Delta\epsilon_i \leq 0.00008$	≤0.0001
$0.00008 < \Delta\epsilon_i < 0.00015$	0.0001

This system was required due to the relative inaccuracy of the inelastic strain data on this order of magnitude and due to the significant effect that these data could exhibit on the linear regressions of inelastic strain. Inelastic strain range data less than 0.0001 (<0.0001) as reported, were not used for regression analyses.

The methodology of summing independent log-linear (or nonlinear) regressions of the elastic and inelastic strain components ($Y = Y_I + Y_E$ where Y = total strain, Y_I = inelastic strain, and Y_E = elastic strain) has been used with excellent agreement with the actual total strain data generated in this program. Figure 49 illustrates this method of component strain summation.

The coefficients and exponents of this model can be rearranged into a more general form (Reference 3):

$$\frac{\Delta\epsilon}{2} = \epsilon_f' (2N_f)^c + \frac{\sigma_f'}{E}(2N_f)^b$$

where:

$\Delta\epsilon$	=	total strain range
N_f	=	cycles to failure
ϵ_f'	=	fatigue ductility coefficient
σ_f'	=	fatigue strength coefficient
c	=	fatigue ductility exponent
b	=	fatigue strength exponent
E	=	elastic modulus

The basic composite exponential function model may be expanded and modified to account for the effects of varying dwell time, mean strain (or mean stress) effects, and dwell mode (strain-hold or stress-hold).

Composite regression curves for all alloys tested at 0.33 Hz (20 cpm) are compared in figures 50 and 51. Similar comparison plots for all 900-sec (15-min) dwell testing are shown in figures 52 and 53.

Cyclic stress-strain curves, reconstructed from the strain control tests, are presented in figure 54. The stress-strain curves were obtained by plotting half the total stress range vs half the total strain range as measured at specimen half-life, $N_f/2$ (Reference 4). Mean stress was nearly zero for all of the tests.

It can be observed from figures 50 through 53 that, for lower strain ranges, the alloys generally exhibit increasing fatigue crack initiation life with increasing alloy tensile (yield) strength for both cyclic and cyclic/hold conditions. The rank order of the alloys changed substantially at higher strain ranges (above approximately 1.5%), approaching the rank order expected from tensile ductilities (higher ductility corresponding to higher life).

The general rank order from best to worst of the alloys under both cyclic and cyclic/dwell test conditions is the same at low strain ranges (strain ranges which yield approximately 100,000 cycles life for cyclic tests, or 10,000 cycles life for dwell tests). This rank order is as follows:

NASA IIB-7
IN 100
Wrought Astroloy
HIP Astroloy
Waspaloy

The effect of the 900-sec hold time on the fatigue life varied from alloy to alloy. A comparison of N_s lives obtained at a total strain range of 1.0% is:

Alloy	*N_s Life (0.33 Hz)*	*N_s Life (900-sec dwell)*	*Percent Reduction in Life*
Waspaloy	2,587	1,517	41
Wrought Astroloy	1,986	1,718	13
NASA IIB-7	13,030	4,838	63
HIP Astroloy	2,527	1,338	47
IN 100	9,999	1,492	85

The wrought Astroloy exhibited the smallest reduction over cyclic, nondwell life at 13%; Waspaloy and HIP-Astroloy exhibited very similar reductions of 41 to 47%, followed by NASA IIB-7 with a reduction of 63%. The IN 100 appeared most affected by the cyclic hold time with a life reduction of 85% over the 0.33 Hz conditions.

The effect of the 900-sec hold time on fatigue life at a total strain range of 0.8% is:

Alloy	*N_s Life (0.33 Hz)*	*N_s Life (900-sec dwell)*	*Percent Reduction in Life*
Waspaloy	10,557	5,613	47
Wrought Astroloy	20,857	10,368	50
NASA IIB-7	834,400	108,750	87
HIP Astroloy	10,947	6,266	43
IN 100	308,000	18,240	94

At the lower strain range (0.8%) level in the table above, which corresponds more closely to engine operating conditions, all alloys experienced significant reductions in life due to the 900-sec dwell time. The HIP-Astroloy exhibited the smallest reduction in life over the cyclic (nondwell) life at 43%; following closely behind HIP-Astroloy are Waspaloy and wrought Astroloy with percent reductions of 47% and 50%, respectively. Again, the high-strength alloys show the most severe degradation in fatigue life due to dwell, with NASA IIB-7 having a reduction of 87%, and IN 100 having a reduction of 94%.

It should be emphasized that the fatigue life determined at the lower strain ranges (i.e., $\Delta\epsilon_t = 0.80\%$ as in the above table) from the strain vs life mean regression curves is very dependent upon curve slope. Note the flat, nearly horizontal slopes of the curves in figures 50 through 53. Changes in the mean regression equations of the elastic and inelastic strain components, as would be expected with additional testing, could alter the fatigue life values given above, and hence, the percent reduction figures due to the 900-sec hold time.

Crack Growth Testing

Test Specimen and Procedures

The modified compact tension (MCT) specimen shown in figures 55 and 56 was used to obtain crack propagation data on the alloys. Testing was conducted on servohydraulic, closed-loop, load-controlled testing machines. Specimens were precracked using procedures outlined in ASTM E-399. Crack lengths were measured directly with a Gaertner traveling microscope after cooling the specimen. The intervals between crack growth measurements were selected to obtain crack growth increments of approximately 0.5 mm (0.02 in.), which normally results in an average of 40 to 50 readings per specimen. The crack propagation tests were conducted with a triangular loading wave form or a triangle wave with a hold time at the tensile peak with all portions of the cycle under tensile load-controlled conditions. All tests were conducted at 650°C (1200°F) with a stress ratio (minimum stress/maximum stress) of 0.05. Table XV lists all crack propagation tests.

Data Analysis Procedures

The direct secant method was used to evaluate crack length (a) vs cycles (N). Discrete values of Δa and ΔN were computed from raw laboratory data. Other approaches to da/dN analysis attempt to fit a vs N with some differentiable equations; da/dN then being obtained as its first derivative. By not smoothing (regressing) the a, N data, the actual local $\Delta a/\Delta N$ perturbations are observable in the final da/dN vs ΔK curve.

Crack propagation under constant amplitude loading conditions is a function of the applied stress intensity range (within the limits of applicability of linear elastic fracture mechanics). The applied stress intensity, ΔK, is the driving force for crack propagation. Many relationships have been developed to correlate observed crack growth rate and stress intensity. Paris and Erdogan presented the simple relationship:

$$da/dn = C\,(\Delta K)^n \tag{1}$$

where C and n are material constants. At elevated temperatures, however, the crack growth process is a complicated function of stress ratio, temperature, load history, and environment. These dependencies make the general use of equations, such as equation (1), more difficult. A new model, developed at P&WA/Florida (Reference 5), was used to describe the effects of cyclic frequency on the crack growth rates of Waspaloy and HIP-Astroloy. The model is based on the hyperbolic sine equation:

$$\log(da/dn) = C_1 \sinh\left(C_2(\log(\Delta K) + C_3)\right) + C_4, \tag{2}$$

where the coefficients have been shown to be functions of test frequency, stress ratio, and temperature:

C_1 = material constant
C_2 = f_2 (R, ν, T)
C_3 = f_3 (C_4, ν, R)
C_4 = f_4 (ν, R, T).

The hyperbolic sine equation was selected as the model for the following reasons:

- It exhibits the overall shape of typical da/dN vs ΔK plots obtained over several decades of crack growth rates.

- All or part of the equation may be used to fit data since the hyperbolic sine has both a concave and a convex half and a nearly linear portion near inflection. Also, the slope at inflection can vary with the fitting constants. (By comparison, the slope of an x^3 model is always zero at inflection.)

- The sinh is not periodic (e.g., trigonometric tangent) nor asymptotic (e.g., tangent, or inverse hyperbolic tangent); therefore, when extrapolation becomes necessary, the sinh behaves well at distances removed from the data, quite unlike most polynominals, periodic, or asymptotic functions.

- This model requires no information other than a, N data. By comparison, some other models in current use require both K_{th} and K_{IC}, in addition to a, N data, to model crack growth behavior. Both K_{th} and K_{IC} are difficult to obtain experimentally; K_{th} because of the extremely small crack growth measurements necessary, and K_{IC} because of gross plasticity at the crack tip encountered in fracture-toughness testing at elevated temperatures.

The hyperbolic sine is defined as

$$y = \sinh x = \frac{e^{x} - e^{-x}}{2} \tag{3}$$

and when presented on Cartesian coordinates, it appears as shown in figure 57. The function is zero at $x = 0$ and has its inflection there.

The introduction of the four regression coefficients C_1 through C_4, permits relocation of the point of inflection and scaling of both axes. In the equation,

$$(y - C_4) = \sinh (x + C_3), \tag{4}$$

C_3 establishes the horizontal location of the hyperbolic sine point of inflection and C_4 locates its vertical position.

To scale the axes, C_1 and C_2 are introduced

$$\frac{(y - C_4)}{C_1} = \sinh (C_2 (x + C_3)) \tag{5}$$

which can be rewritten as

$$y = C_1 \sinh (C_2 (x + C_3)) + C_4 \tag{6}$$

of which equation (2) is a special case where $y = \log (da/dN)$ and $x = \log (\Delta K)$. Note that C_3 has units of log (ΔK) and C_4 has units of log (da/dN); C_1 and C_2 are dimensionless and can be conceptualized as stretching the curve vertically and horizontally, respectively. Experience indicates that, for a given material, C_1 can be fixed without adversely affecting model flexibility (Reference 6).

The hyperbolic sine model is easily adapted to describe the fundamental parametric effects of stress ratio, frequency, and temperature on crack growth rate. Only frequency effects were characterized for this contract.

Experience with turbine disk alloys indicates that changing test frequency, while holding stress ratio and temperature constant, produces crack growth curves similar in shape but shifted along a nearly vertical line passing through the points of inflection. The location of these

inflection points is related to test frequency. Figure 58 schematically depicts the qualitative effects of frequency on crack propagation rates.

The fundamental strength of the hyperbolic sine model is its interpolative capacity. The four sinh model coefficients can be determined as follows:

C_1 = material constant (0.5 for these materials)
C_2 = $m_2 \log(\nu) + b_2$
C_3 = $m_3 C_4 + b_3$
C_4 = $m_4 \log(\nu) + b_4$.

Computation of a crack growth rate equation for any given frequency (with stress ratio and temperature held constant) is a straightforward calculation once the above linear relationships have been established.

Test Program

Figures 59 through 63 show the 0.33 Hz crack growth curves with data for each individual alloy. A minimum of two specimens were run at these conditions for each alloy. Figure 64 is a composite of the 0.33 Hz crack growth curves of all five alloys. The curves tend to converge at low ΔK. As ΔK increases, the curves diverge, and the differences in crack growth rates become more pronounced. Waspaloy (alloy 1) has the slowest crack growth rate and HIP-Astroloy (alloy 4), the second slowest. The crack growth rate for Wrought-Astroloy (alloy 2) is consistently 1.5 times as fast as the growth rate for HIP-Astroloy above a ΔK of 20 MPa $\sqrt{m}$. IN 100 (alloy 5) and NASA IIB-7 (alloy 3) have nearly the same crack growth rates for ΔK less than 30 MPa $\sqrt{m}$, but the NASA IIB-7 propagation rate increases more rapidly above this ΔK. From the crack propagation data it appears that the alloys may have very similar threshold applied stress intensities (ΔK_{th}) but vastly different fracture toughness (K_{IC}). Waspaloy would be expected to have the highest fracture toughness and NASA IIB-7 the lowest.

Figures 65 through 69 show the 900-sec (15-min) dwell crack propagation curves with data for each individual alloy. A composite of these curves is illustrated in figure 70. Again, Waspaloy and HIP-Astroloy have the best crack growth rates followed by Wrought-Astroloy, IN 100, and NASA IIB-7. This is the same order as the crack growth rates at 0.33 Hz, but much larger differences exist between the alloys at the 900-sec (15-min) dwell test condition. IN 100 is approximately an order of magnitude faster than Waspaloy or HIP-Astroloy, and NASA IIB-7 has a crack growth rate more than two orders of magnitude faster than Waspaloy and HIP-Astroloy.

The attempt to sustain low crack propagation rates in 900-sec tensile dwell tests with $\Delta K < 20$ MPa $\sqrt{m}$ was met with considerable difficulty. Under these conditions crack tip blunting was frequently observed and often resulted in crack arrest. Such interruptions in crack propagation under low levels of applied ΔK have been attributed to crack tip inelasticity and oxide formation at the crack tip during extended hold times at elevated temperatures. In cases in which crack tip blunting does not result in arrest, multiple secondary cracking can contribute to discontinuous crack propagation, and large scatter in data is frequently observed. These problems are eliminated as the applied stress intensity range increases such that the stress intensity, during the dwell, exceeds the threshold for crack growth under sustained load.

Comparisons of 900-sec (15-min) dwell and 0.33 Hz crack propagation rates for each of the five alloys are presented in figures 71 through 75. The effect of the dwell loading is observed to be most severe for NASA IIB-7.

The HIP-Astroloy crack growth rates for cyclic frequencies of 0.0083 and 20 Hz are shown individually in figures 76 and 77, respectively. The comparison of these crack growth rates with the 0.33 Hz curve is shown in figure 78. The basis for development of the interpolative frequency model was the crack growth equation,

$$\log (da/dN) = C_1 \sinh (C_2 (\log (\Delta K) + C_3)) + C_4,$$

described in the Data Analysis Procedures section. Figure 79 illustrates the relationships between C_2, C_4, and frequency. Knowing these relationships, the hyperbolic sine crack growth curve can be calculated for any frequency between 0.0083 and 20 Hz (holding stress ratio and temperature constant).

The individual data sets (0.0083, 0.33, and 20 Hz) used in the IN 100 frequency model are shown in figures 80, 63, and 81. The comparison of these crack growth rates is shown in figure 82. The sinh crack growth rate curve can be calculated for any frequency between 0.0083 and 20 Hz by using the relationships between C_2, C_4, and frequency given in figure 83.

Figures 84 and 85 present the crack propagation data for Waspaloy under 120- and 300-sec (2- and 5-min) dwell loading, respectively. A composite of these curves and the 900-sec (15-min) dwell Waspaloy data of figure 65 is shown in figure 86. Figure 87 completes the dwell model with the C_2, C_4, and frequency relationships.

Crack propagation data for HIP-Astroloy under 120- and 300-sec dwell loading are presented in figures 88 and 89. A composite plot of HIP-Astroloy in 120-, 300-, and 900-sec dwell conditions is given in figure 90. The dwell model is completed with the presentation of the C_2, C_4, and frequency relationships in figure 91.

The effect of frequency on the crack growth rates of Waspaloy and Wrought-Astroloy are shown in figures 92 and 93. There were not enough data obtained on these alloys to construct a frequency model.

The coefficients for the hyperbolic sine crack growth curves are listed in table XVI for every condition tested.

Disk Life Analysis

Introduction

The disk life analysis was performed to provide a comparison of the fatigue life capability of four alloys under simulated turbine disk operating conditions. Fatigue life predictions were based on a direct material property substitution for each alloy into a disk having a fixed design and operating cycle. The four alloys selected for the disk life analysis were alloys 1, 2, 3, and 5 (Waspaloy, Wrought Astroloy, NASA IIB-7, and IN 100).

Alloy 4, HIP-Astroloy, was not directly analyzed. However, it is very similar to alloy 1, Waspaloy, in material properties, low cycle fatigue (LCF) capability, and crack growth rate under the conditions evaluated. Consequently, it is assumed that life predictions for HIP Astroloy would be similar to those determined for Waspaloy.

The 2nd-stage high-pressure turbine disk for the F100 engine was selected as the vehicle for the disk life analysis. The Pratt and Whitney Aircraft (P&WA) F100 engine is an advanced, high-performance afterburning turbofan engine which utilizes powder metallurgy GATORIZED® IN 100 turbine disks. The fracture critical location for the disk is the tie-bolthole located in the

web section of the disk. Frontal and side view photographs of the disk are shown in figures 94 and 95. A cross section of the high-pressure turbine showing the bolthole location in the 2nd-stage disk is presented in figure 96.

The flight point selected for the analysis was Mach 2.5 at 15,240 meters (50,000 ft) altitude. Metal temperature at the bolthole location for this condition is approximately 650°C (1200°F). This flight point was chosen because of its expected severity in terms of mechanically induced strain range at the bolthole location and the stress field around the bolthole.

The MARC nonlinear finite element program was used to carry out the plane-stress elastic-plastic disk analyses. The nonlinear problem is essentially solved by MARC as a series of piecewise linear problems.

Because of symmetry, only 1/40 of the disk was idealized with the two-dimensional (2-D) finite element meshes as shown in figure 97 (20 boltholes are contained in the disk). This 2-D disk model with stepwise thickness variation was aimed at obtaining quasi 3-D results at reasonable cost without sacrificing accuracy in conducting the costly elastic-plastic disk analyses. High order isoparametric elements of linear strain were used in the disk model which has 887-degrees of freedom. The inner radius of the 2-D disk model was chosen to coincide with the inner radius of the designed disk. However, the outer radius of the 2-D model is smaller than the actual outer radius of the disk. The outer radius location of the finite element model was selected to satisfy the St. Venant principle that the elastic stress state at this outer radius boundary should not be affected by the local yielding near the bolthole location. The radial elastic stress on the outer radius of the 2-D disk model shown in figure 97 was obtained from a disk analysis using ring elements. Physically, this radial stress loading at the outer radius of the model stems from the centrifugal body forces due to the blade pull and the disk material situated between the outer boundary of the finite element model and the outer radius of the actual disk. In addition to the tractions on the outer radius of the model, the centrifugal body forces at the selected flight point were included so that the actual disk loading conditions were represented.

In addition to the effects off the various tensile properties, the coefficients of thermal expansion and material density variations from alloy to alloy were accounted for in the analysis. Differences in the linear coefficient of expansion from room temperature to 650°C were relatively small, ranging from 13.7 to 14.6 μm/m/°C (7.6 to 8.1 μin./in./°F from room temperature to 1200°F) and were assumed to have no significant impact on the analysis. Densities, however, varied significantly. Densities used in the analysis for Waspaloy, wrought Astroloy, NASA IIB-7, HIP Astroloy, and IN 100 were 8.25, 7.94, 9.02, 7.80, and 7.86 gm/cm^3 (0.298, 0.287, 0.326, 0.289, and 0.284 lb/in.^{3} respectively.) The higher density for the NASA IIB-7 alloy resulted in significantly increased loads due to the increased body forces.

Disk Crack Initiation Life

The 1st-cycle stress-strain response for each of the four alloys was determined by the elastic-plastic analysis. Each alloy was subjected to a single cycle from zero load and room temperature to maximum load at approximately 217 revolutions of the disk per second (13,000 rpm) and a temperature of 650°C (1200°F). For the bolthole location of the disk, the finite element results showed that the elastic tangential stress at location "A" is larger than the maximum radial stress at location "B" (figure 97).

The local stress-strain response at this fracture critical location is schematically illustrated in figure 98. The first quarter cycle (or maximum) strain occurs at the flight point of Mach 2.5, 15,240 meters altitude (50,000 ft) and 650°C (1200°F). This corresponds to the disk rotational speed of approximately 217 Hz (13,000 rpm). Minimum strain occurs when the disk rotational velocity returns to zero.

Maximum strain, inelastic offset, minimum tangential strain, and the resulting total strain range encountered during the first complete loading cycle were determined for each alloy. These strains are presented in table XVII. Strain ranges were relatively low (less than 0.8%) and were all positive (tensile).

As expected, peak or maximum strain generally decreased as alloy tensile strength increased. The exception was that the NASA IIB-7 exhibited slightly higher peak strain than the IN 100, probably due to the higher material density of the NASA IIB-7 alloy.

The extent of yielding around the bolthole varied considerably from alloy to alloy and was indicative of relative strengths of the alloys. Boundaries of the yield zone are shown for each alloy in figure 99.

Differences in strain range from alloy to alloy were relatively small, ranging from 0.722% range for IN 100 to 0.777% for NASA IIB-7. As with peak strain, strain range generally decreased with increasing alloy strength, except in the case of the NASA IIB-7, which exhibited the highest total strain range.

None of the alloys exhibited yielding in compression during the unloading cycle. An isotropic hardening model was assumed for the unloading cycle, which does not account for the Bauschinger effect of a reduced compressive yield strength following tensile yielding. This model was selected based on the stress-strain behavior of the alloys observed in the strain control LCF tests.

Since the strain ranges were low and all of the alloys are cyclically stable at low strain ranges and 650°C (1200°F), the first cycle strain ranges were assumed to be representative of the stable cyclic strain ranges.

Analytical determination of the local cyclic creep strains or creep stress relaxation resulting from sustained loading of the disk at elevated temperature was beyond the scope of this investigation. The analytically determined strain range was used to estimate both cyclic and cyclic/dwell lives for each alloy using the appropriate strain range vs life curves for crack initiation (N_s) life (figures 50 and 52). Calculated disk lives to crack initiation for the cyclic and cyclic/dwell conditions are presented in table XVIII.

Both cyclic and cyclic/dwell crack initiation lives predicted for this single cycle generally increased with increasing alloy strength. The only exception is the relationship between NASA IIB-7 and IN 100 for cyclic (0.33 Hz) conditions. Here, the IN 100 exhibits higher predicted life than the NASA IIB-7. The IN 100 experienced a lower strain range than the NASA IIB-7 which resulted in higher life. The more severe effect of the hold time on IN 100 caused a reversal in the relative lives of the two alloys for 900-sec (15-min) dwell. The NASA IIB-7 exhibited the highest predicted life under the cyclic/dwell conditions.

The predicted cyclic and cyclic/dwell lives are shown in figure 100 for comparison. The life (cycles) axis is logarithmic for convenience; however, differences in component life-cycle costs due to the different fatigue lives predicted for the alloys would be better represented on a Cartesian scale. The differences in estimated fatigue life would then appear far more significant.

The disk life analysis showed that each material experienced an all-tensile strain cycle at the fracture critical location. Corresponding mean stresses for the alloys were significant and positive (tensile). The strain range-life relationships, however, were established using fully reversed strain cycles (mean strain equals zero) which also resulted in zero or near-zero mean stress. Consequently, the effects of mean stress or strain on fatigue life were not accounted for in the life predictions.

Crack Growth Life Analysis Results

The crack propagation life analysis was performed from initial flaw sizes (total surface crack length) of 0.25 and 0.51 mm (0.010 and 0.020 in.). Life was calculated at representative turbine disk operating conditions using the Component Life Analysis computer program developed at the P&WA/Commercial Products Division (P&WA/CPD). This program calculates the number of cycles for a crack in a bolt hole to grow large enough for the stress intensity (K) to surpass the critical stress intensity (K_{IC}). Inputs into the program are the hyperbolic sine crack growth equation coefficients, initial crack length, K_{IC}, and the uncracked stress field surrounding the bolthole. The elastic stress distributions for the four alloys are shown in figures 101 through 104.

A surface crack geometry was selected for the alloy comparison, and the results are presented in table XIX. A K_{IC} of 110 MPa $\sqrt{m}$ (100 ksi $\sqrt{in.}$) was used for all alloys except NASA IIB-7. The crack growth rates exhibited by NASA IIB-7 tend to approach infinity below a stress intensity of 77 MPa $\sqrt{m}$; therefore, a critical stress intensity of 77 MPa $\sqrt{m}$ (70 ksi $\sqrt{in.}$) was used for the NASA IIB-7 material.

At 0.33 Hz the alloys showed increasing crack propagation life with decreasing tensile strength. The only exception to this trend was for the wrought-Astroloy and IN 100 life calculations from a 0.25 mm flaw. The IN 100 life is longer than the Wrought-Astroloy life from a 0.25 mm crack but shorter from a 0.51 mm crack due to crossing of the crack growth rate curves at low ΔK. This trend at low ΔK indicates that IN 100 has a higher ΔK_{th} (threshold applied stress intensity) than Wrought-Astroloy, while Wrought-Astroloy has more resistance to crack growth at higher ΔK's. Figure 105 compares the results of the life analysis for 0.33 Hz.

The crack growth rate curve for the Waspaloy 900-sec dwell tests intersected the 0.33 Hz curve at a ΔK = 22 MPa $\sqrt{m}$ (20 ksi $\sqrt{in.}$). No 900-sec dwell data were obtained below this intersection due to crack tip blunting causing crack arrest or multiple crack tips. Since these tests were performed with long cracks and low stresses, it is possible that for short cracks and high stresses (disk application), crack growth may be possible in this region. With dwell data unavailable (but crack growth possible) below ΔK=22 MPa$\sqrt{m}$, the Waspaloy 900 sec dwell life analysis was made using the 0.33 Hz crack propagation curve from the initial flaw size until ΔK=22 $MP_a\sqrt{m}$ (20 ksi $\sqrt{in}$). The 900-sec dwell curve was then used for the remainder of the analysis and the two results added together.

The 900-sec dwell results are illustrated in figure 106. Notice that the order is the same as the 0.33 Hz results, and the detrimental effect of the 900-sec dwell was severe for all alloys. However, the NASA IIB-7 disk lost 99% of the 0.33 Hz cyclic life due to the dwell. For a 0.51 mm flaw the amount of reduction in propagation life for the other alloys is as follows: Wrought-Astroloy — 85%, Waspaloy — 89%, and IN 100 — 95%.

The effect of the 900-sec dwell on the Astroloy, IN 100, and NASA IIB-7 crack propagation life is the same whether the life is calculated from a 0.25- or 0.51-mm (0.010- or 0.020-in.) flaw. For Waspaloy, there is a significant difference when crack propagation life is calculated from a 0.25-mm flaw. The Waspaloy disk loses only 80% of the propagation life due to the dwell effect. This is probably due to the fact that at low stress intensities (at least for long cracks and low stresses), cracks in Waspaloy tend to blunt when subjected to long hold times resulting in slower than normally expected crack growth rates.

Disk Total Life

The elevated temperature fatigue or rupture process can be conceptualized as occurring in three stages (Reference 7): (1) nucleation and linkup of surface and subsurface microcracks, (2) subcritical crack propagation through local plasticity due to yielding at a notch, and (3) crack propagation through basically elastic material. The ideal for total fatigue life prediction might be a unification of lives predicted for each stage of the fracture process. It is, however, difficult to experimentally separate and quantify the initiation phase and continuum crack propagation in high-strength materials. For a comparison of total disk life for each alloy in this program, a simple addition of mean cycles to crack initiation and mean cycles of crack propagation was performed. Crack initiation life was approximated using the mean strain control curve relating total strain range and cycles to 5% stress range drop (N_s life). The crack propagation life was determined using the hyperbolic sine relationship of stress intensity factor range (ΔK) and crack growth rate. Crack propagation life was calculated, assuming starting crack lengths of 0.25 and 0.51 mm (0.010 and 0.020 in.). Lives were determined for both 0.33 Hz (20 cpm) and 900-sec (15-min) hold time conditions.

The resulting estimated total fatigue lives are presented in table XX and are shown schematically for comparison of the alloys in figures 107 and 108. Total propagation life from a 0.51-mm starting crack (0.020-in.) is distinguished from the mean crack initiation life (N_s) by shading in the figures.

Figure 107 shows schematically the relative magnitudes of crack initiation and crack propagation lives for the alloys under cyclic (0.33 Hz) conditions. Nearly all of the total fatigue life for the alloys was in crack initiation, with IN 100 exhibiting somewhat longer life than NASA IIB-7.

Figure 108 shows schematically the relative magnitudes of crack initiation and crack propagation lives for the the alloys under cyclic/dwell (900-sec hold) conditions. As for the cyclic (0.33 Hz) condition, the Wrought Astroloy appeared slightly superior to Waspaloy in total fatigue life, but both alloys had somewhat lower total lives than NASA IIB-7 and IN 100. Again, nearly all of the predicted life for the alloys was due to fatigue crack initiation. In a reversal from the cyclic condition, however, cyclic/dwell life for NASA IIB-7 was superior to that predicted for IN 100.

The disk life analysis was intended to provide a comparison of the alloys under simulated turbine disk operating conditions. Several factors normally considered in the design and evaluation of a disk were eliminated from this analysis in the interest of simplicity and due to limitations in program cost and scope. Some of these simplifications could affect the relative lives (rank order) of the alloys, particularly the calculated total disk lives.

In general, higher alloy yield strength correlated with better fatigue crack initiation resistance, but, reduced resistance to fatigue crack propagation. Consequently, any simplifications or changes to the disk life analysis which affect the relative magnitudes of crack initiation lives or crack propagation lives could also affect the rank order of total lives calculated for the alloys. Some examples of these changes are: changes in disk design, change in fracture critical location (geometry), statistical consideration such as predicting minimum rather than mean life, effects of steady or mean stress, and changes in operating cycles.

CONCLUSIONS AND SUMMARY OF RESULTS

Five turbine disk alloys representing varying tensile strengths and processing histories were evaluated for resistance to fatigue crack initiation and propagation under both cyclic and cyclic/dwell conditions at 650°C (1200°F). Results were used to perform a direct material comparison of the five alloys.

For realistic comparison under simulated operating conditions, an advanced turbine disk having a fixed design and operating cycle was analyzed. Predicted lives to crack initiation and to complete failure of the disk were determined based on a direct material property substitution for four of the alloys.

1. At total strain ranges of interest for turbine disk applications the alloys exhibited generally increasing initiation life with increasing tensile yield strength for both cyclic (0.33 Hz) and cyclic/dwell (900-sec hold per cycle) conditions. The rank order from highest life to lowest life for strain ranges below approximately 1.0% was as follows:

   NASA IIB-7
   IN 100
   Wrought Astroloy
   HIP-Astroloy
   Waspaloy

2. Rank order of the alloys by LCF initiation life changed substantially at higher strain ranges, approaching the rank order expected from monotonic tensile ductilities for total strain ranges above approximately 1.5%. For cyclic (0.33 Hz), nondwell tests, the rank order of the alloys from highest to lowest LCF initiation life was as follows:

   HIP-Astroloy
   Waspaloy
   Wrought Astroloy
   IN 100
   NASA IIB-7

3. The effect of the 900-sec (15-min) hold time on the fatigue life varied significantly from alloy to alloy. Generally, the NASA IIB-7 and the IN 100 exhibited more significant reductions in fatigue life due to the dwell than Waspaloy, Astroloy, and HIP-Astroloy. For a total strain range of 0.8% (approximate range determined by the disk analysis), percentage reductions in N_s life for the alloys was as follows:

HIP-Astroloy	43%
Waspaloy	47%
Wrought Astroloy	50%
NASA IIB-7	87%
IN 100	94%

4. All of the alloys exhibited nearly stable cyclic stress-strain response for the conditions evaluated. Waspaloy cyclically softened at high strain ranges during cyclic testing, and at all strain ranges evaluated under cyclic/dwell conditions. IN 100 exhibited some cyclic hardening for higher strain ranges under cyclic (0.33 Hz) test conditions.

5. A comparison of crack growth rates at 0.33 Hz (20 cpm) shows that crack growth rates generally increase with increasing tensile strengths. The rank order from best (lowest crack growth rate) to worst is as follows:

   Waspaloy
   HIP-Astroloy
   Wrought Astroloy
   IN 100
   NASA IIB-7

6. The effect of the 900-sec hold time on crack propagation rates varied considerably from alloy to alloy but did not change the relative order seen with the 0.33 Hz testing. NASA IIB-7 showed the severest degradation due to the dwell time, and Waspaloy crack growth rates were least affected by the hold time at stress intensities below 25 MPa $\sqrt{m}$.

7. The effects of frequency on the crack growth rates of IN 100 and HIP-Astroloy were uniform and predictable. A model was developed to predict crack growth rates for any frequency between 0.0083 and 20 Hz for R = 0.05, 650°C using empirically determined relationships between coefficients of the hyperbolic sine model.

8. The effect on crack growth rates of varying hold time was not as uniform as for varying frequency. However, a dwell model was developed for Waspaloy and HIP-Astroloy to predict crack growth rates for any dwell time between 120 and 900 sec.

Waspaloy, Wrought Astroloy, NASA IIB-7, and IN 100 were included in the disk life analysis. Although HIP-Astroloy was not directly analyzed, life estimations for HIP-Astroloy are expected to be substantially the same as those determined for Waspaloy. Conclusions and a summary of results of the disk life analysis are presented below.

1. Total strain ranges determined for the selected disk operating cycle varied slightly from alloy to alloy and were all positive (tensile). Total strain ranges for the Waspaloy, Astroloy, NASA IIB-7, and IN 100 were 0.753, 0.733, 0.777, and 0.722%, respectively. NASA IIB-7 exhibited the highest calculated total strain range, probably because of its higher density.

2. Higher strengths for the alloys generally correlated with longer predicted lives to crack initiation (N_s life). Rank order of the alloys from highest to lowest in predicted disk life to crack initiation was as follows:

Cyclic (0.33 Hz)	*Cyclic/Dwell (900-sec Hold)*
IN 100	NASA IIB-7
NASA IIB-7	IN 100
Wrought Astroloy	Wrought Astroloy
Waspaloy	Waspaloy

3. At stresses representative of turbine disk applications, the alloys exhibited increasing crack propagation life with decreasing tensile (yield) strength for both the cyclic (0.33 Hz) and the 900-sec dwell conditions. The rank order from highest propagation life to the lowest (from a 0.51 mm flaw) is as follows:

   Waspaloy
   Wrought Astroloy
   IN 100
   NASA IIB-7

4. The detrimental effect of the 900-sec hold time on the crack propagation life from a 0.51-cm (0.020-in.) flaw was severe for all alloys. However, the NASA IIB-7 disk lost 99% of the 0.33 Hz cyclic life. The following list shows the percent reduction in crack propagation life from a 0.51-cm (0.020-in.) flaw due to the 900-sec dwell:

Wrought Astroloy	85%
Waspaloy	89%
IN 100	95%
NASA IIB-7	99%

5. The effect of the 900-sec dwell on crack propagation life from a 0.25-mm (0.010-in.) flaw is about the same for Astroloy, IN 100, and NASA IIB-7 as the effect from the larger 0.51-mm (0.020-in.) flaw. For Waspaloy there is a significant difference when crack propagation life is calculated from an 0.25-mm flaw; the Waspaloy disk loses only 80% of the propagation life due to the dwell effect. This is apparently due to the fact that at low stress intensities (at least for long cracks and low stresses), cracks in Waspaloy tend to blunt when subjected to long hold times resulting in lower crack growth rates.

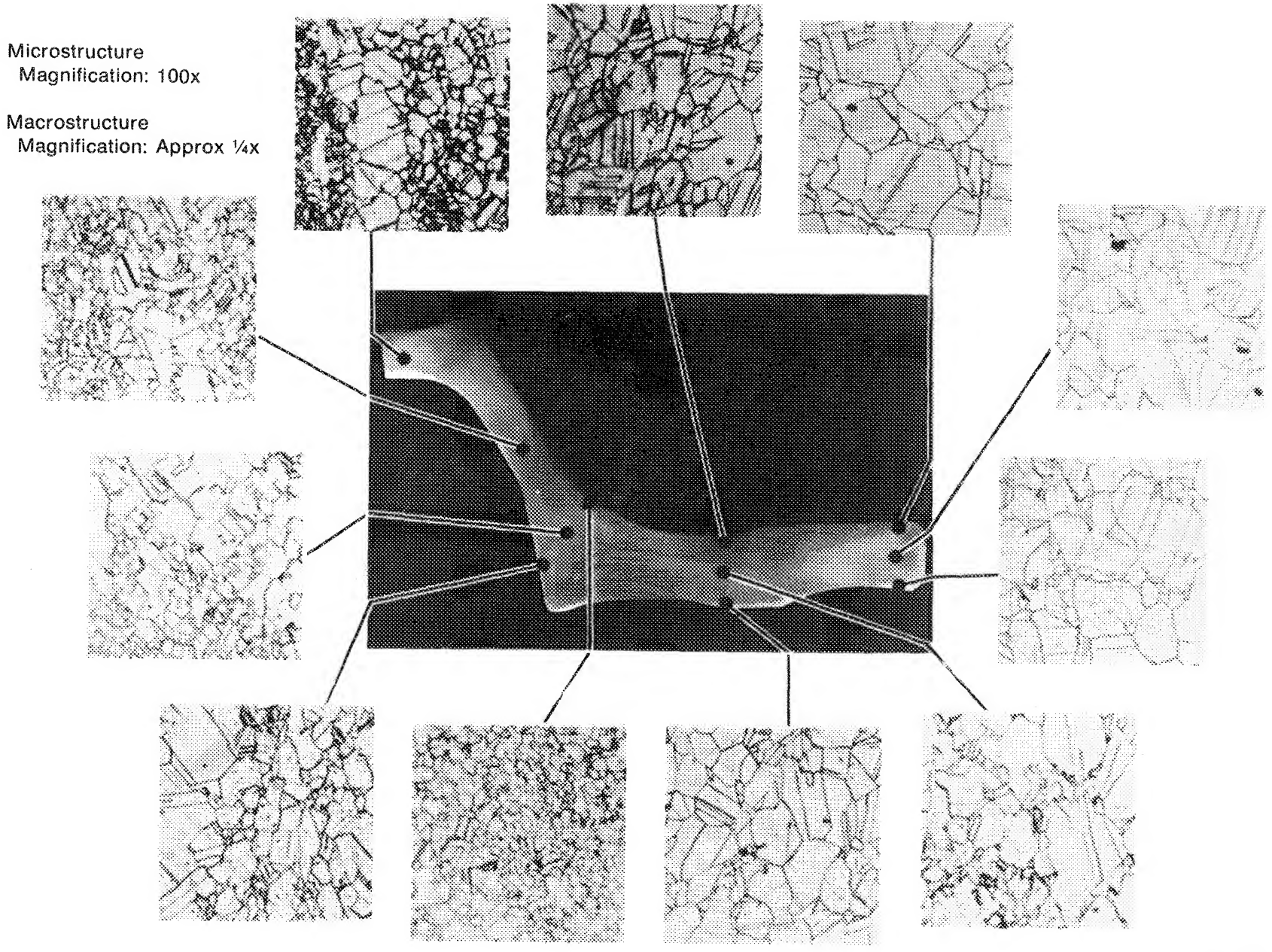

Figure 1. Typical Microstructure of Alloy 1, Wrought Waspaloy Turbine Disk Forging

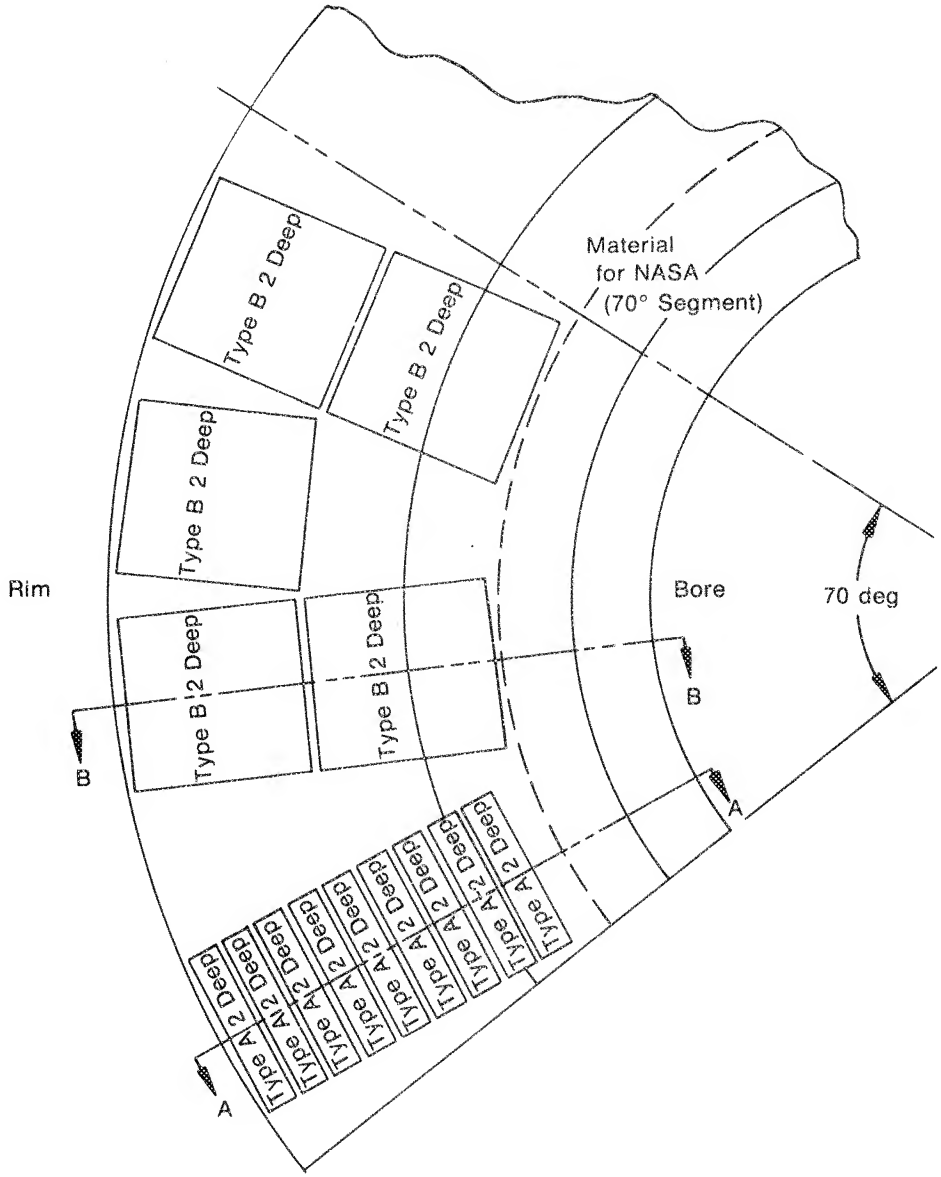

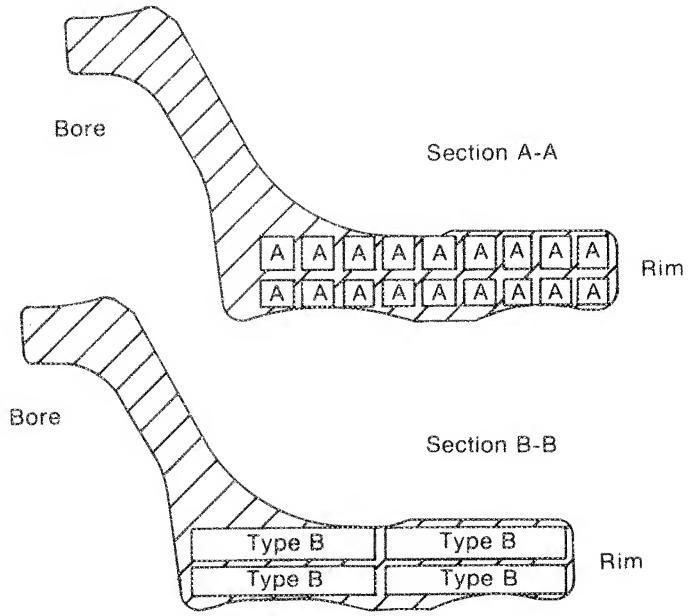

Specimen Blank
Type A - Strain Control LCF
Type B - Modified Compact Tension

FD 105627

Figure 2. Alloy 1 — Wrought Waspaloy Turbine Disk Forging Schematic Layout Showing Location and Orientation of Specimen Blanks

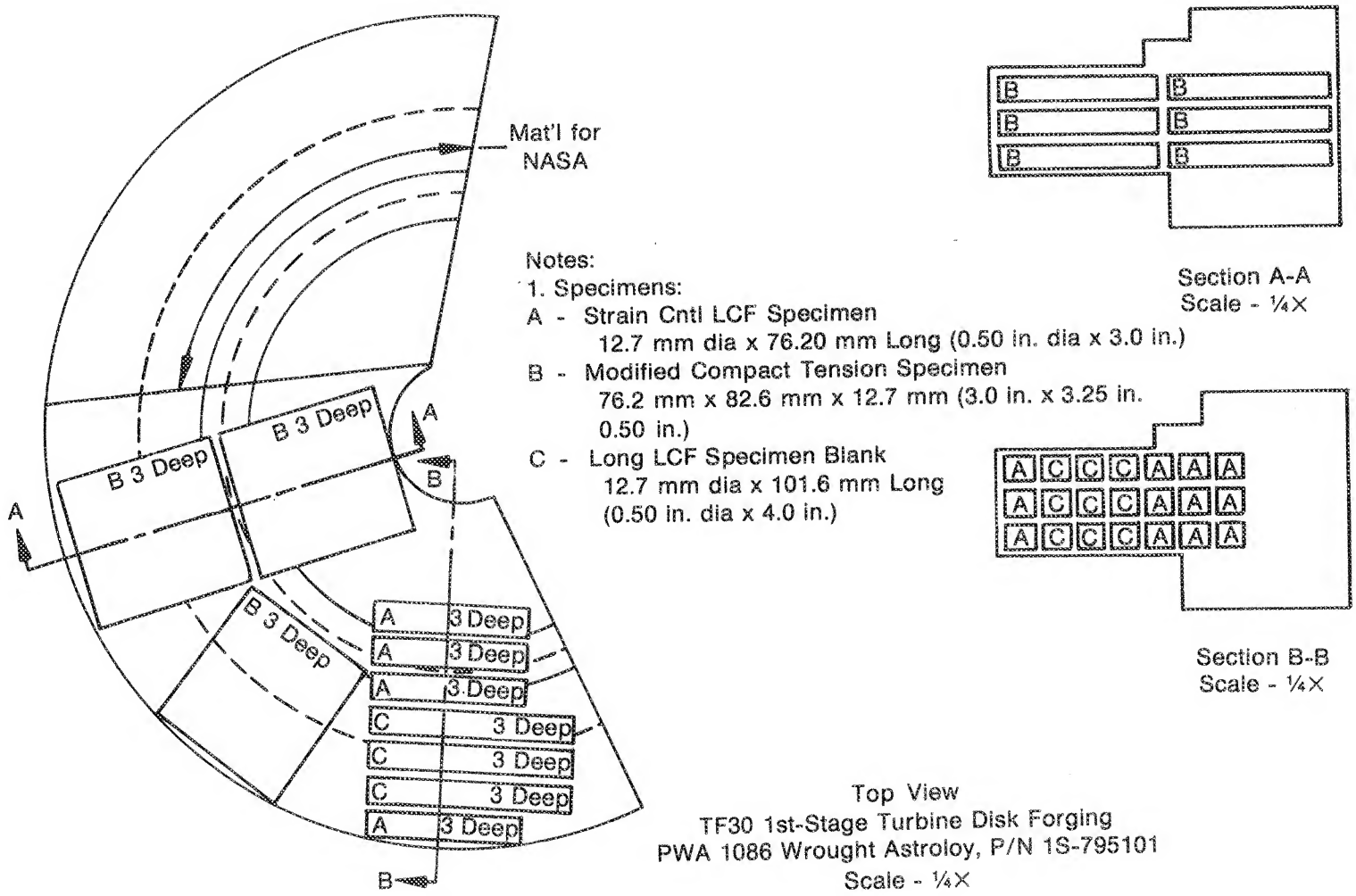

FD 143382

Figure 3. Specimen Schematic Layout for Alloy 2, Wrought Astroloy

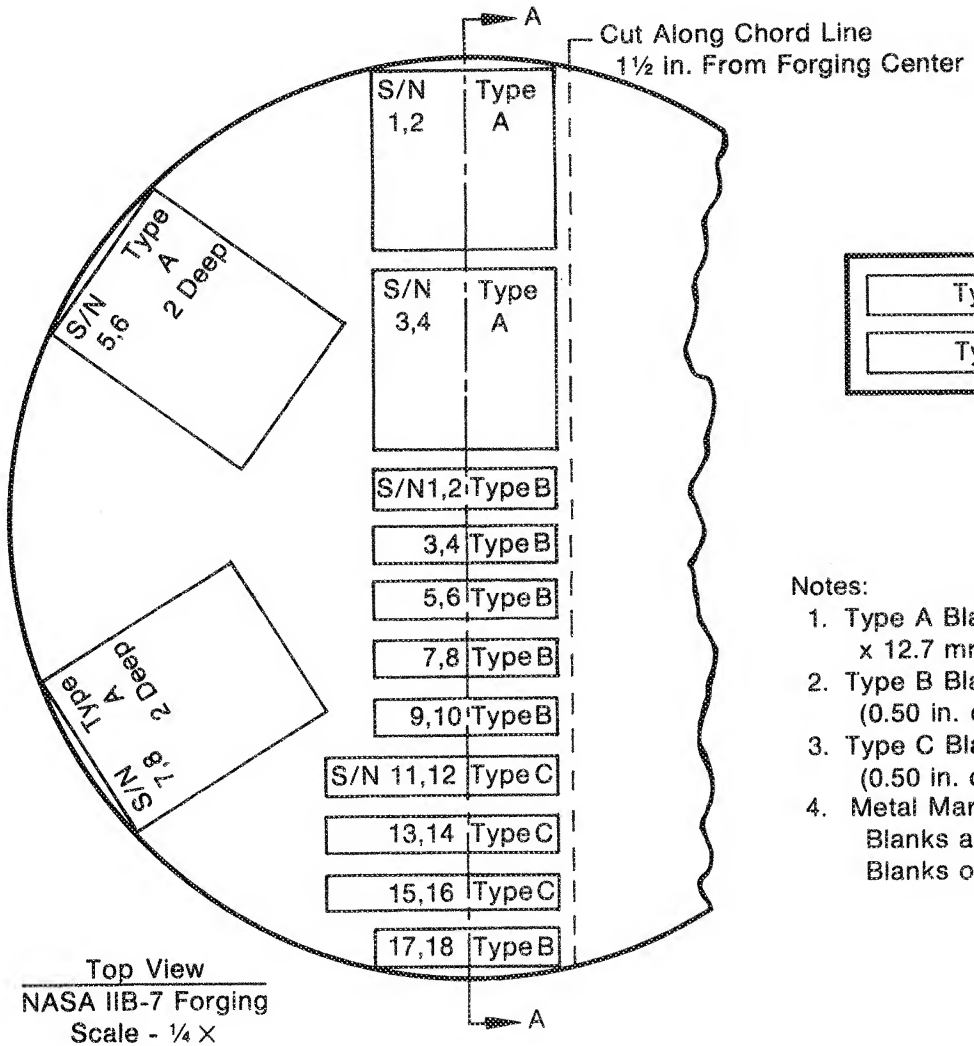

Top View
NASA IIB-7 Forging
Scale - ¼ X
Heat KR376-8

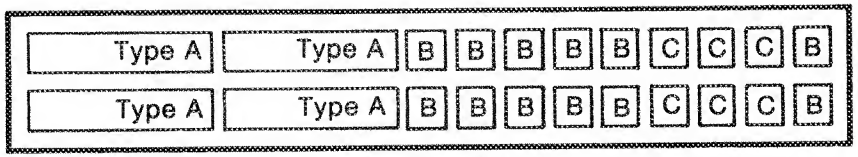

Section A-A
Scale ¼x

Notes:

1. Type A Blanks - Modified Contract Tension - 76.2 mm x 82.6 mm x 12.7 mm (3.0 in. x 3.25 in. x 0.50 in.)
2. Type B Blanks - LCF Specimen - 12.7 mm dia x 70 mm Long (0.50 in. dia x 2.50 in.)
3. Type C Blanks - LCF Specimen - 12.7 mm dia x 101.6 mm Long (0.50 in. dia x 4.0 in.)
4. Metal Mark All Specimens With S/N Mark Type A Blanks as Shown in Top View, Mark Type B and C Blanks on End

FD 143383A
781010
gen-509

FD 143383

Figure 4. Specimen Schematic Layout for Alloy 3, NASA IIB-7

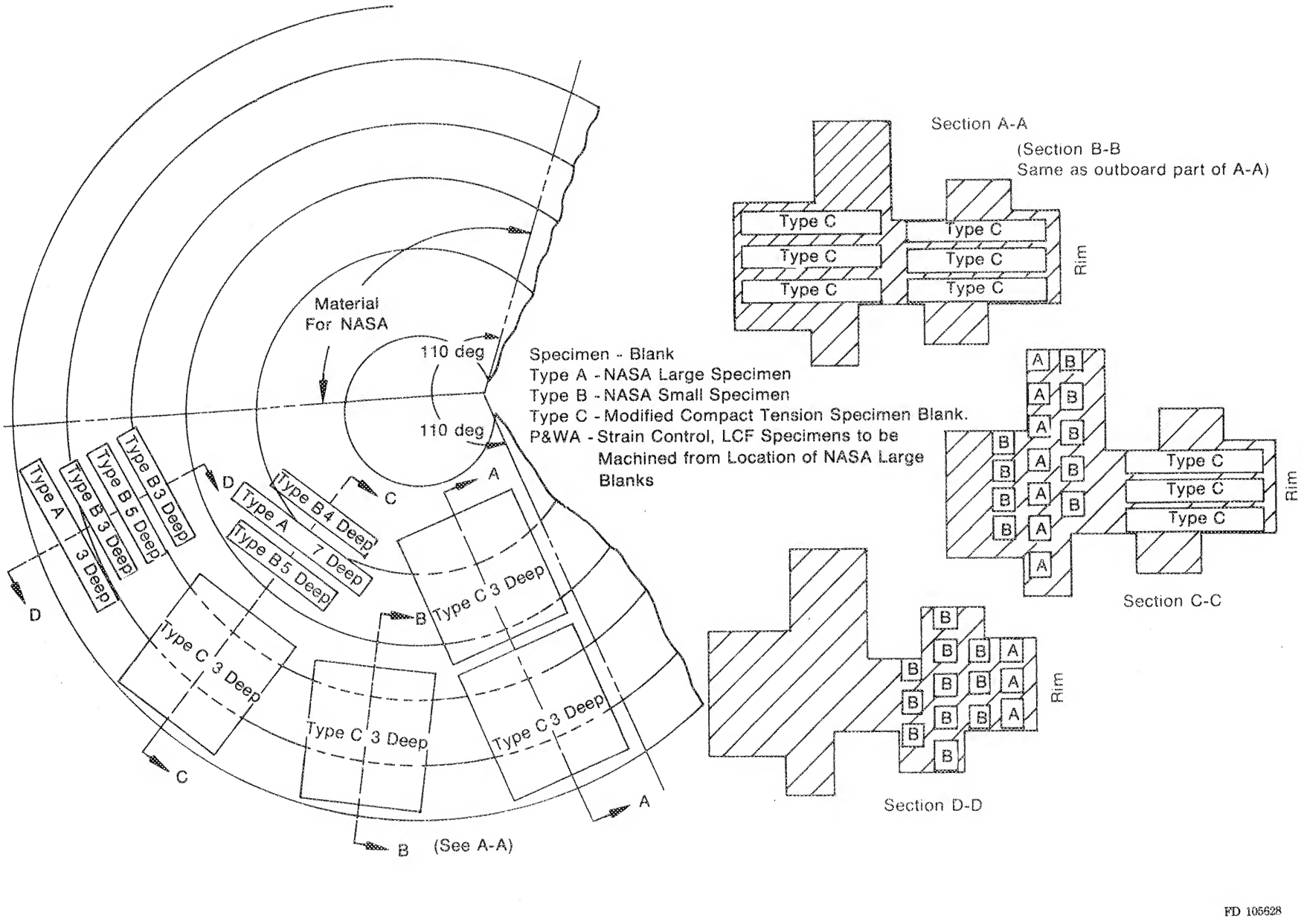

Figure 5. Alloy 4, HIP-Astroloy Turbine Disk Form Schematic Layout Showing Location and Orientation of Specimen Blanks

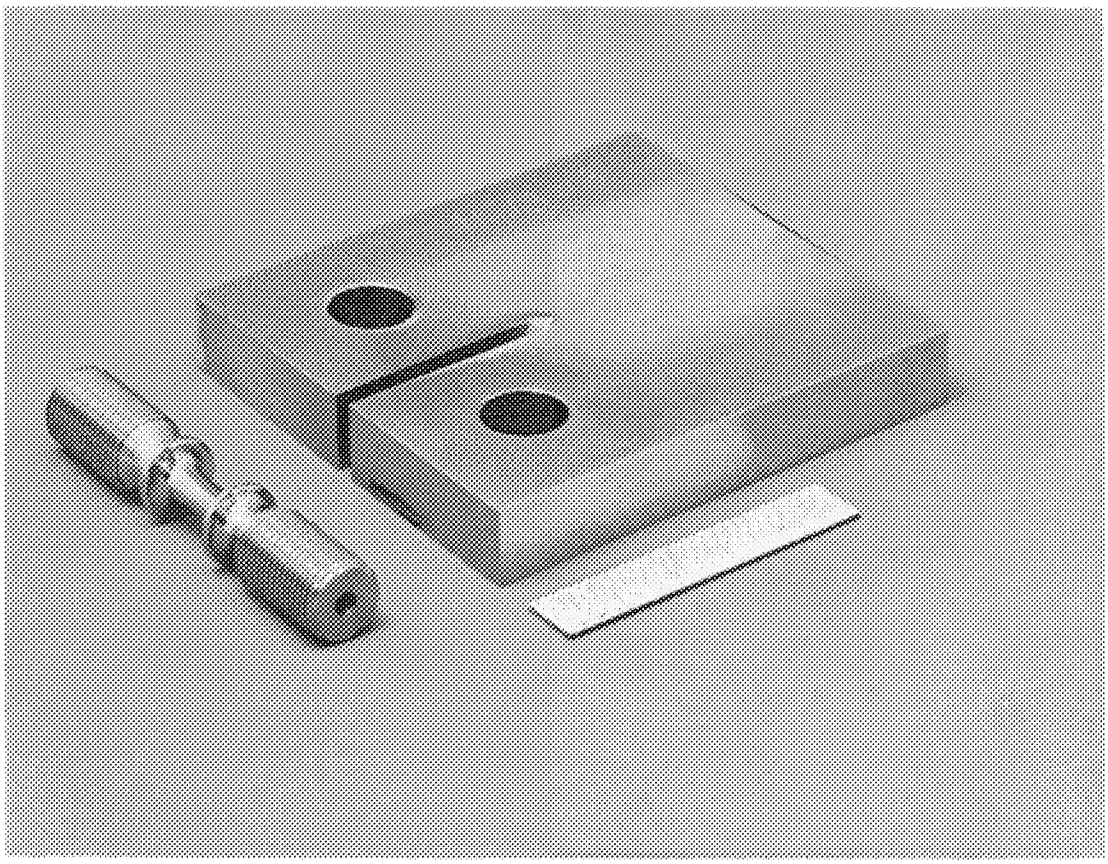

FE 169461

Figure 6. Strain Control LCF and Modified Compact Tension Specimens

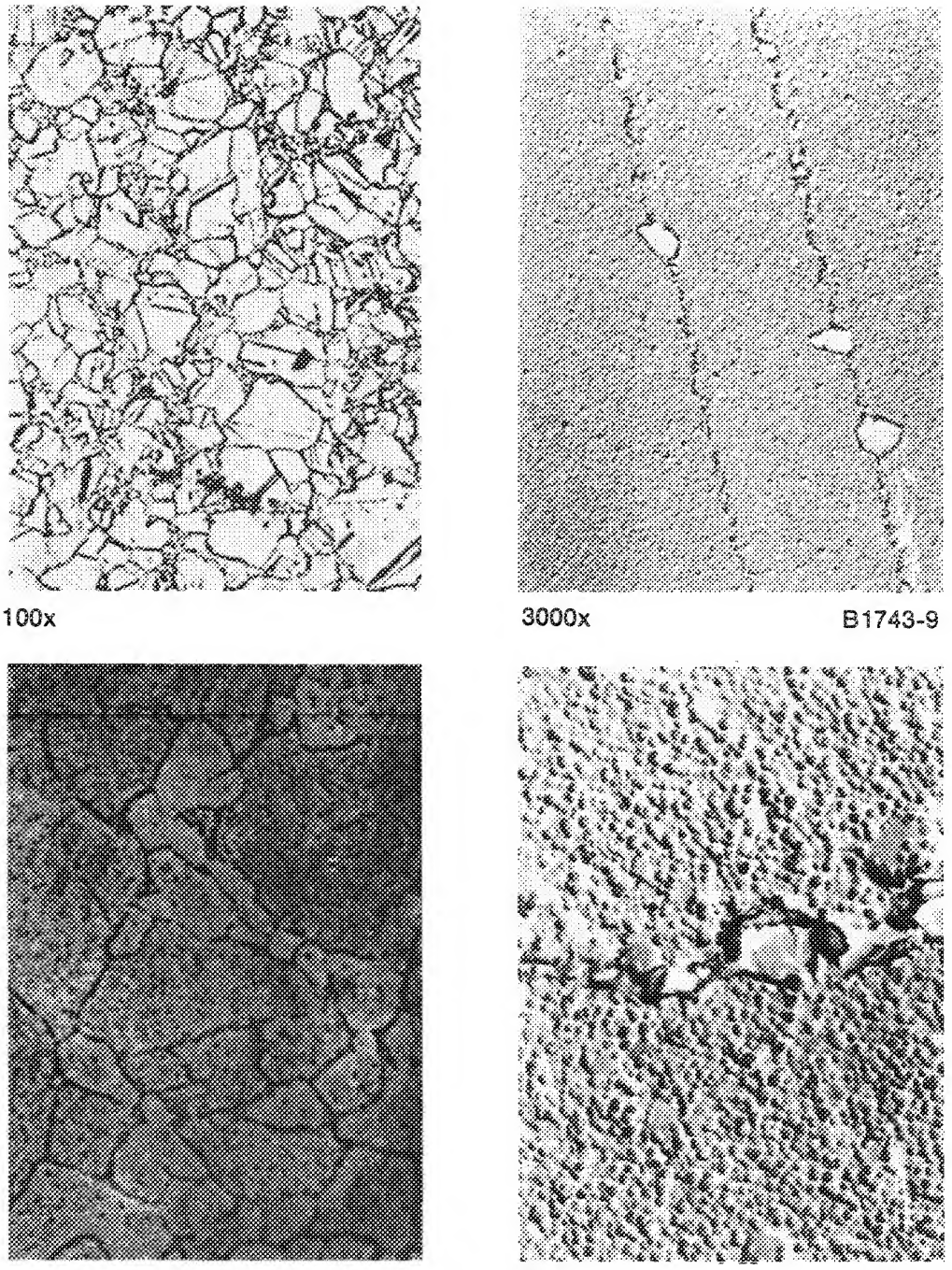

Figure 7. Optical Microstructure and Transmission Electron Micrographs of Alloy 1, Waspaloy

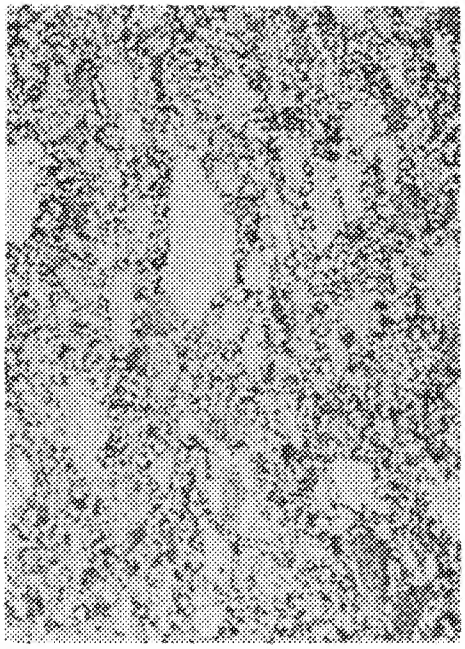

100x

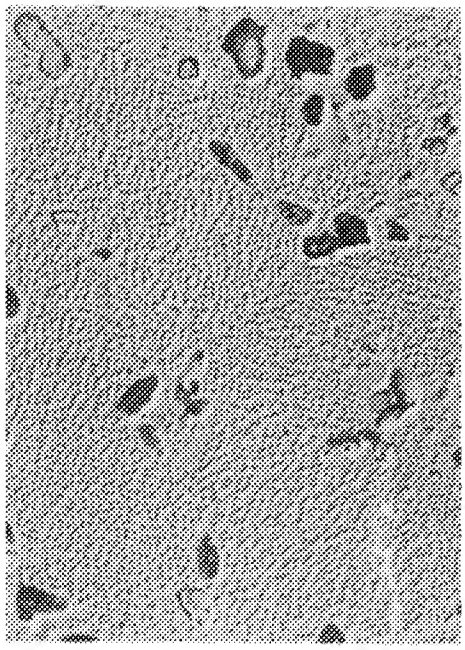

3000x B1743-21

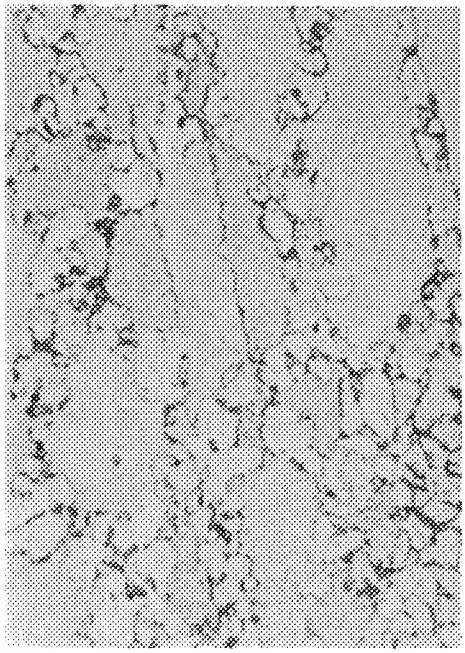

1000x

Alloy 2 - Wrought Astroloy

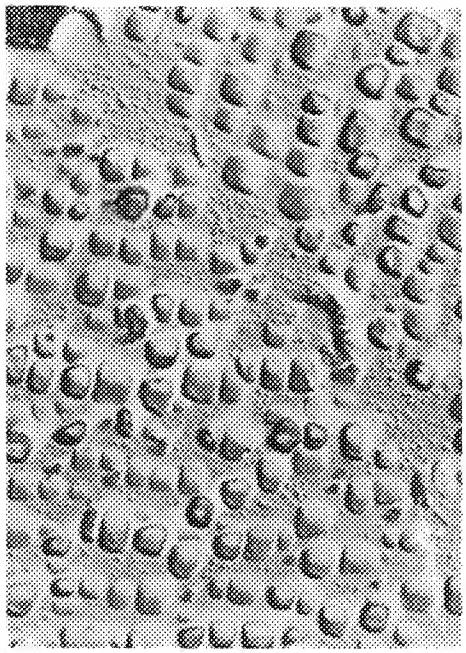

20,000x B1743-23

Alloy 2 - Wrought Astroloy

FD 148006

Figure 8. Optical Microstructure and Transmission Electron Micrographs of Alloy 2, Wrought Astroloy

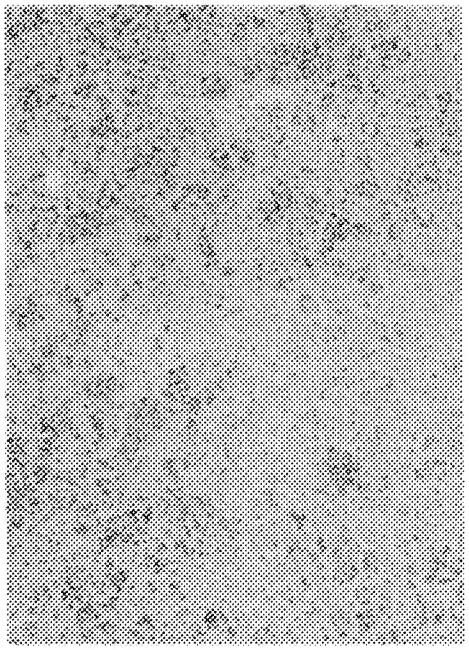

100x

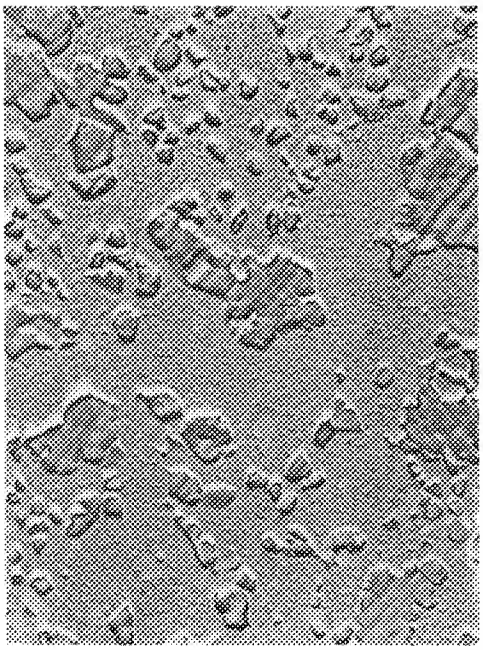

3000x B1743-33

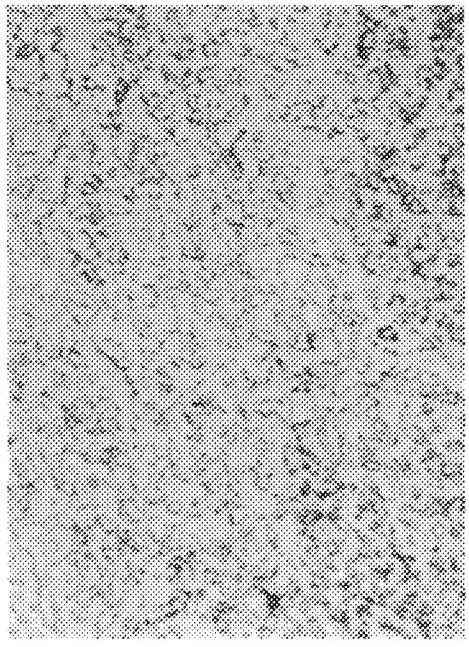

1000x

Alloy 3 - NASA IIB-7

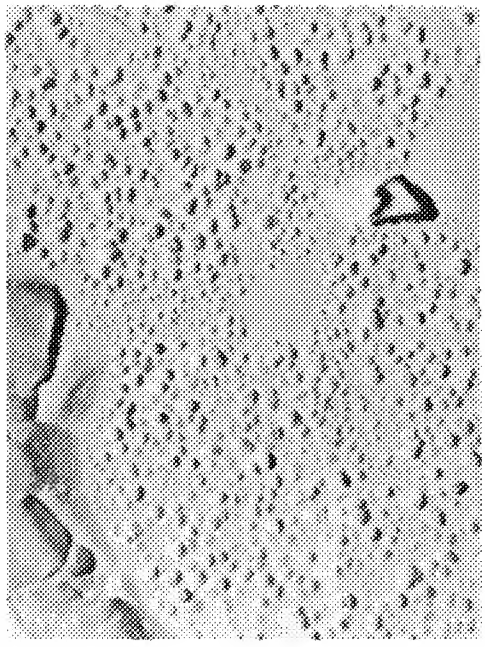

20,000x B1743-35

Alloy 3 - NASA IIB-7

FD 148007

Figure 9. Optical Microstructure and Transmission Electron Micrographs of Alloy 3, NASA II B-7

100x

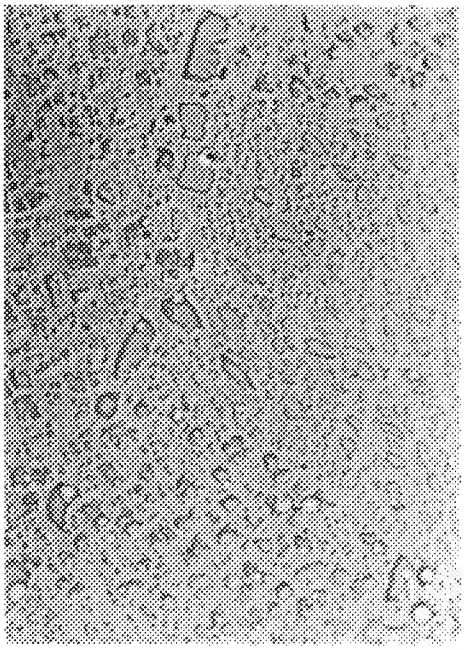

3000x B1556-25

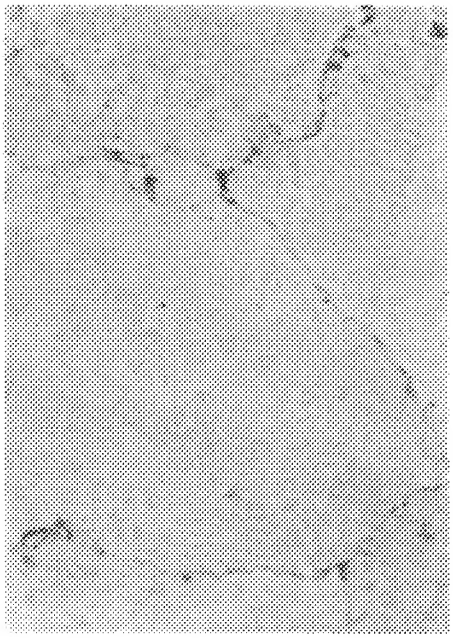

1000x

Alloy 4 - HIP Astroloy

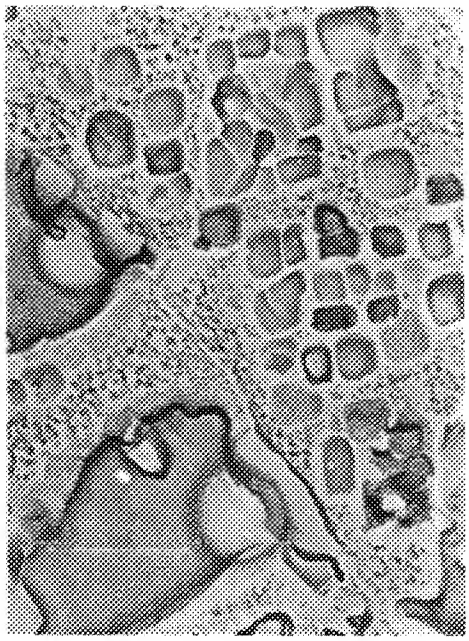

20,000x B1556-27

Alloy 4 - HIP Astroloy

FD 148008

Figure 10. Optical Microstructure and Transmission Electron Micrographs of Alloy 4, HIP Astroloy

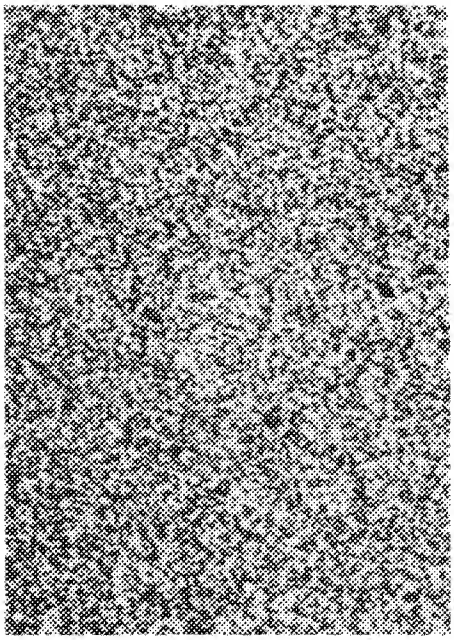

100x

3000x B1563-1

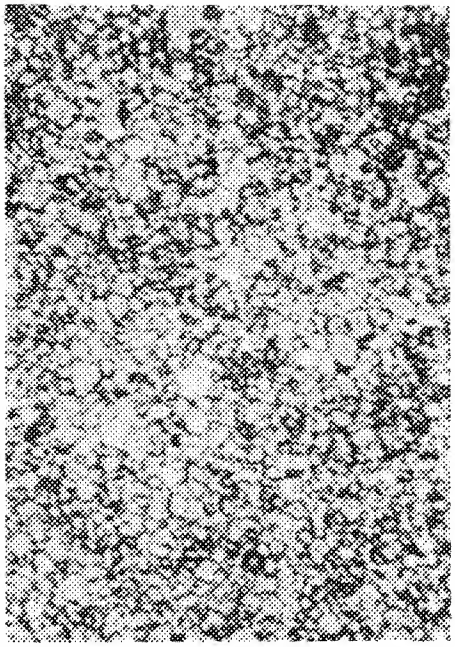

1000x

Alloy 5 - GATORIZED® IN 100

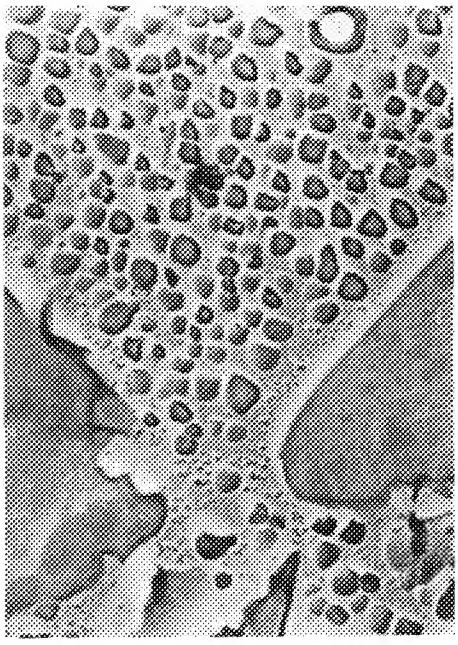

20,000x B1563-3

Alloy 5 - GATORIZED® IN 100

FD 148009

Figure 11. Optical Microstructure and Transmission Electron Micrographs of Alloy 5, GATORIZED® IN 100

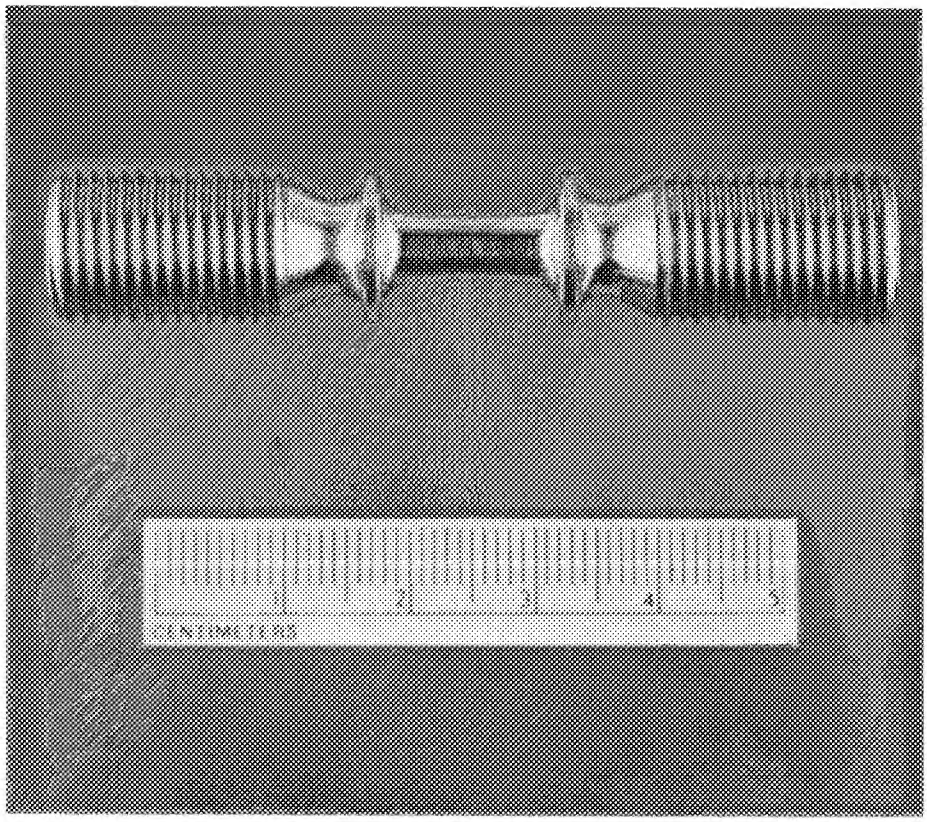

FE 169457

Figure 12. Strain Controlled LCF Specimen

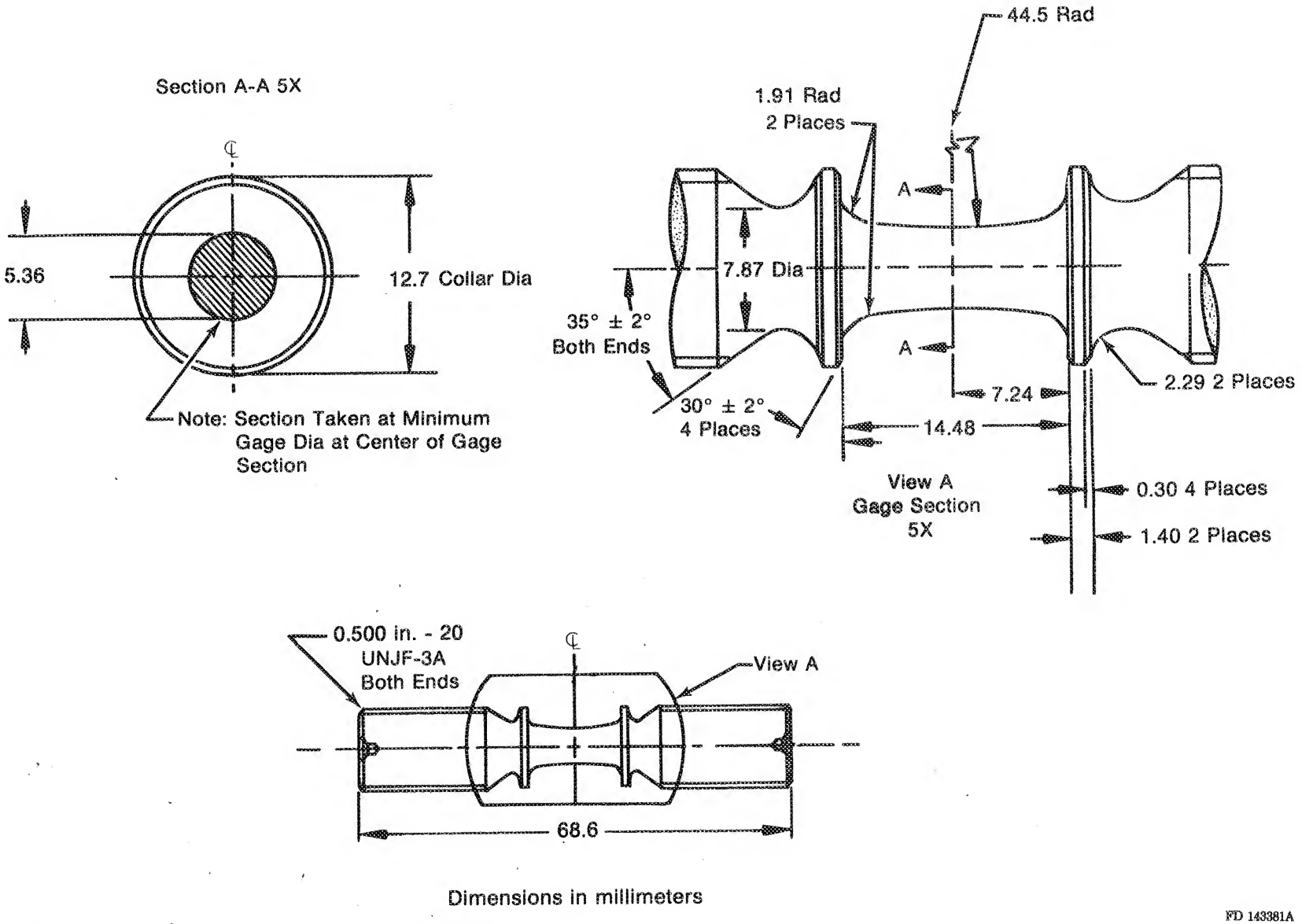

Figure 13. Strain Controlled LCF Specimen Print

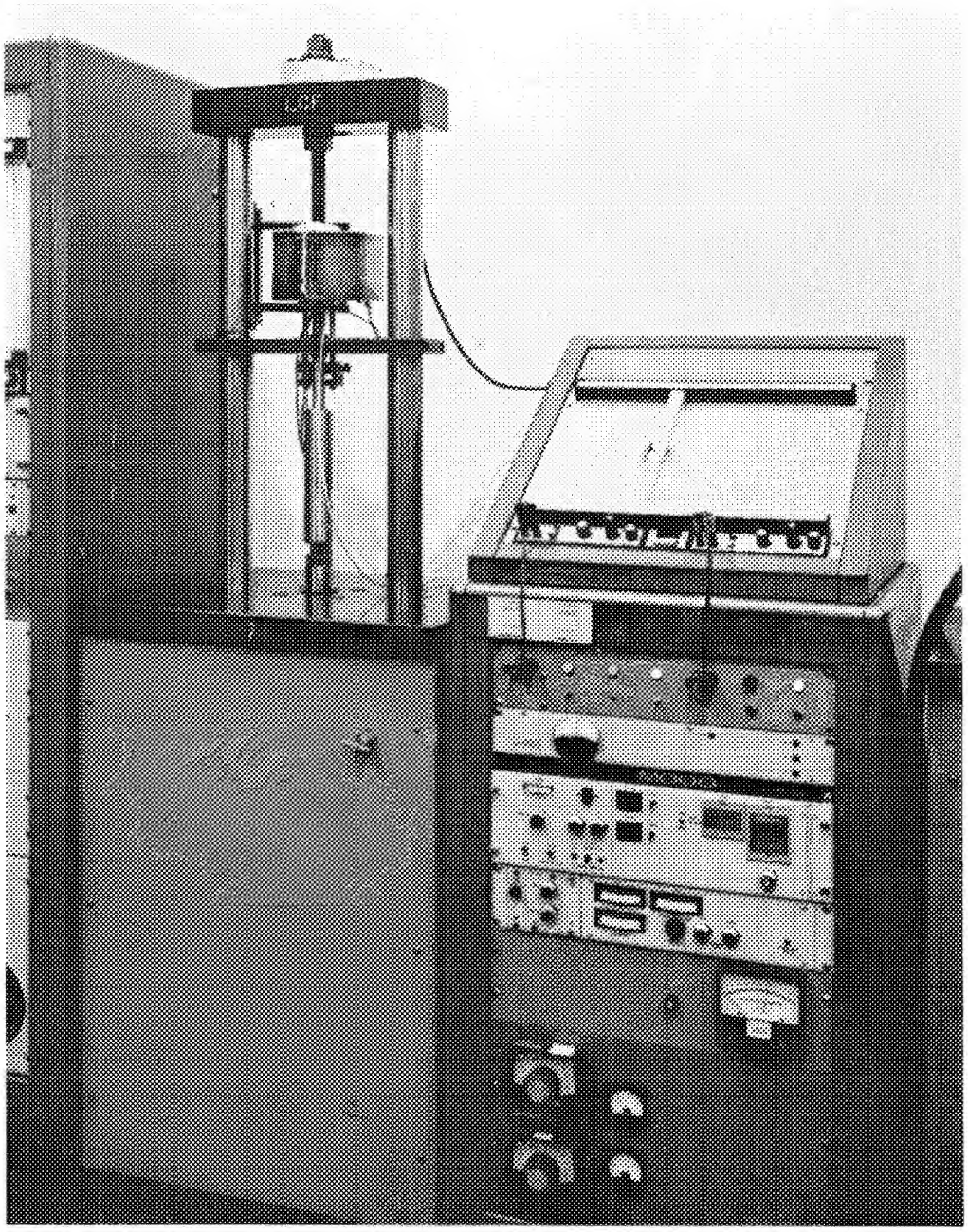

FAC 39397

Figure 14. Servohydraulic Closed-Loop LCF Test Machine

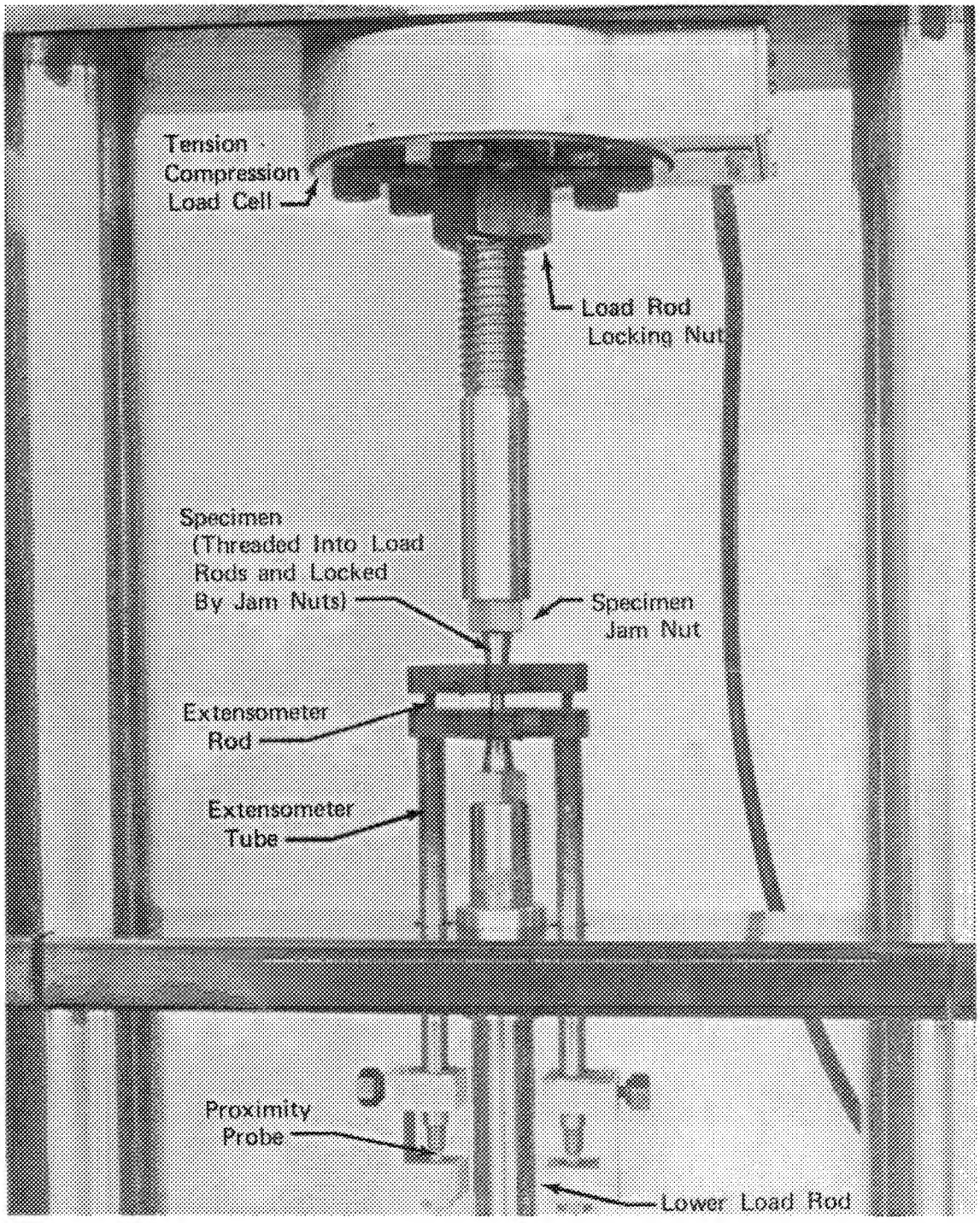

FD 92637

Figure 15. Load Cell, Load Rod, Specimen, and Extensometer Assembly Mounted in LCF Testing Machine

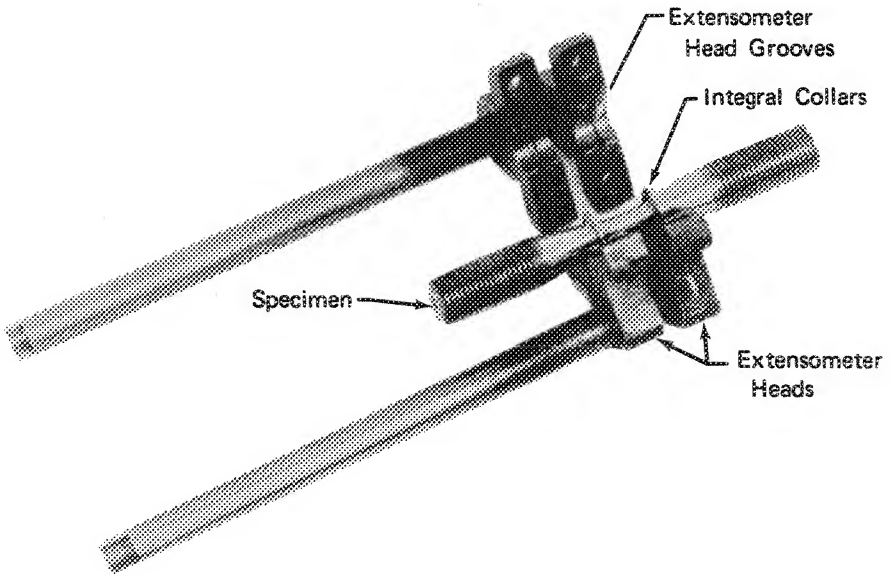

Figure 16. Extensometer Head Assembly and LCF Specimen

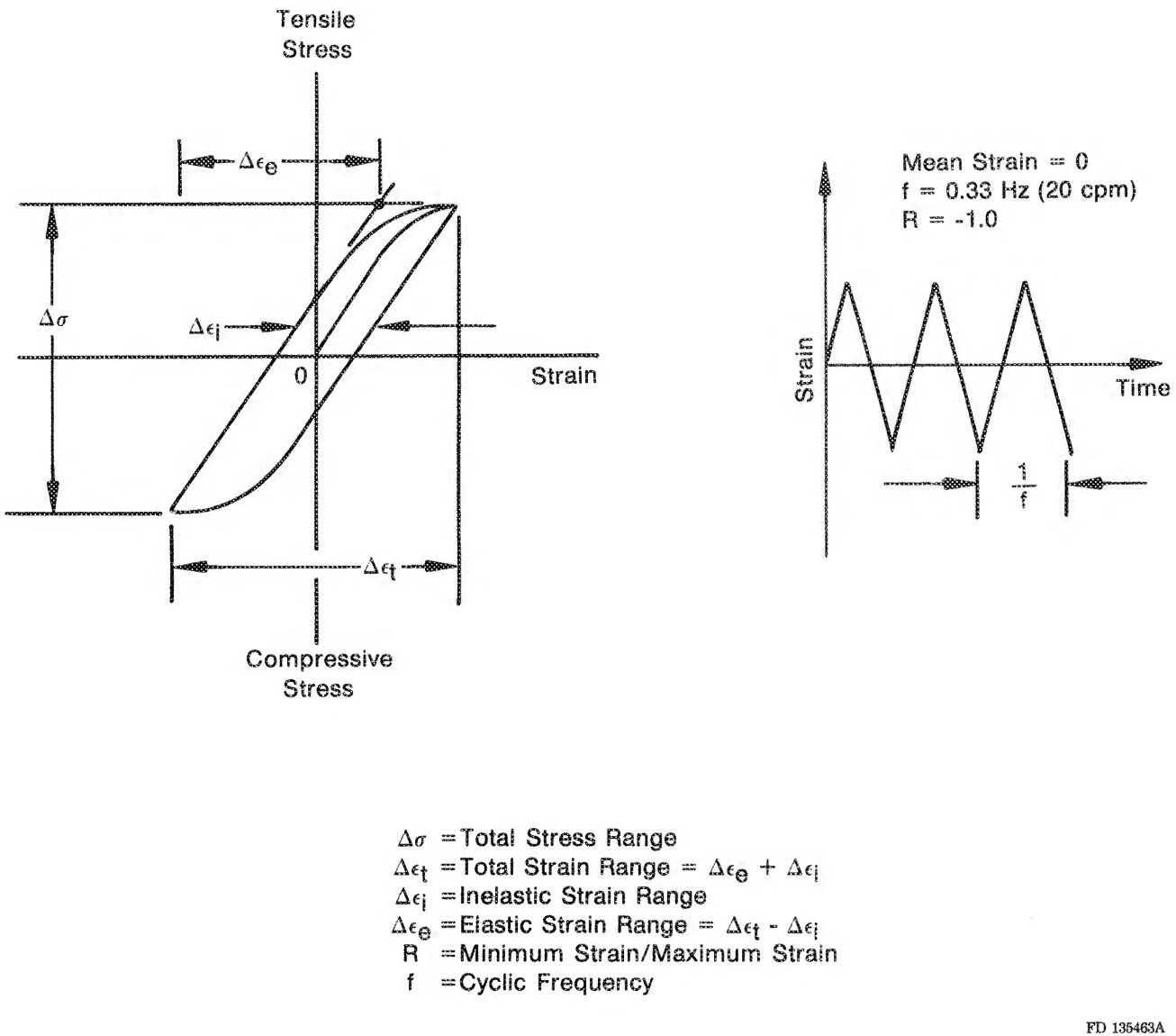

$\Delta\sigma$ = Total Stress Range
$\Delta\epsilon_t$ = Total Strain Range = $\Delta\epsilon_e + \Delta\epsilon_i$
$\Delta\epsilon_i$ = Inelastic Strain Range
$\Delta\epsilon_e$ = Elastic Strain Range = $\Delta\epsilon_t - \Delta\epsilon_i$
R = Minimum Strain/Maximum Strain
f = Cyclic Frequency

FD 135463A

Figure 17. Typical Nondwell LCF Test With Mean Strain of Zero

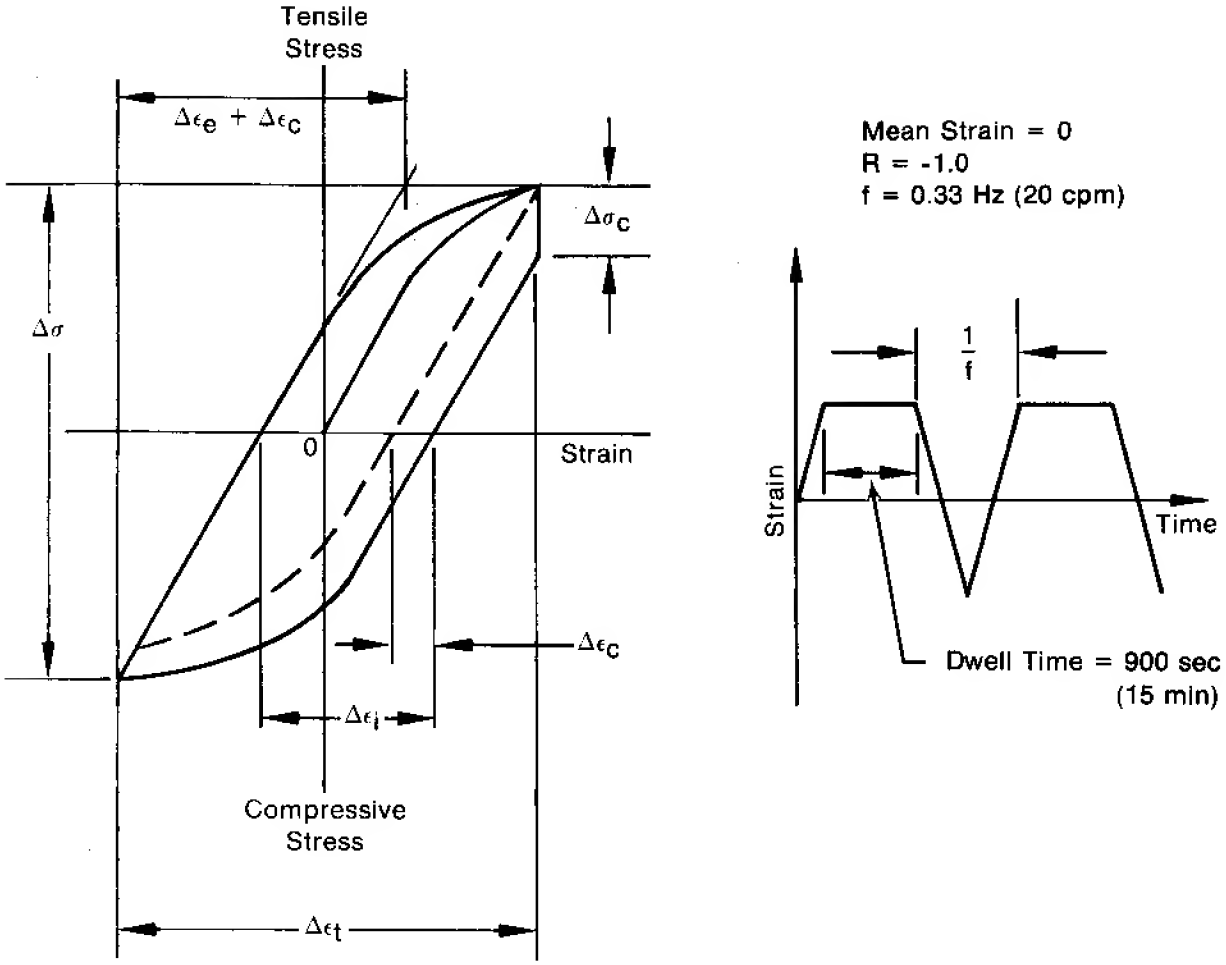

$\Delta\sigma$ = Total Stress Range
$\Delta\sigma_c$ = Creep Relaxation Stress
$\Delta\epsilon_t$ = Total Strain Range = $\Delta\epsilon_e + \Delta\epsilon_i$
$\Delta\epsilon_i$ = Inelastic Strain Range
$\Delta\epsilon_c$ = Creep Strain Range = $\Delta\sigma_c/E$
$\Delta\epsilon_e$ = Elastic Strain Range = $\Delta\epsilon_t - \Delta\epsilon_i$
R = Minimum Strain/Maximum Strain
f = Ramp Frequency (Equivalent to 20 cpm No-dwell Test)

FD 135462A

Figure 18. Typical Strain-Dwell LCF Test With Mean Strain of Zero

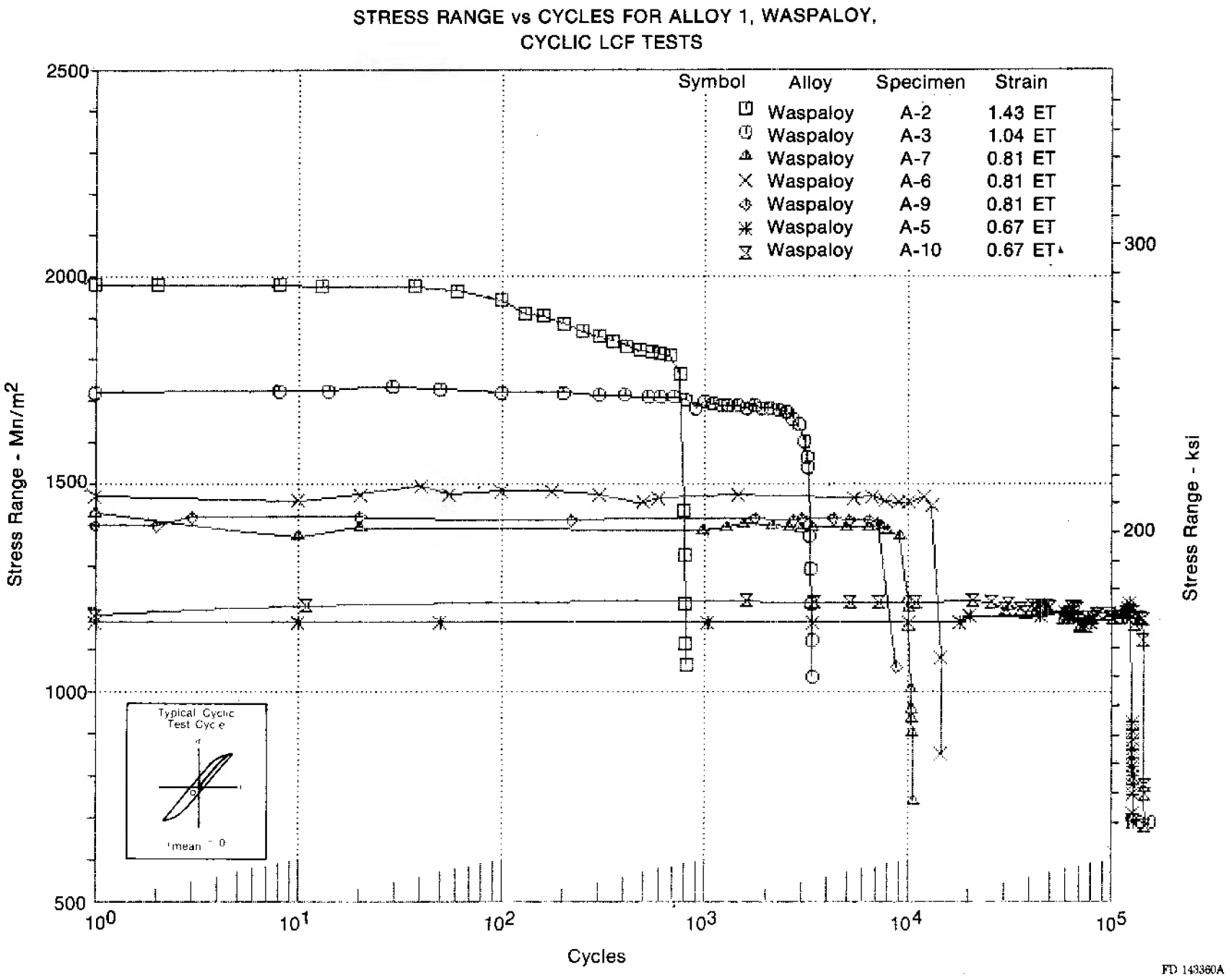

Figure 19. Stress Range vs Cycles for Alloy 1, Waspaloy, Cyclic LCF Tests

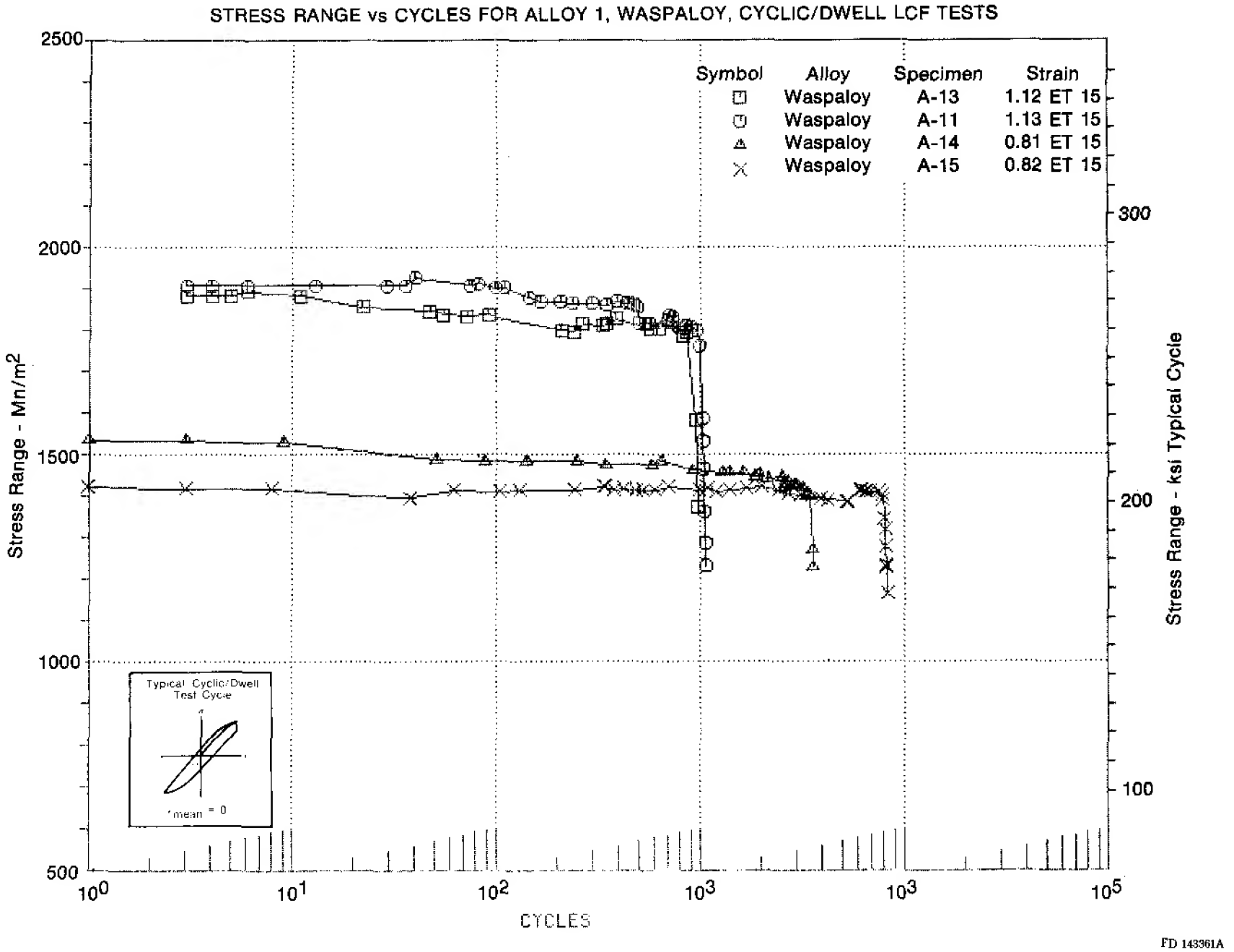

Figure 20. Stress Range vs Cycles for Alloy 1, Waspaloy, Cyclic/Dwell LCF Tests

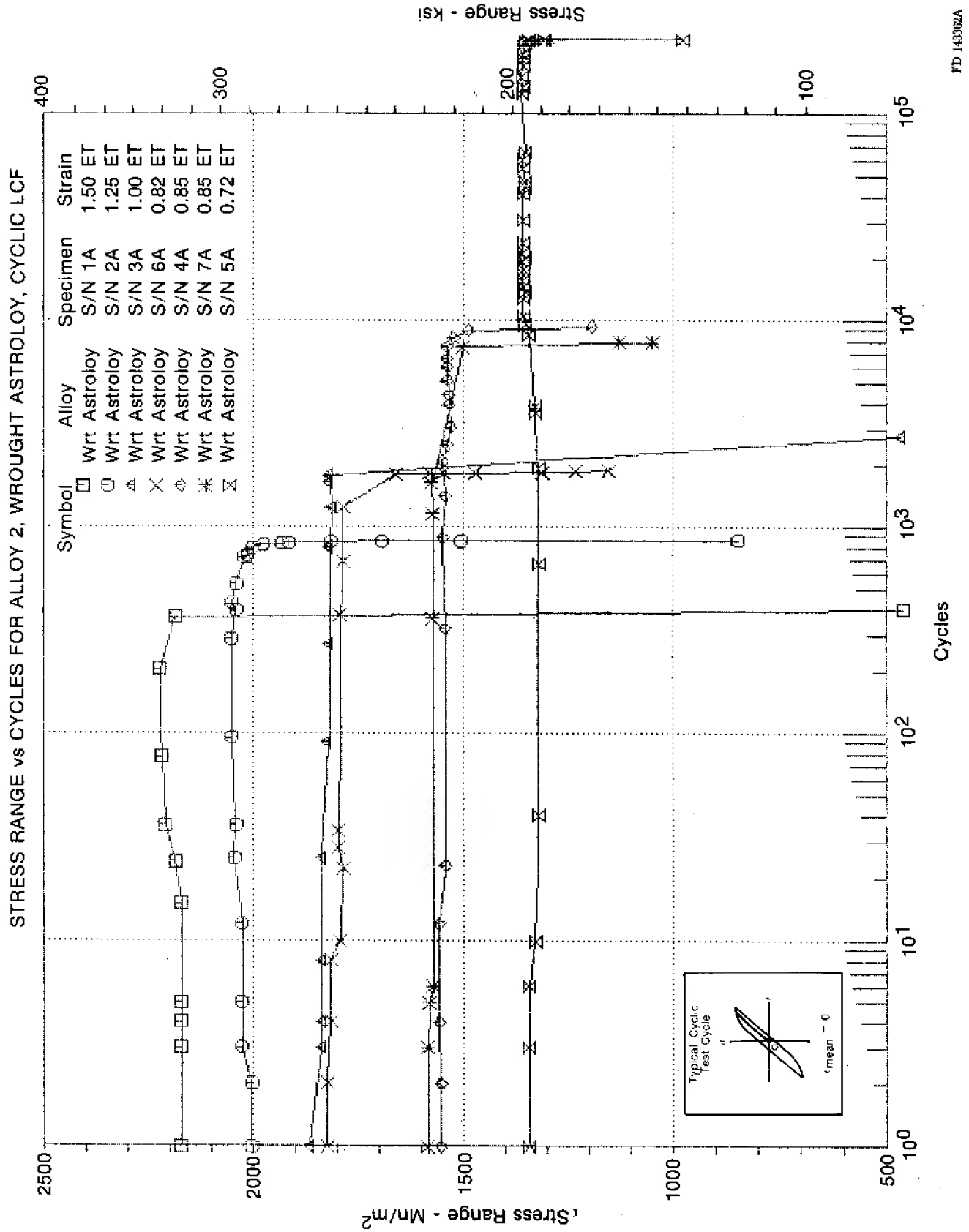

Figure 21. Stress Range vs Cycles for Alloy 2, Wrought Astroloy, Cyclic LCF Tests

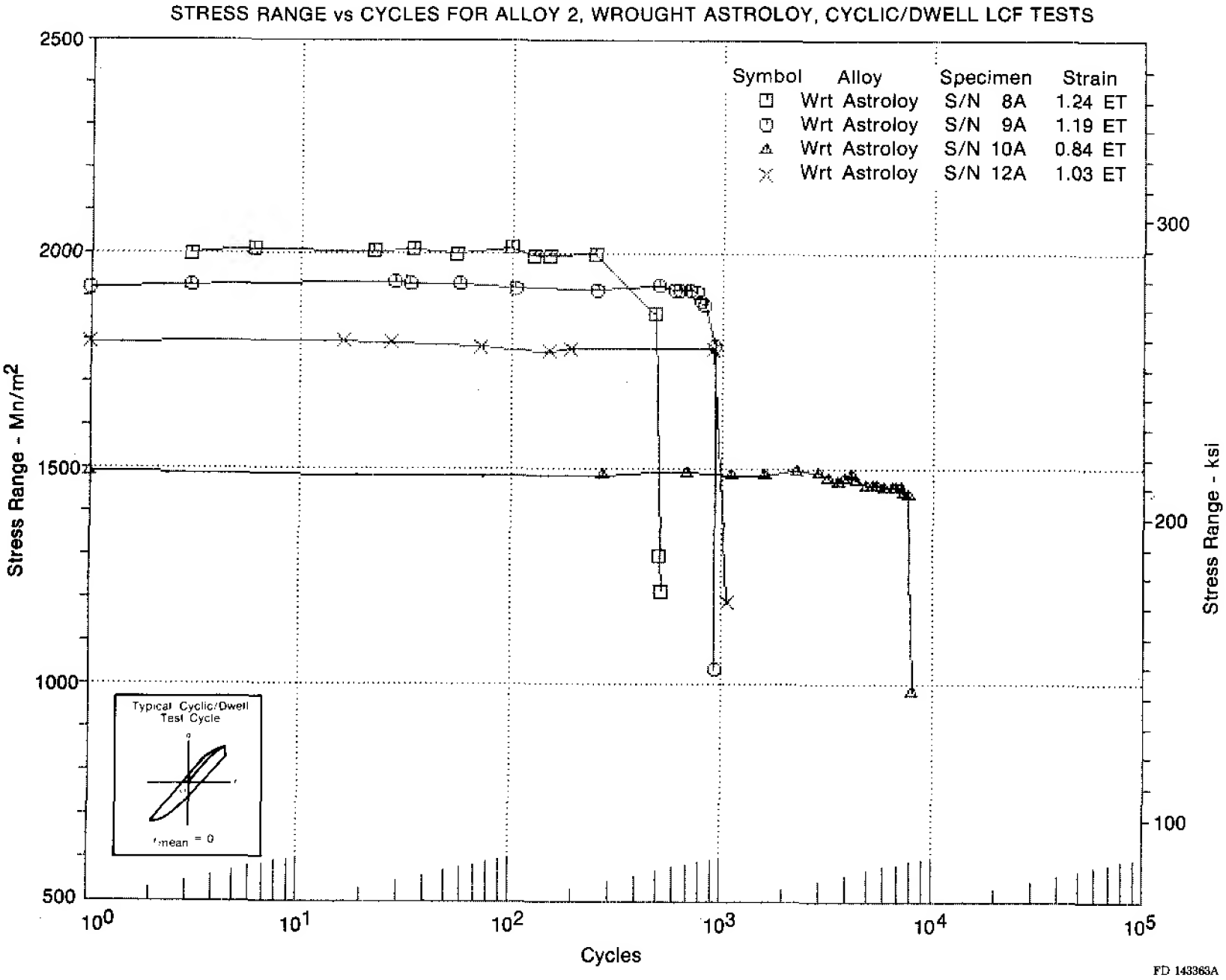

Figure 22. Stress Range vs Cycles for Alloy 2, Wrought Astroloy, Cyclic/Dwell LCF Tests

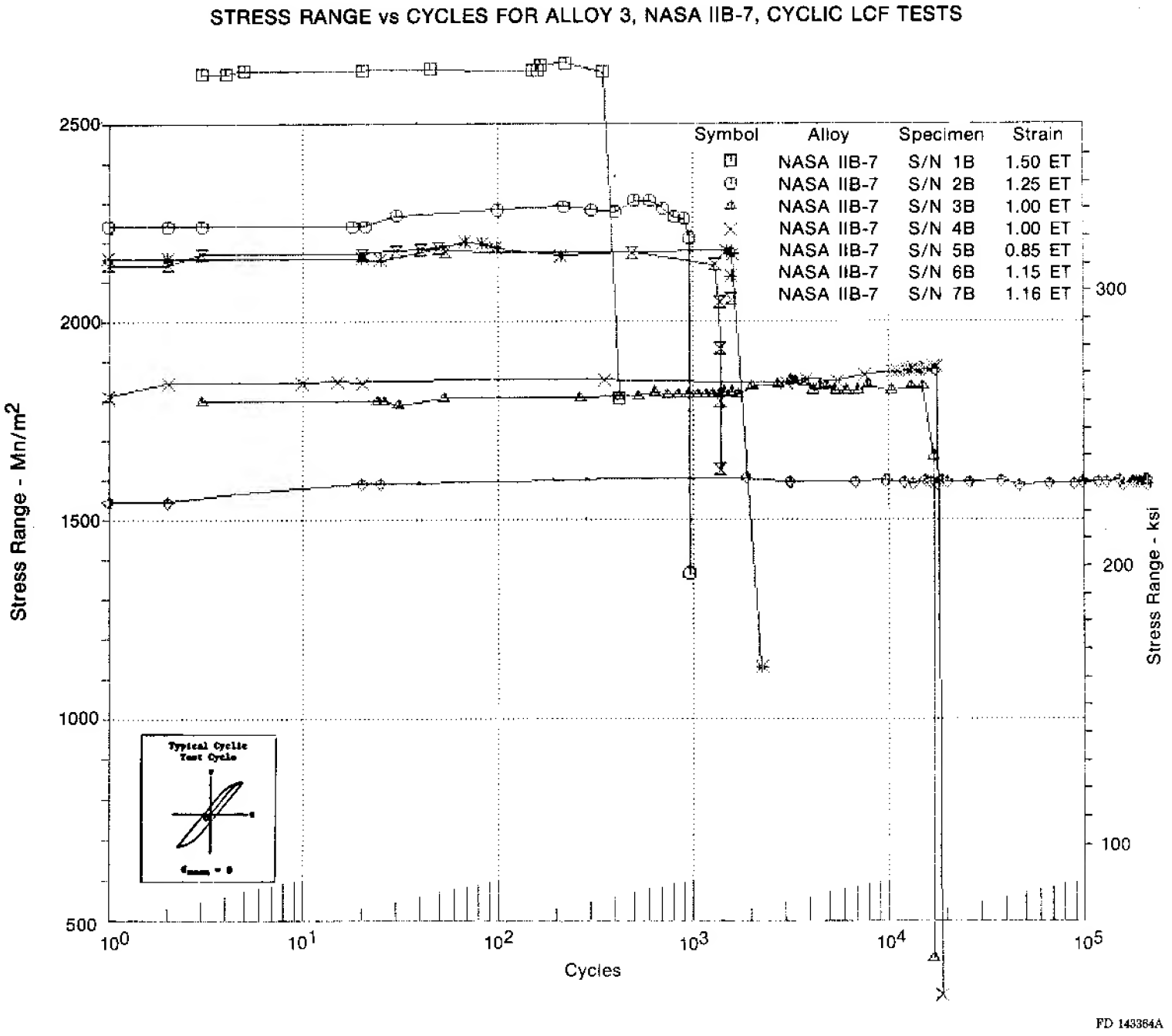

Figure 23. Stress Range vs Cycles for Alloy 3, NASA IIB-7, Cyclic LCF Tests

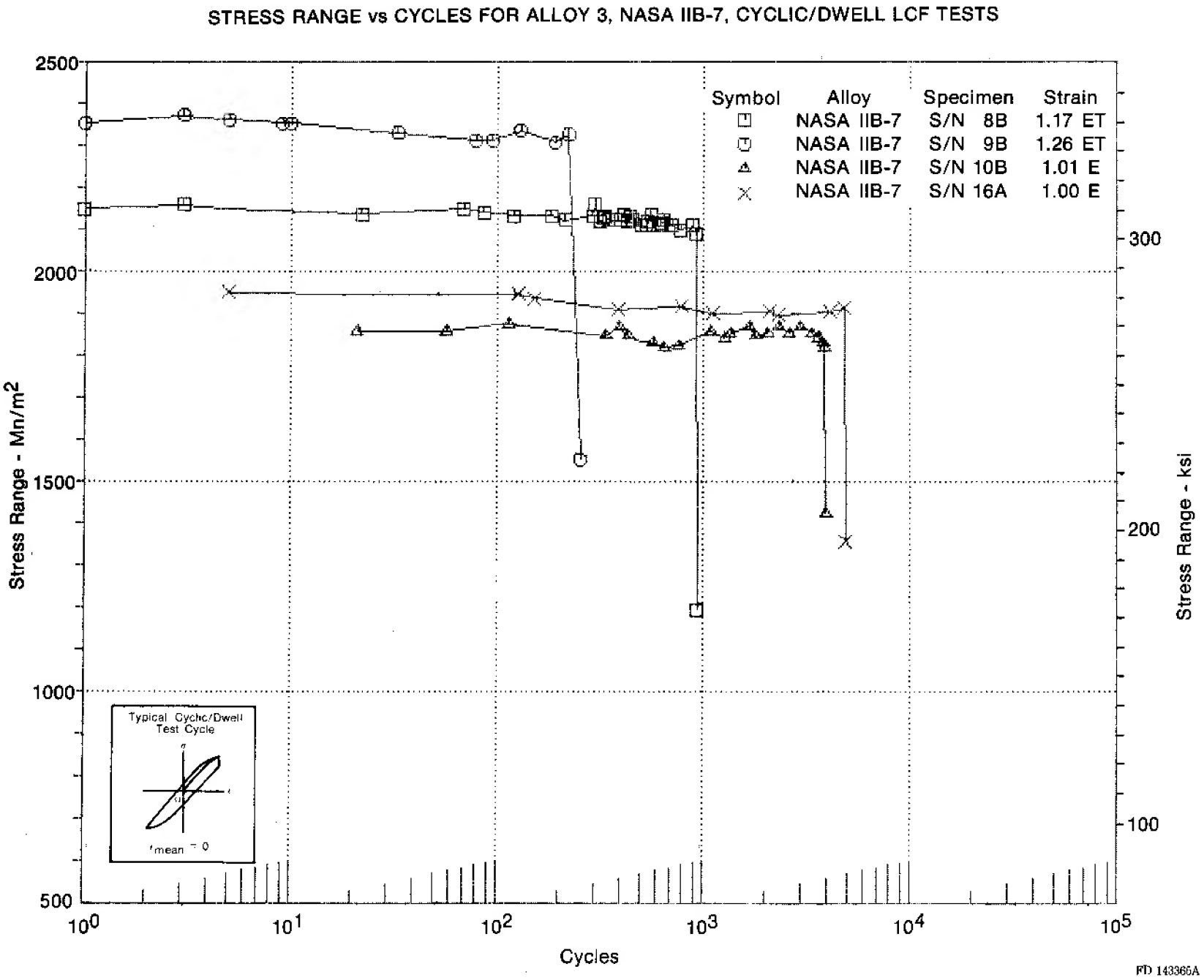

Figure 24. Stress Range vs Cycles for Alloy 3, NASA IIB-7, Cyclic/Dwell LCF Tests

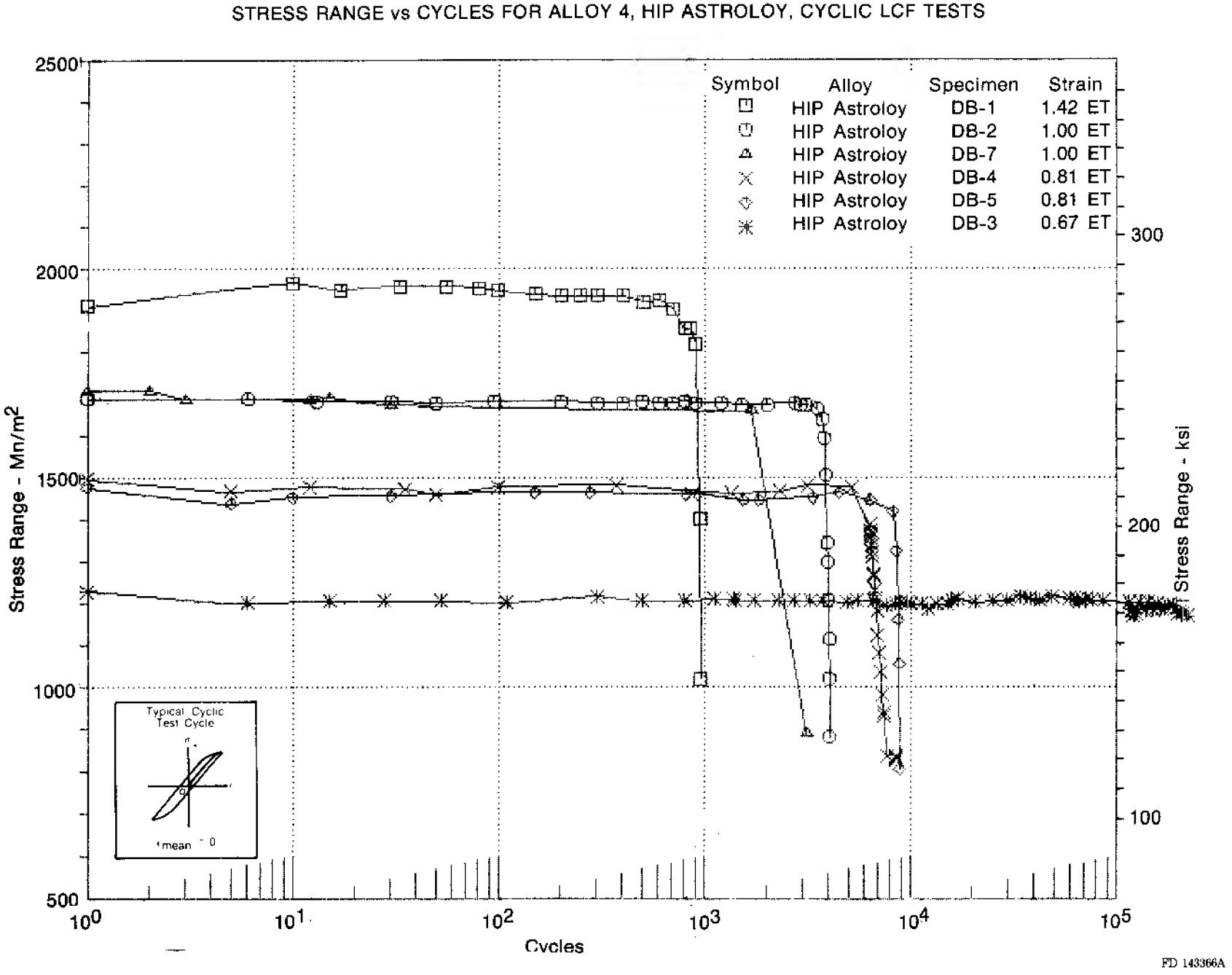

Figure 25. Stress Range vs Cycles for Alloy 4, HIP-Astroloy, Cyclic LCF Tests

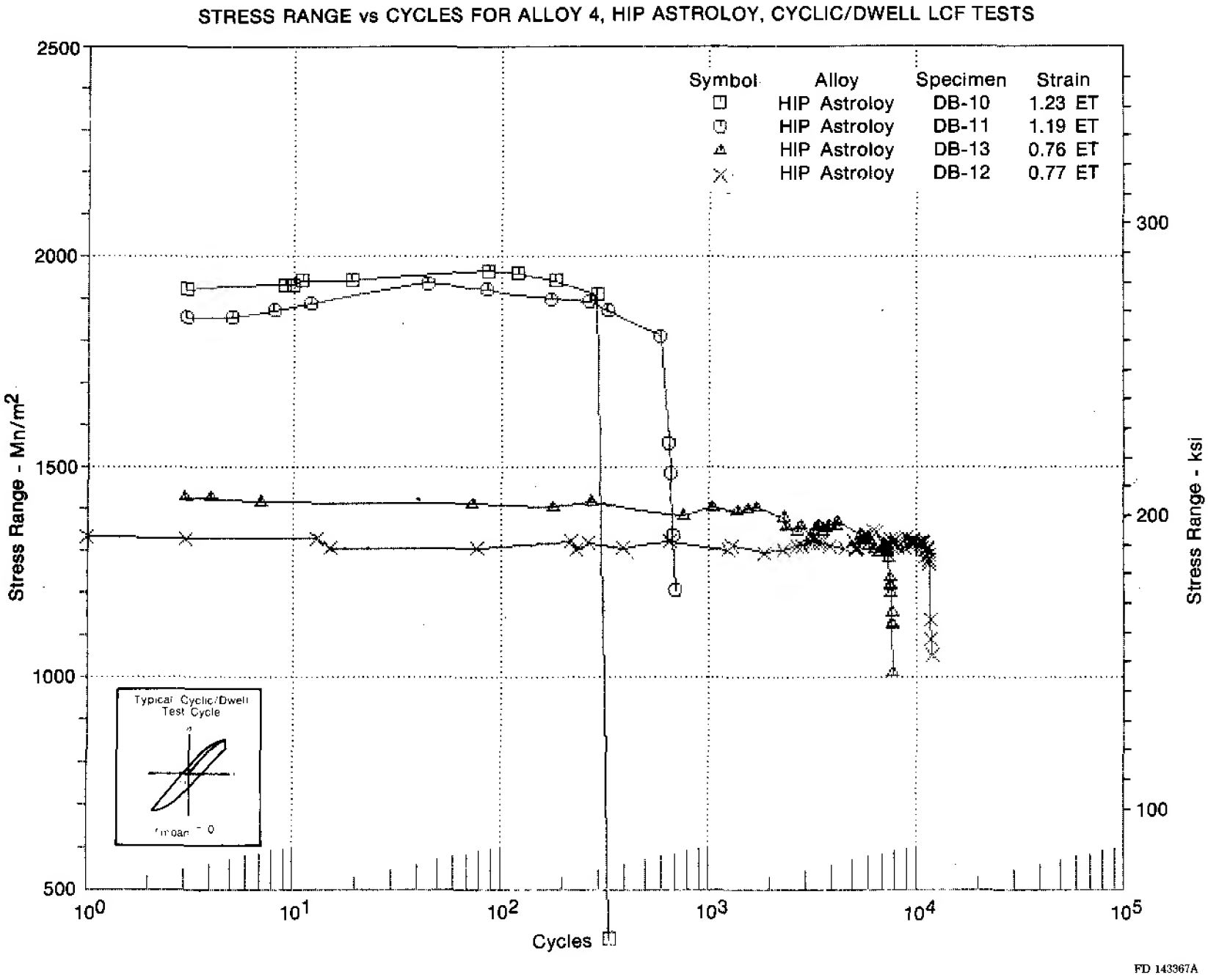

Figure 26. Stress Range vs Cycles for Alloy 4, HIP-Astroloy, Cyclic/Dwell LCF Tests

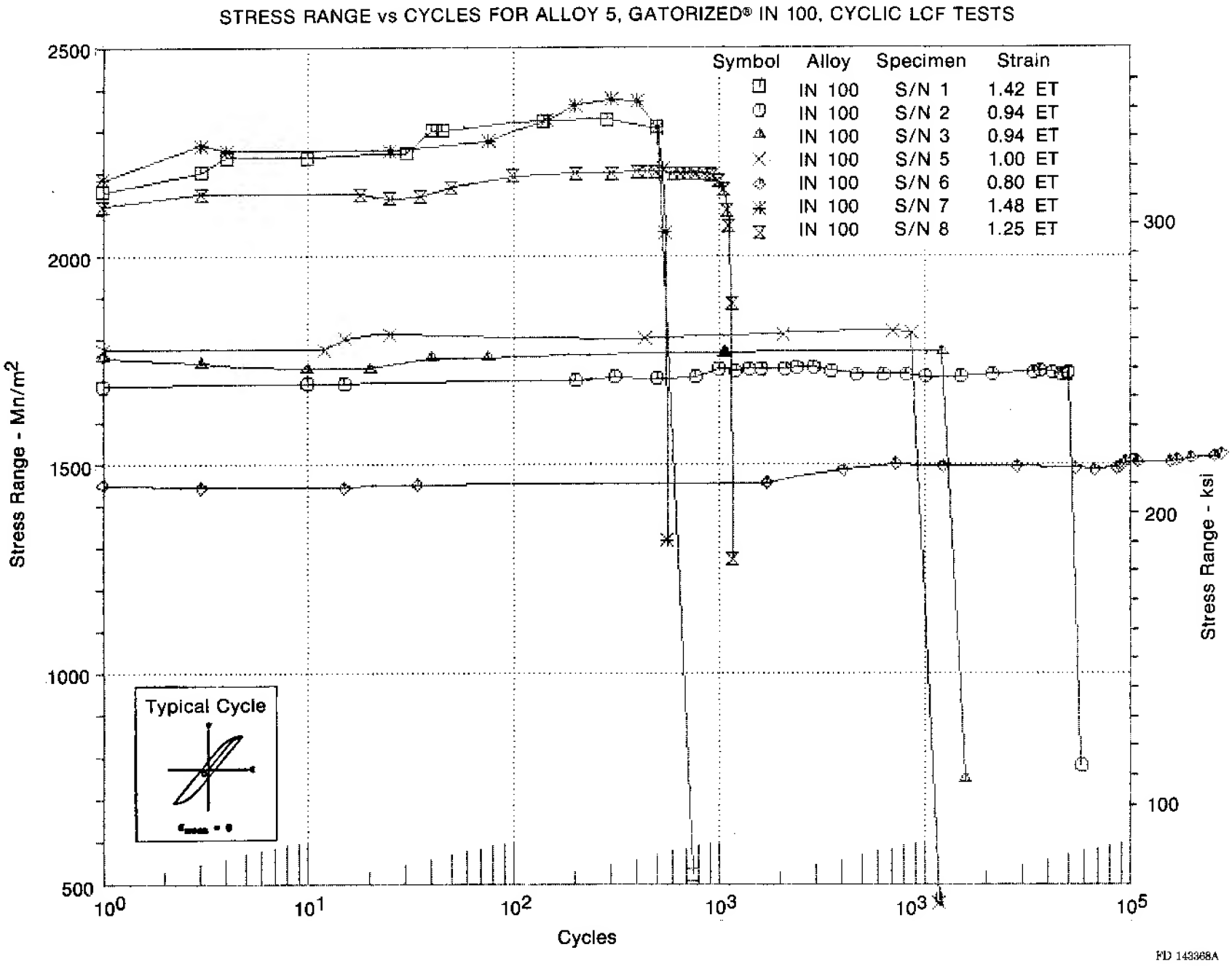

Figure 27. Stress Range vs Cycles for Alloy 5, GATORIZED® IN 100, Cyclic LCF Tests

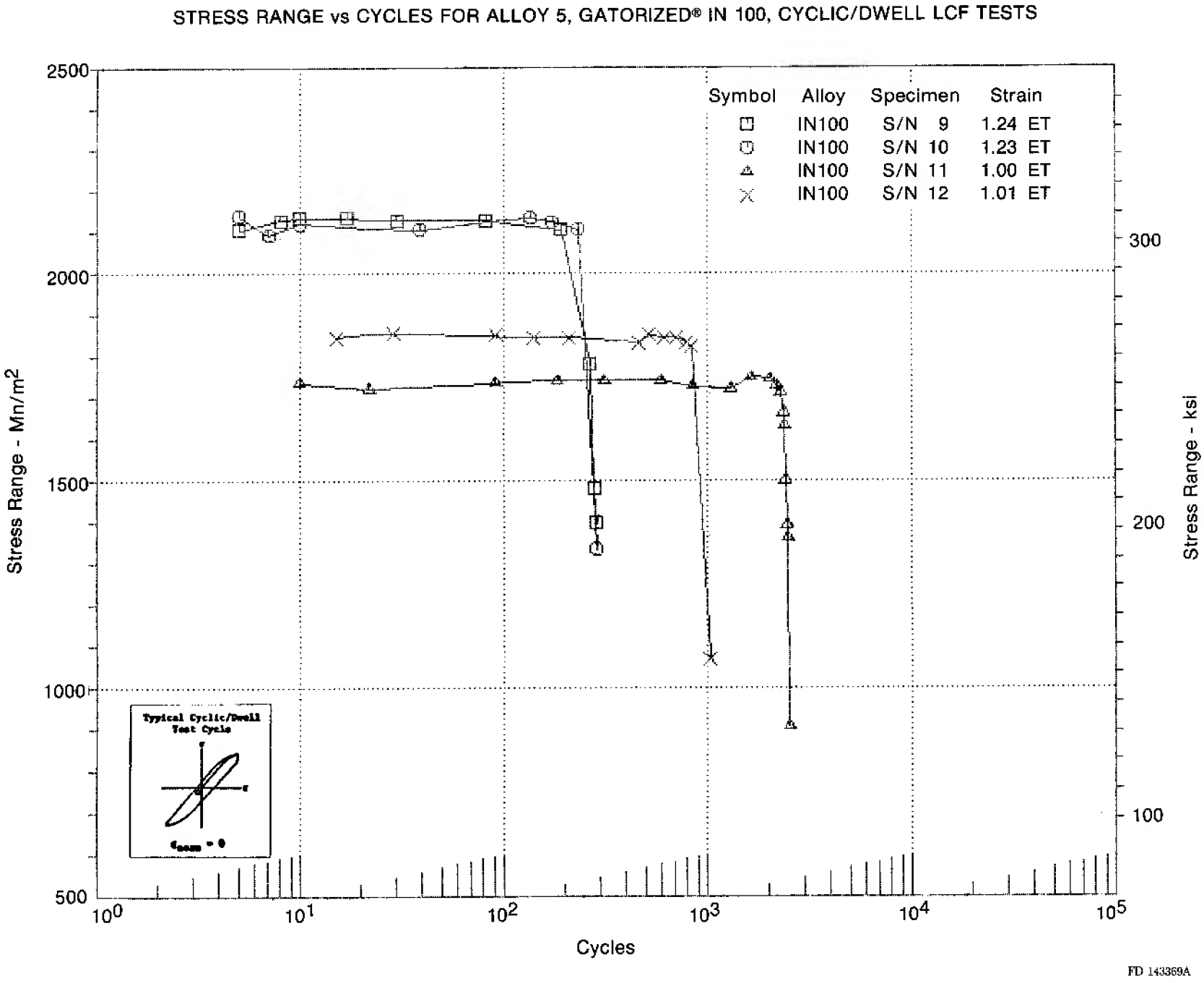

Figure 28. Stress Range vs Cycles for Alloy 5, GATORIZED® IN 100, Cyclic/Dwell LCF Tests

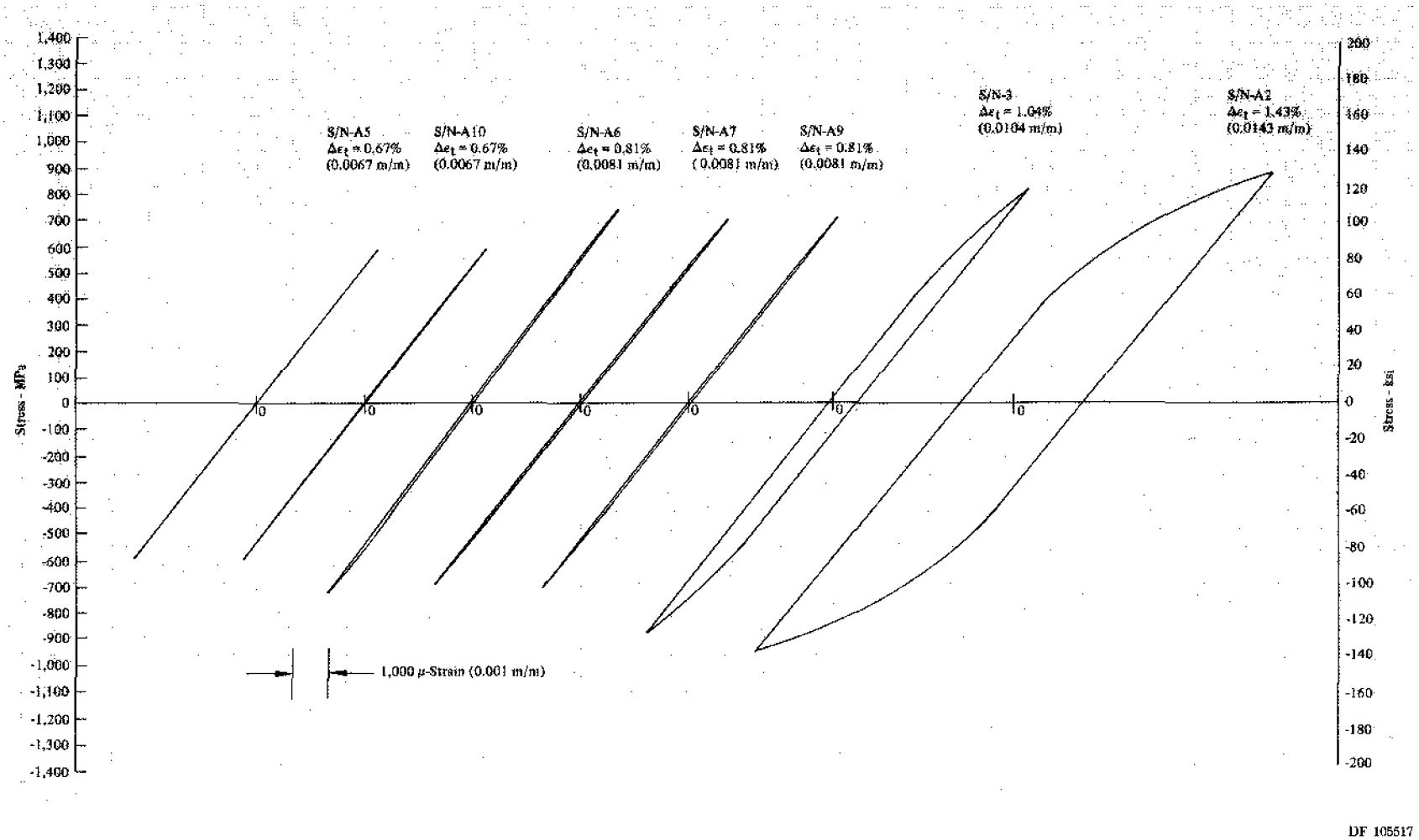

Figure 29. Typical Stress-Strain Hysteresis Loops for All Waspaloy Cyclic Strain-Controlled LCF Tests (Test Frequency = 0.33 Hz, Temp = 650°C, 1200°F, Cycles Shown Taken at $N_F/2$)

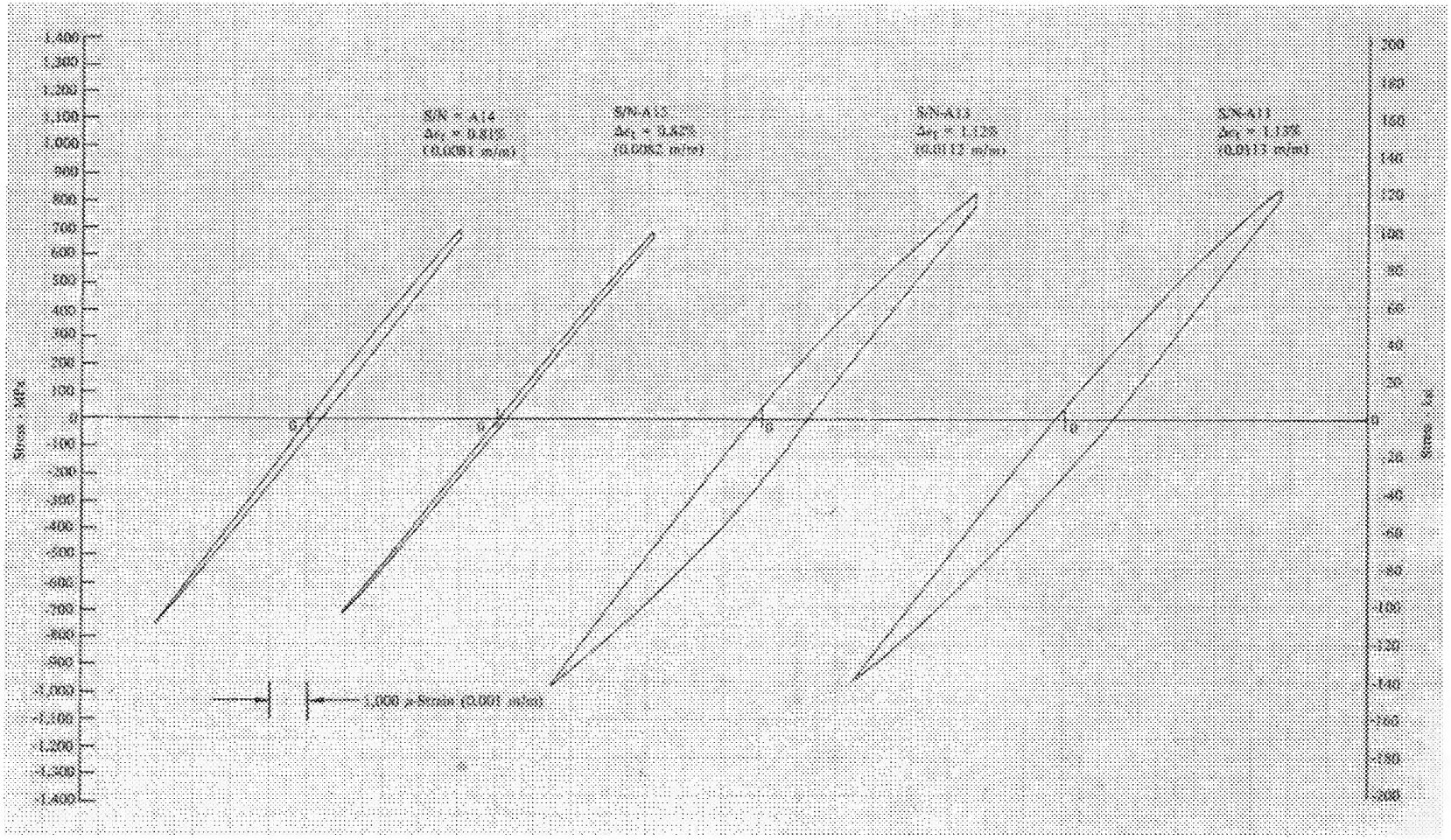

DF 105501

Figure 30. Typical Stress-Strain Hysteresis Loops for All Waspaloy Cyclic/Dwell Strain-Controlled LCF Tests (Dwell Time = 900 sec, Temp = 650°C, 1200°F, Cycles Shown Taken at $N_F/2$)

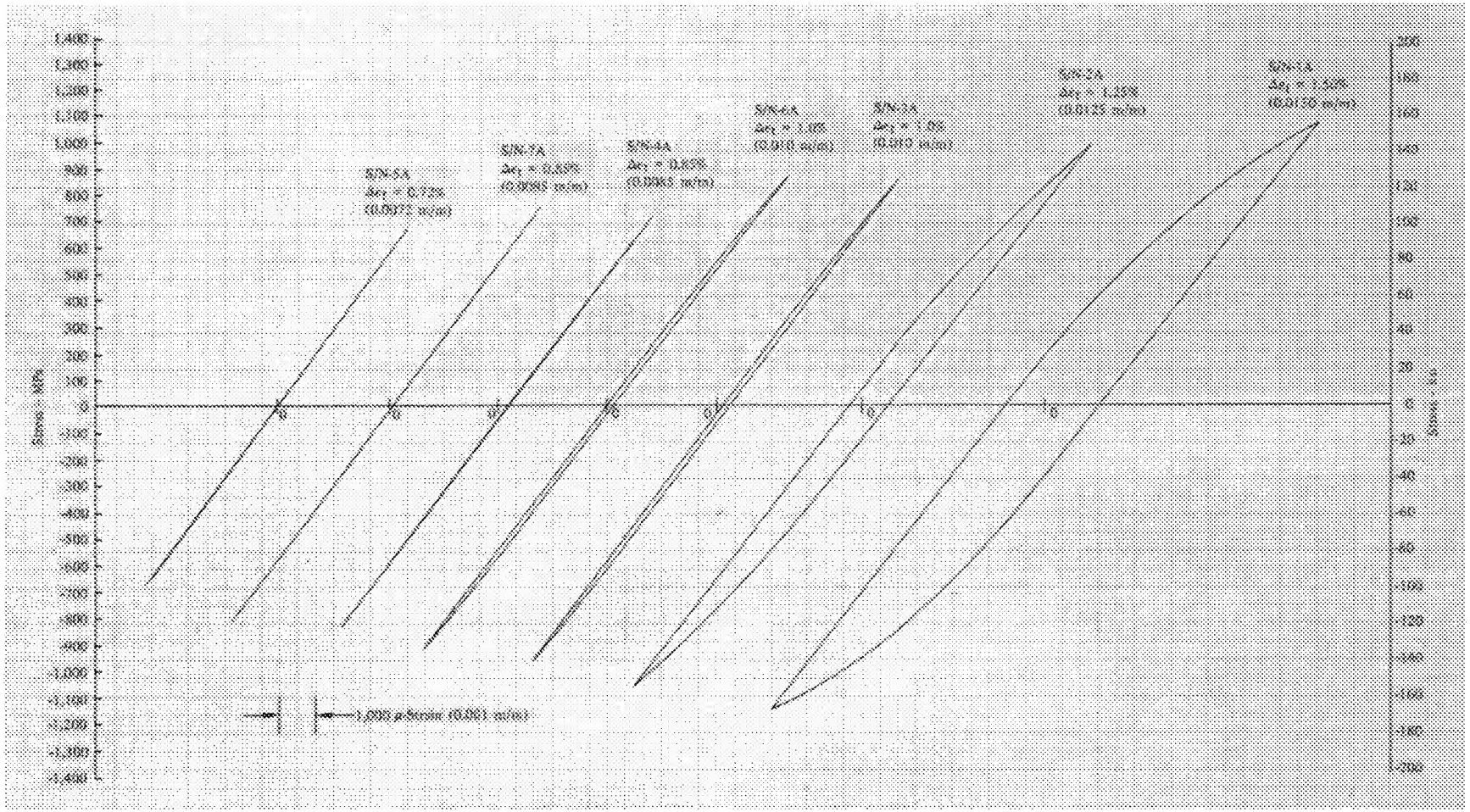

Figure 31. Typical Stress-Strain Hysteresis Loops for All Wrought Astroloy Cyclic Strain Controlled LCF Tests (Test Frequency = 0.33 Hz, Temp = 650°C, 1200°F, Cycles Shown Taken at $N_F/2$)

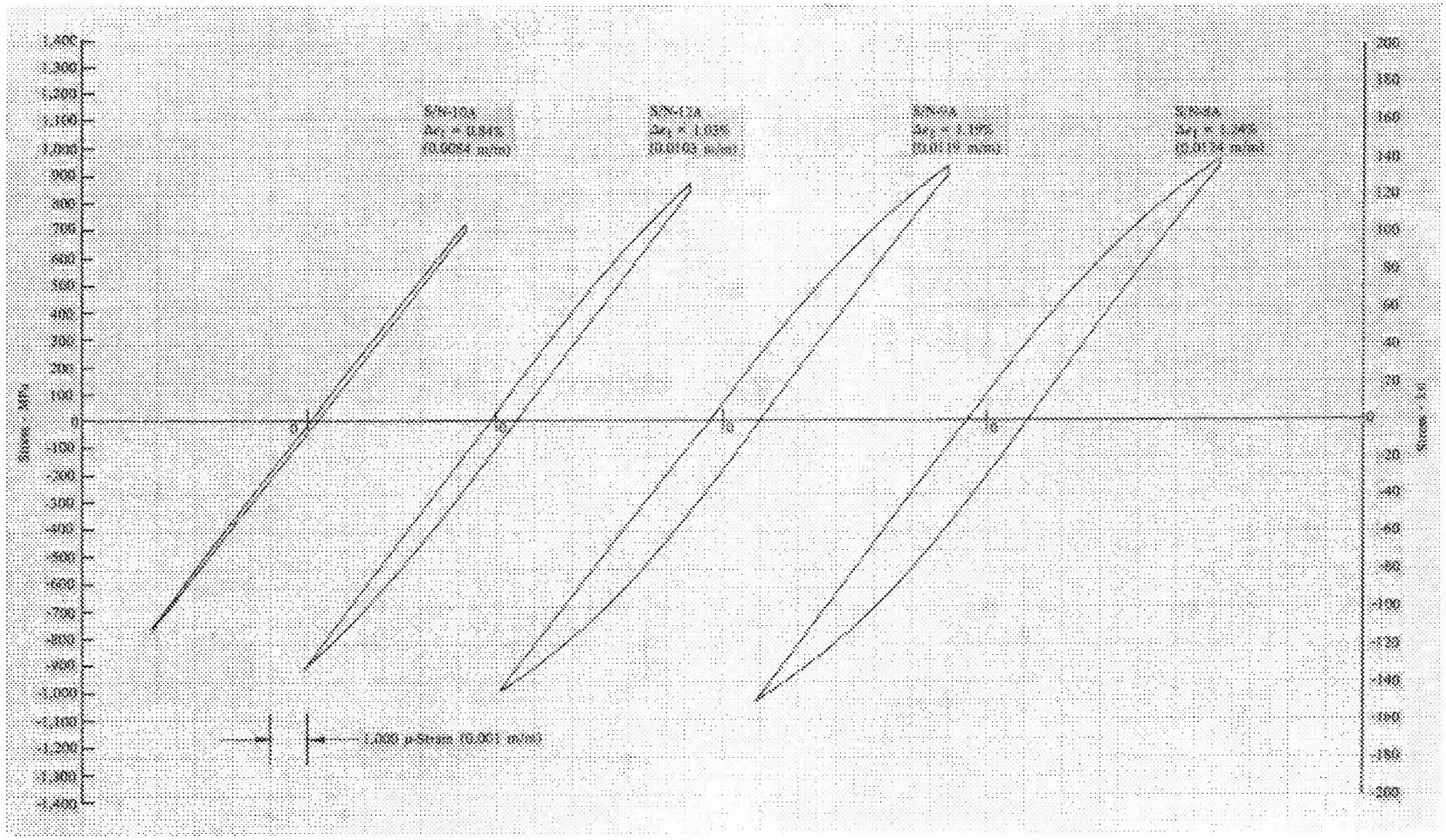

DF 105503

Figure 32. Typical Stress-Strain Hysteresis Loops for All Wrought Astroloy Cyclic/Dwell Strain-Controlled LCF Tests (Dwell Time = 900 sec, Temp = 650°C, 1200°F, Cycles Shown Taken at $N_F/2$)

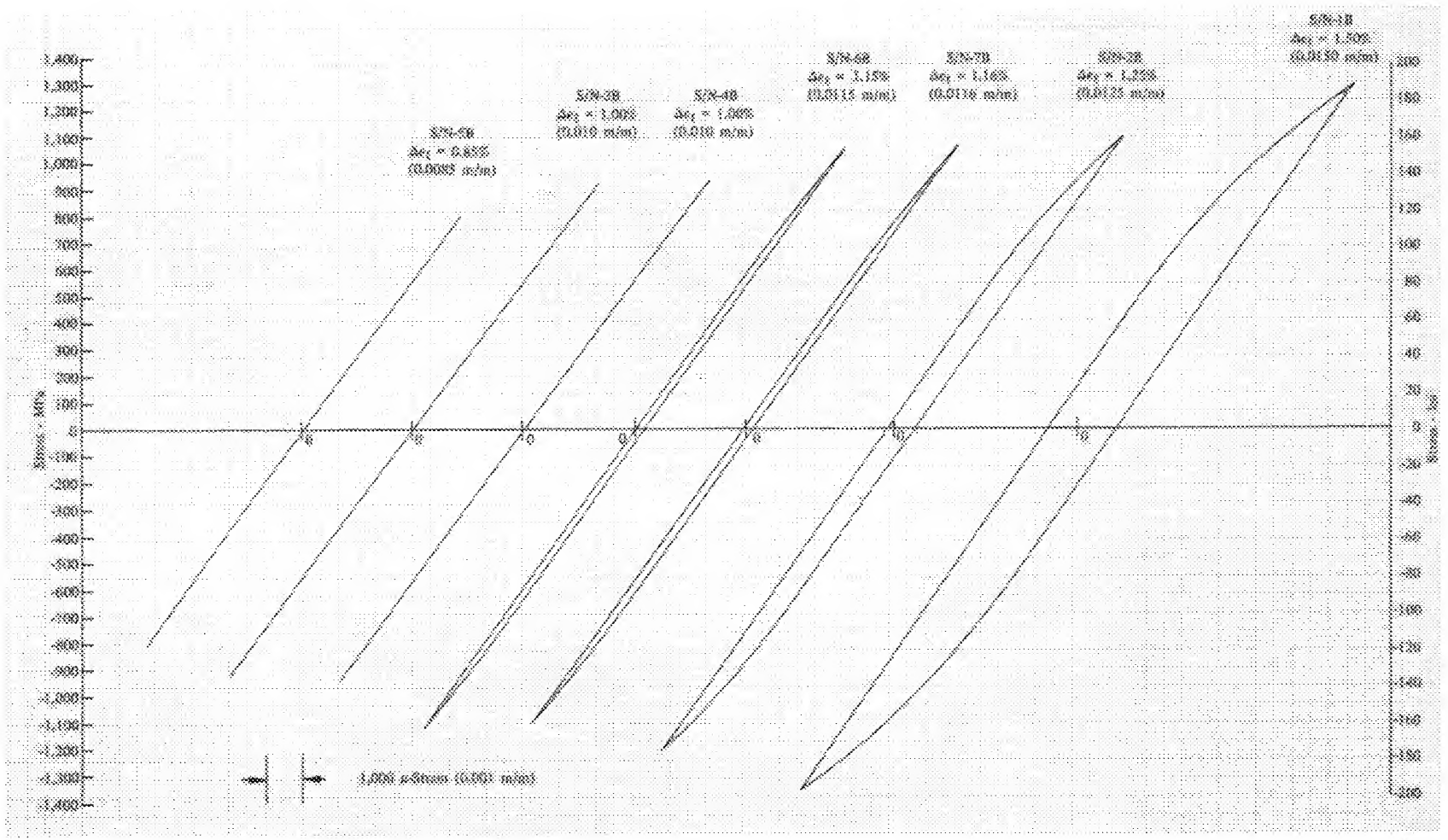

Figure 33. Typical Stress-Strain Hysteresis Loops for All NASA IIB-7 Cyclic Strain-Controlled LCF Tests (Test Frequency = 0.33 Hz, Temp = 650°C, 1200°F, Cycles Shown Taken at $N_F/2$)

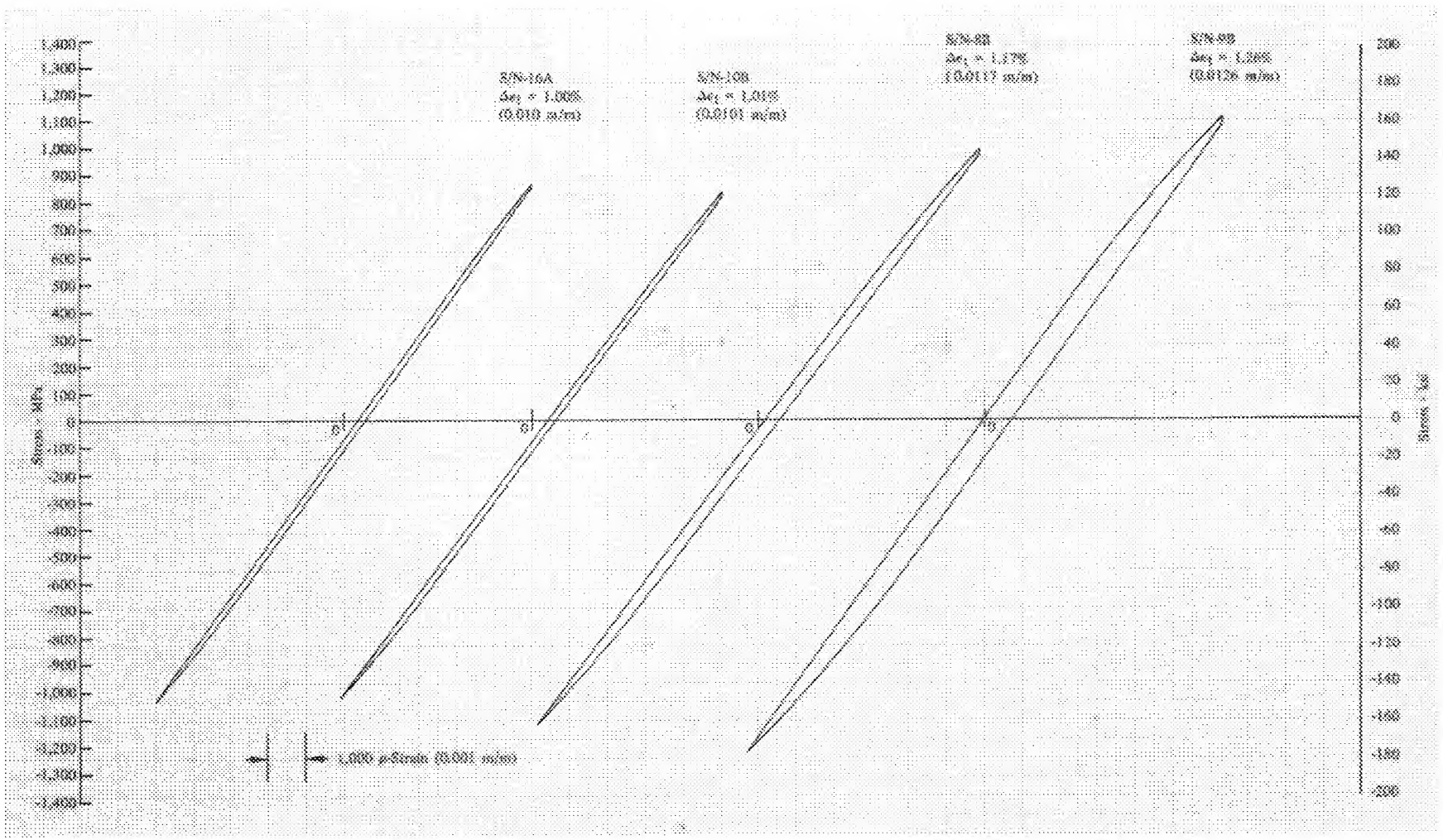

Figure 34. Typical Stress-Strain Hysteresis Loops for All NASA IIB-7 Cyclic/Dwell Strain-Controlled LCF Tests (Dwell Time = 900 sec, Temp = 650°C, 1200°F, Cycles Shown Taken at $N_f/2$)

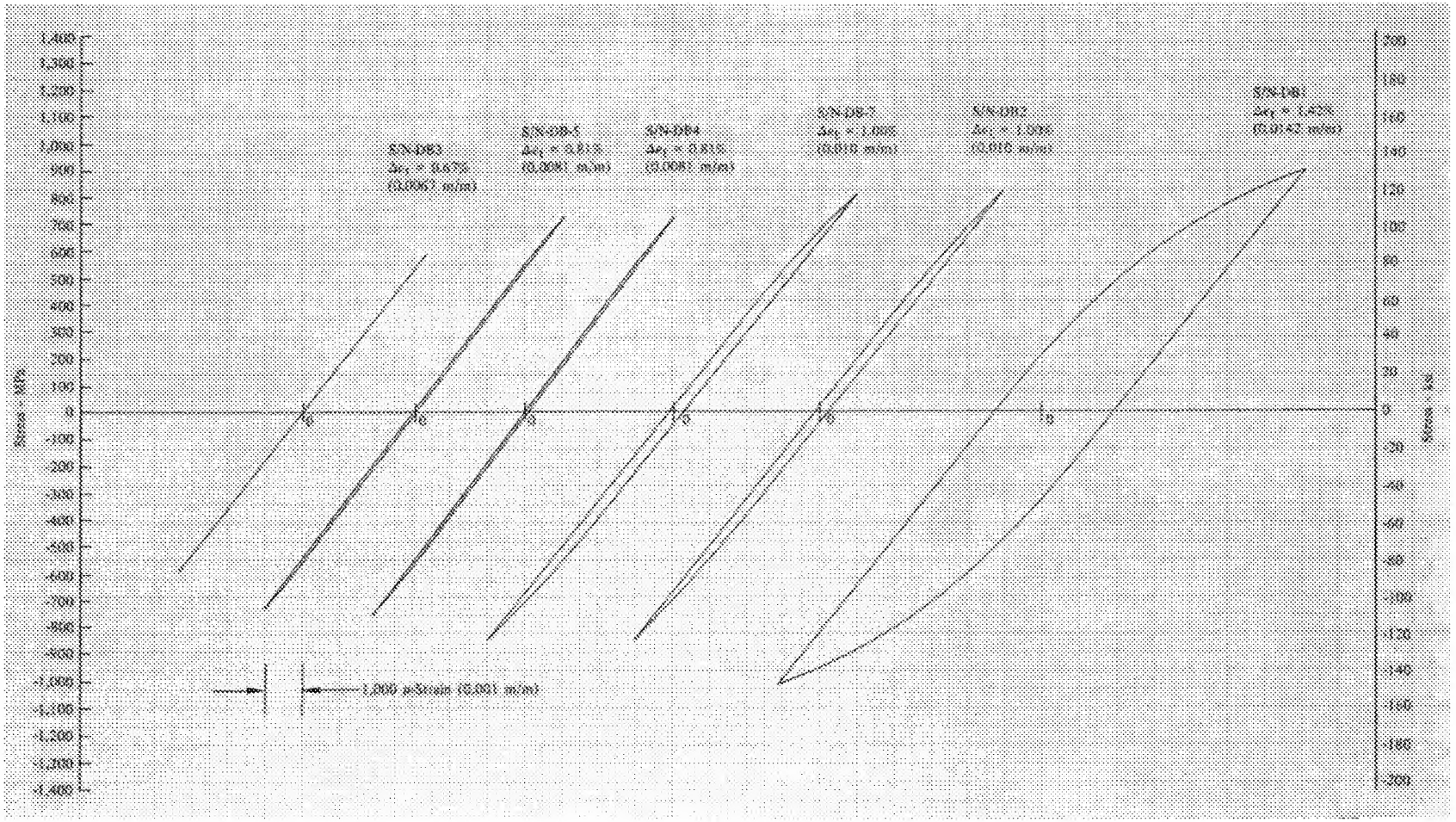

Figure 35. Typical Stress-Strain Hysteresis Loops for All HIP-Astroloy Cyclic Strain-Controlled LCF Tests (Test Frequency = 650°C, 1200°F, Cycles Shown at $N_F/2$)

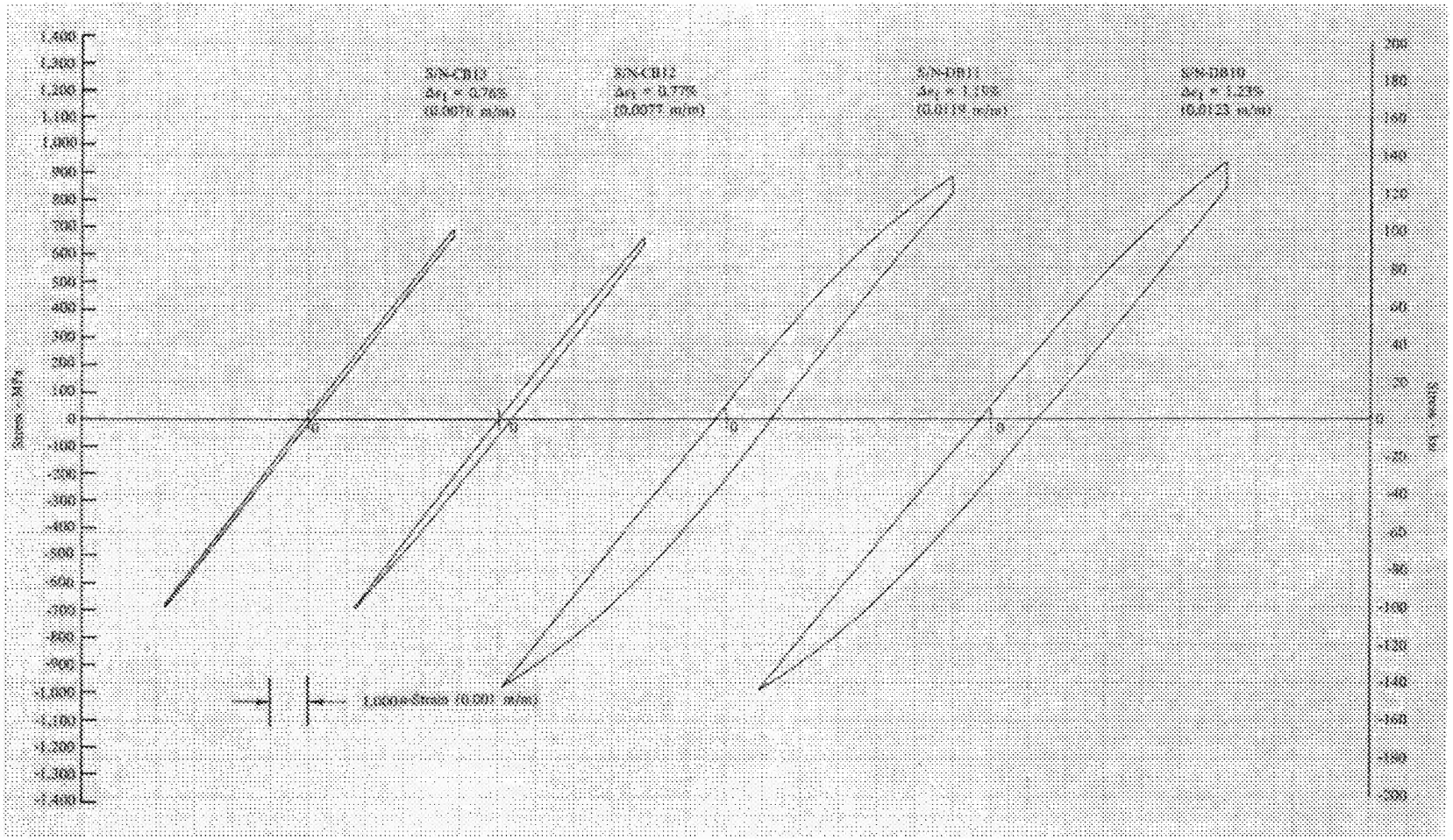

DF 105507

Figure 36. Typical Stress-Strain Hysteresis Loops for All HIP-Astroloy Cyclic/Dwell Strain-Controlled LCF Tests (Dwell Time = 900 sec, Temp = 650°C, 1200°F, Cycles Shown Taken at $N_F/2$)

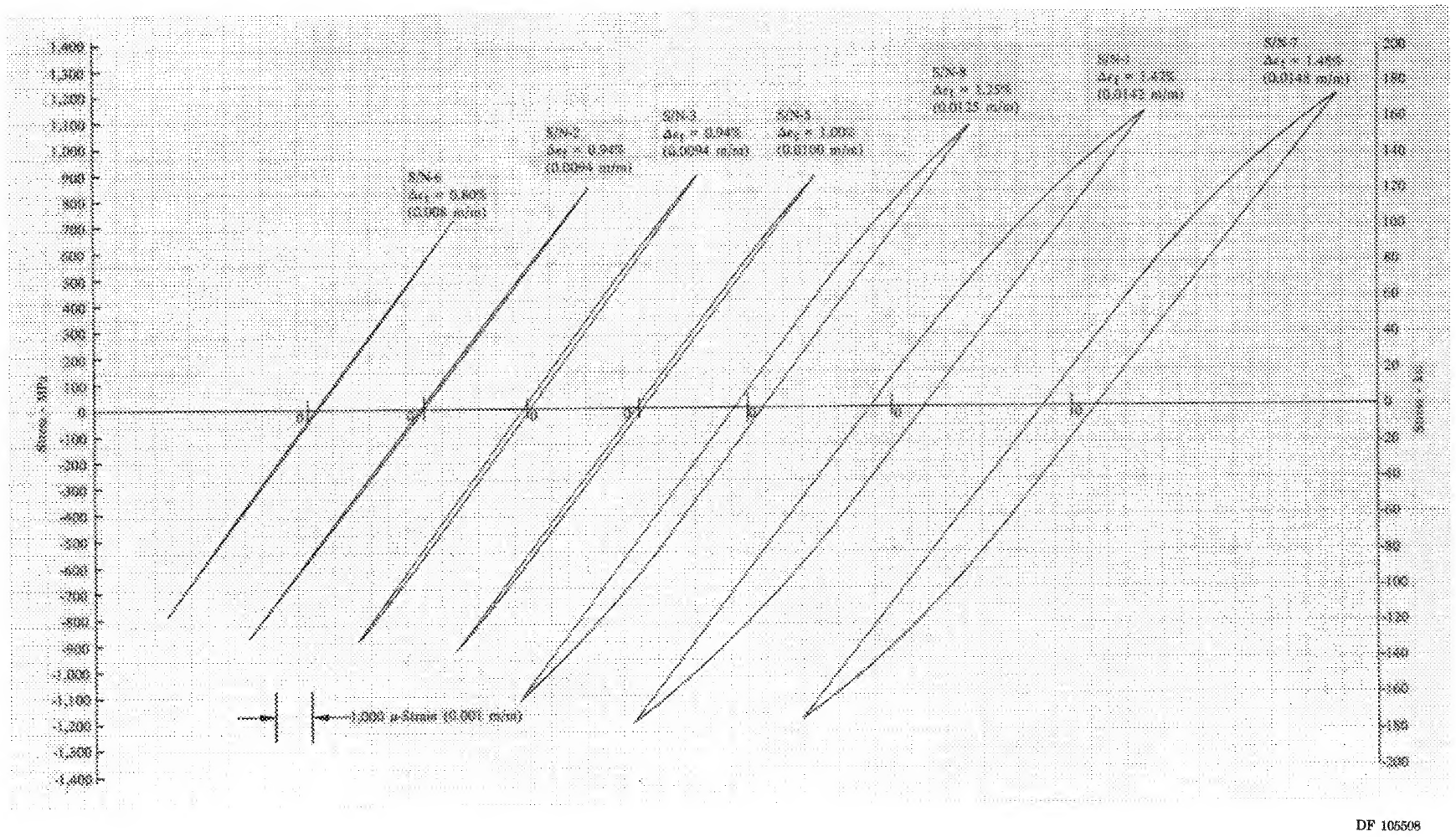

Figure 37. Typical Stress-Strain Hysteresis Loops for All GATORIZED® IN 100 Cyclic Strain-Controlled LCF Tests (Test Frequency = 0.33 Hz, Temp = 650°C, 1200°F, Cycles Shown Taken at $N_F/2$)

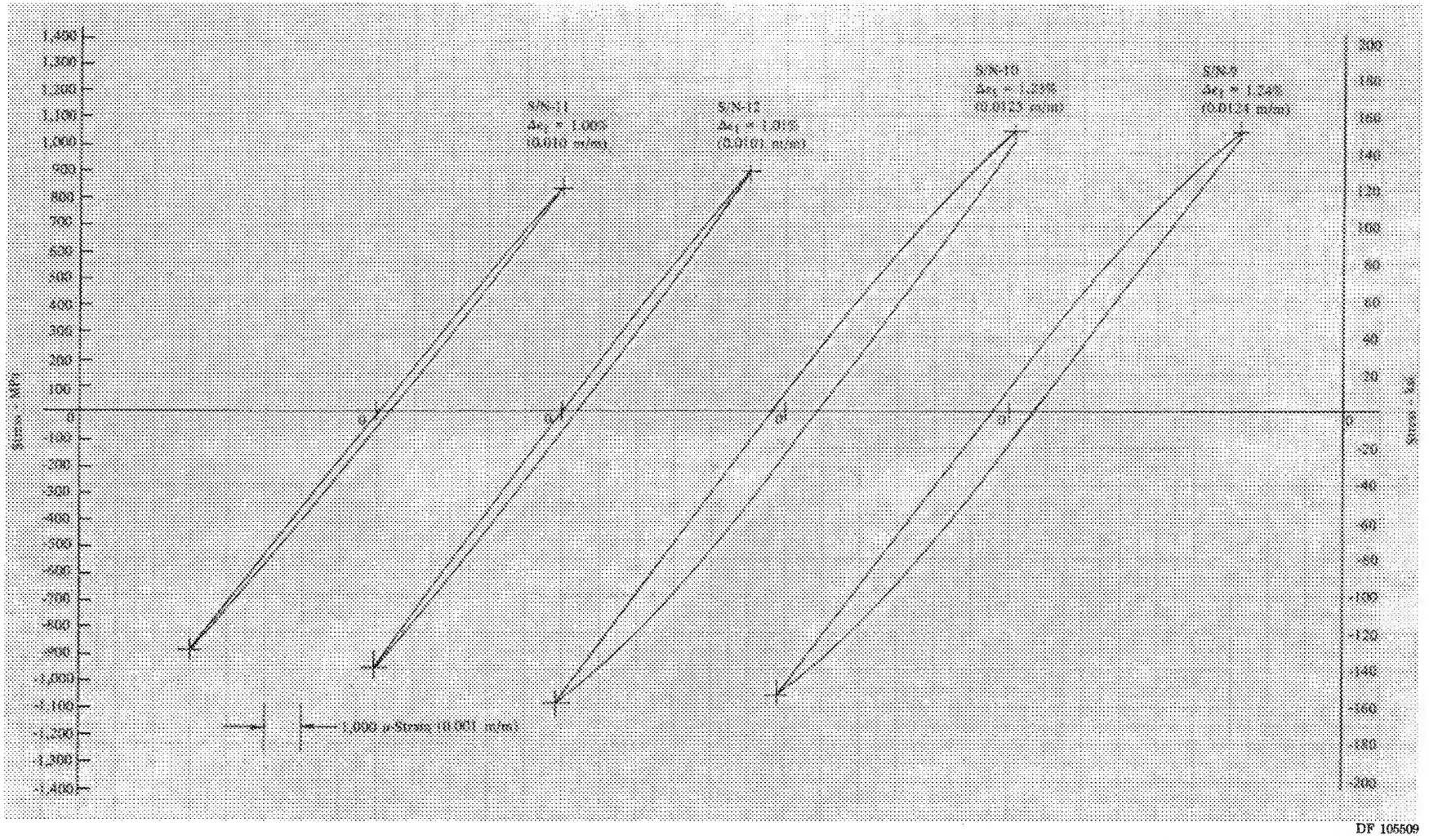

Figure 38. Typical Stress-Strain Hysteresis Loops for All GATORIZED® IN 100 Cyclic/Dwell Strain-Controlled LCF Tests (Dwell Time = 900 sec, Temp = 650°C, 1200°F, Cycles Shown Taken at $N_F/2$)

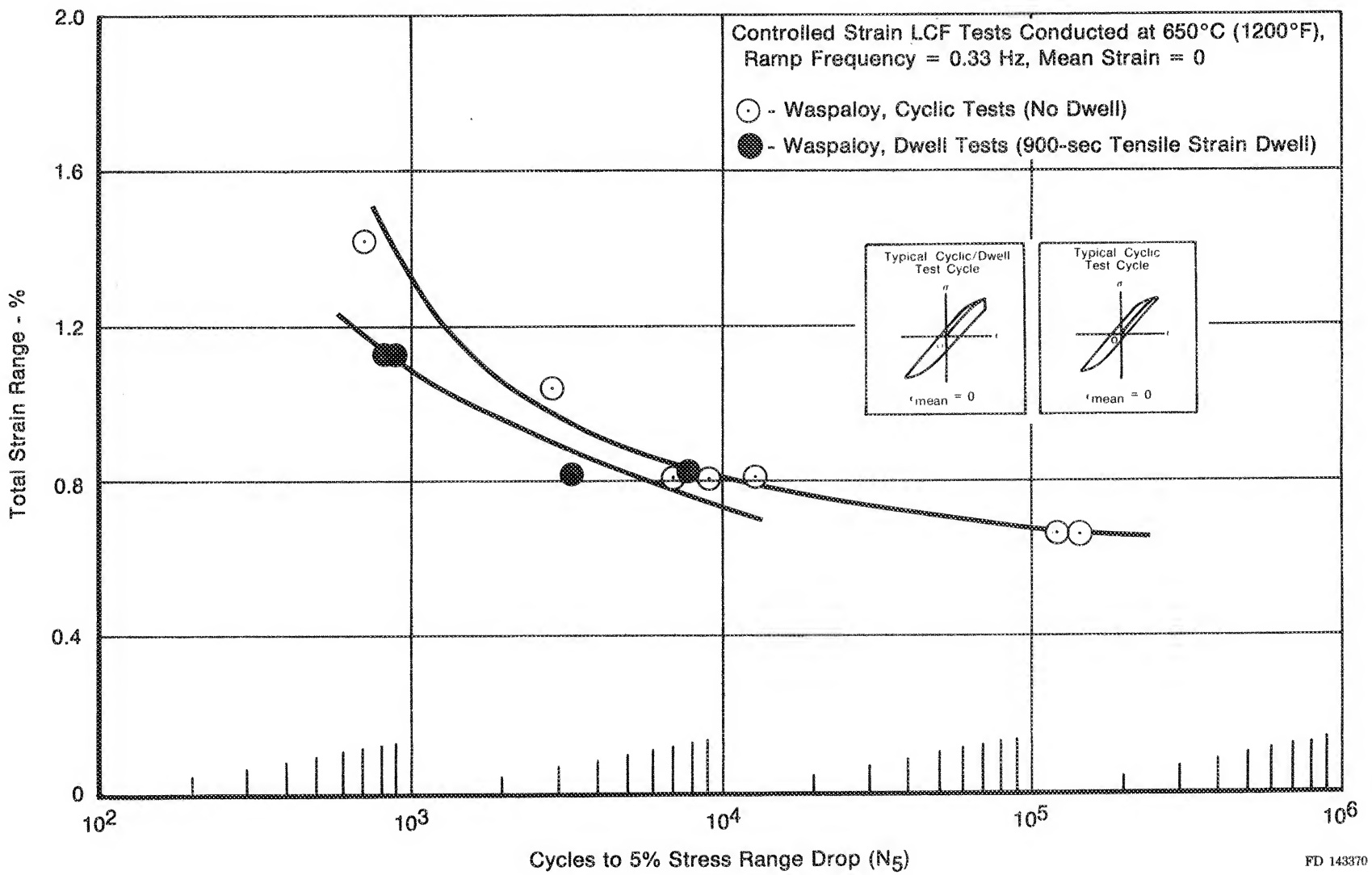

Figure 39. Strain Control LCF Results for Alloy 1, Wrought Waspaloy

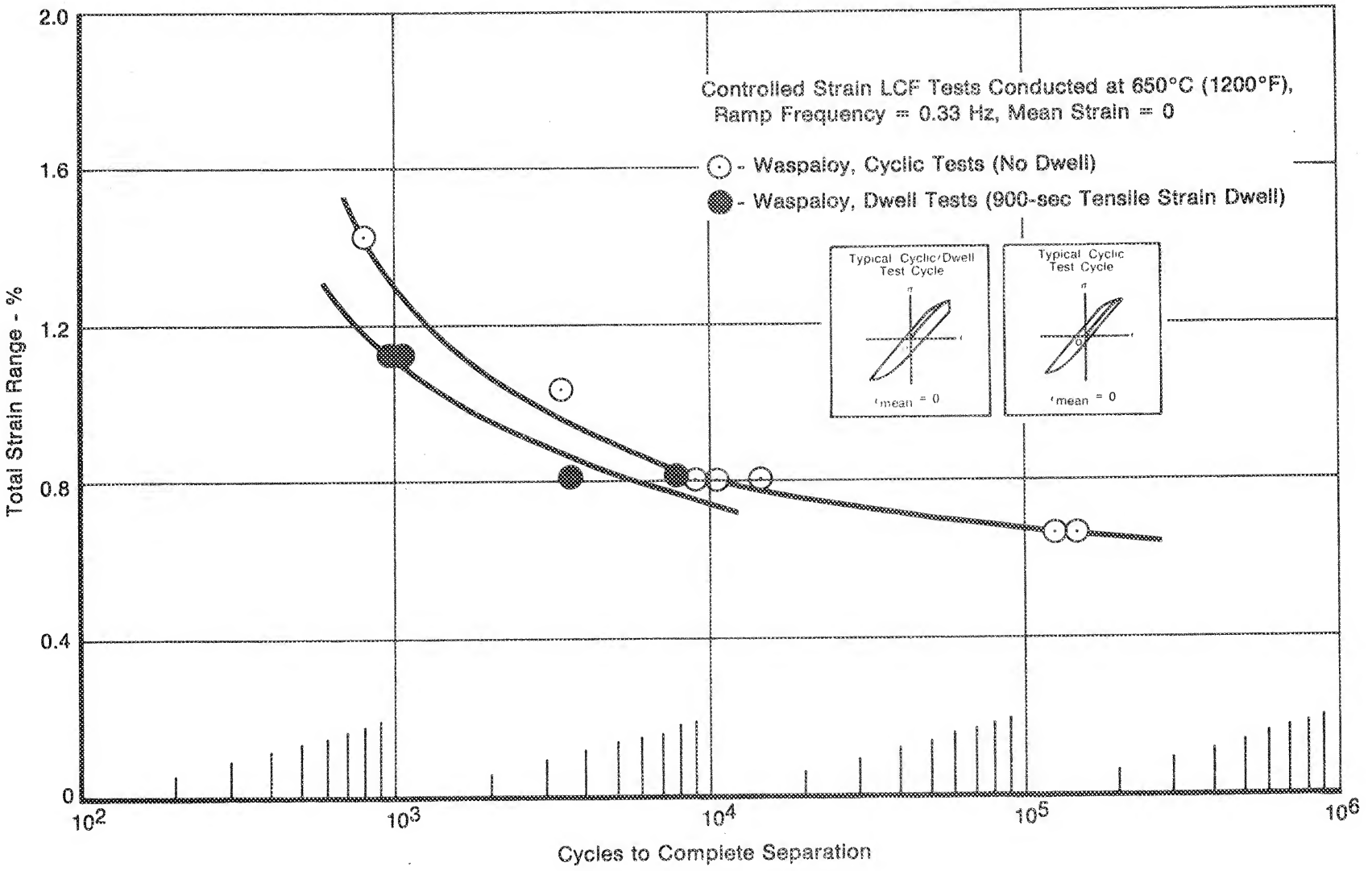

Figure 40. Strain Control LCF Results for Alloy 1, Wrought Waspaloy

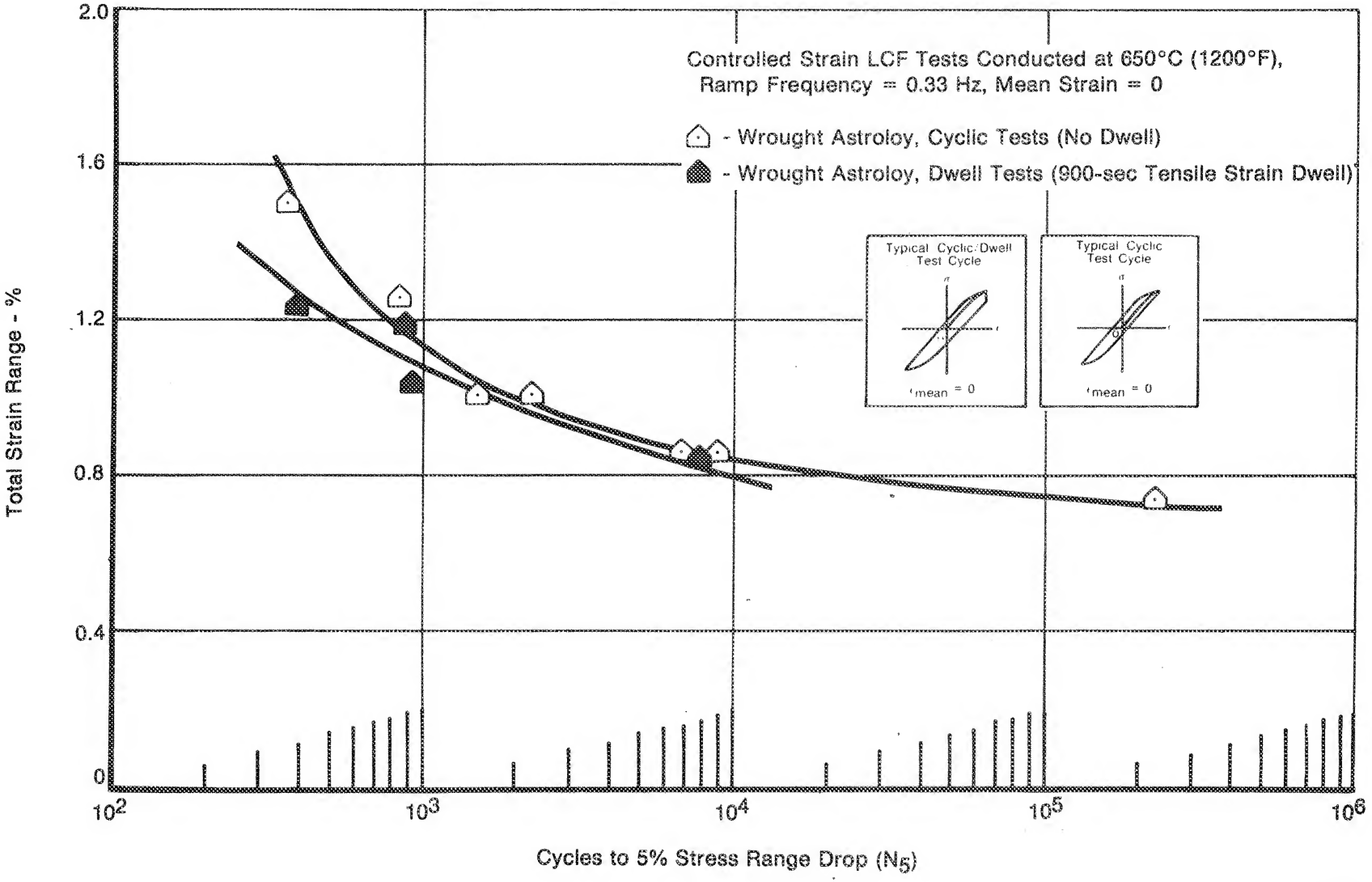

Figure 41. Strain Control LCF Results for Alloy 2, Wrought Astroloy

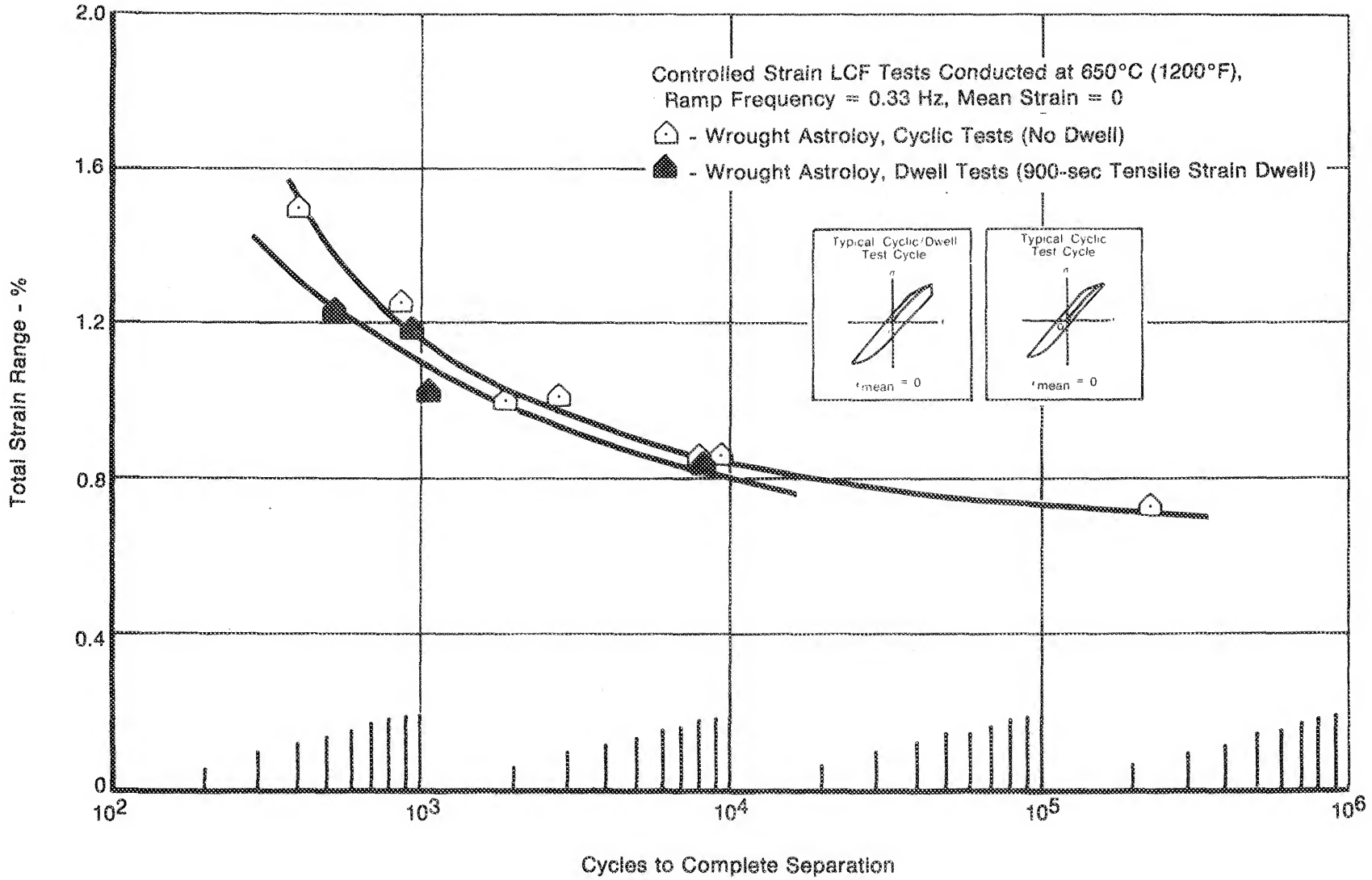

Figure 42. Strain Control LCF Results for Alloy 2, Wrought Astroloy

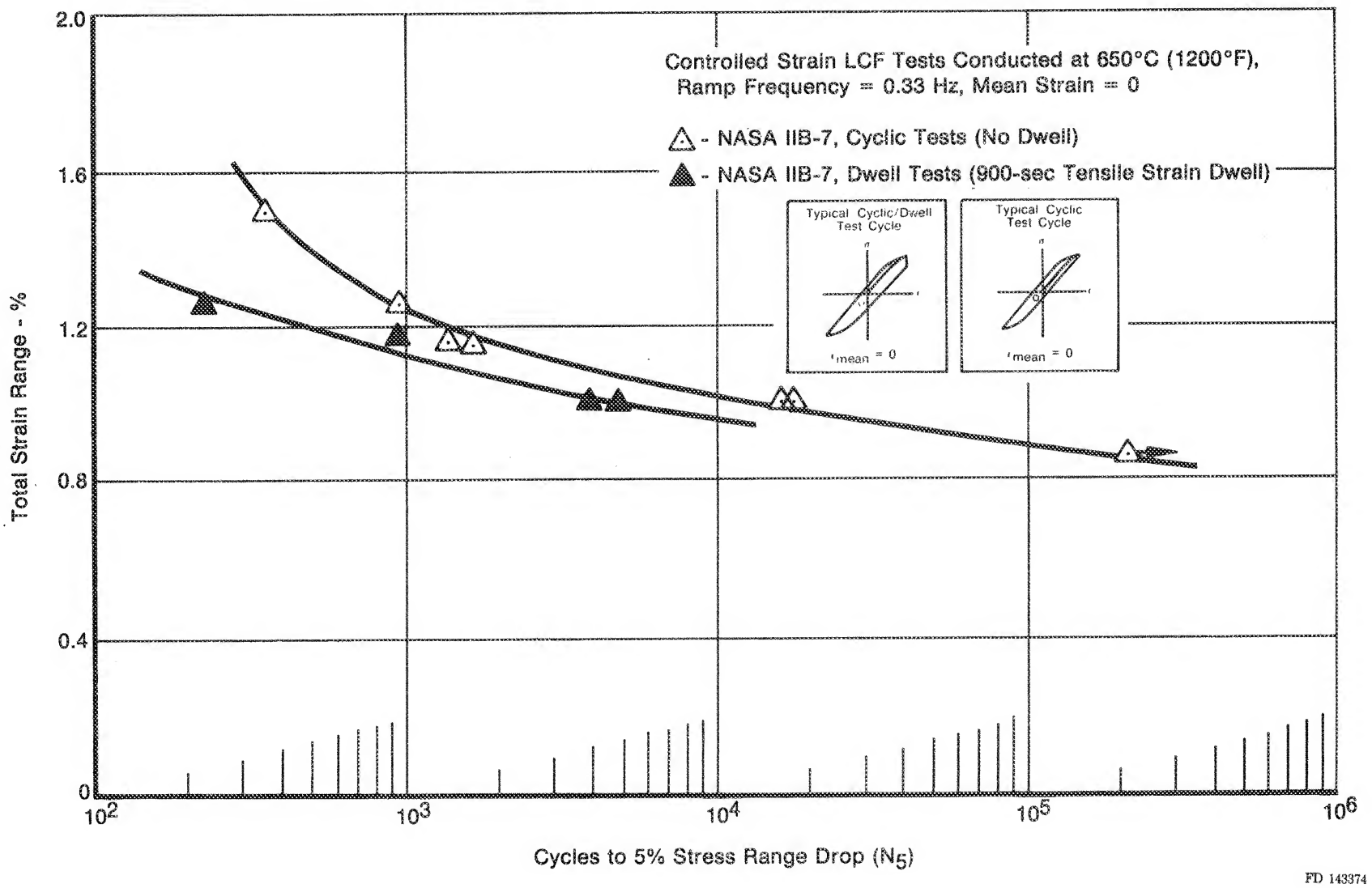

Figure 43. Strain Control LCF Results for Alloy 3, NASA IIB-7

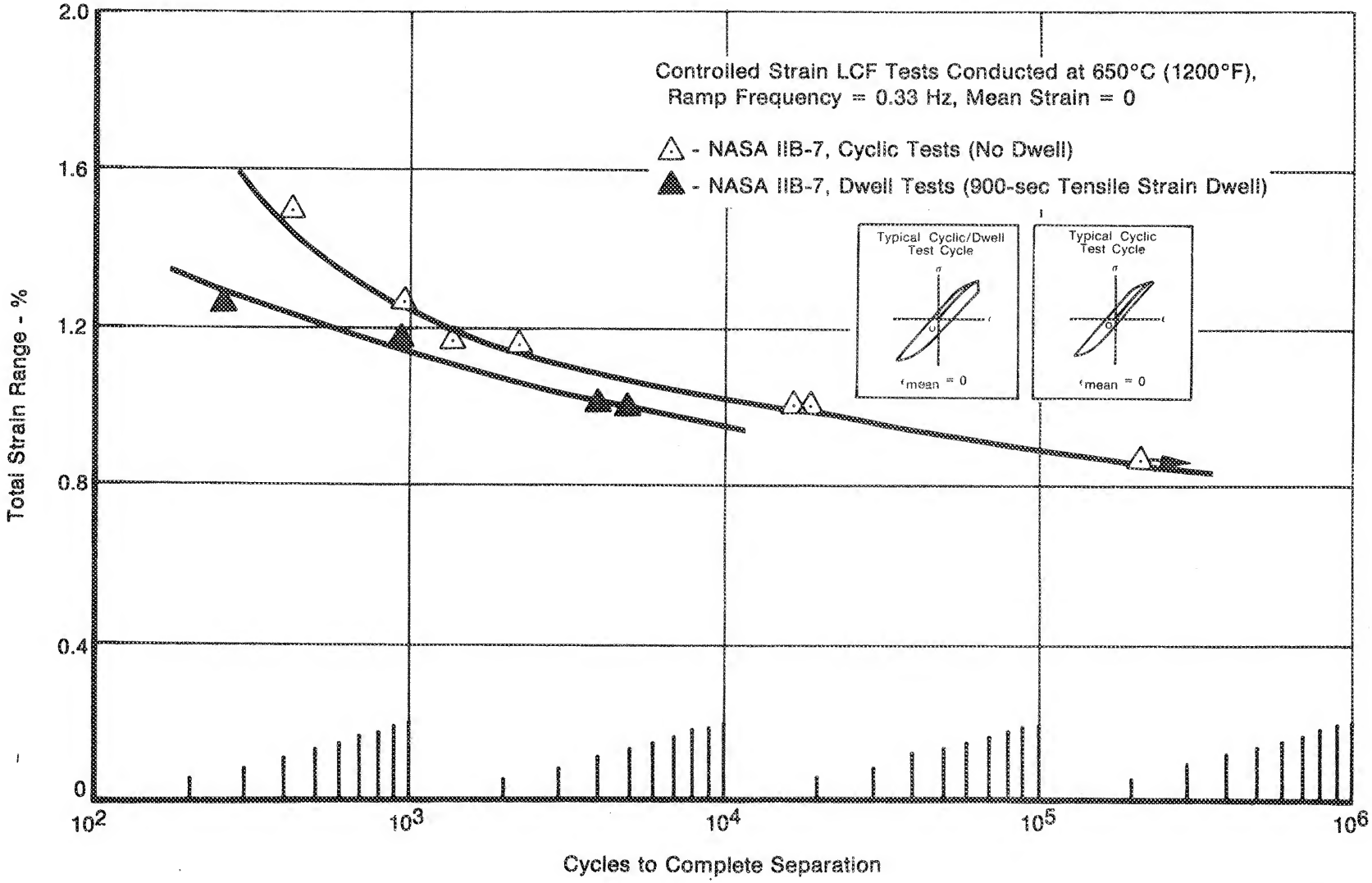

FD 143375

Figure 44. Strain Control LCF Results for Alloy 3, NASA IIB-7

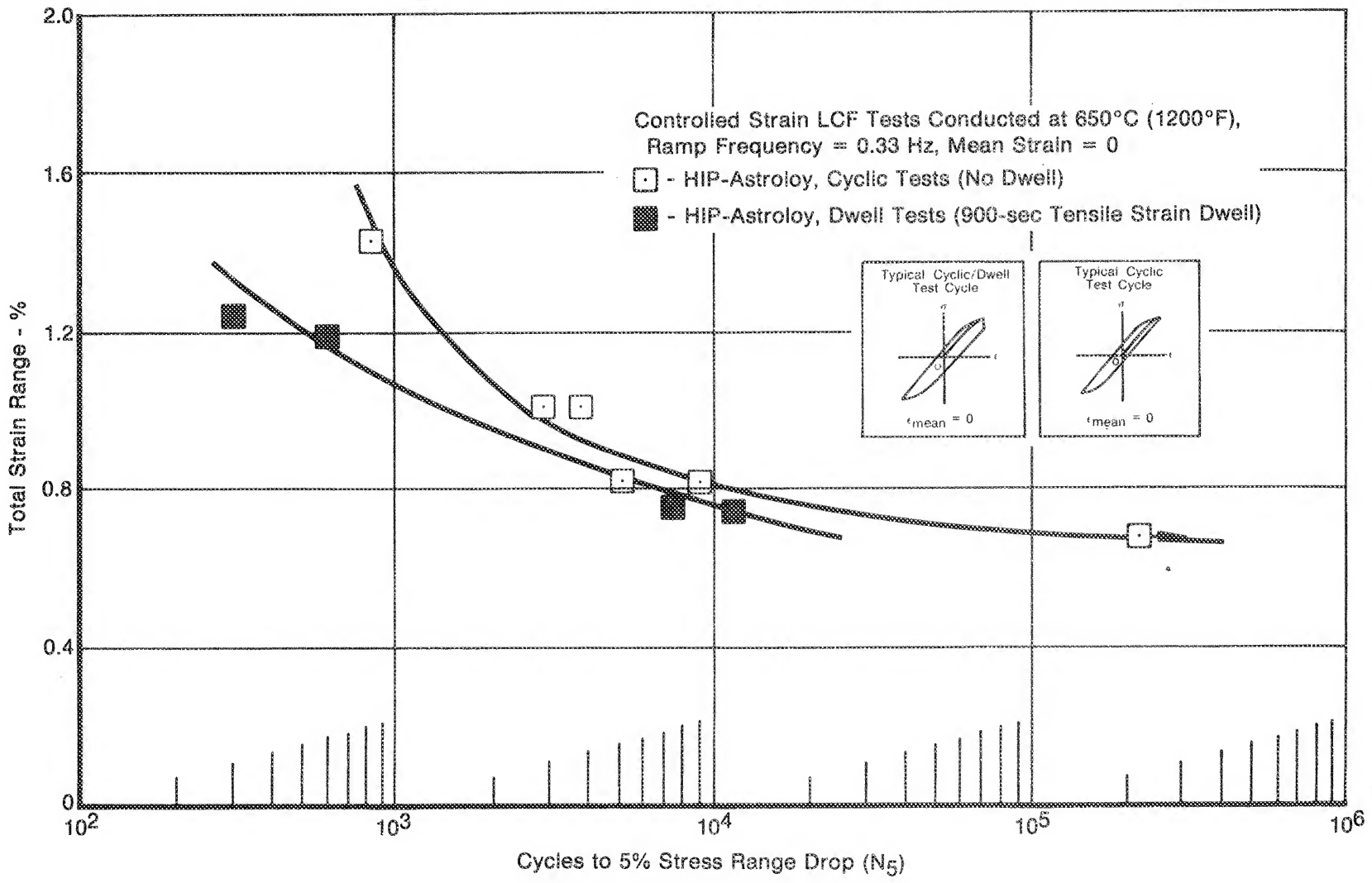

Figure 45. Strain Control LCF Results for Alloy 4, HIP-Astroloy

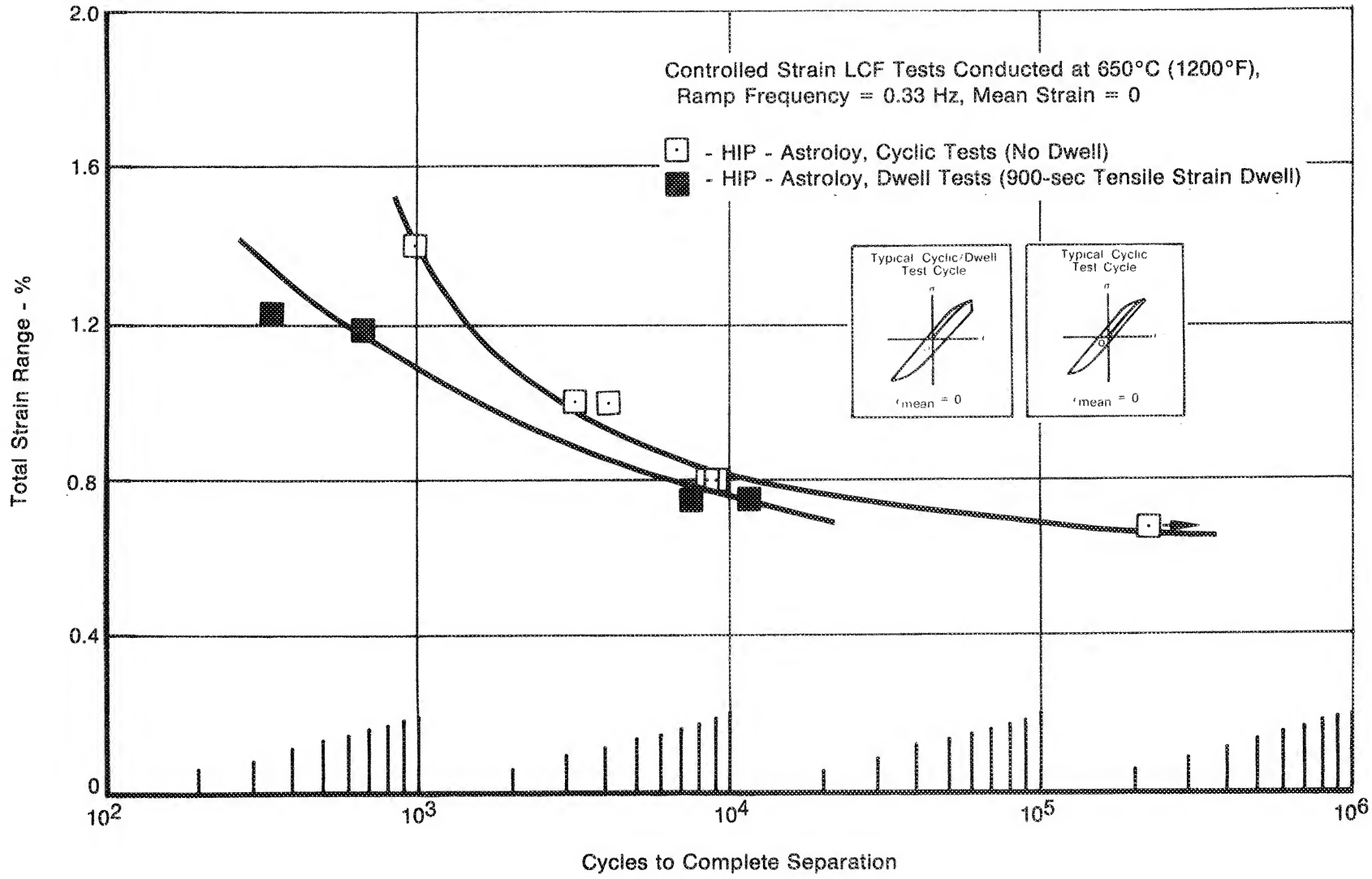

FD 143377

Figure 46. Strain Control LCF Results for Alloy 4, HIP-Astroloy

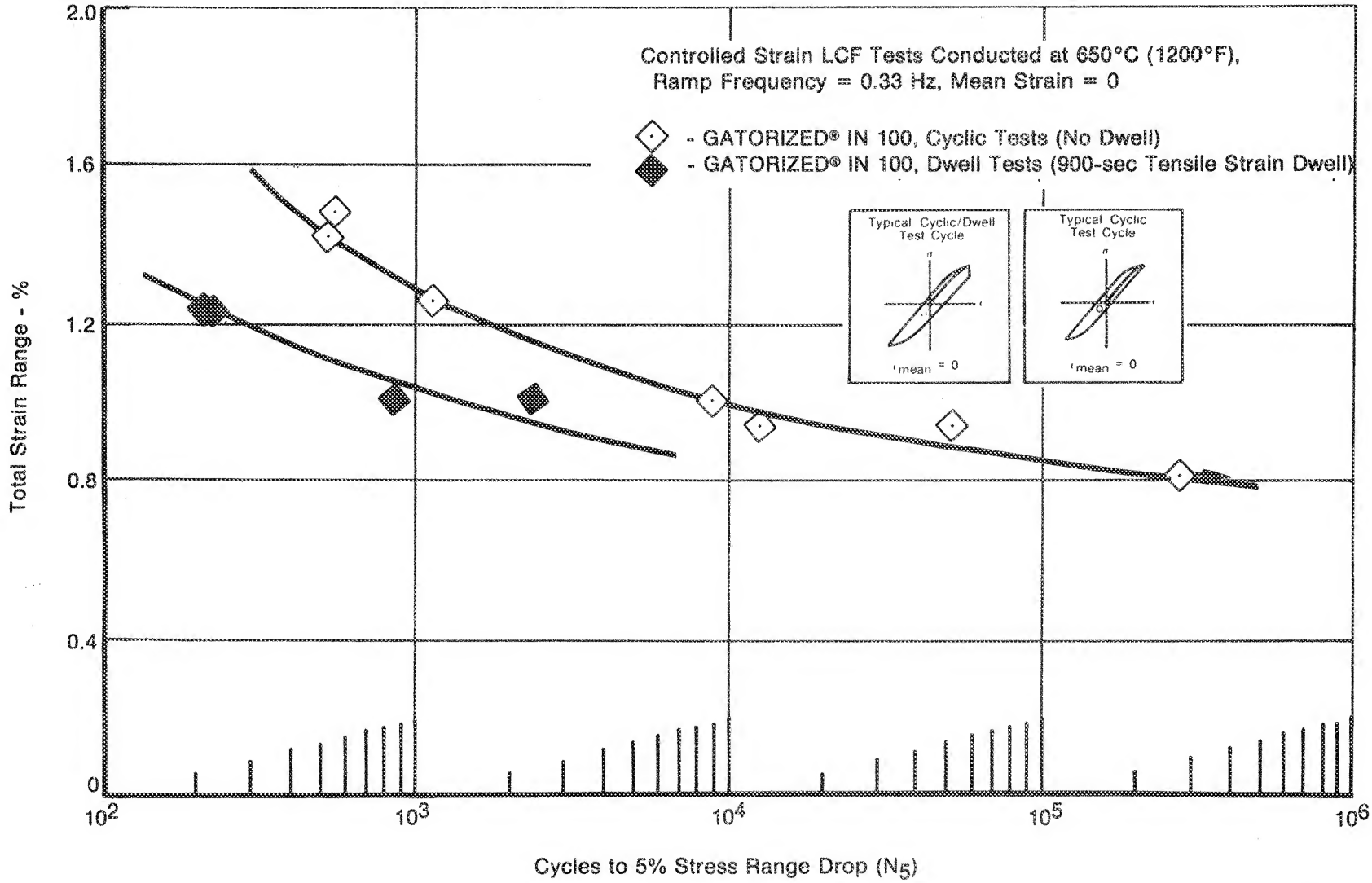

Figure 47. Strain Control LCF Results for Alloy 5, GATORIZED® IN 100

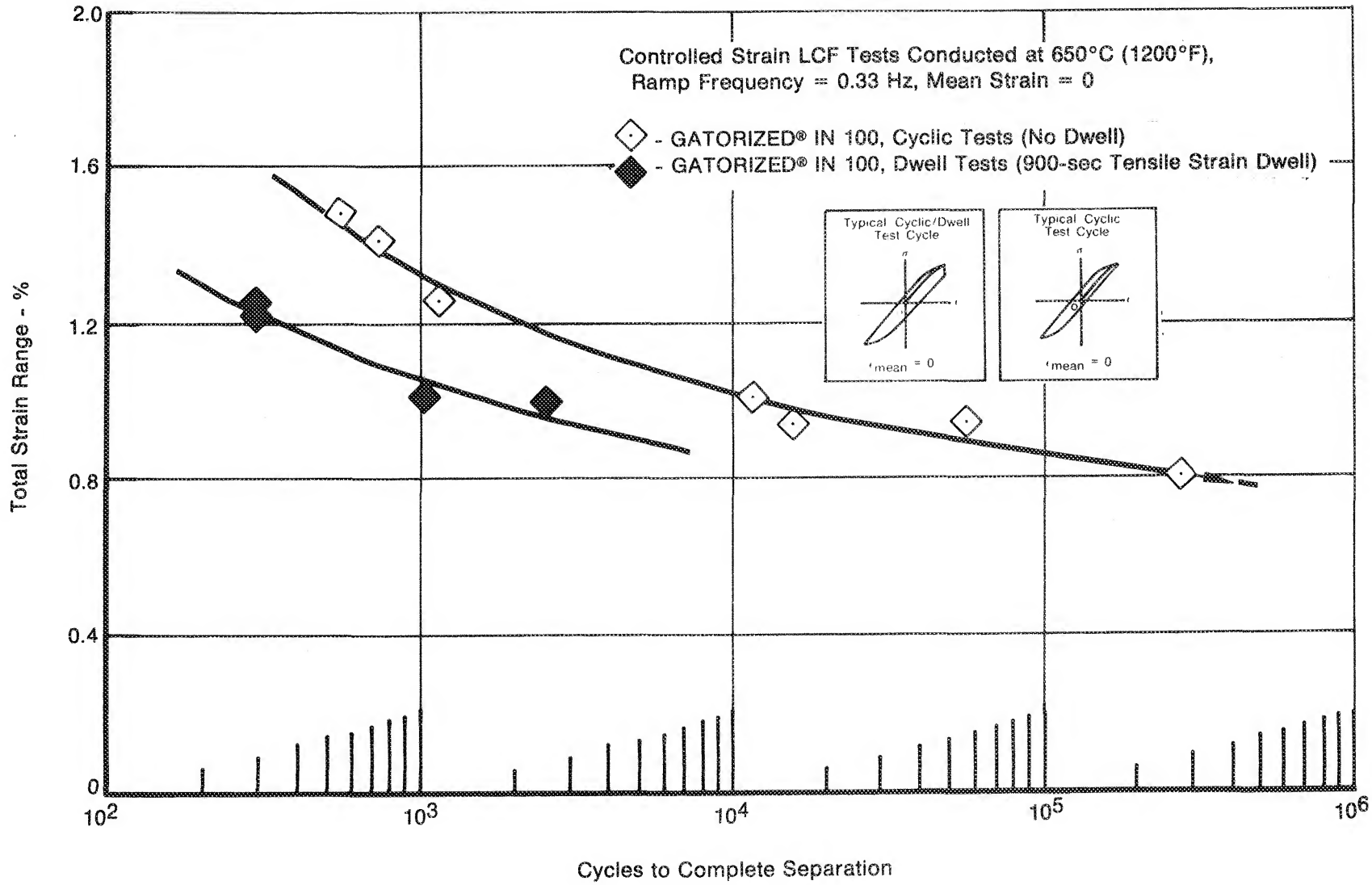

Figure 48. Strain Control LCF Results for Alloy 5, GATORIZED® IN 100

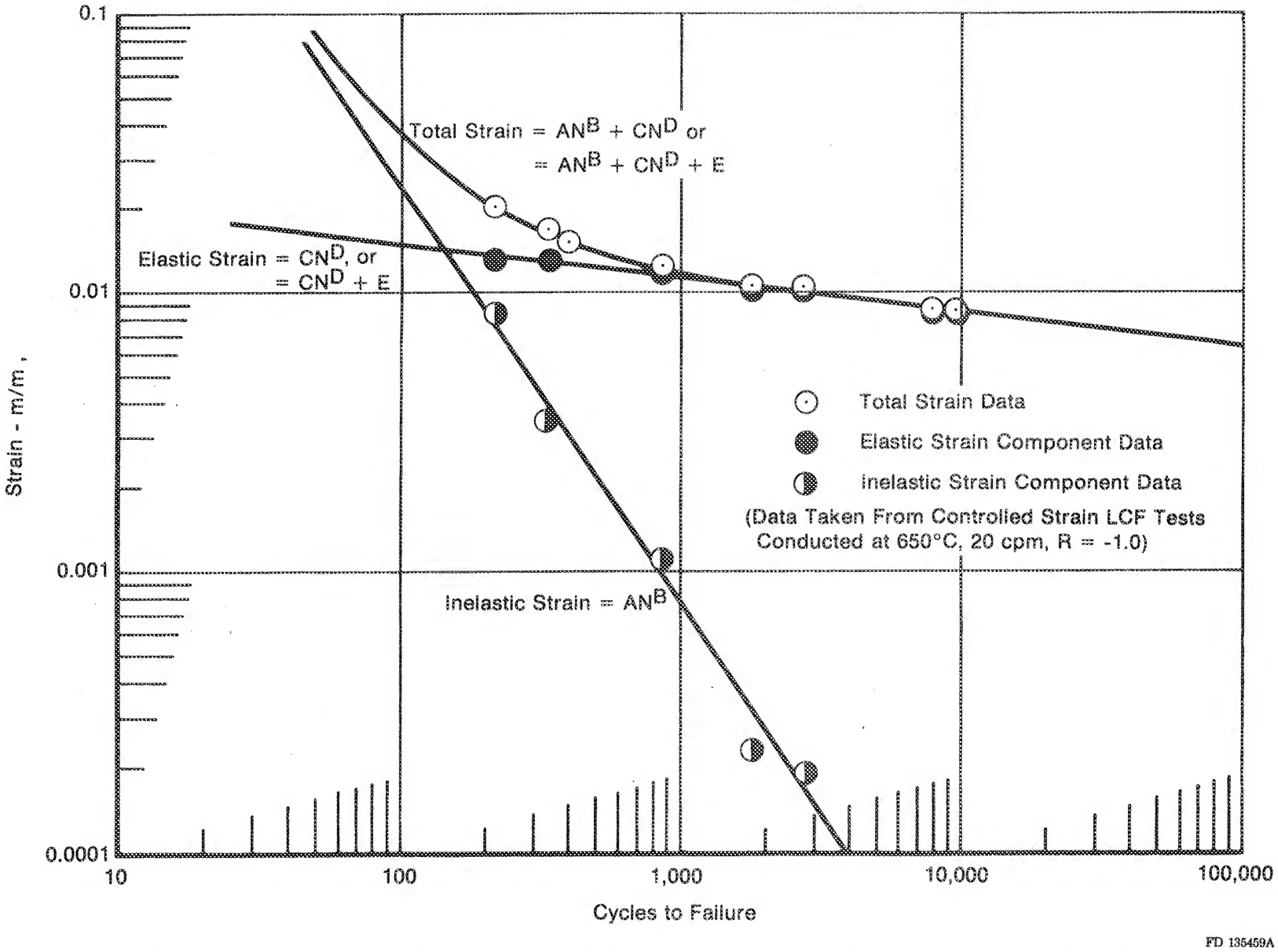

Figure 49. Composite Experimental Fatigue Life Model Using Summation of Elastic and Inelastic Strain Components

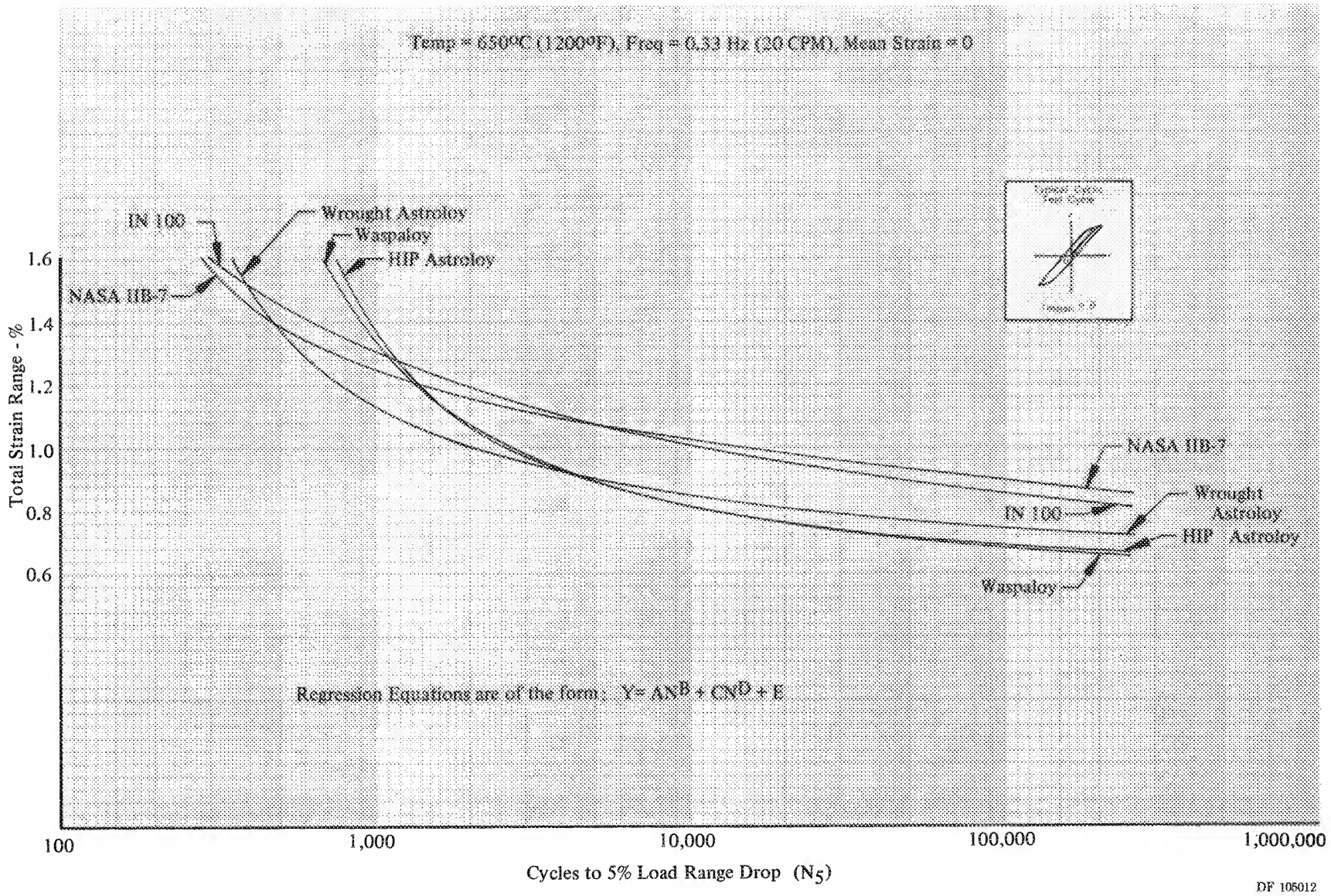

Figure 50. Cyclic Strain Range vs N_5 Life (5% Load Range Drop) for All Five Alloys

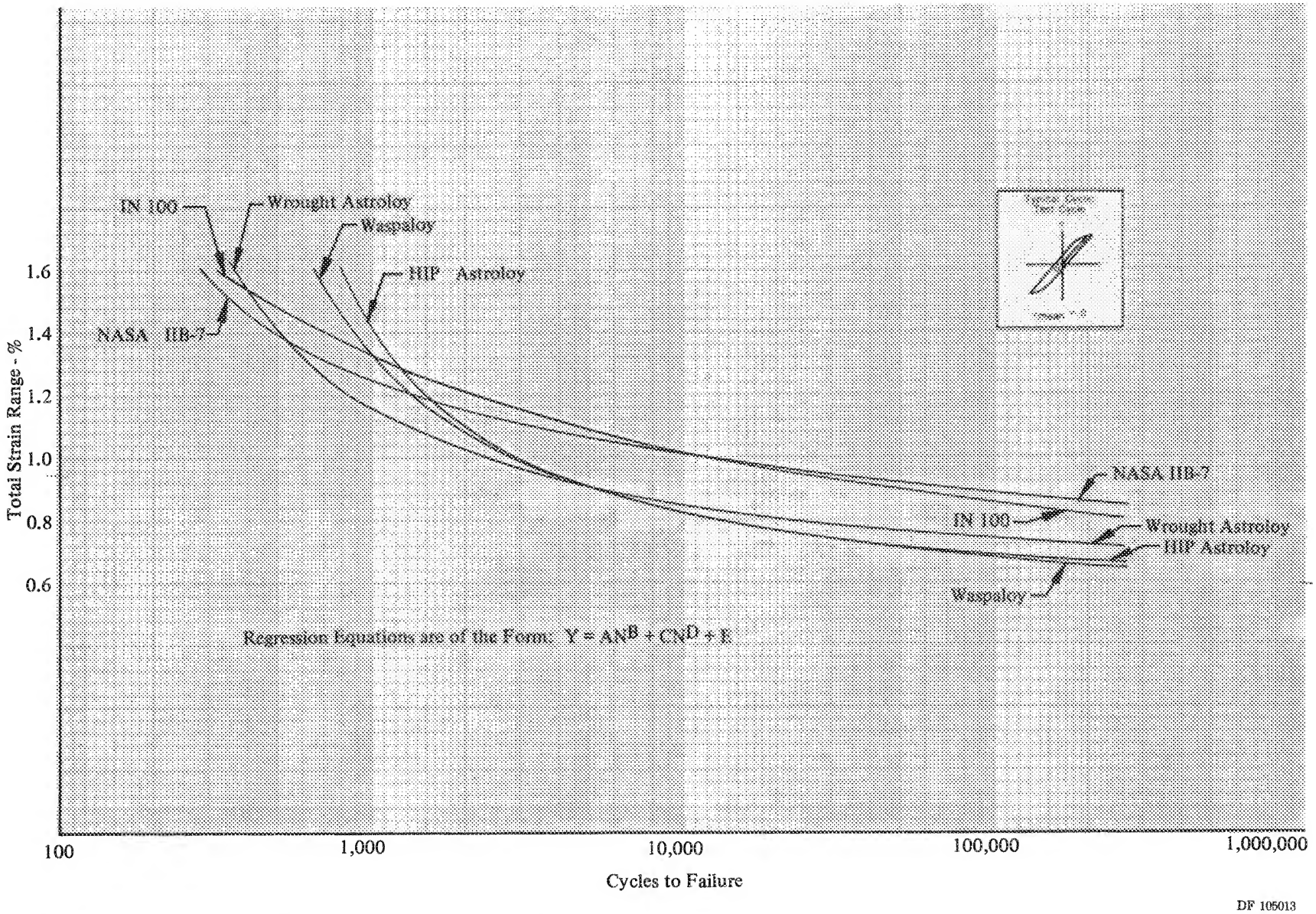

Figure 51. Cyclic Strain Range vs Total Life for All Five Alloys

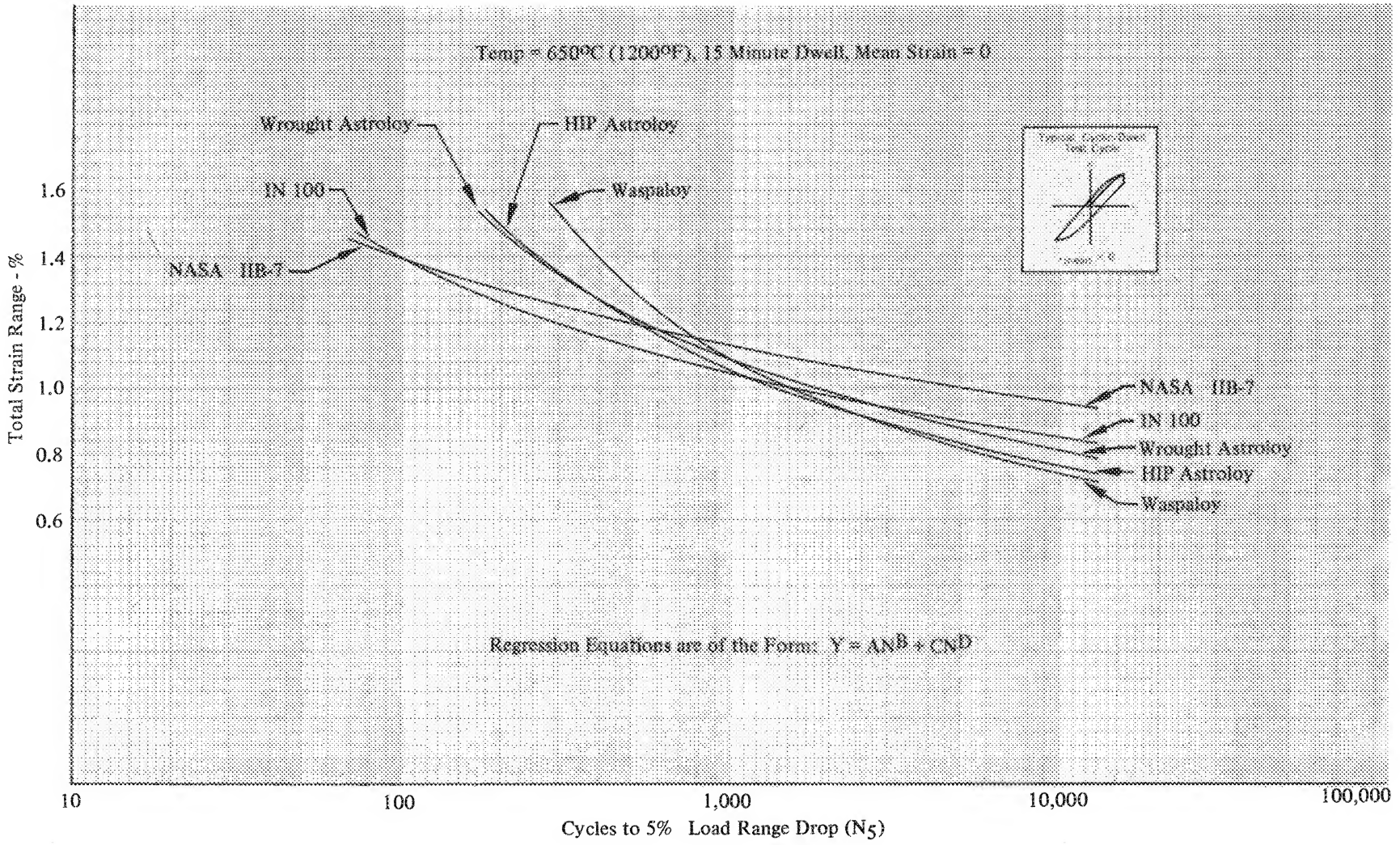

Figure 52. Cyclic/Dwell Strain Range vs N_5 Life (5% Load Range Drop) for All Five Alloys

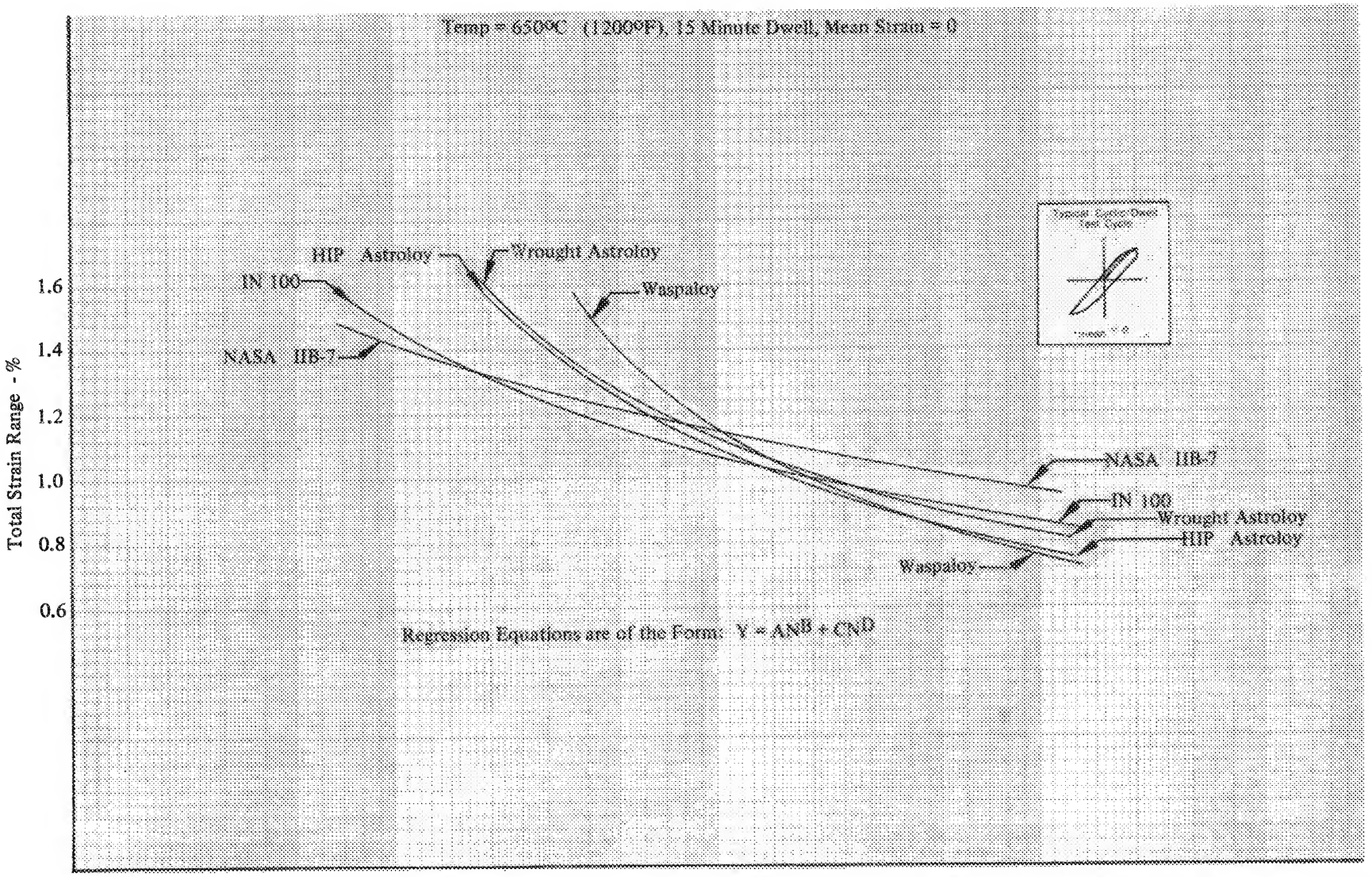

Figure 53. Cyclic/Dwell Strain Range vs Total Life for All Five Alloys

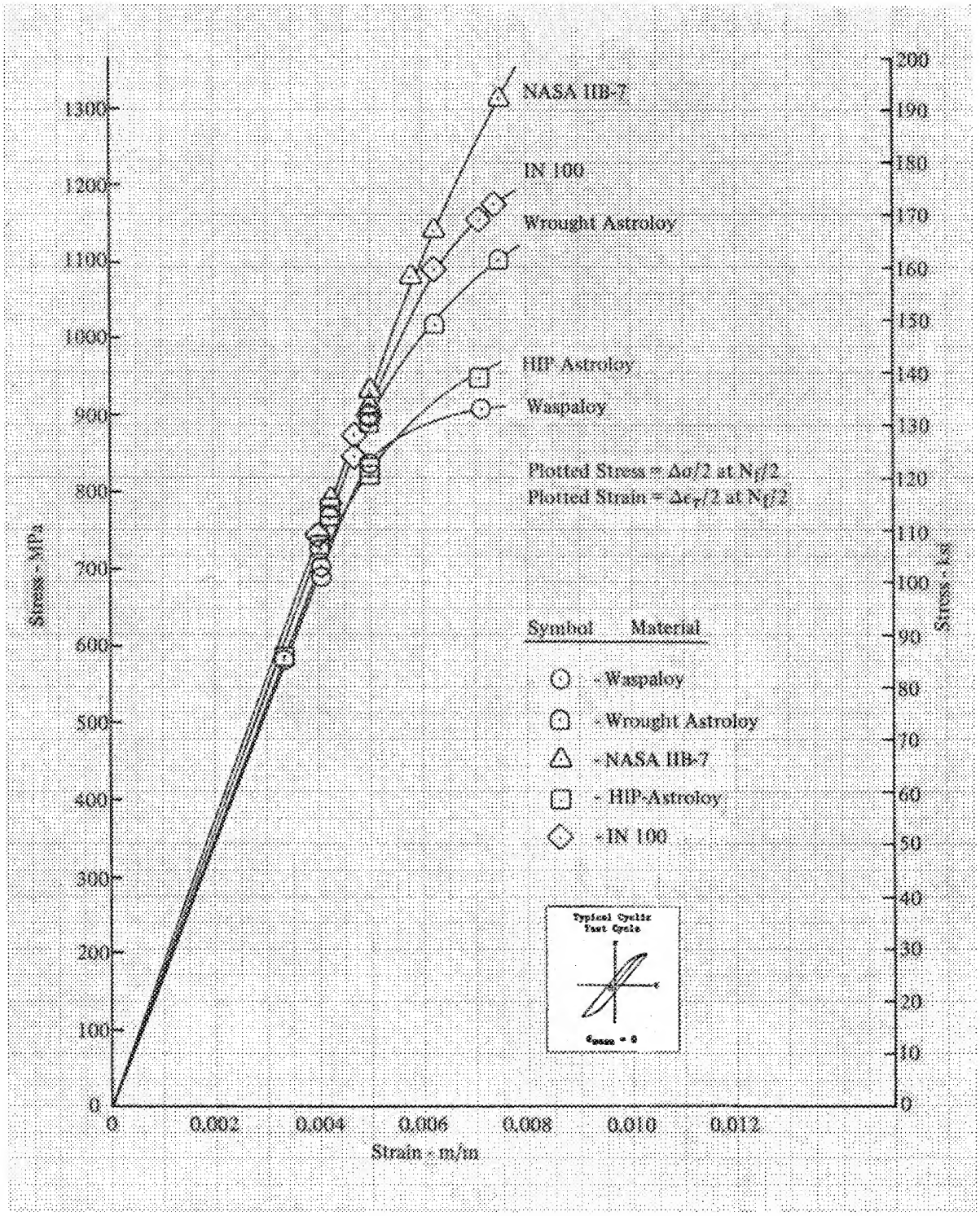

DF 105016

Figure 54. Reconstructed Cyclic Stress-Strain Curves for All Five Alloys

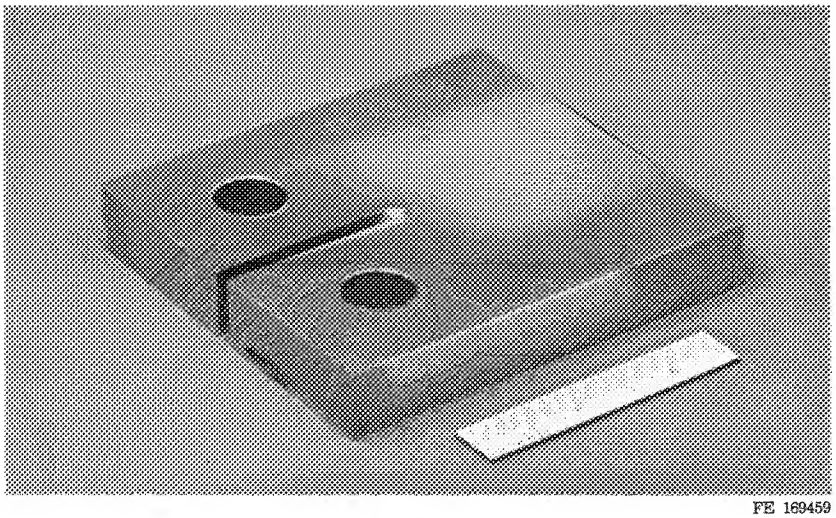

FE 169459

Figure 55. Photograph of Modified Compact Tension Specimen

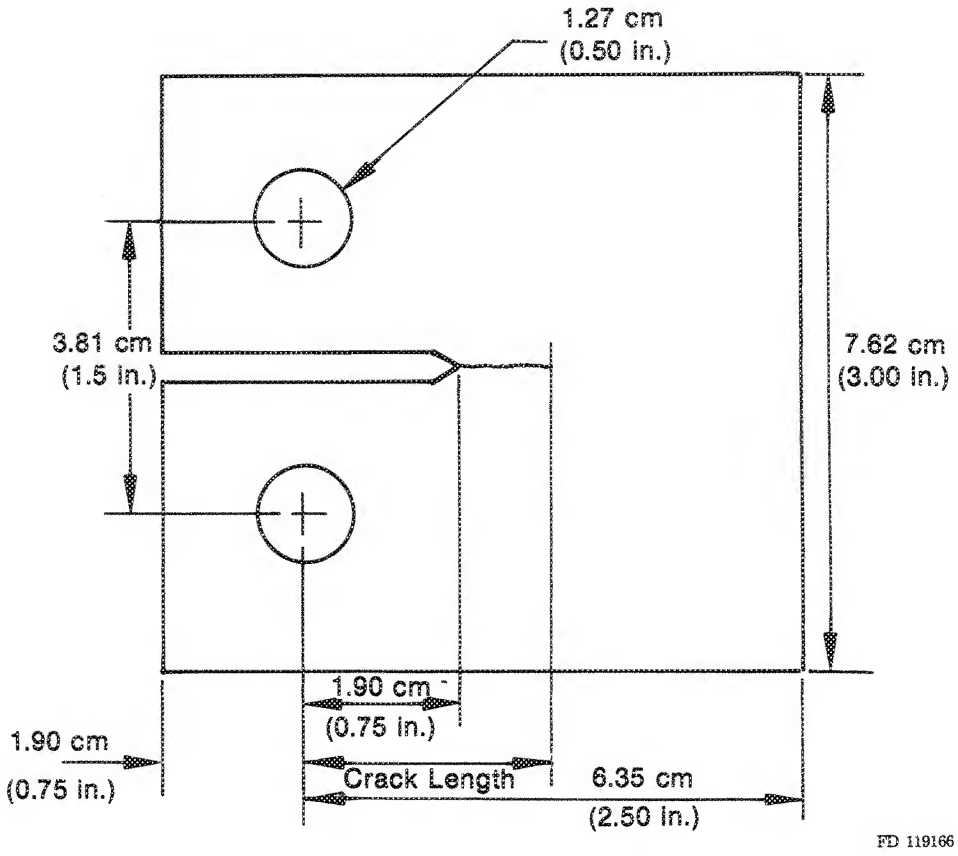

FD 119166

Figure 56. Modified Compact Tension Specimen

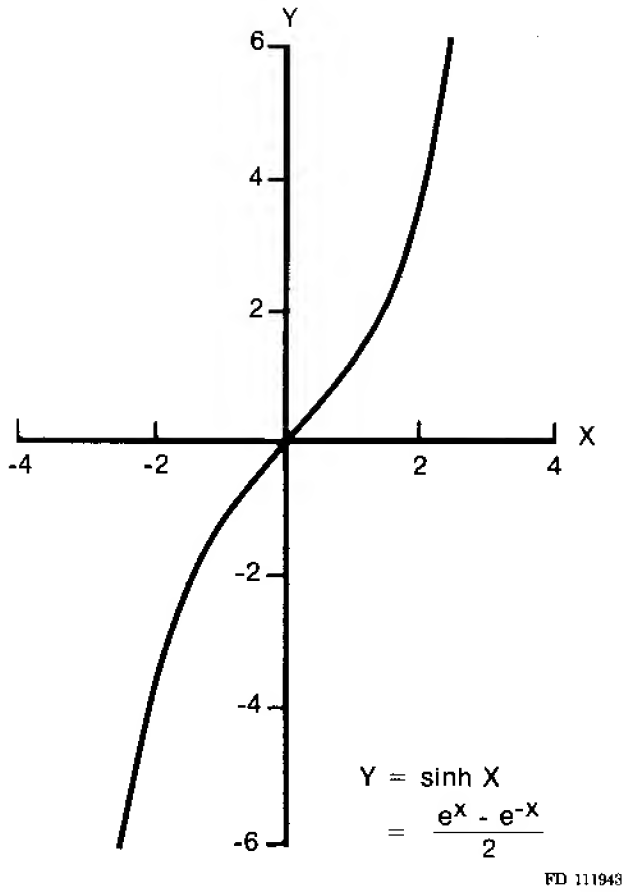

Figure 57. Hyperbolic Sine on Cartesian Coordinates

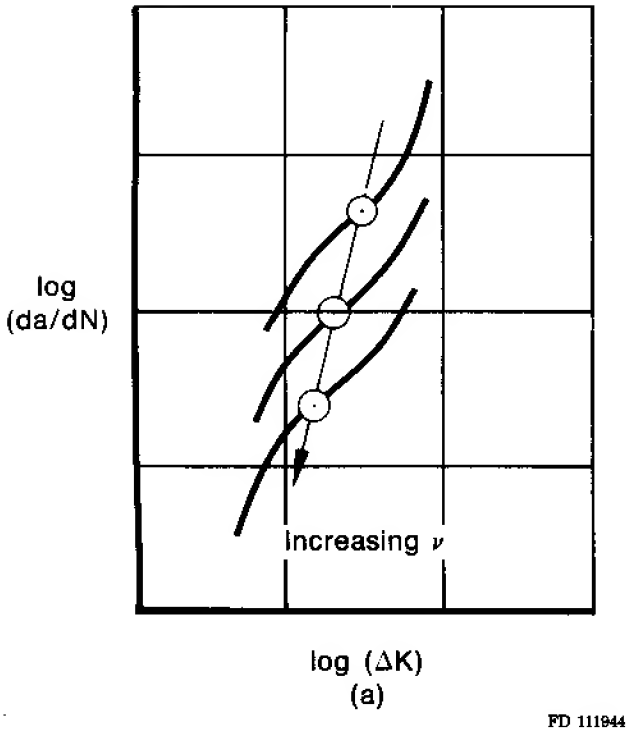

Figure 58. Crack Propagation Rate Is Influenced by Frequency

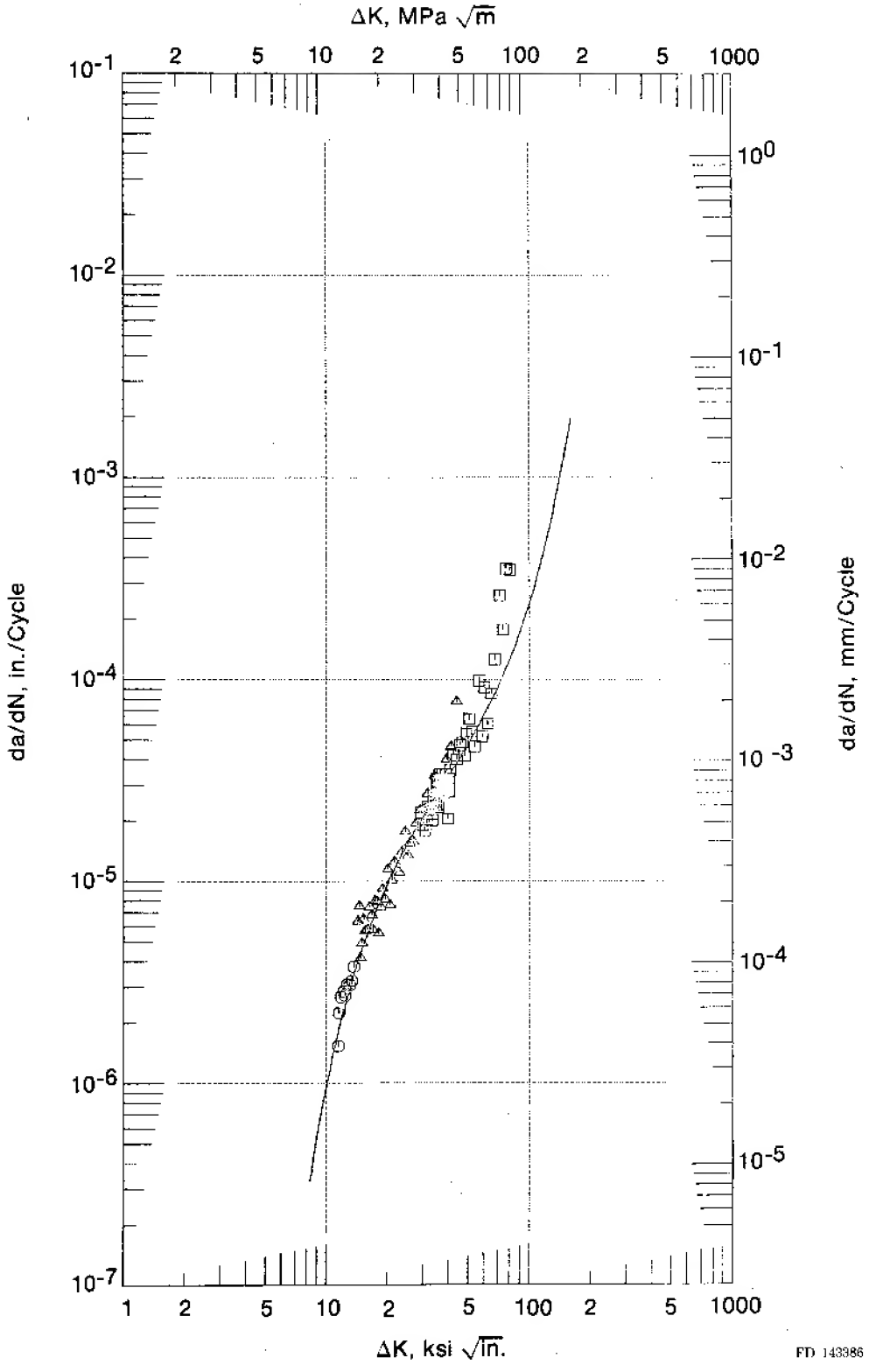

Figure 59. Crack Growth Rate for Waspaloy at 0.33 Hz, R = 0.05, 650°C (1200°F)

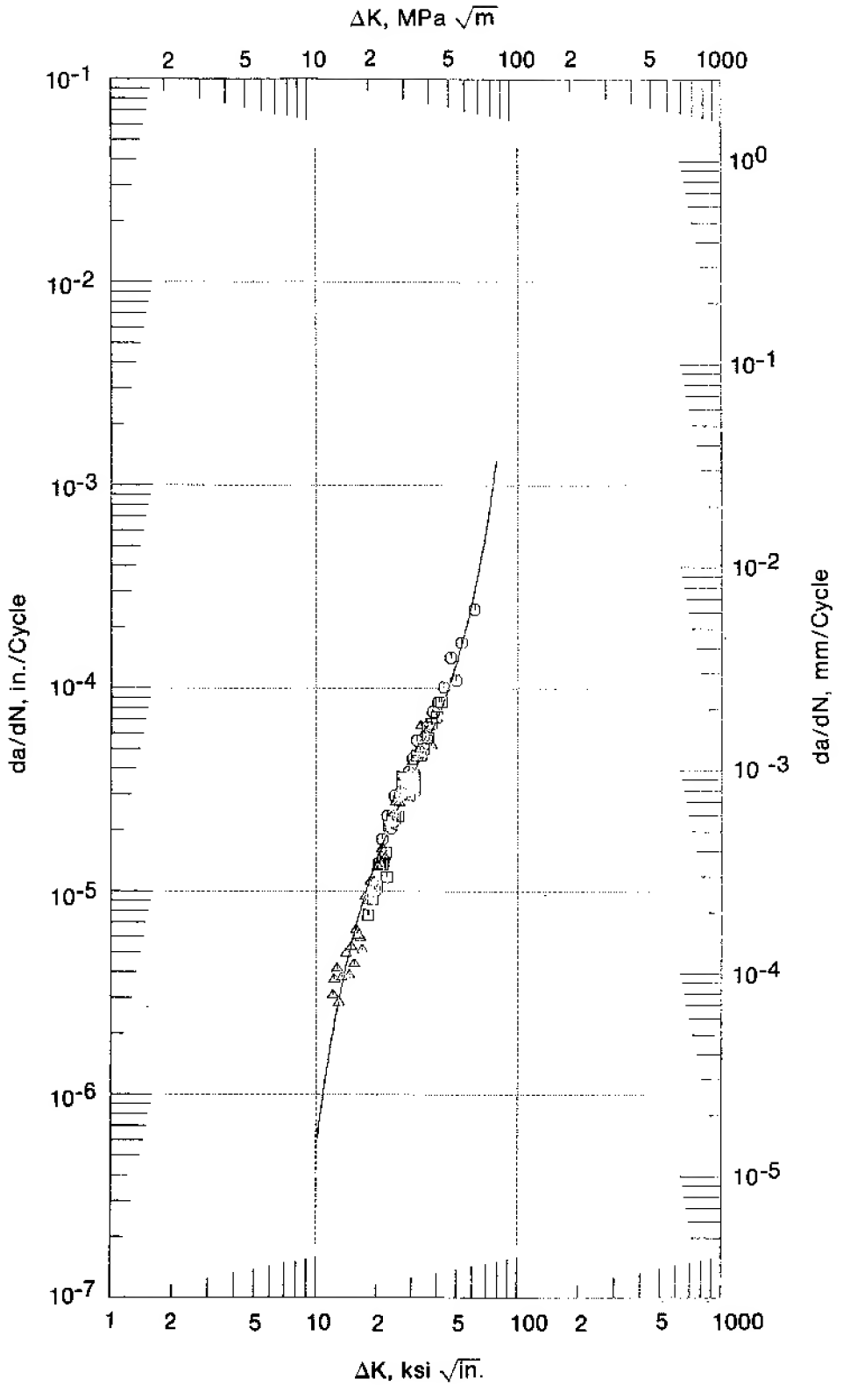

Figure 60. Crack Growth Rate for Wrought Astroloy at 0.33 Hz, R = 0.05, 650°C (1200°F)

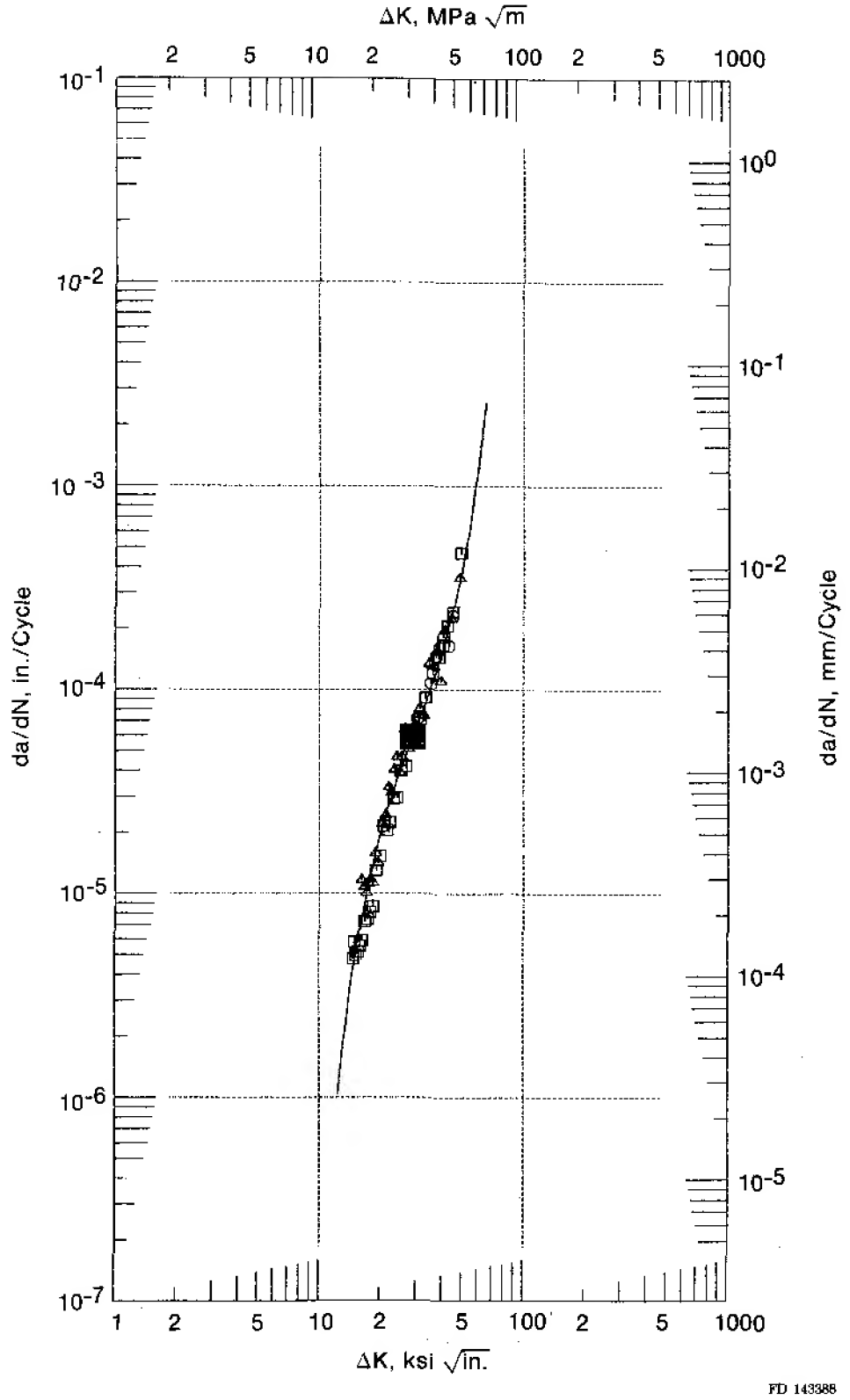

Figure 61. Crack Growth Rate for NASA IIB-7 at 0.33 Hz, R = 0.05, 650°C (1200°F)

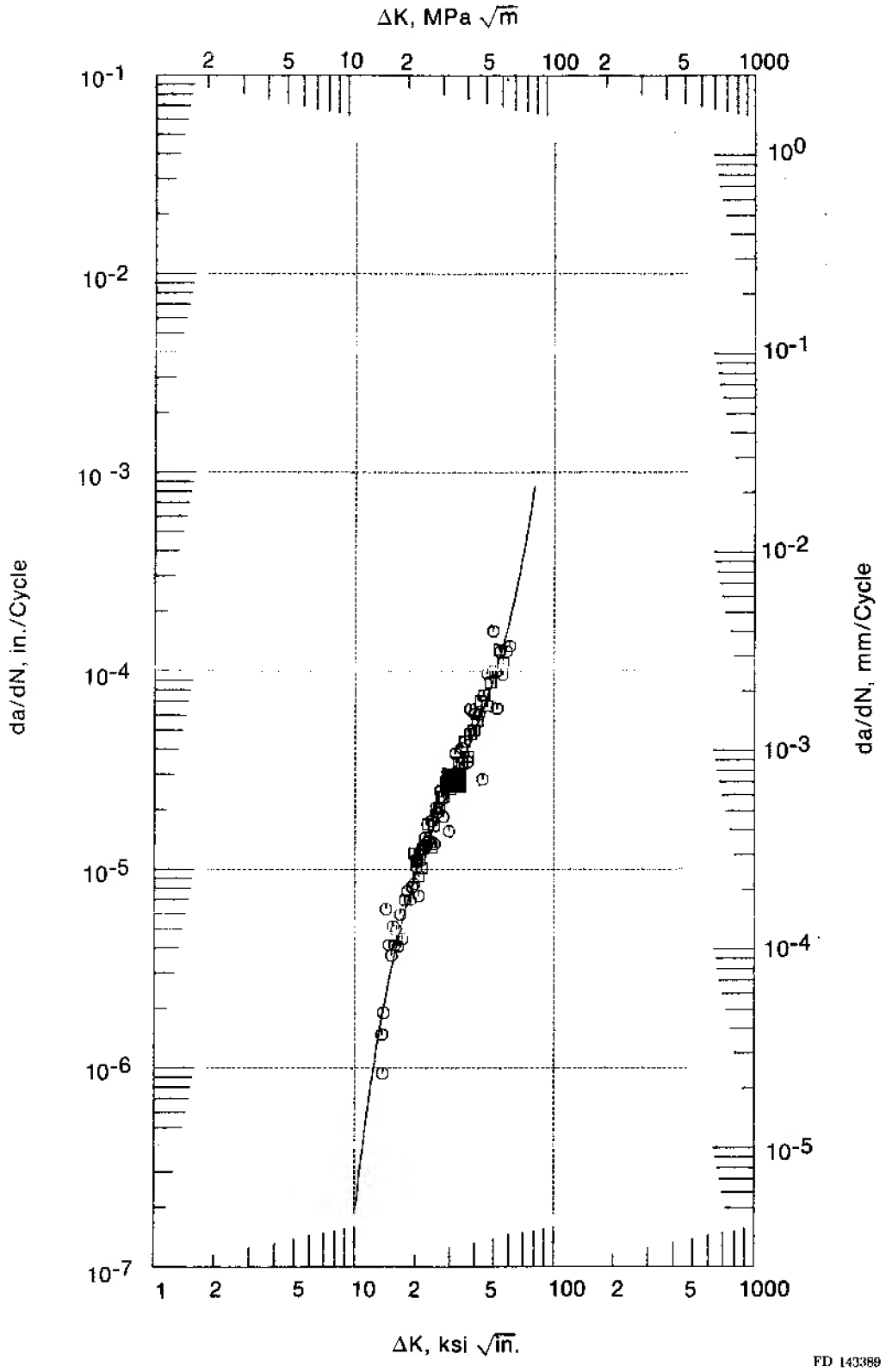

Figure 62. Crack Growth Rate for HIP-Astroloy at 0.33 Hz, R = 0.05, 650°C (1200°F)

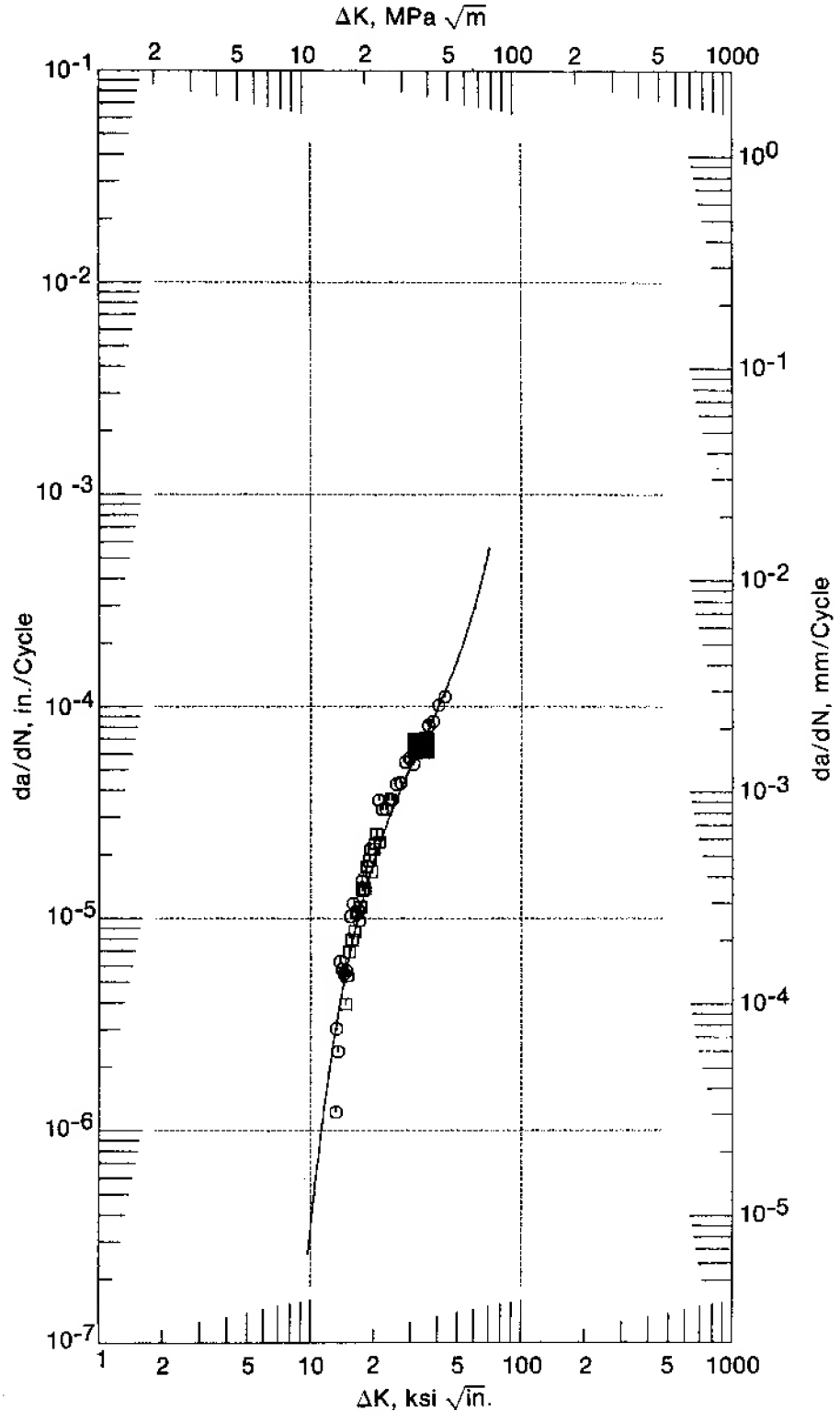

Figure 63. Crack Growth Rate for IN 100 at 0.33 Hz, R = 0.05, 650°C (1200°F)

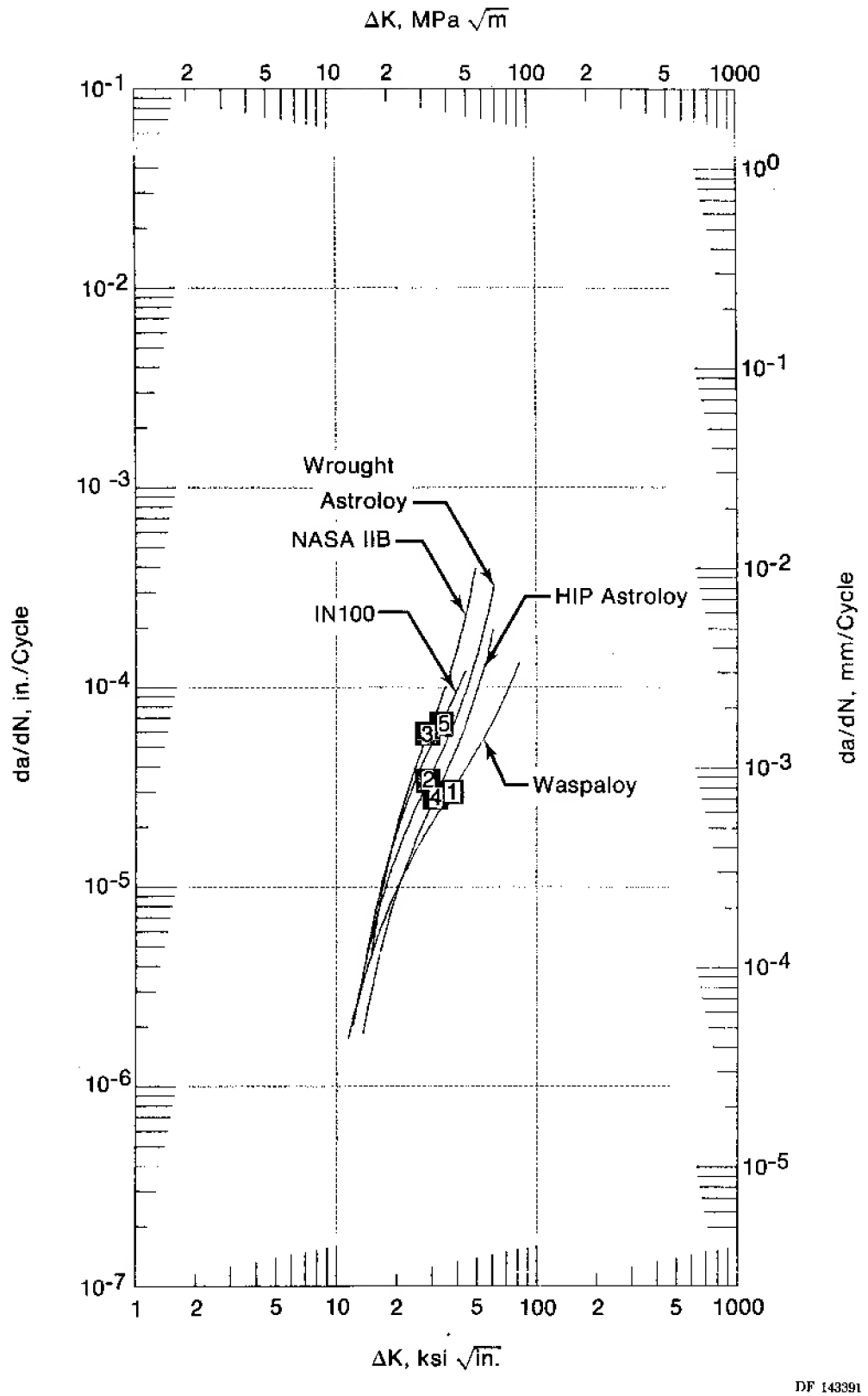

Figure 64. Crack Growth Rate of All Five Alloys at 0.33 Hz, R = 0.05, 650°C (1200°F)

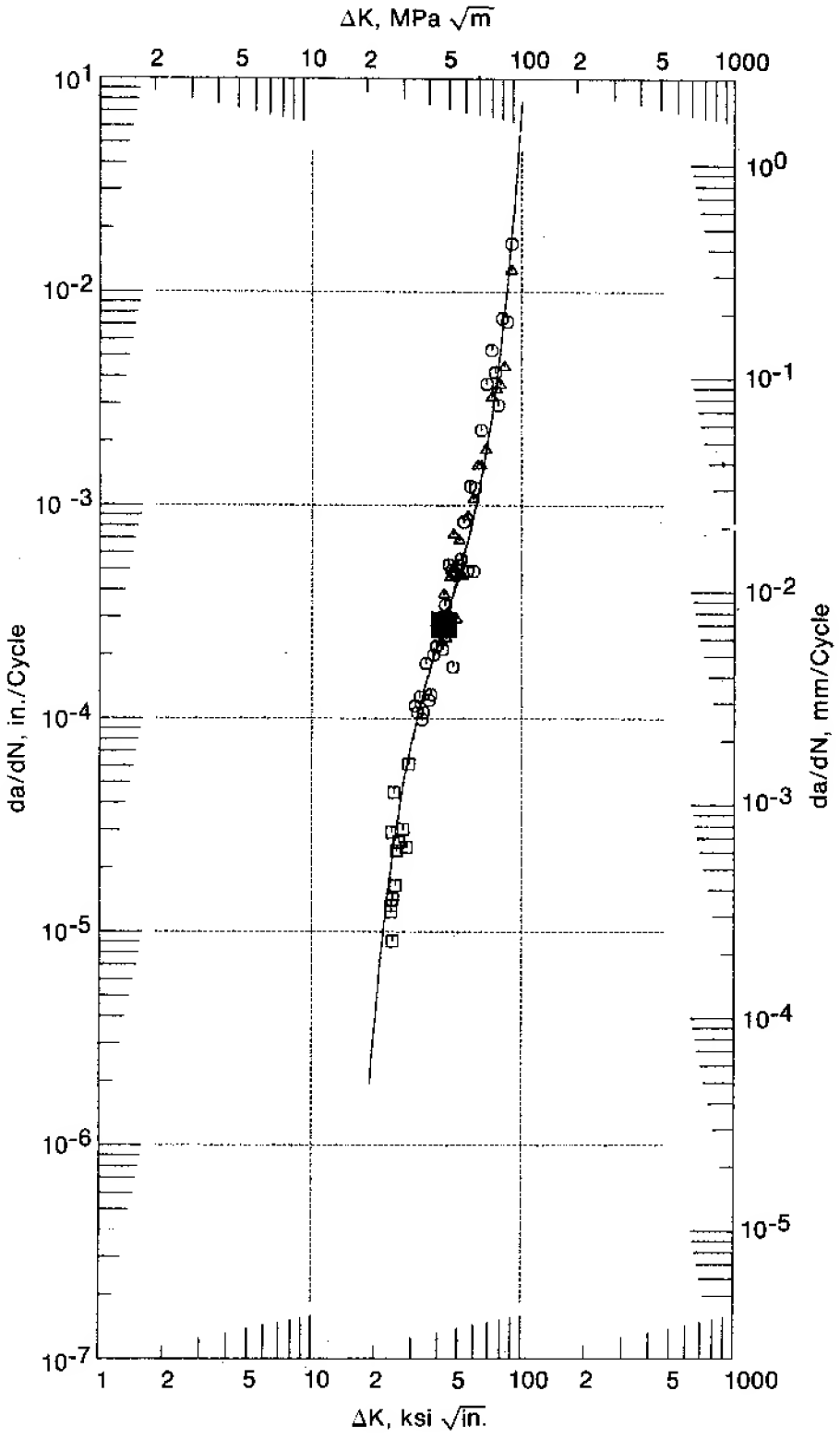

Figure 65. Waspaloy Crack Growth Rate for 900-sec Dwell, R = 0.05, 650°C (1200°F)

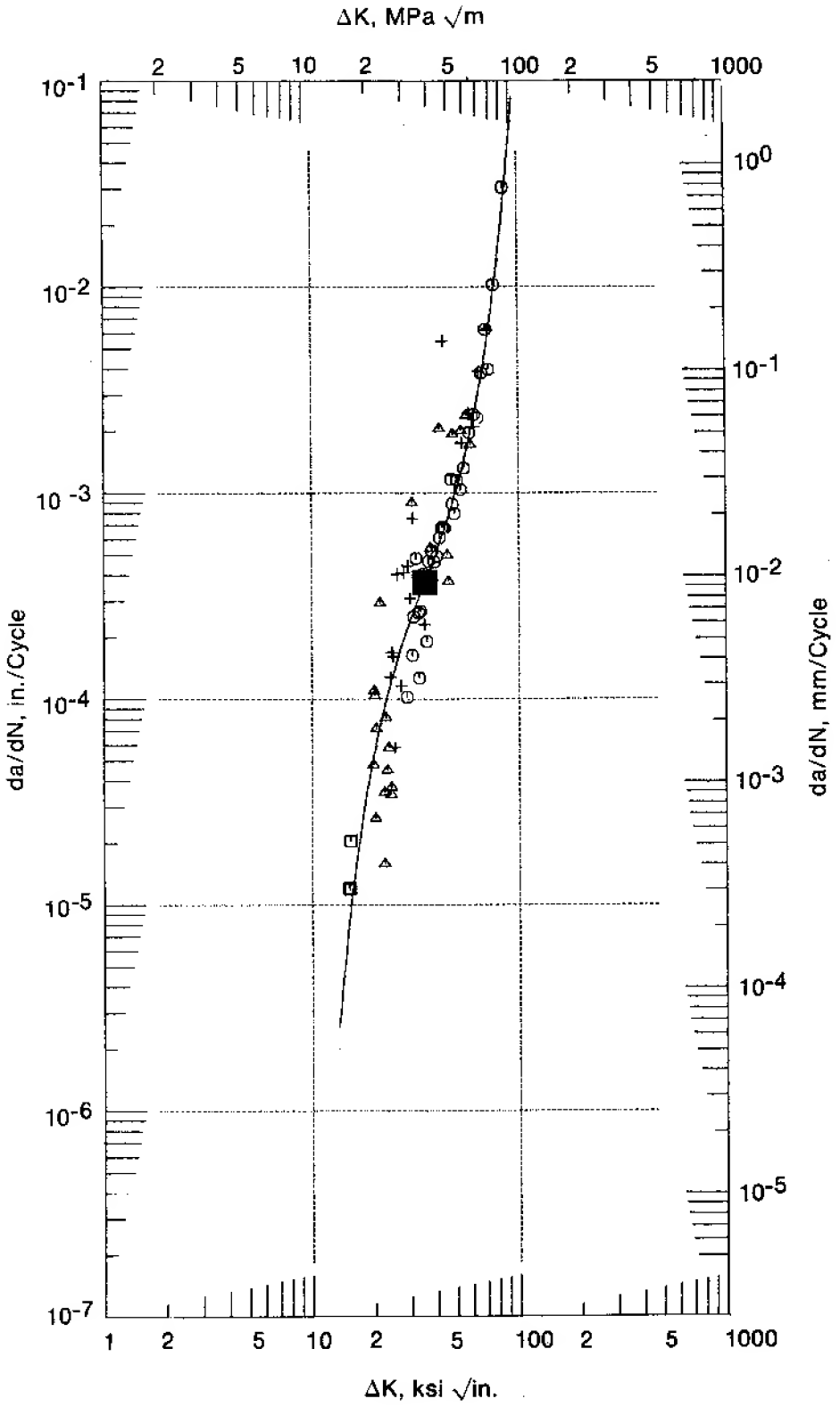

Figure 66. Wrought Astroloy Crack Growth Rate for 900-sec Dwell, R = 0.05, 650°C (1200°F)

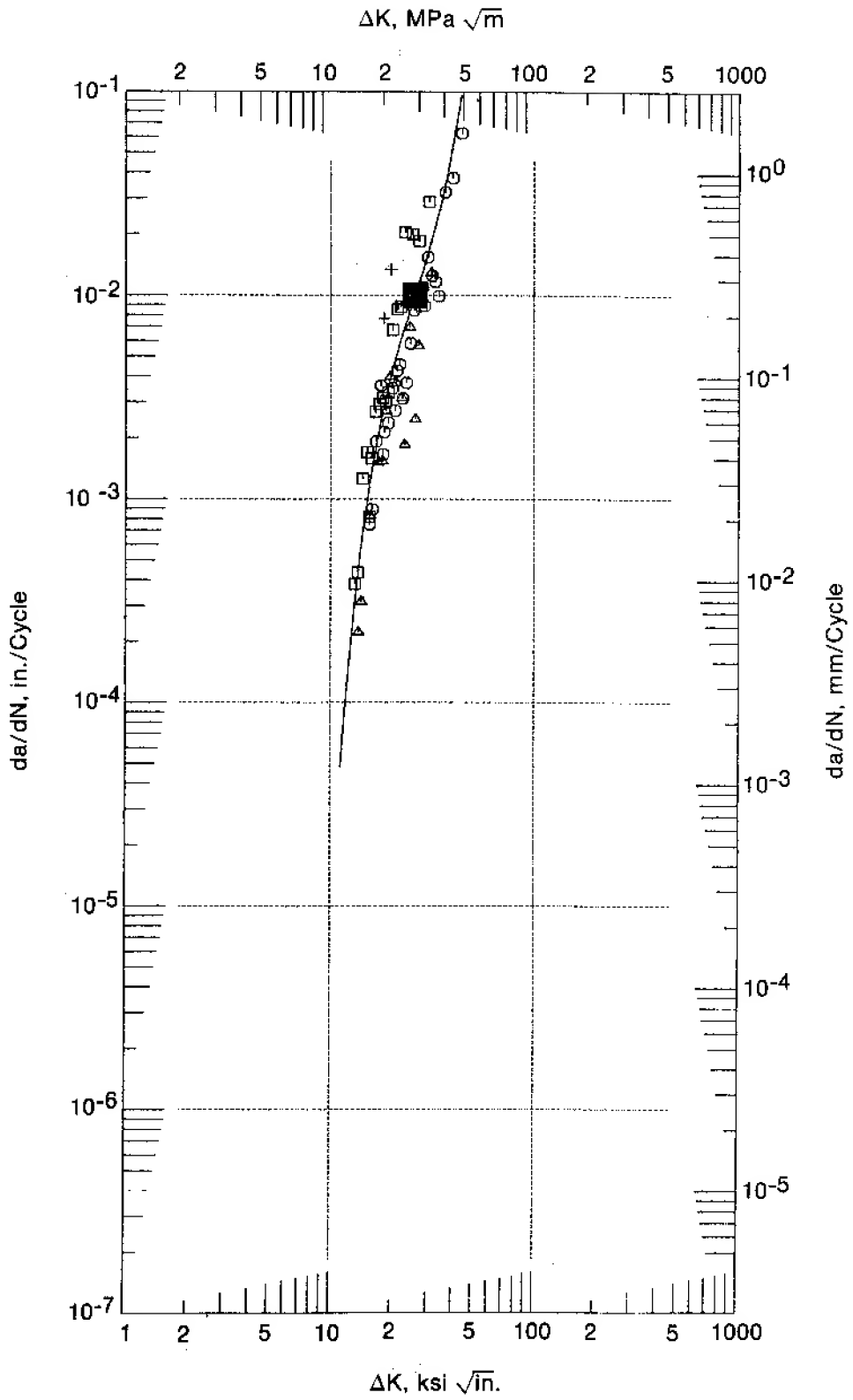

Figure 67. NASA IIB-7 Crack Growth Rate for 900-sec Dwell, R = 0.05, 650°C (1200°F)

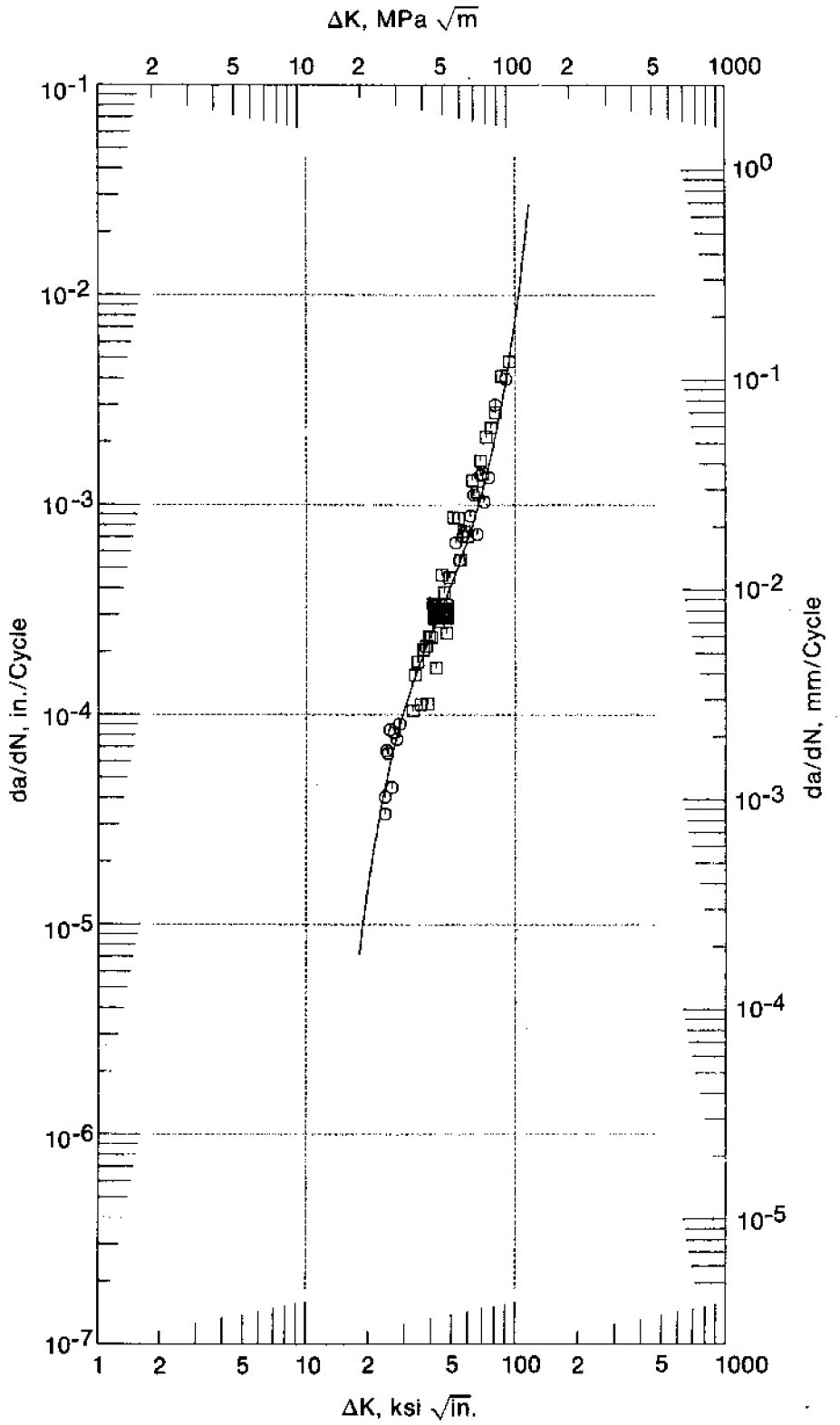

Figure 68. HIP-Astroloy Crack Growth Rate for 900-sec Dwell, R = 0.05, 650°C (1200°F)

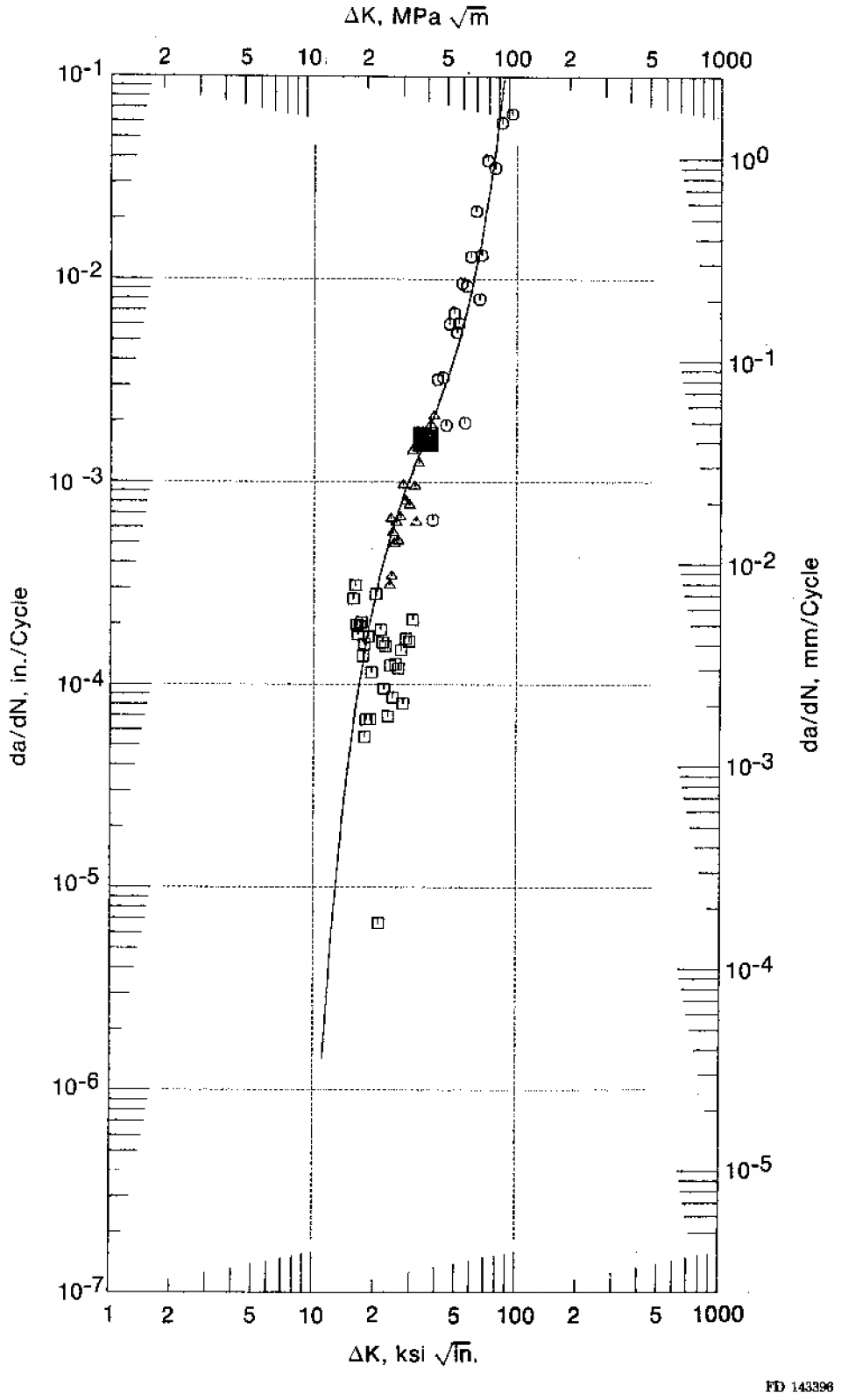

Figure 69. IN 100 Crack Growth Rate for 900-sec Dwell, R = 0.05, 650°C (1200°F)

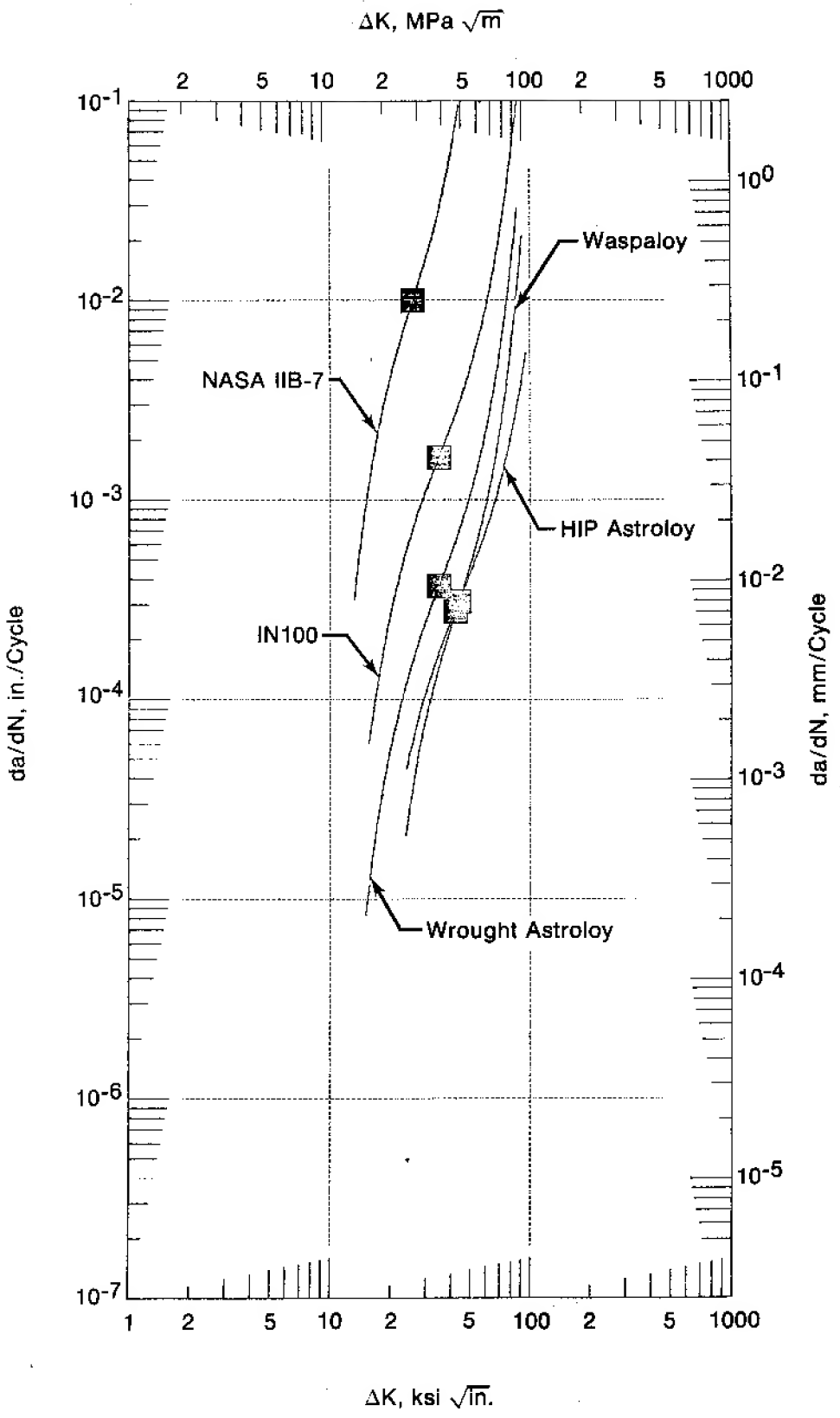

Figure 70. Crack Growth Rates of All Five Alloys for 900-sec Dwell, R = 0.05, 650°C (1200°F)

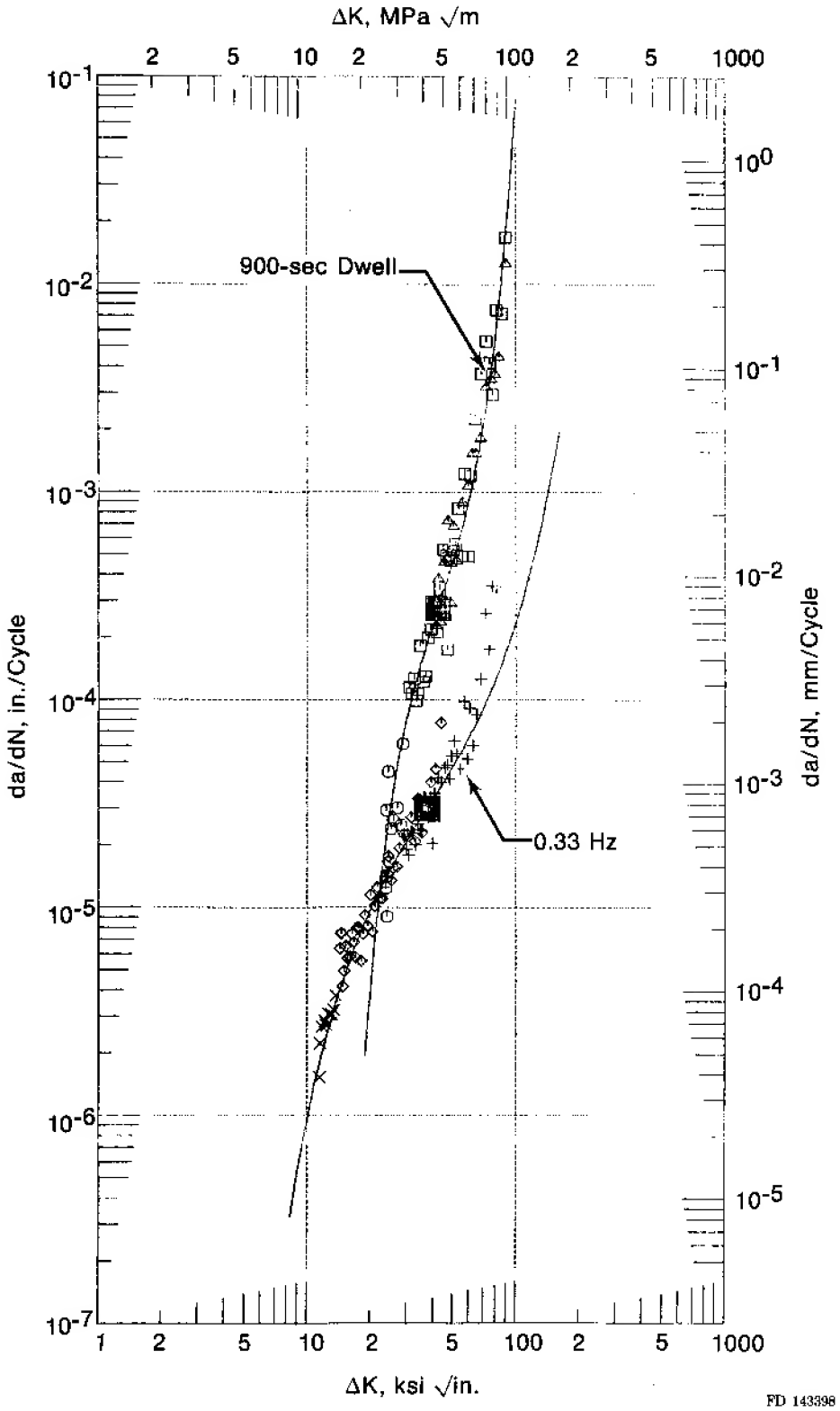

Figure 71. Comparison of Waspaloy 900-sec Dwell and 0.33 Hz Crack Growth Rates at R = 0.05, 650°C (1200°F)

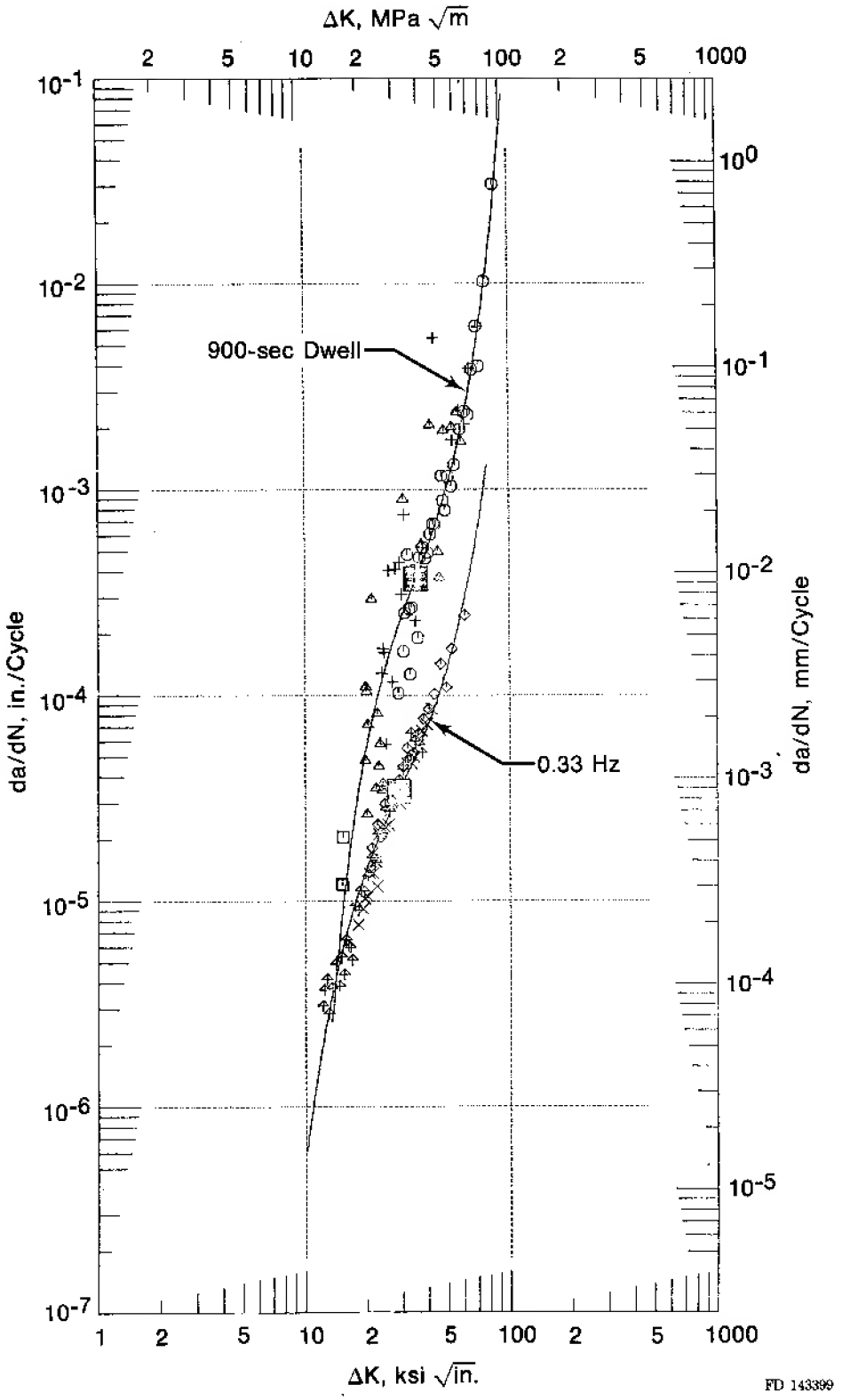

Figure 72. Comparison of Wrought-Astroloy 900-sec Dwell and 0.33 Hz Crack Growth Rates at R = 0.05, 650°C (1200°F)

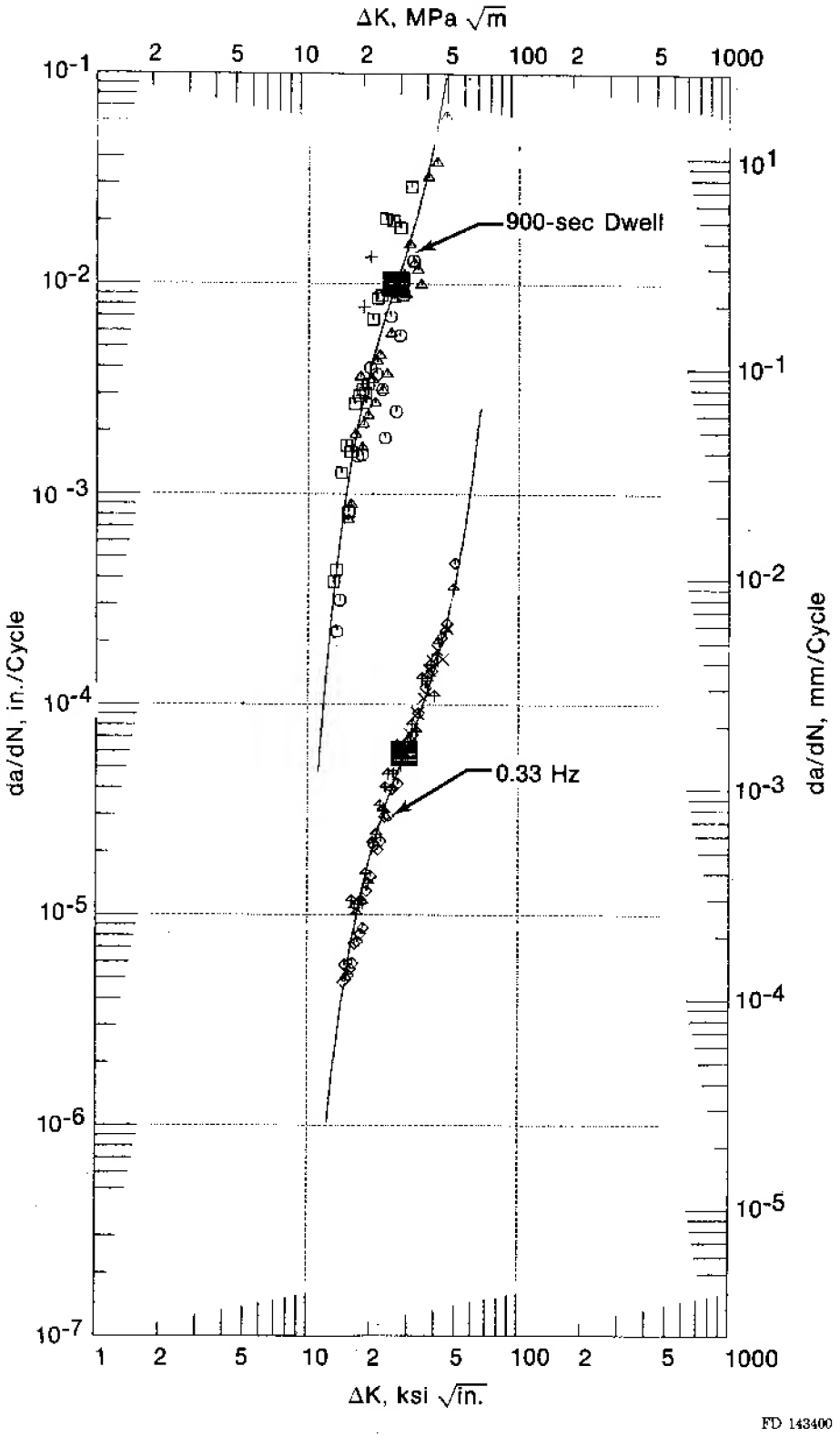

Figure 73. Comparison of NASA IIB-7 900-sec Dwell and 0.33 Hz Crack Growth Rates at R = 0.05, 650°C (1200°F)

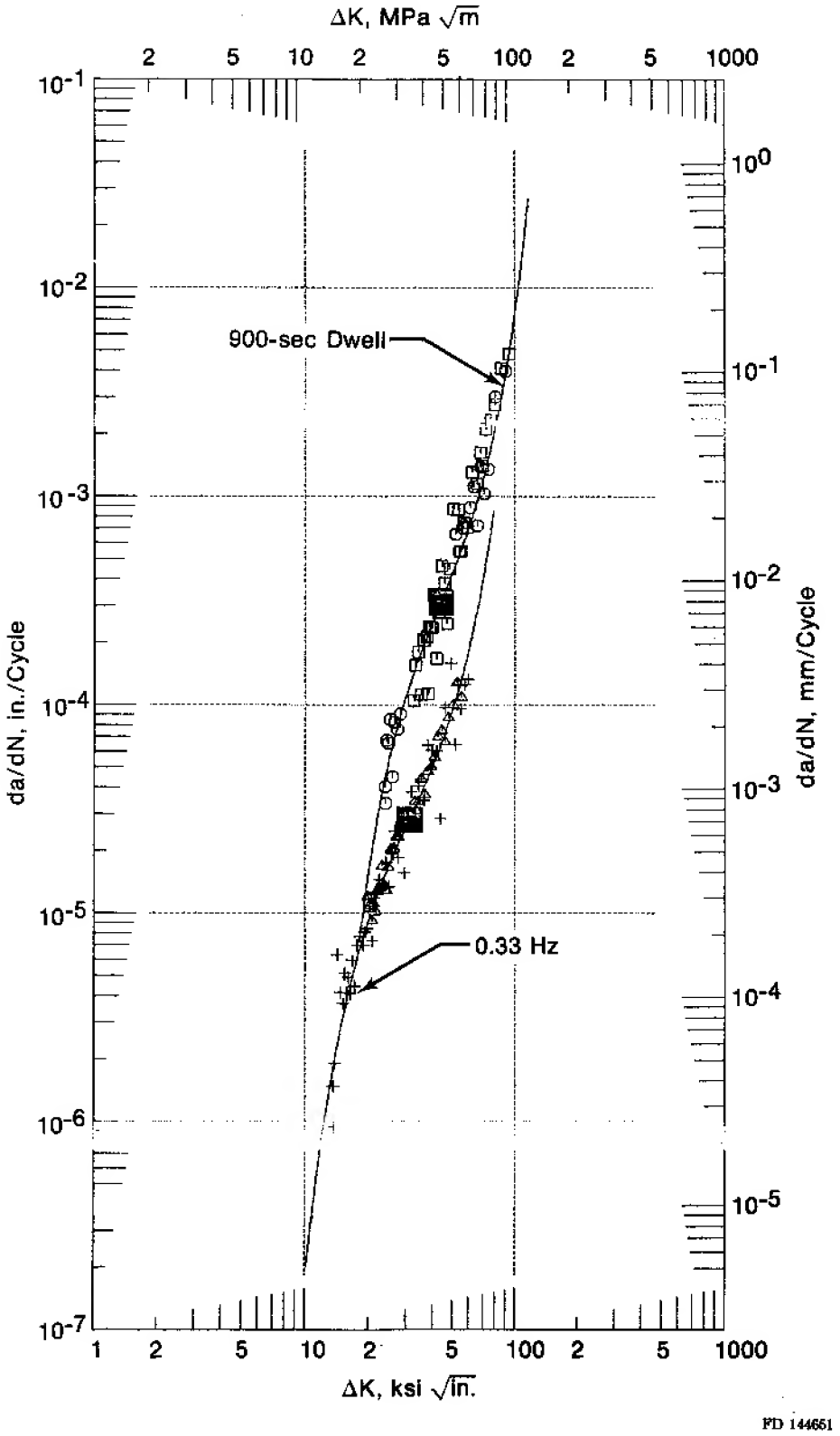

Figure 74. Comparison of HIP-Astroloy 900-sec Dwell and 0.33 Hz Crack Growth Rates at R = 0.05, 650°C (1200°F)

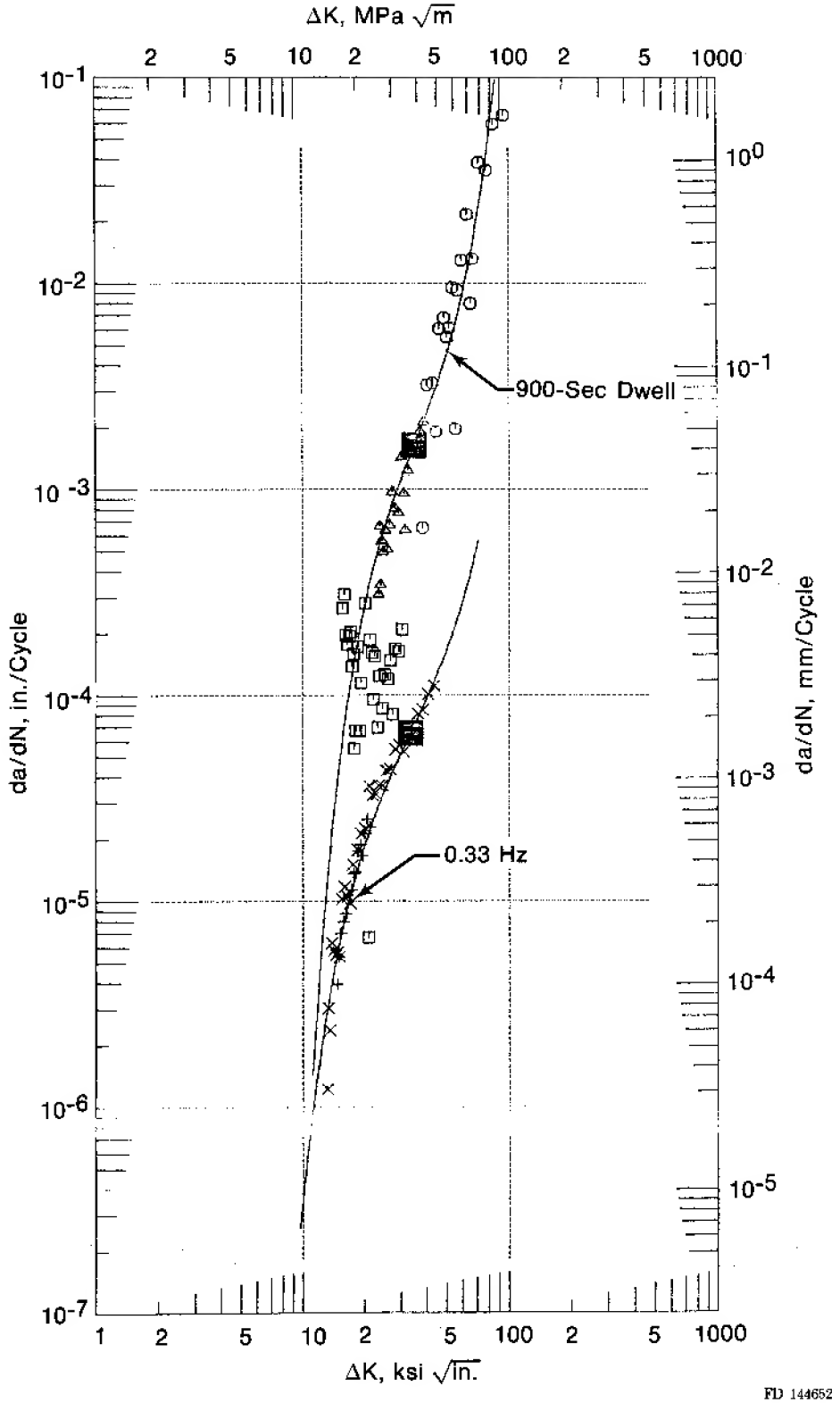

Figure 75. Comparison of IN 100 900-sec Dwell and 0.33 Hz Crack Growth Rates at R = 0.05, 650°C (1200°F)

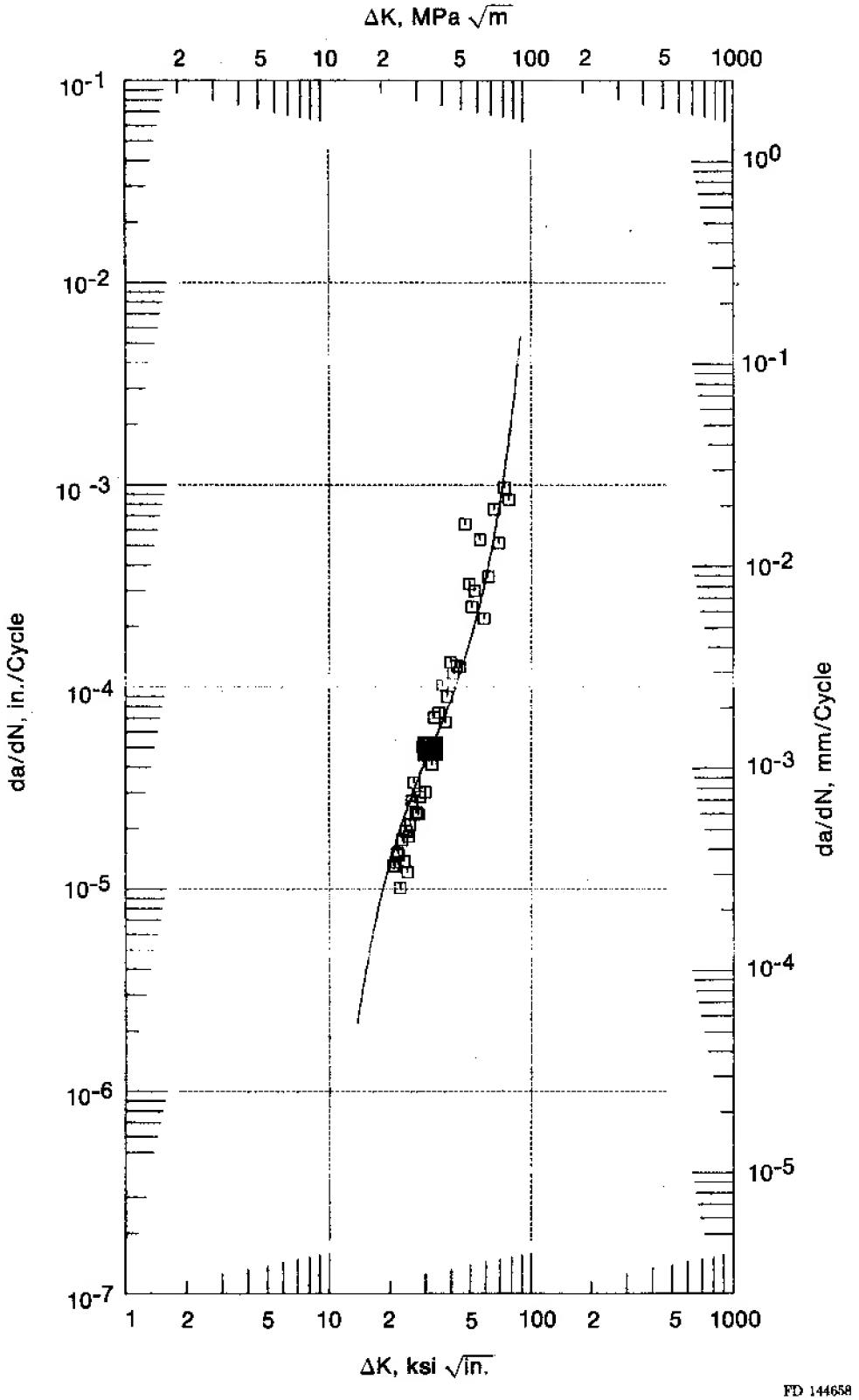

Figure 76. HIP-Astroloy Crack Growth Rate for 0.0083 Hz, R = 0.05, 650°C (1200°F)

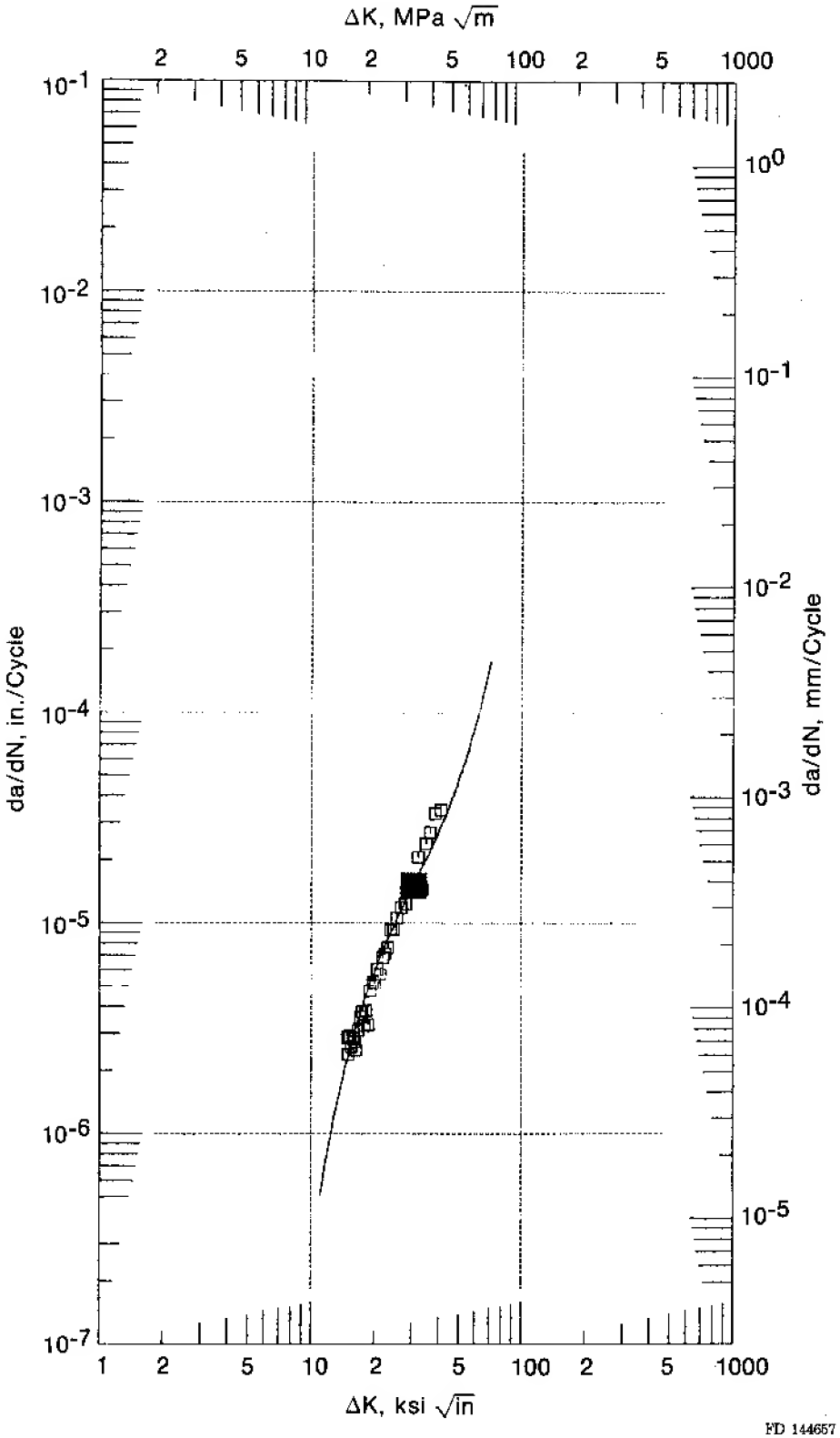

Figure 77. HIP-Astroloy Crack Growth Rate for 20 Hz, R = 0.05, 650°C (1200°F)

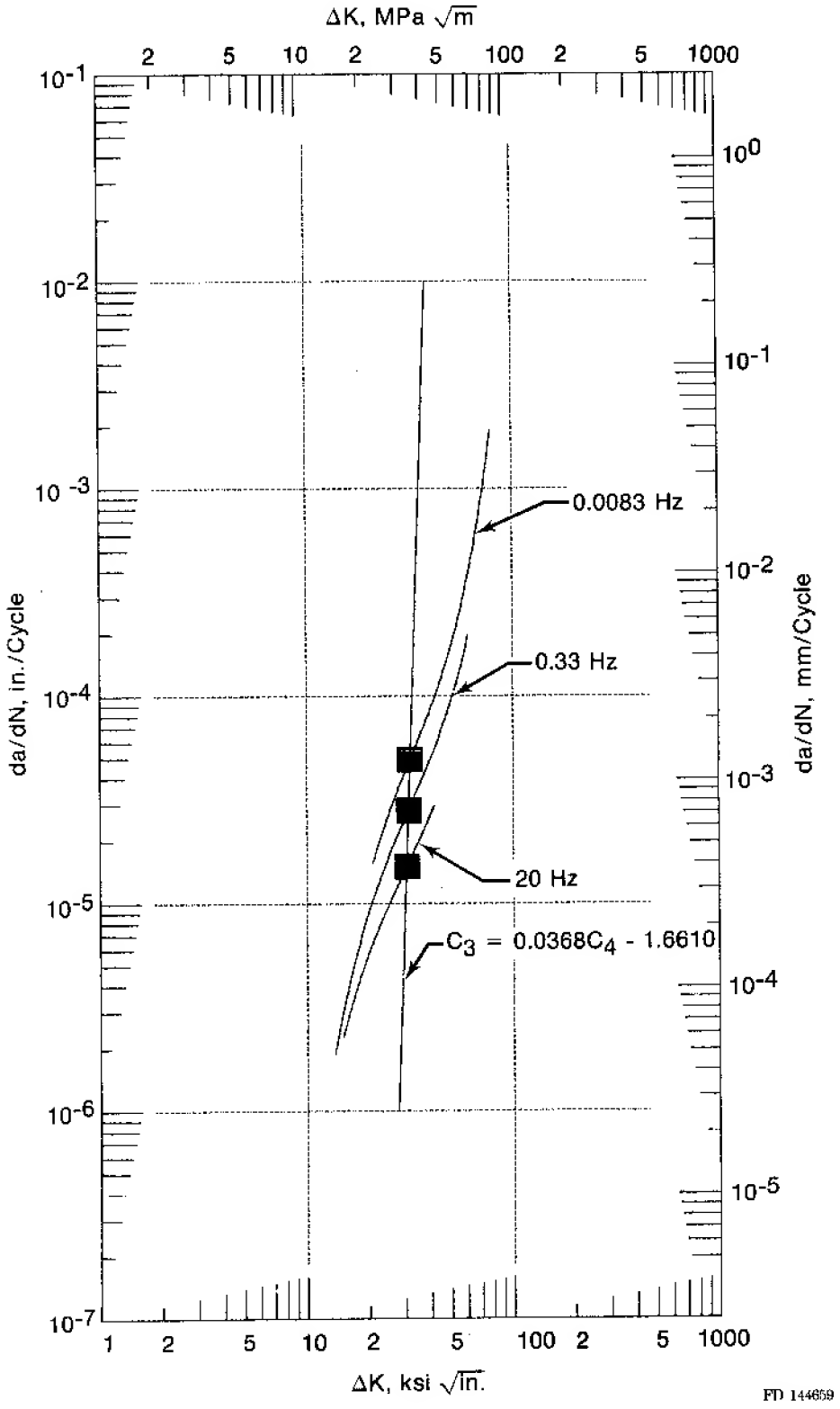

Figure 78. Effect of Frequency on HIP-Astroloy Crack Growth Rate at R = 0.05, 650°C (1200°F)

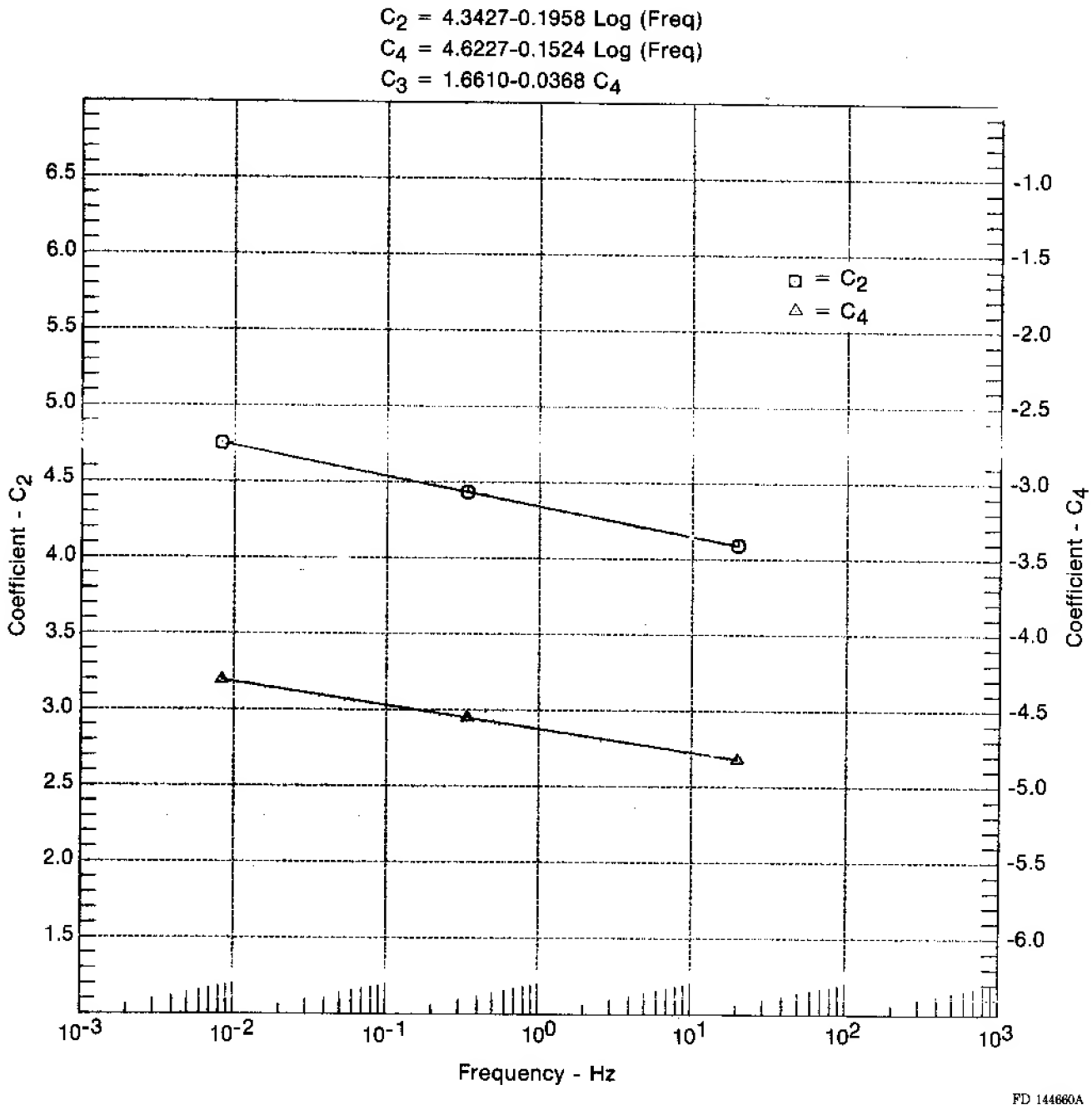

Figure 79. Effect of Frequency on Sinh Model Coefficients C_2 and C_4 for HIP-Astroloy

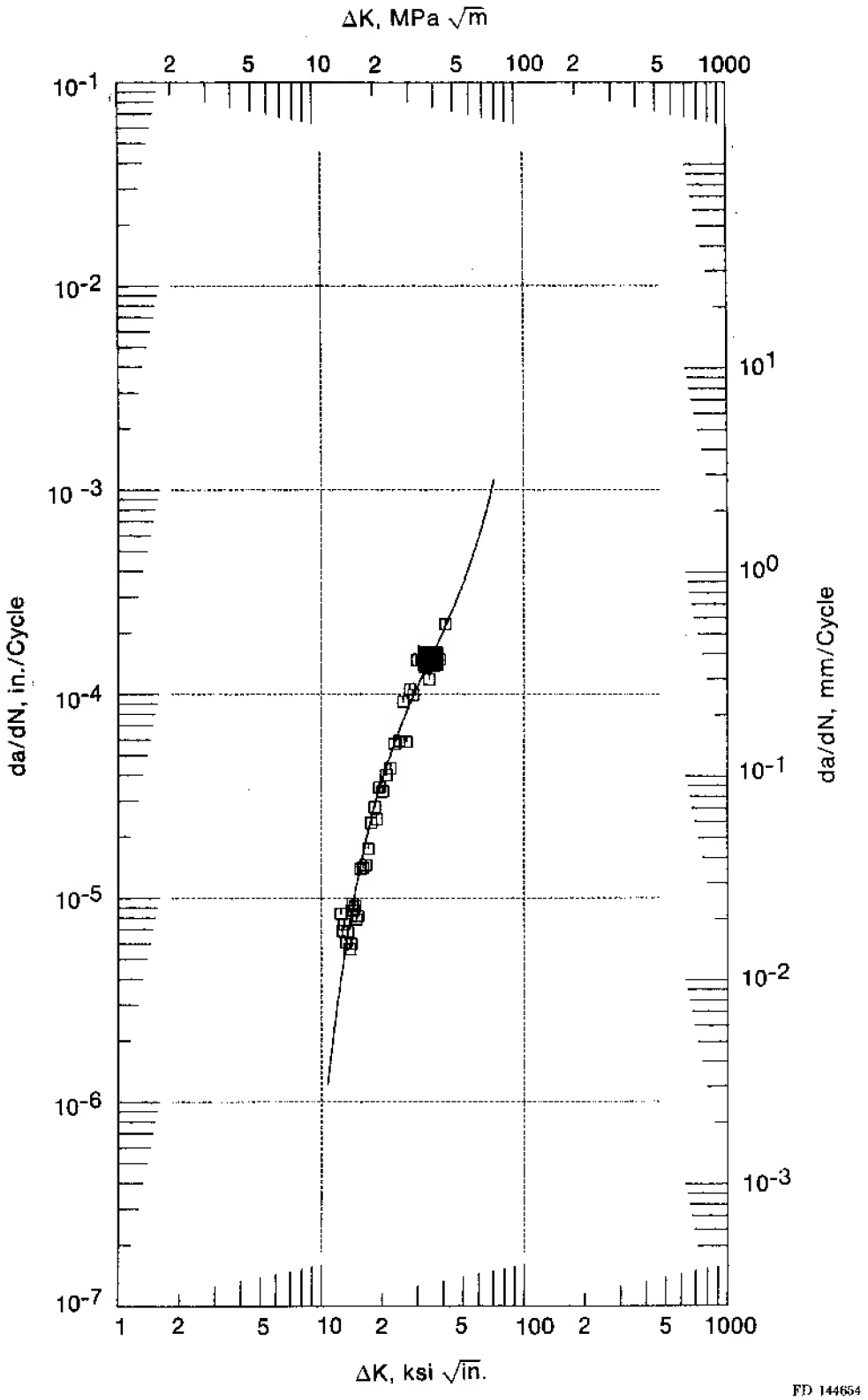

Figure 80. IN 100 Crack Growth Rate for 0.0083 Hz, R = 0.05, 650°C (1200°F)

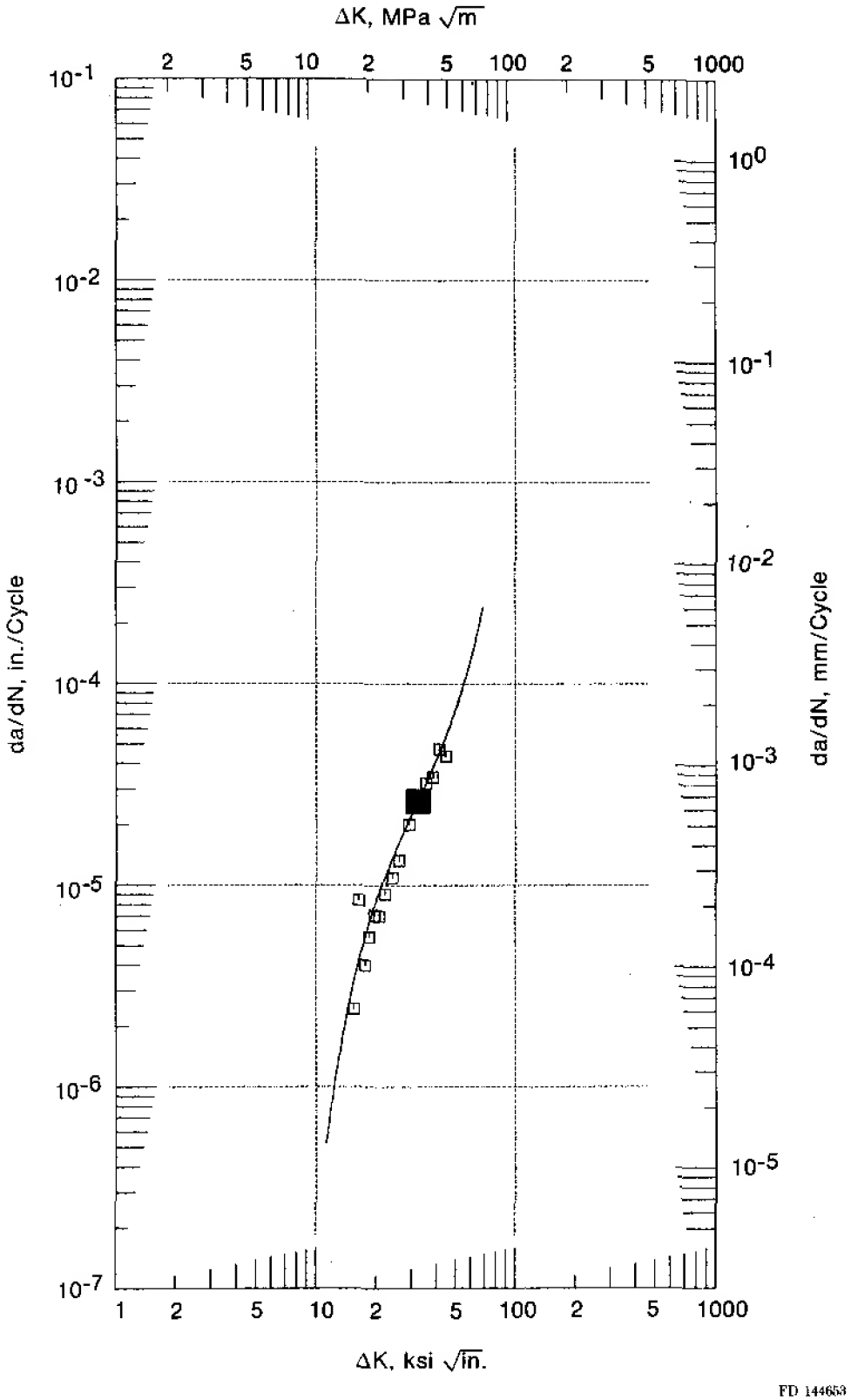

Figure 81. IN 100 Crack Growth Rate for 20 Hz, R = 0.05, 650°C (1200°F)

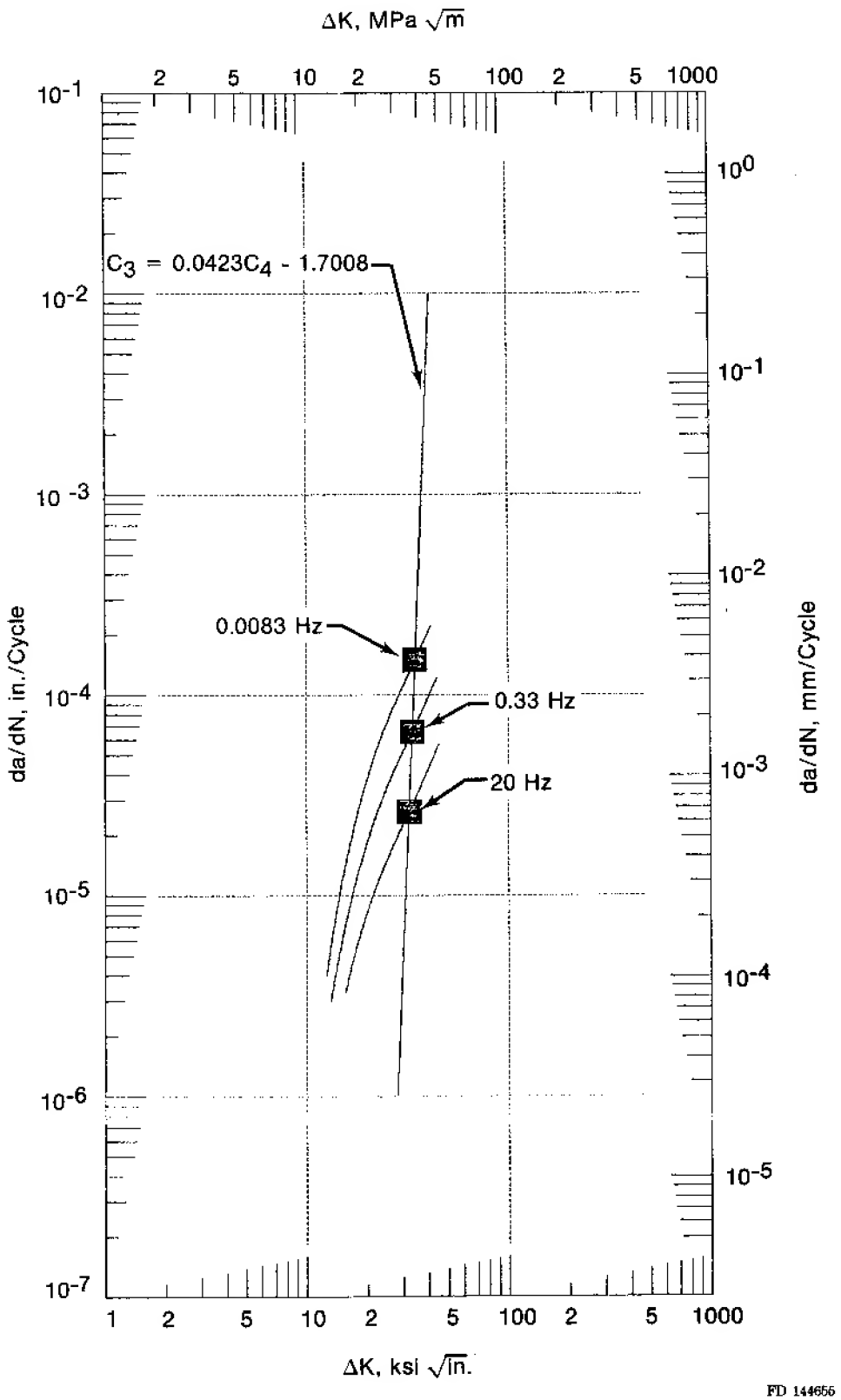

Figure 82. Effect of Frequency on IN 100 Crack Growth Rate at R = 0.05, 650°C (1200°F)

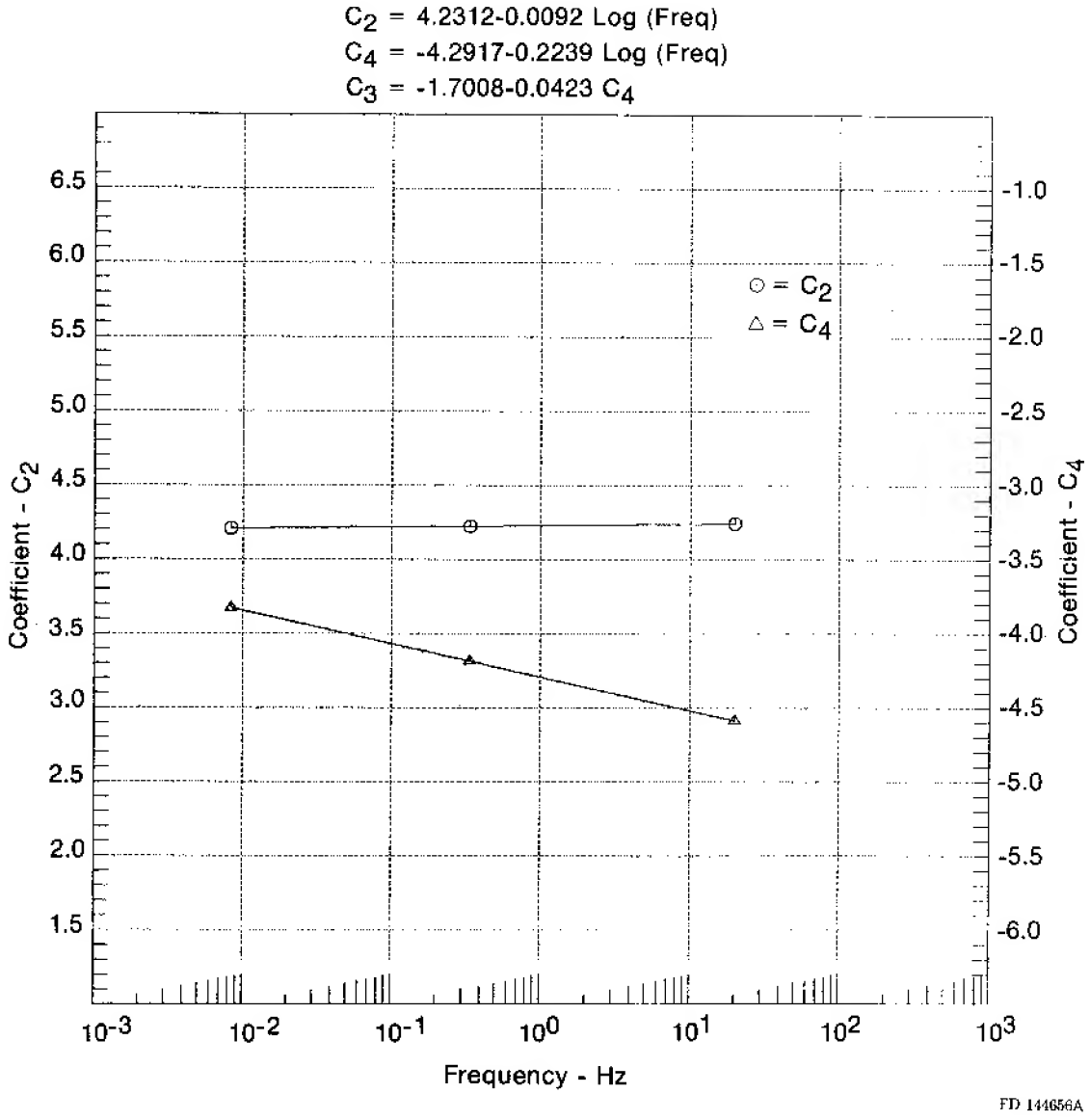

Figure 83. Effect of Frequency on Sinh Model Coefficients C_2 and C_4 for IN 100

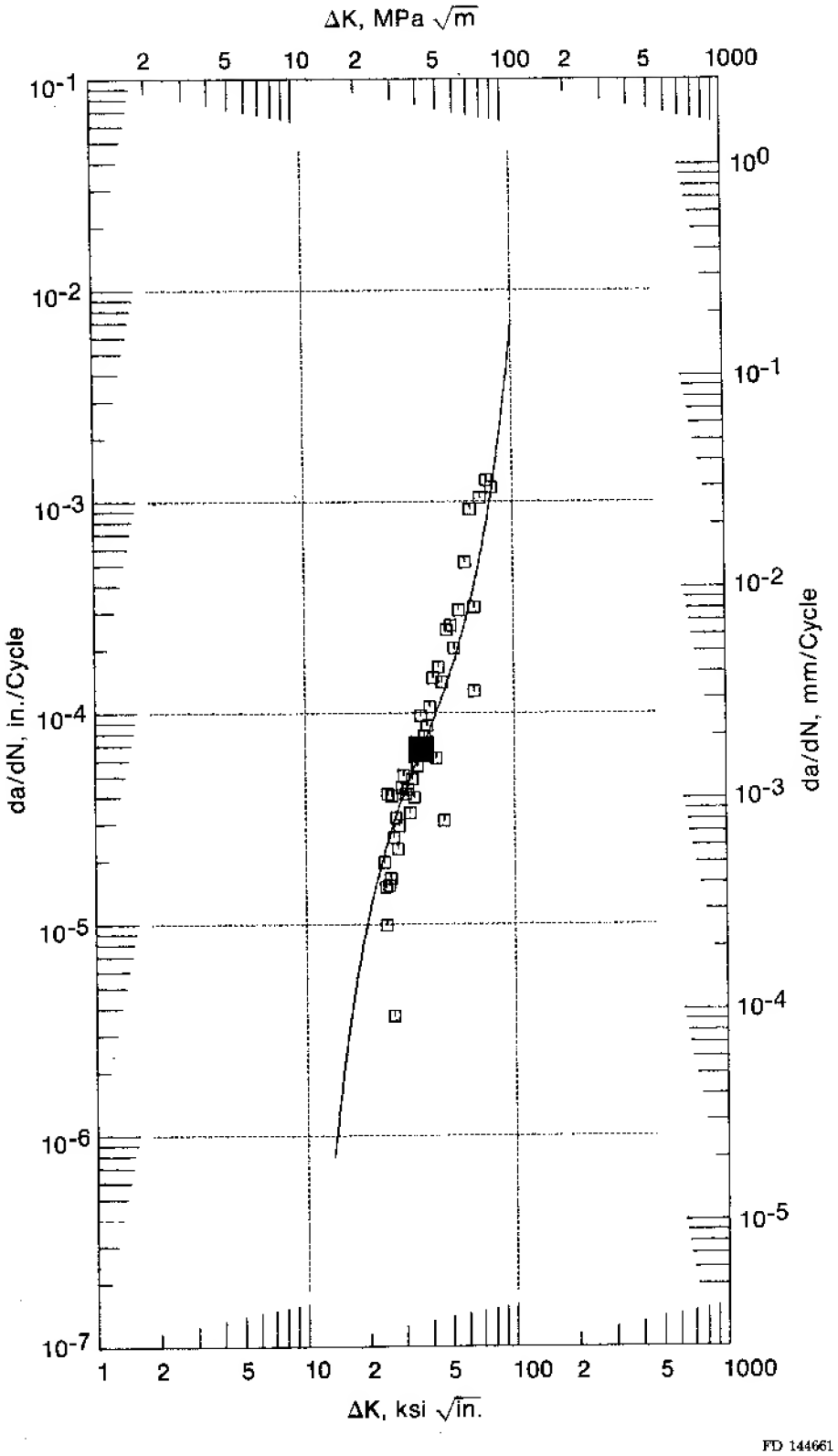

Figure 84. Waspaloy Crack Growth Rate for 120-sec Dwell, R = 0.05, 650°C (1200°F)

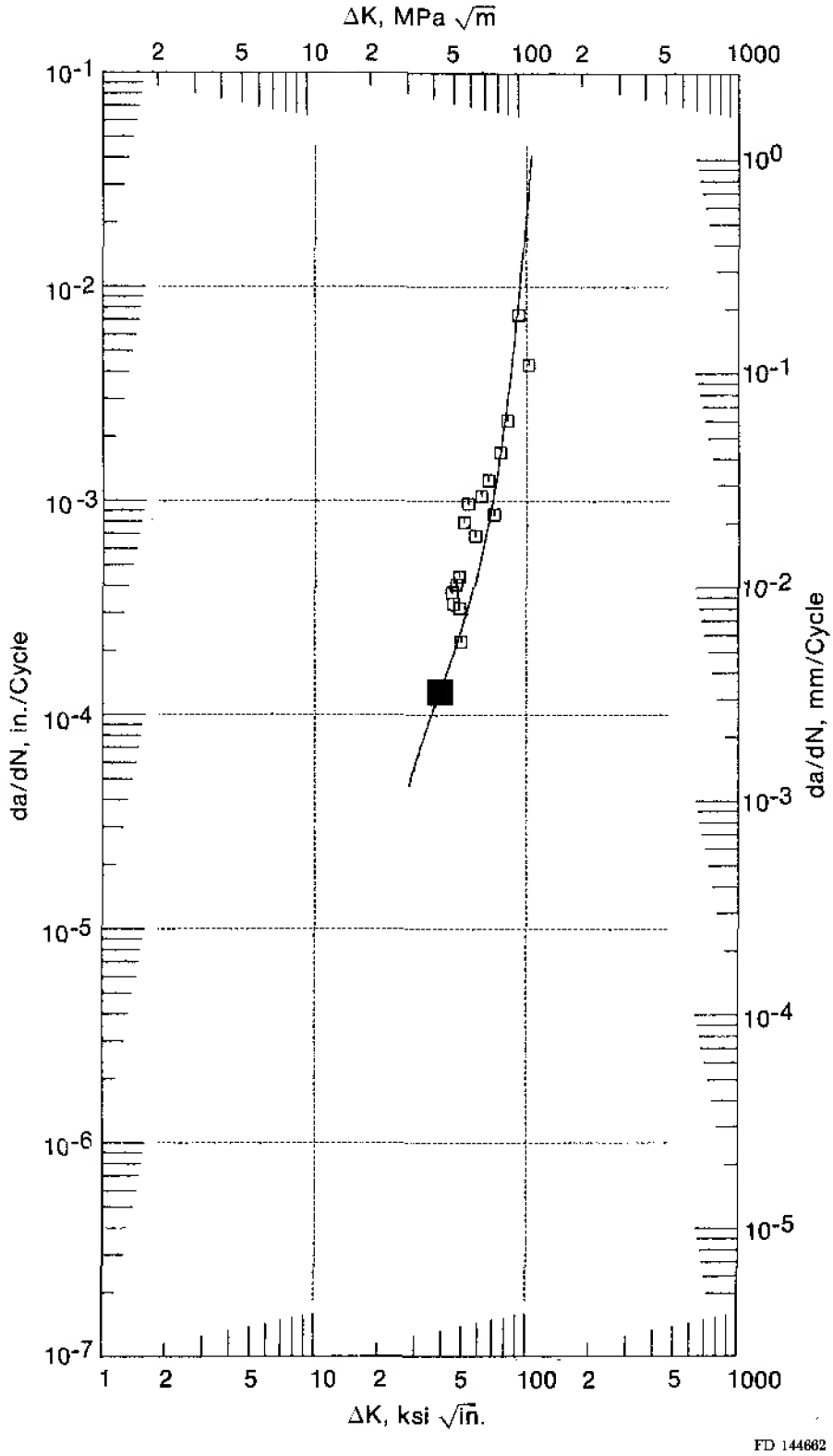

Figure 85. Waspaloy Crack Growth Rate for 300-sec Dwell, R = 0.05, 650°C (1200°F)

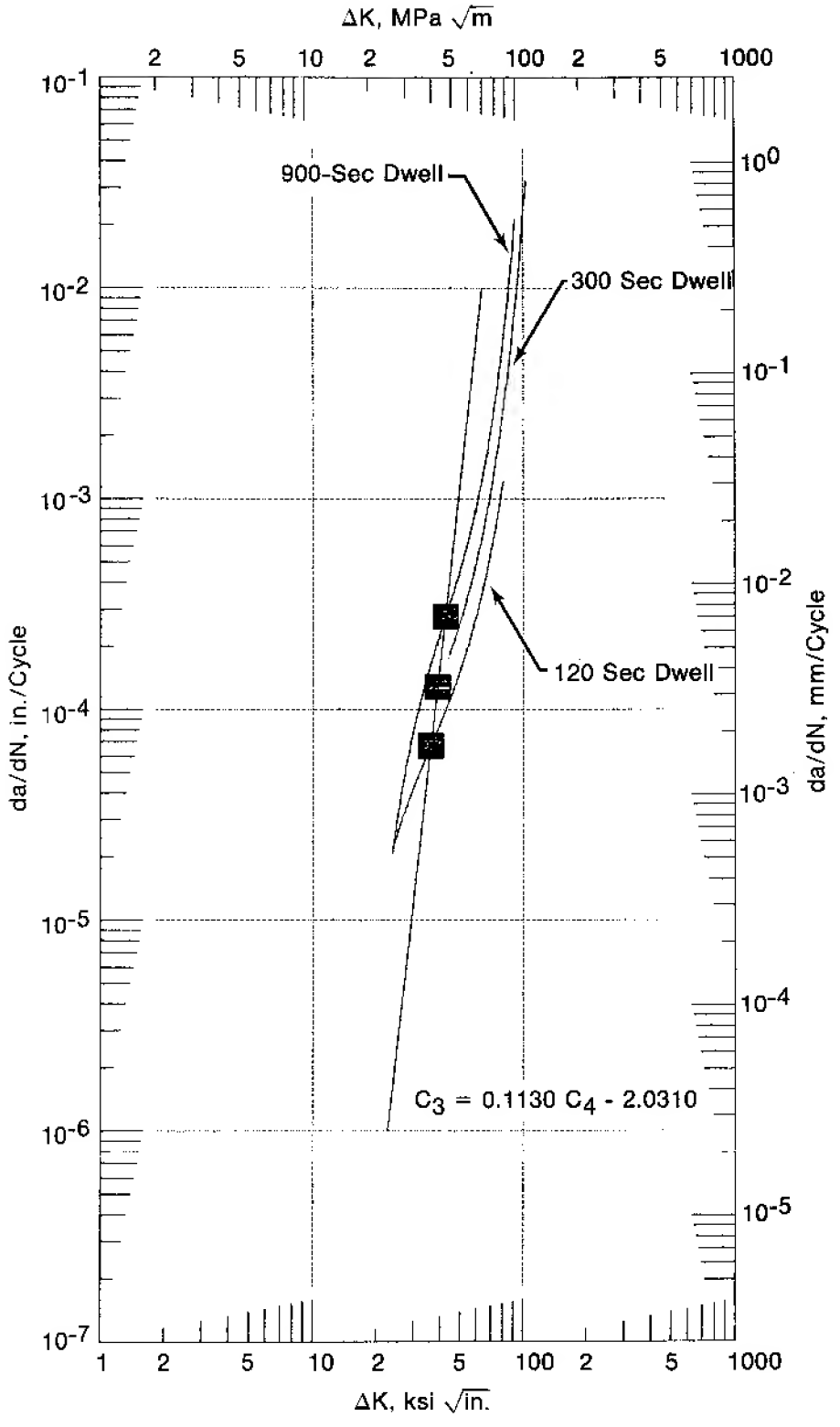

Figure 86. Comparison of 120-, 300-, and 900-sec Dwell Crack Growth Rates at 650°C (1200°F), R = 0.05 for Waspaloy

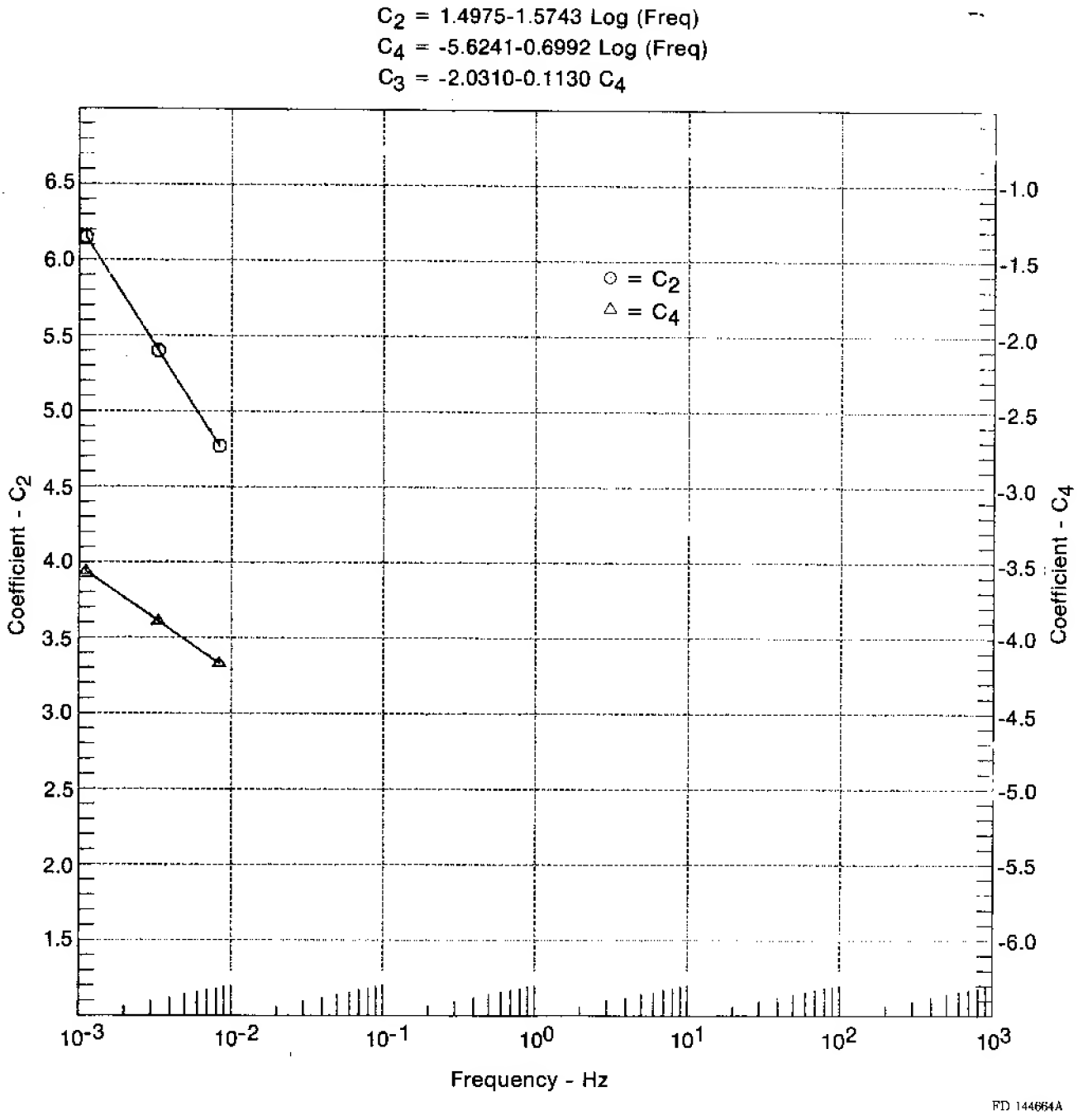

Figure 87. Effect of Dwell Time on Sinh Model Coefficients C_2 and C_4 for Waspaloy

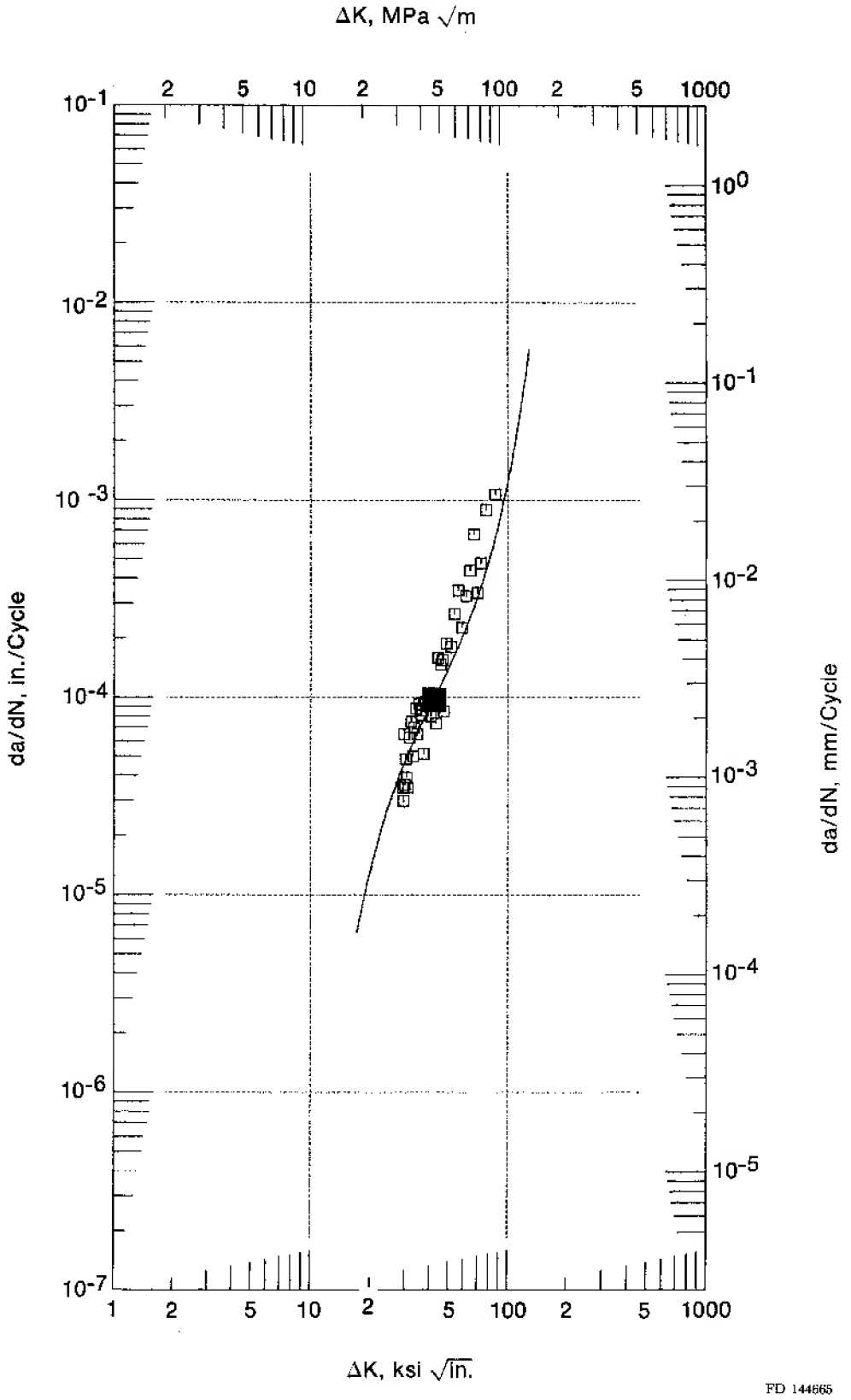

Figure 88. HIP-Astroloy Crack Growth Rate for 120-sec Dwell, R = 0.05, 650°C (1200°F)

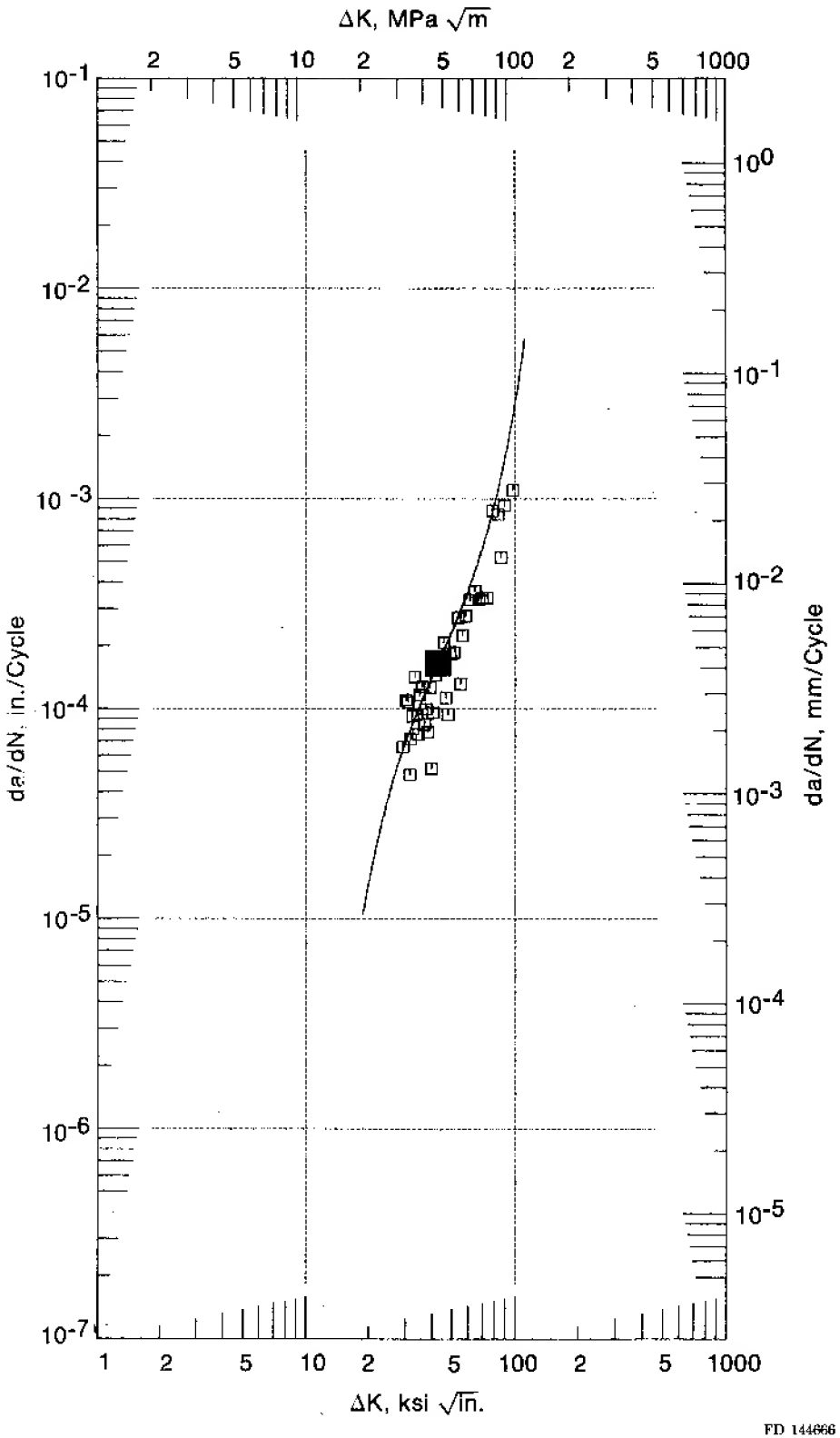

Figure 89. HIP-Astroloy Crack Growth Rate for 300-sec Dwell, R = 0.05, 650°C (1200°F)

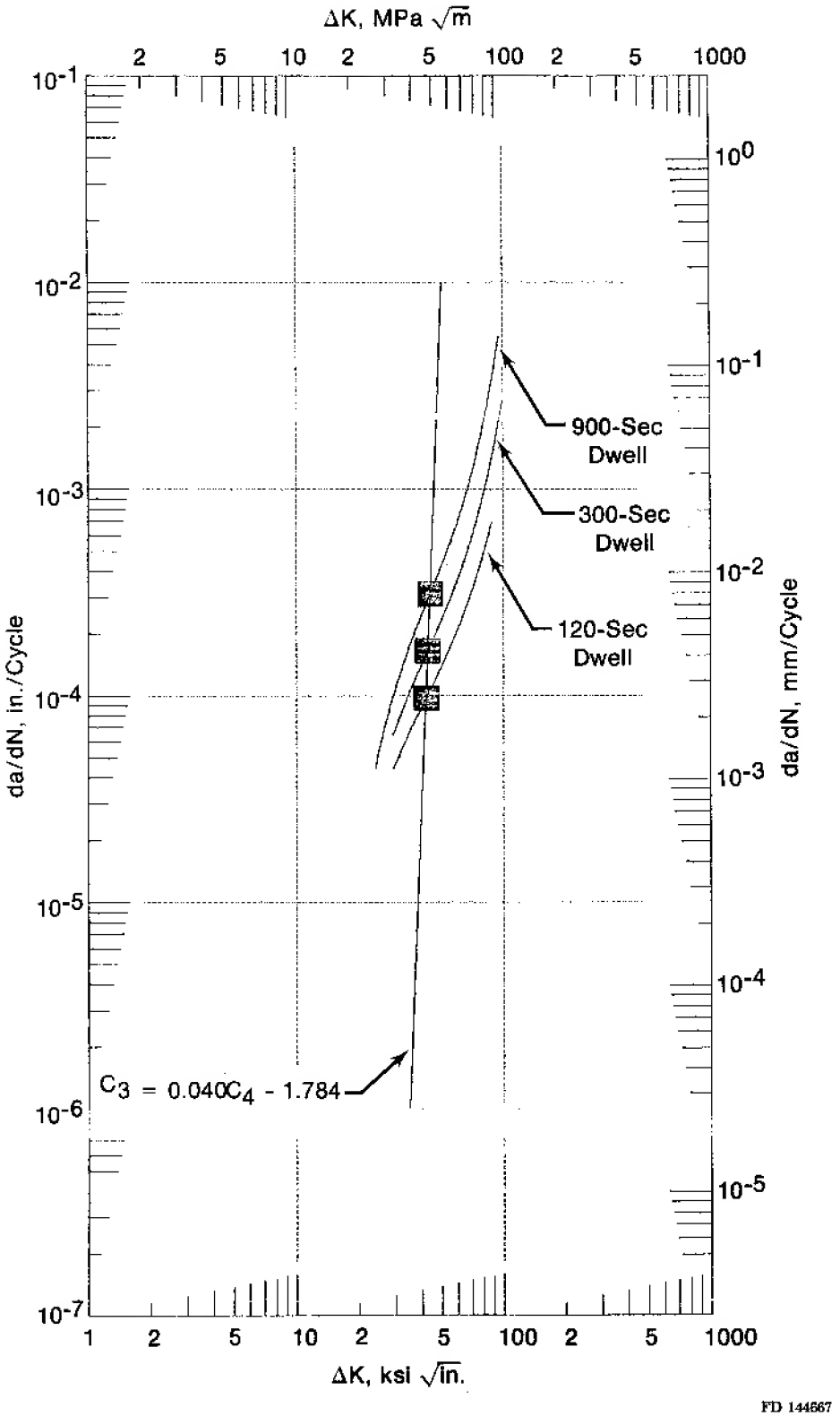

Figure 90. Comparison of 120-, 300-, and 900-sec Dwell Crack Growth Rates at 650°C (1200°F), R = 0.05 for HIP-Astroloy

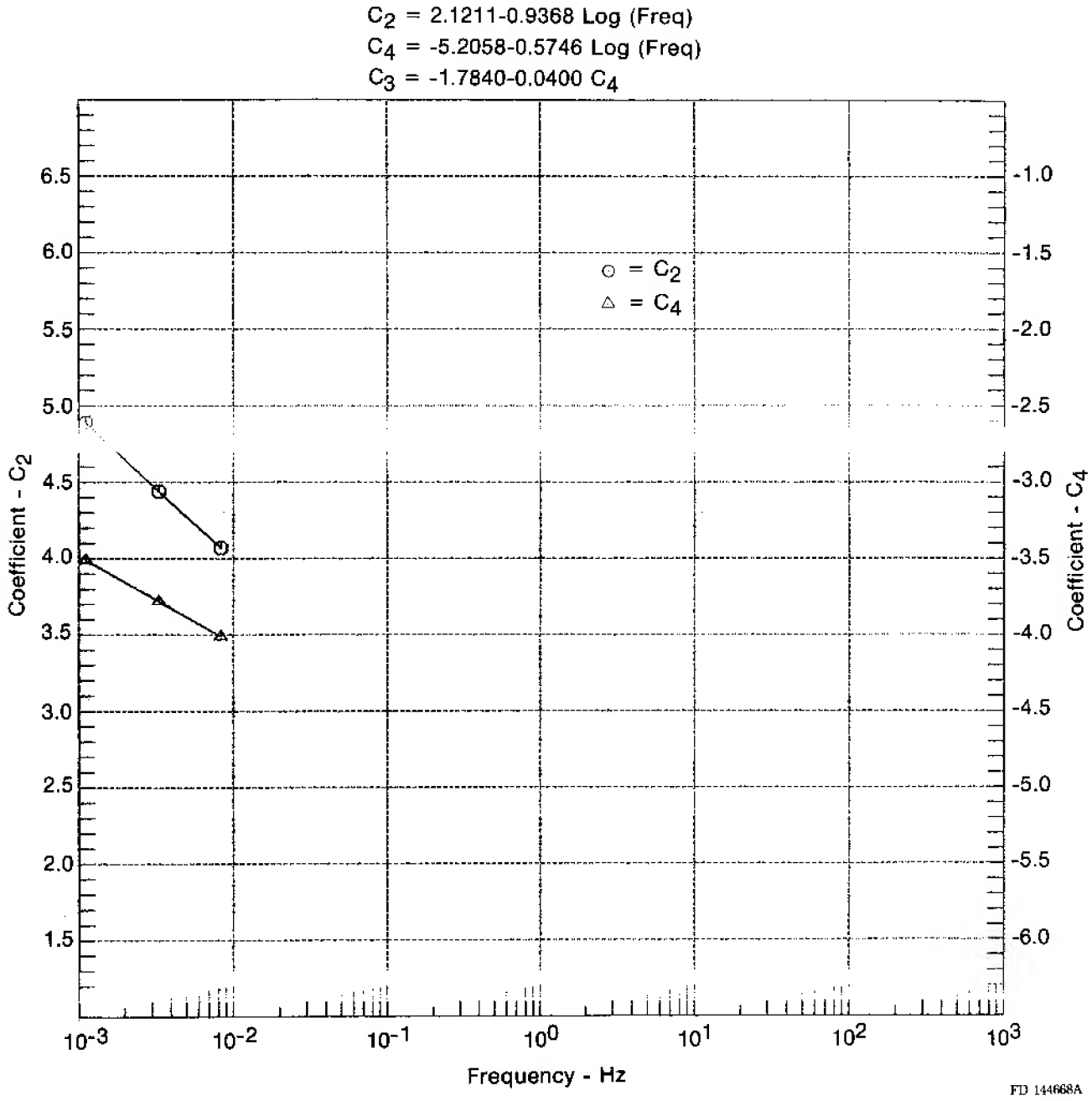

Figure 91. Effect of Dwell Time on Sinh Model Coefficients C_2 and C_4 for HIP-Astroloy

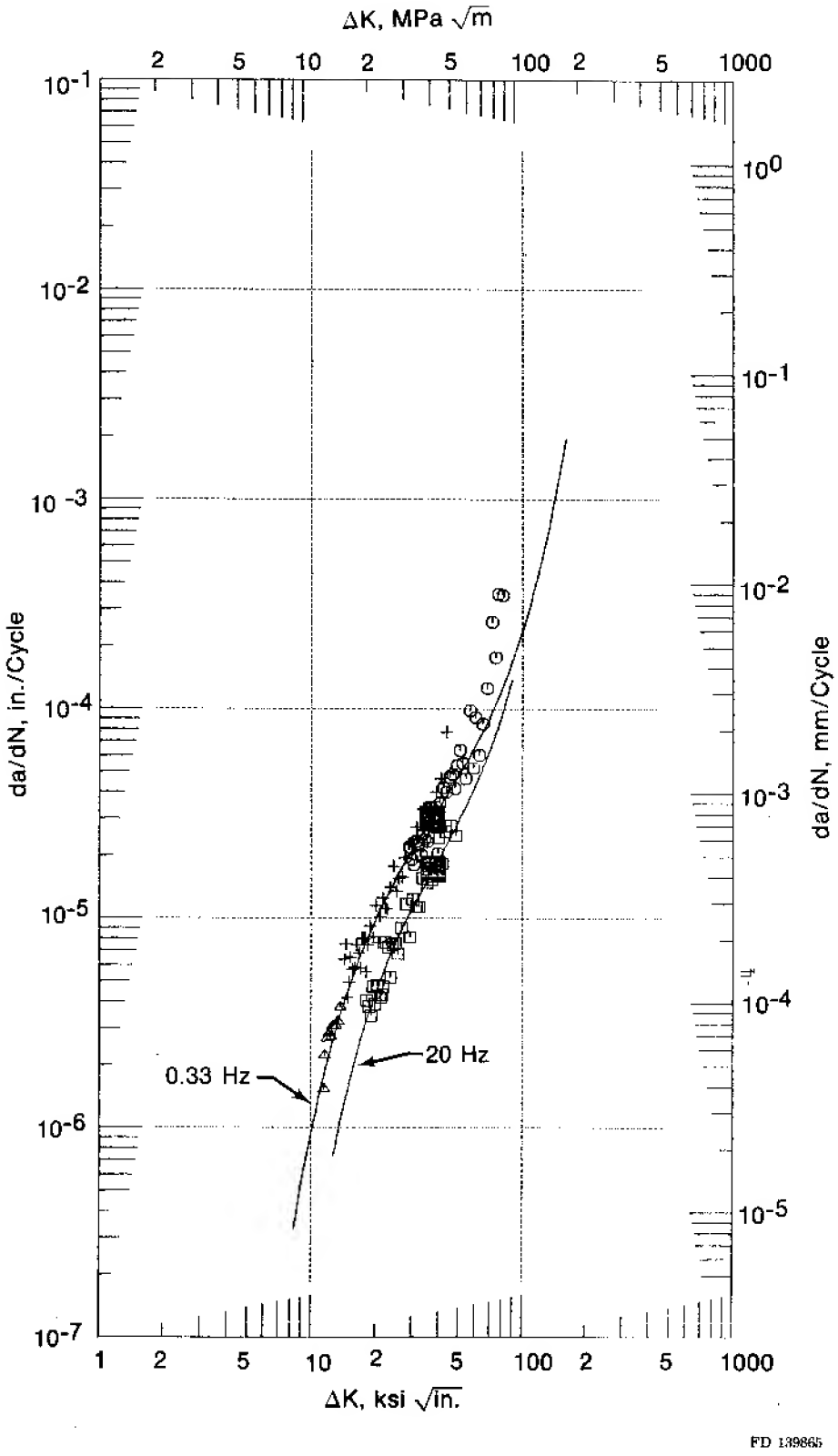

Figure 92. Effect of Frequency on Waspaloy Crack Growth Rate at R = 0.05, 650°C (1200°F)

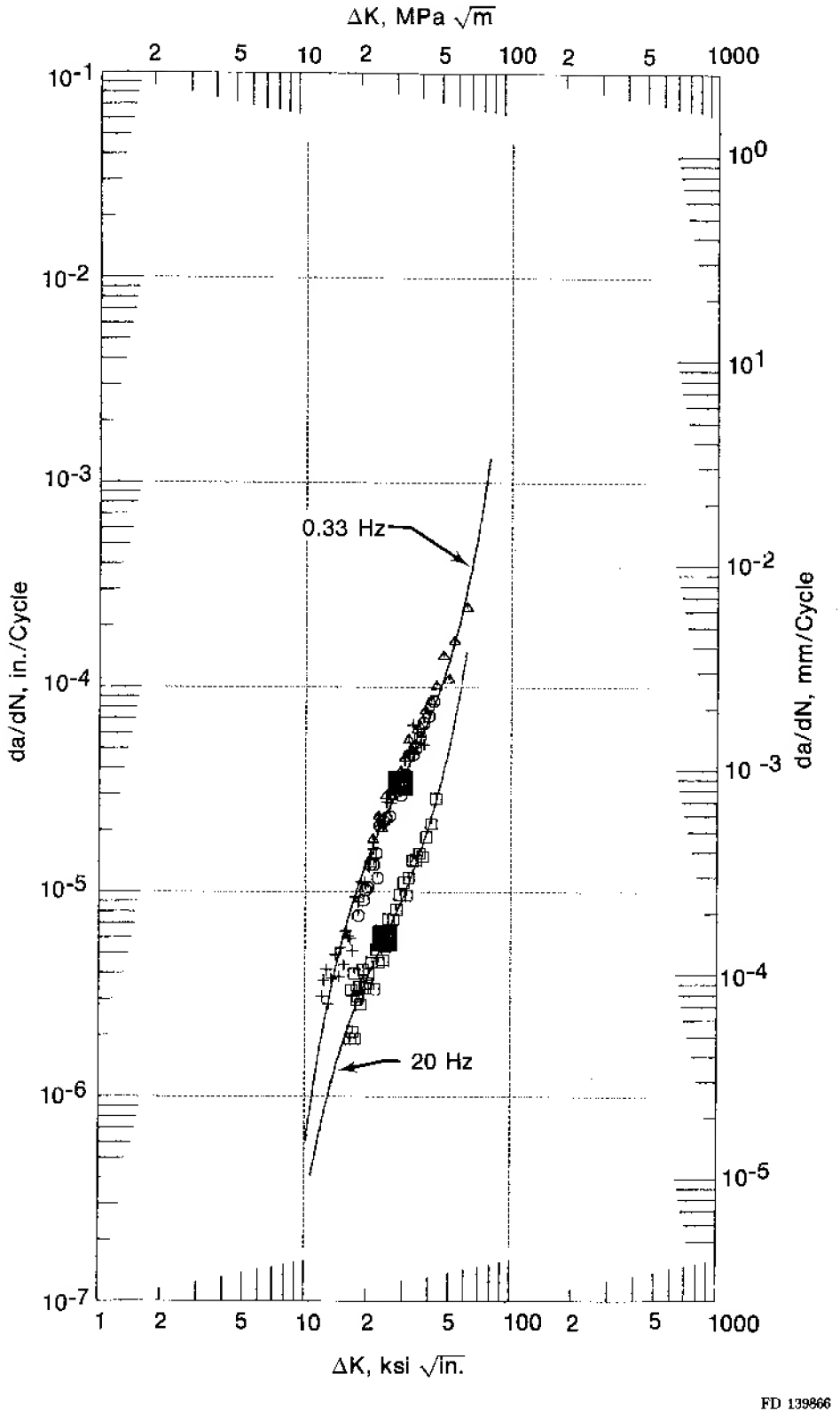

Figure 93. Effect of Frequency on Wrought Astroloy Crack Growth Rate at R = 0.05, 650°C (1200°F)

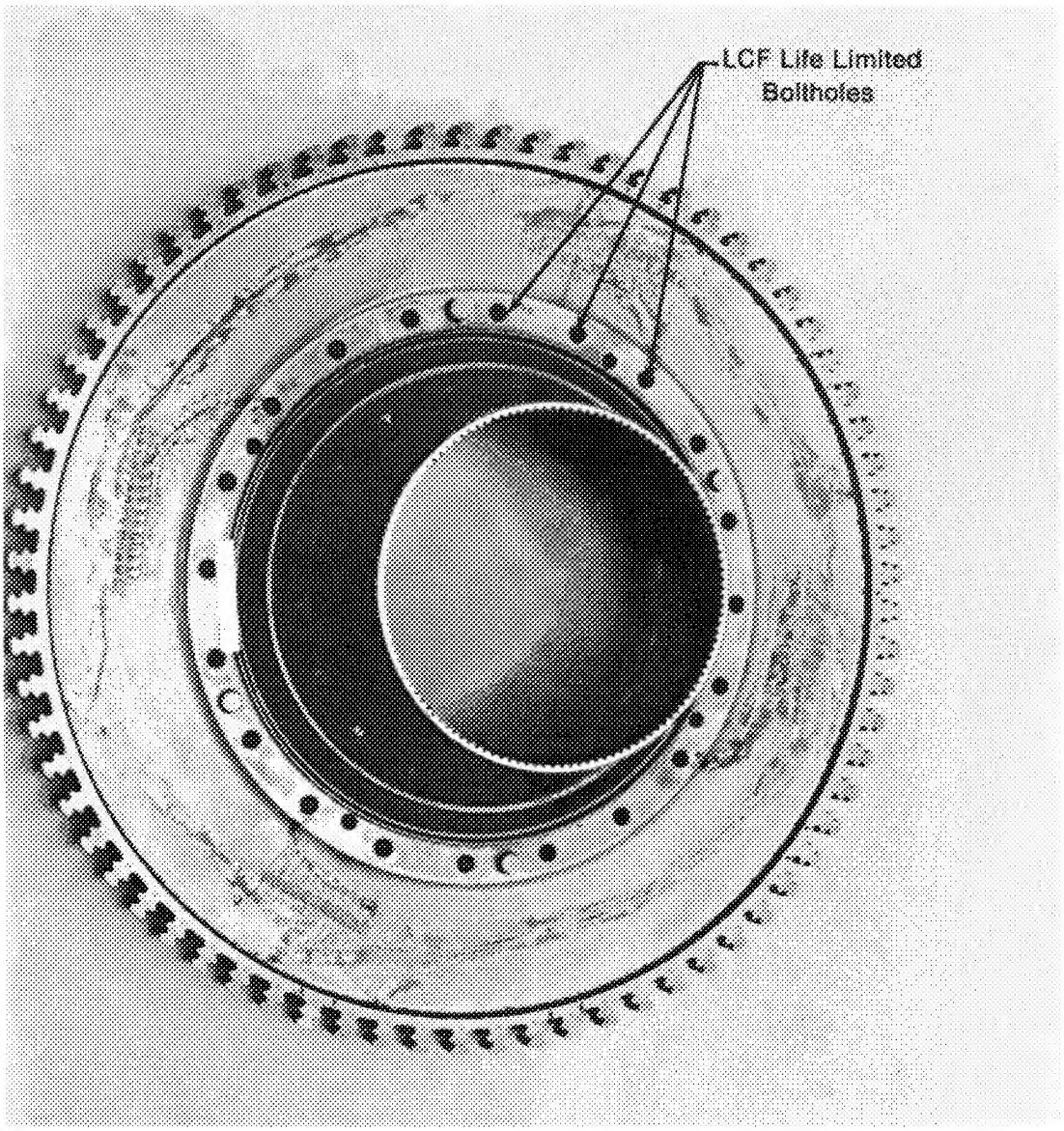

FE 169462A

Figure 94. F100 2nd-Stage Turbine Disk (Frontal View)

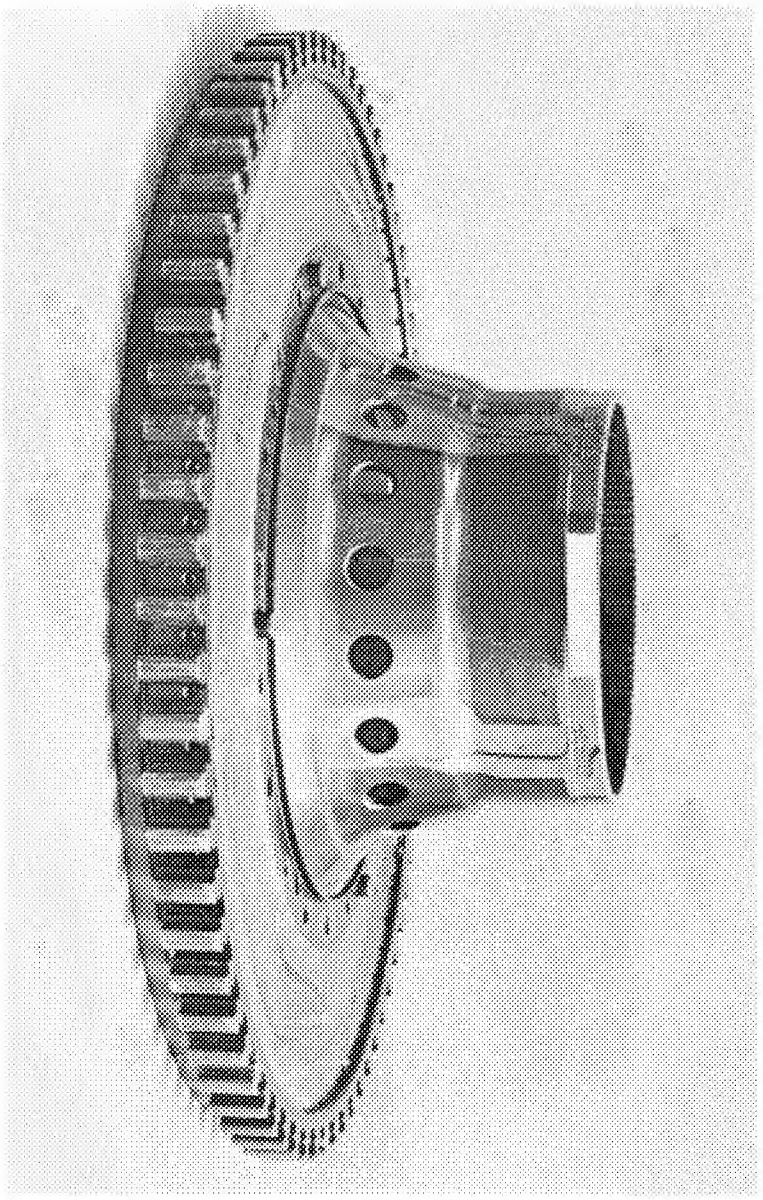

FE 169463

Figure 95. F100 2nd-Stage Turbine Disk (Side View)

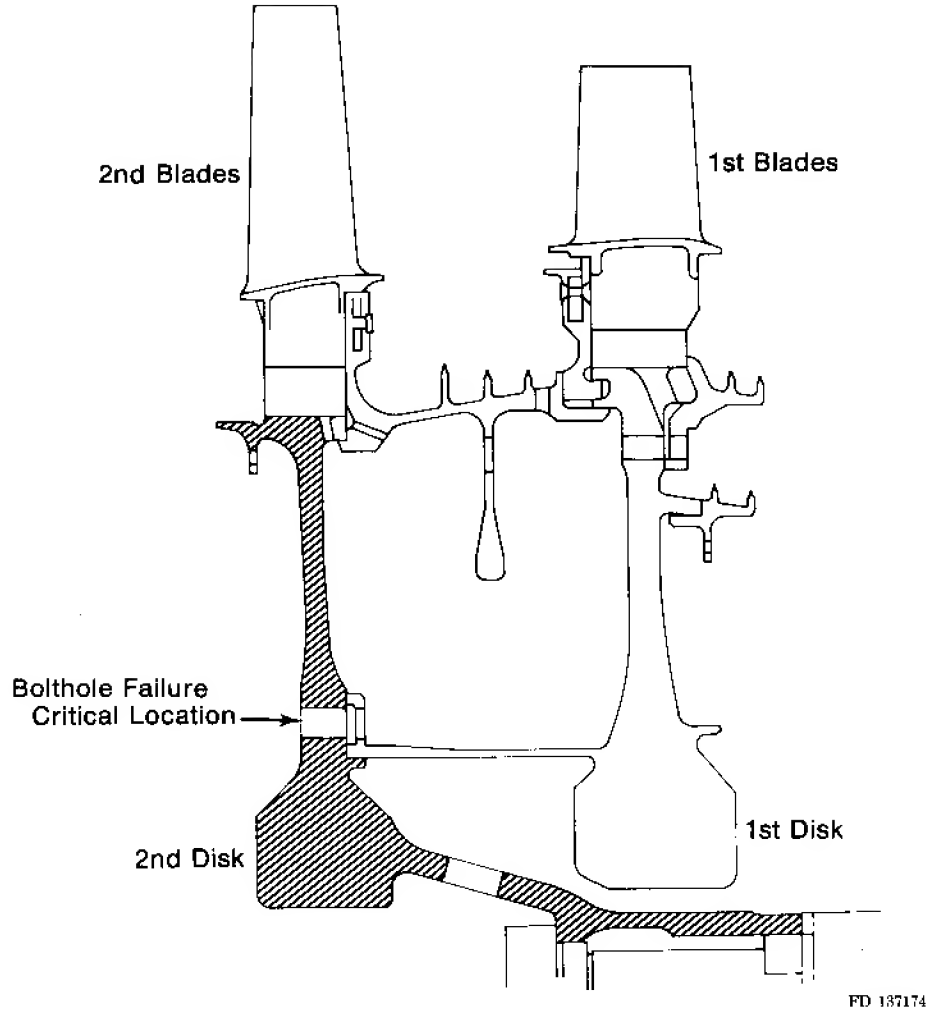

Figure 96. Advanced 2nd-Stage High-Pressure Turbine Disk Cross Section

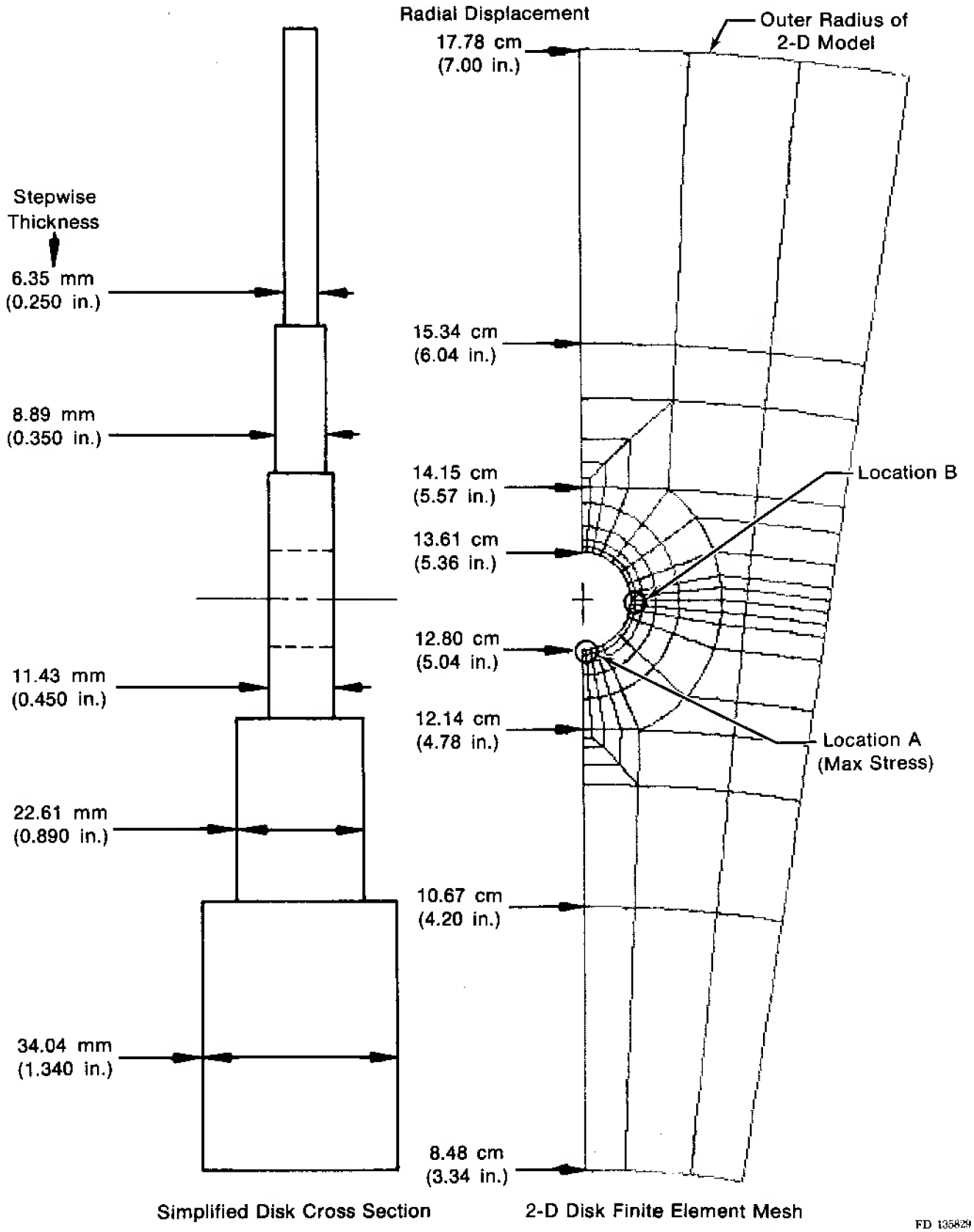

Figure 97. Idealized 2-D Finite Element Mesh and Stepwise Cross Section for Elastic-Plastic Analysis of an Advanced F100 2nd-Stage Turbine Disk

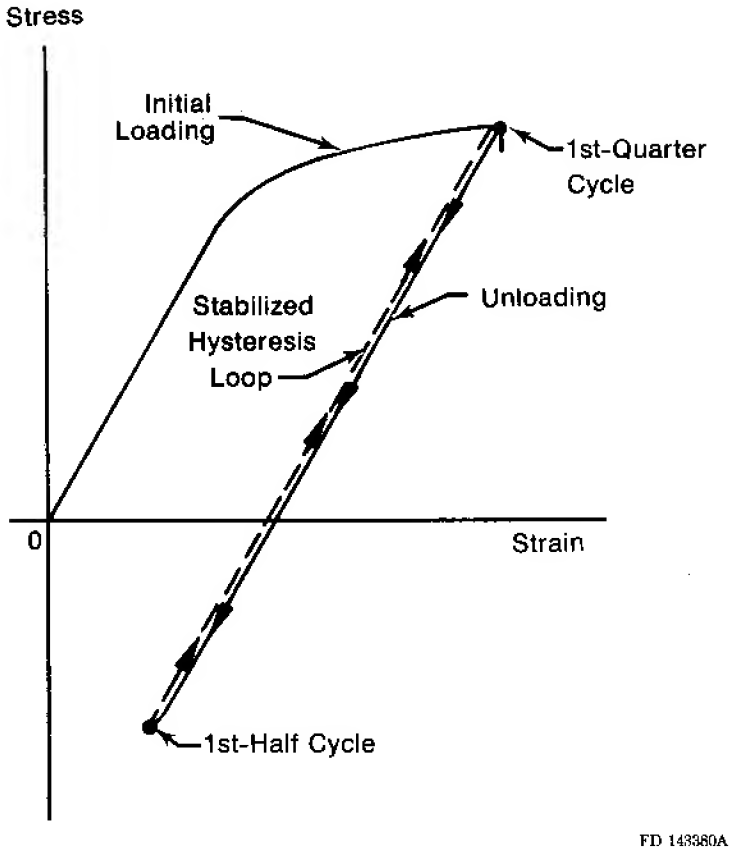

Figure 98. Typical 1st-Cycle Disk Loading Material Response

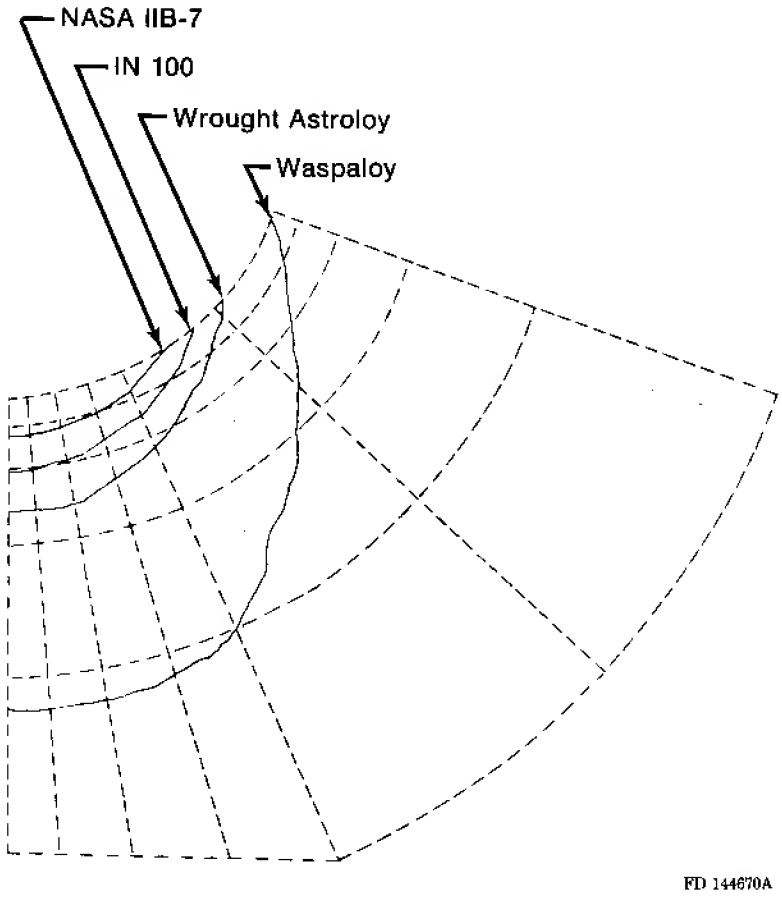

Figure 99. Von Mises Yield Surfaces

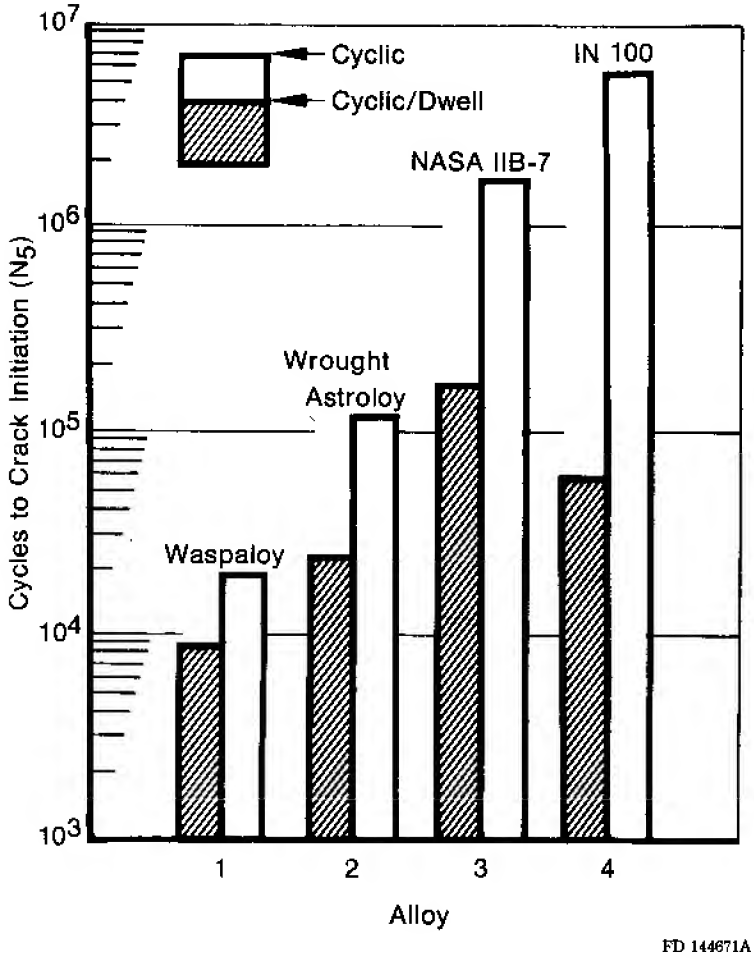

Figure 100. Predicted Disk Cyclic and Cyclic/Dwell Crack Initiation Lives for Four Alloys

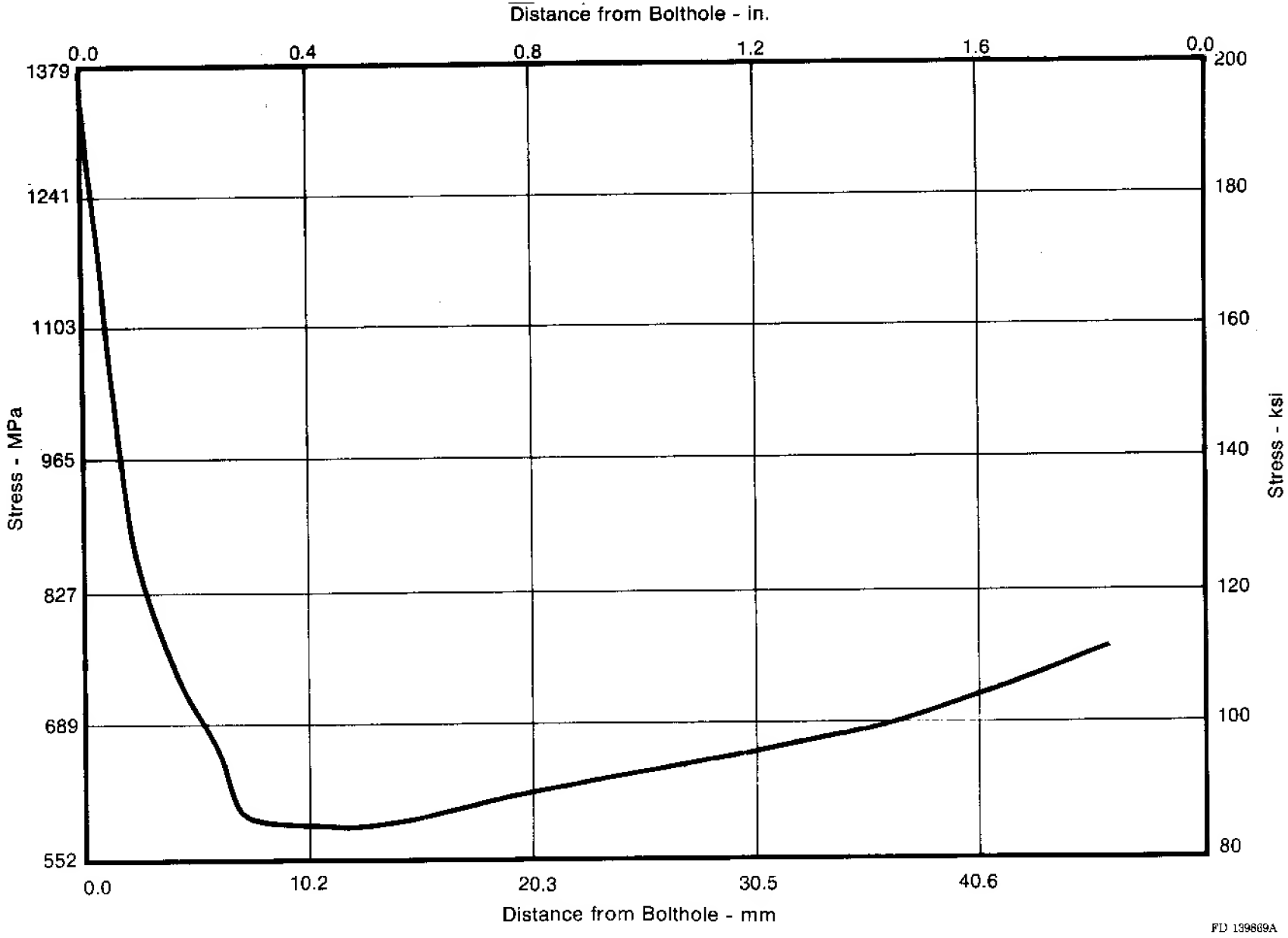

Figure 101. Uncracked Stress Distribution Around the Bolthole for Waspaloy

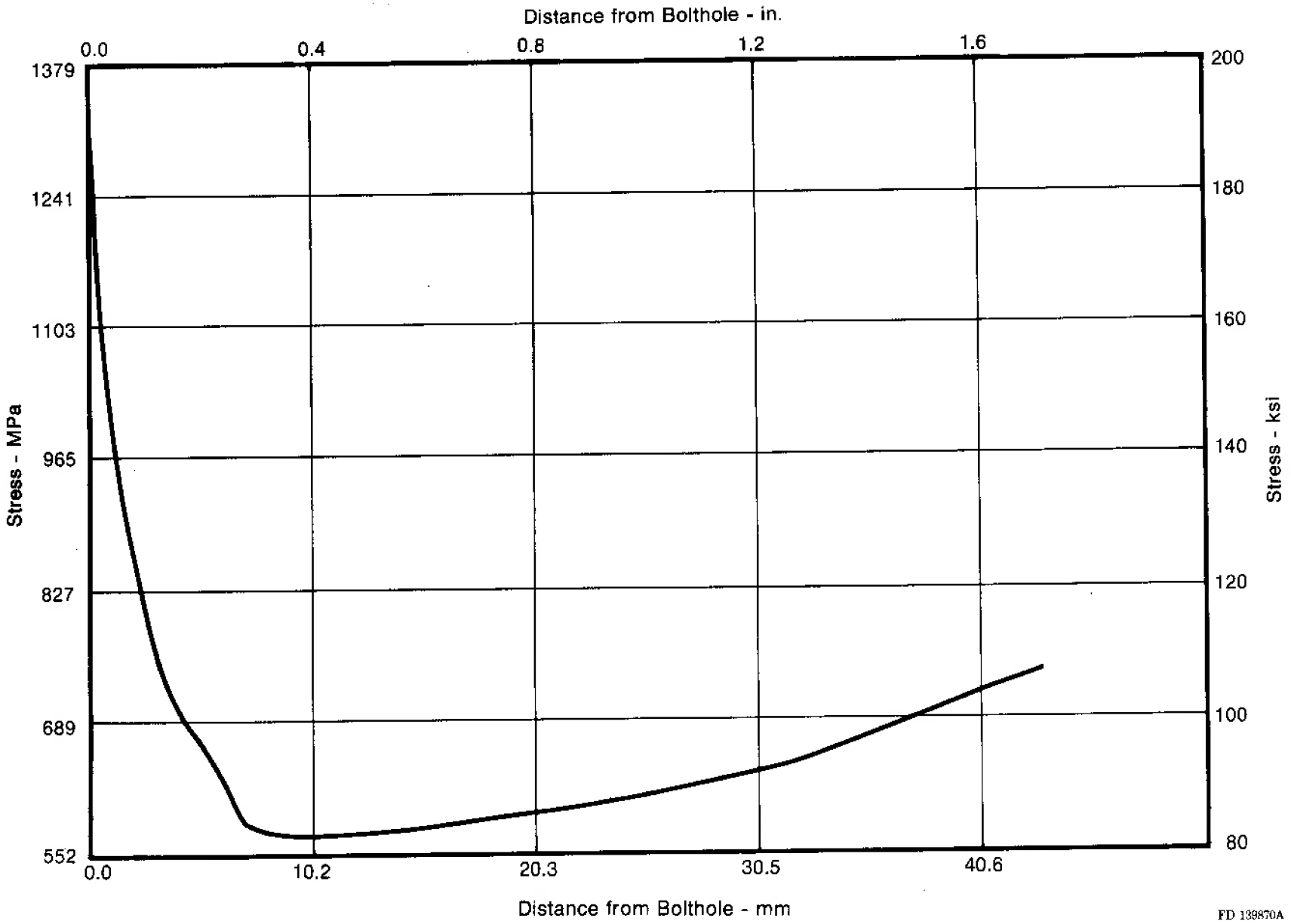

Figure 102. Uncracked Stress Distribution Around the Bolthole for Wrought Astroloy

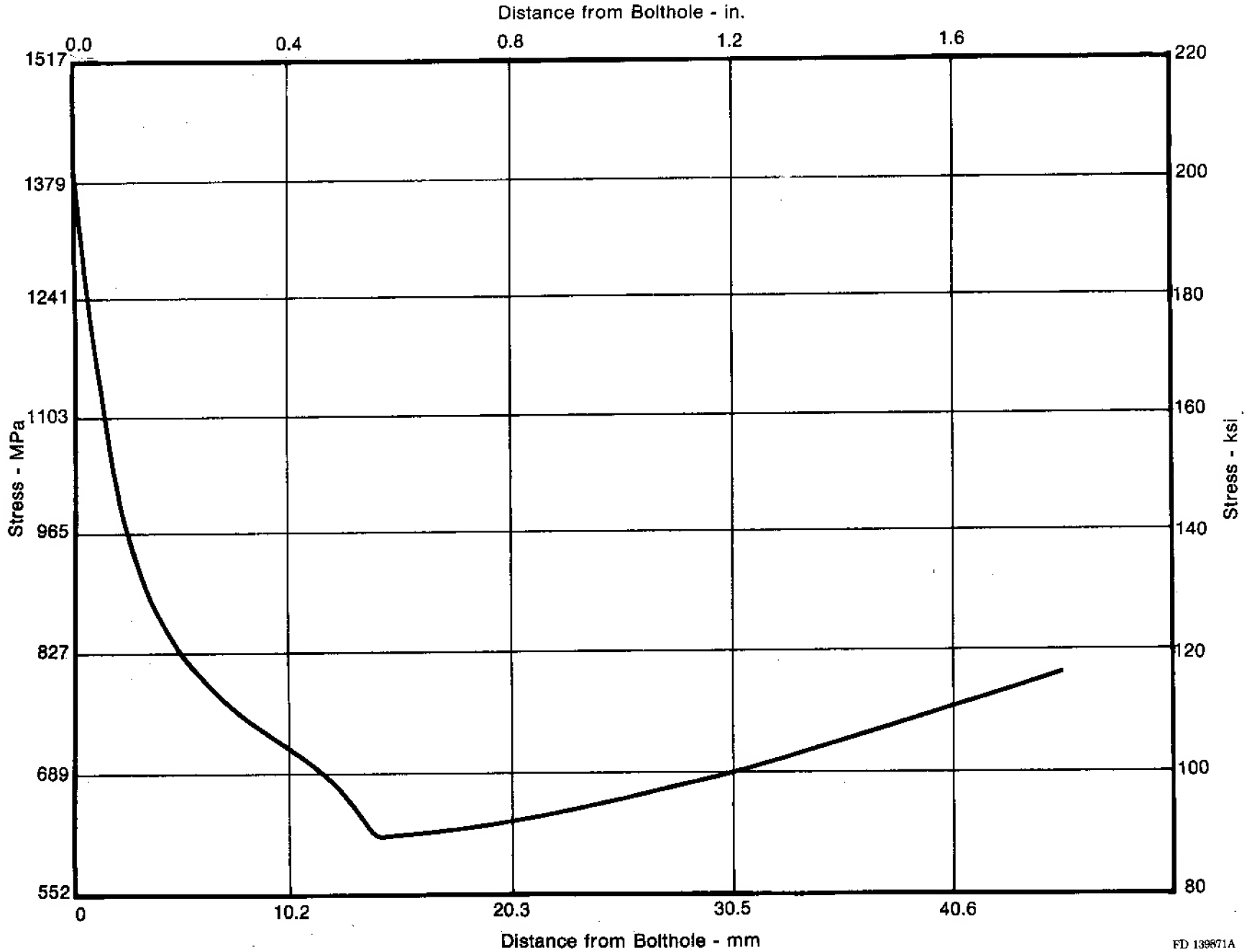

Figure 103. Uncracked Stress Distribution Around the Bolthole for NASA IIB-7

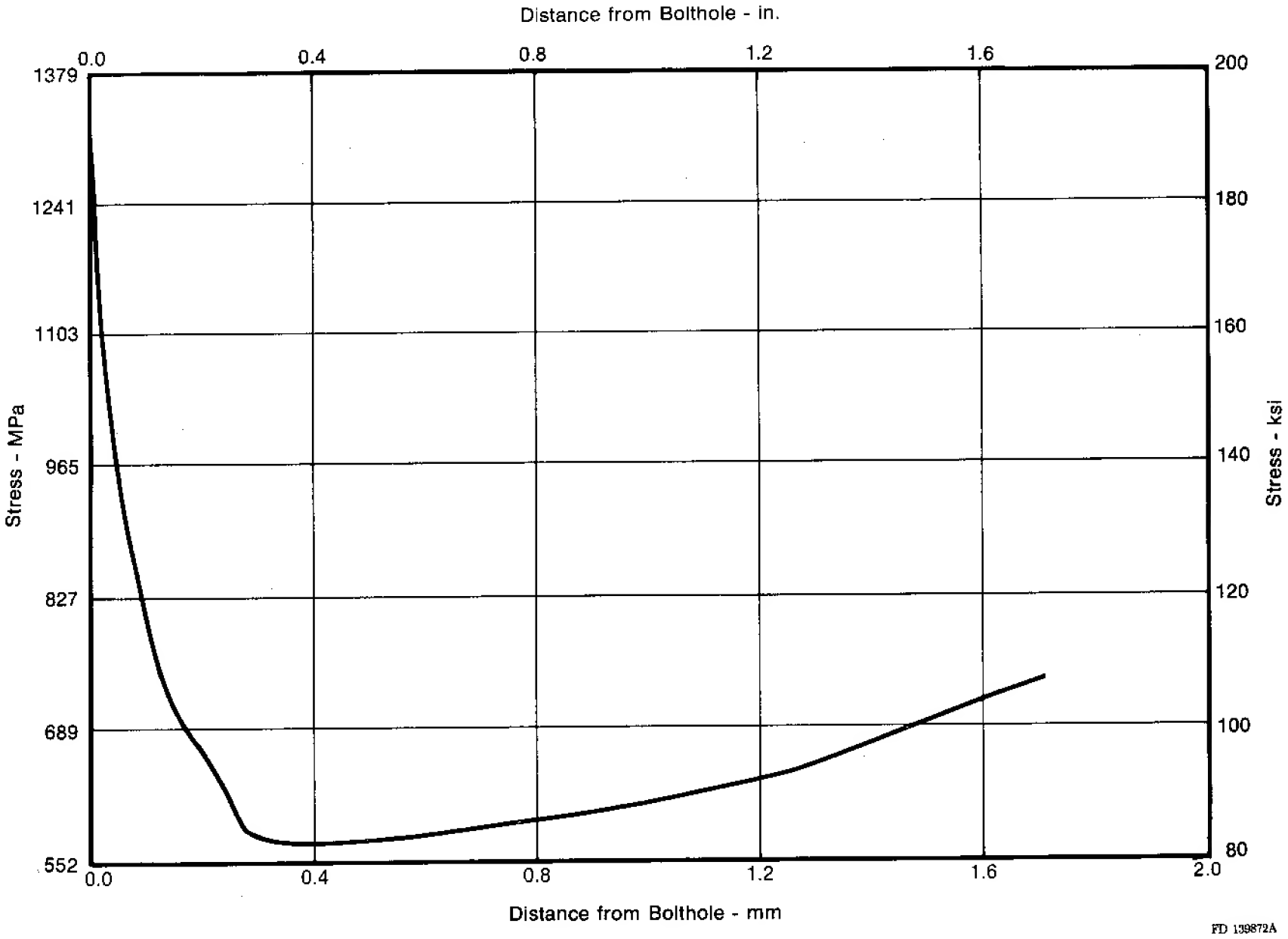

Figure 104. Uncracked Stress Distribution Around the Bolthole for IN 100

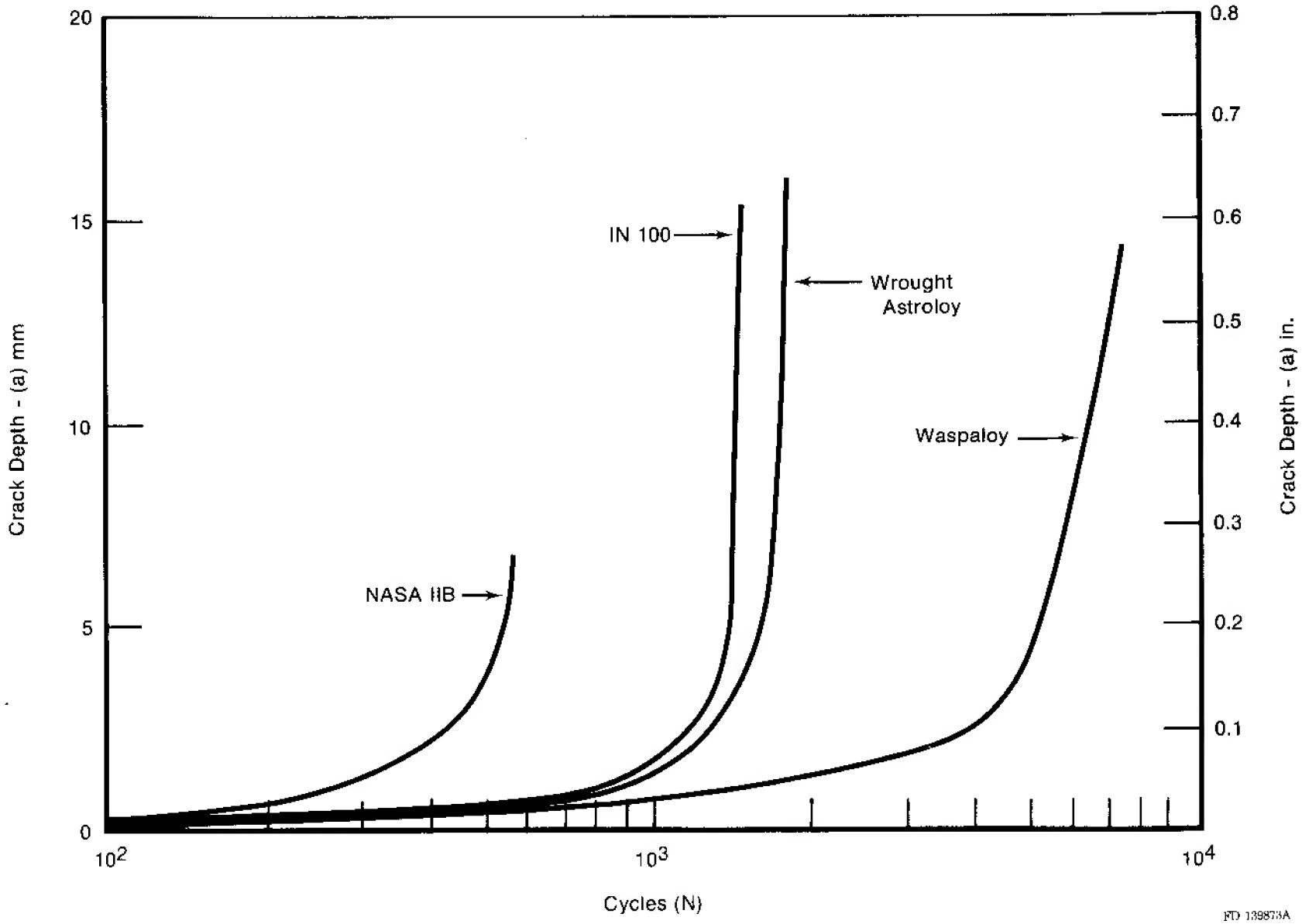

Figure 105. Life Prediction Comparisons Using 0.33 Hz Crack Growth Data

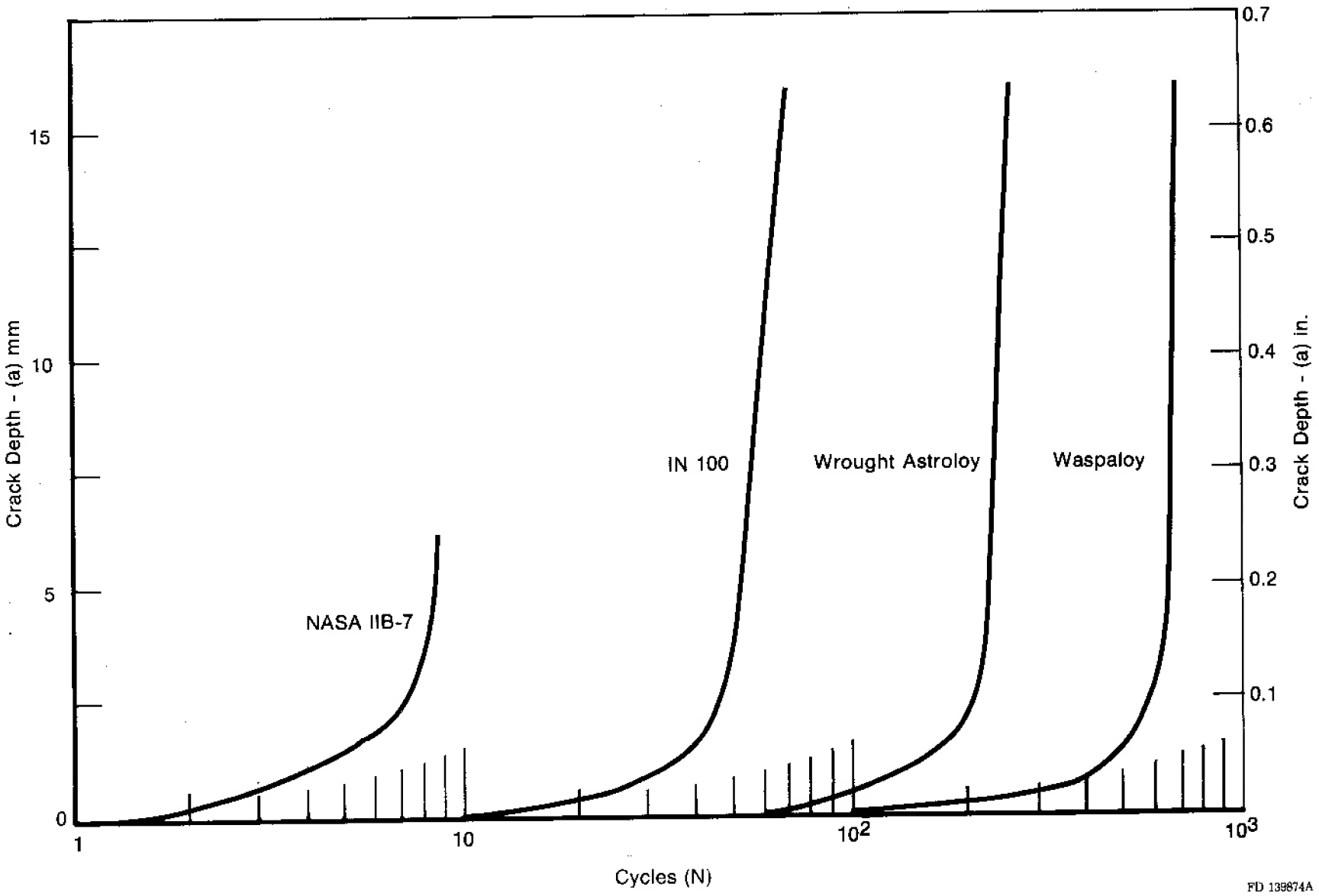

Figure 106. Life Prediction Comparison Using 900-sec Dwell Crack Growth Data

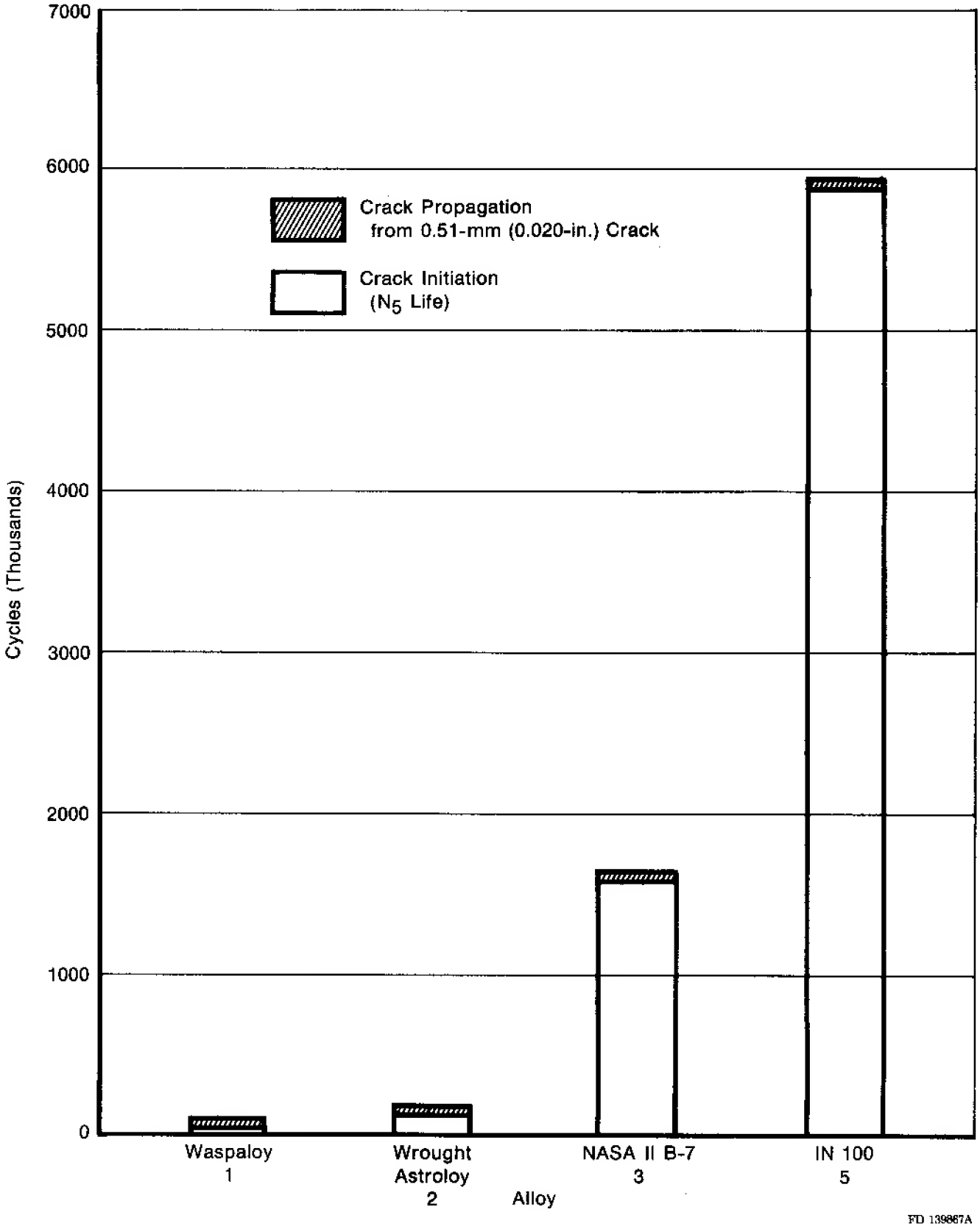

Figure 107. Comparison of Total Predicted Disk LCF Life for Cycle (0.33 Hz) Conditions

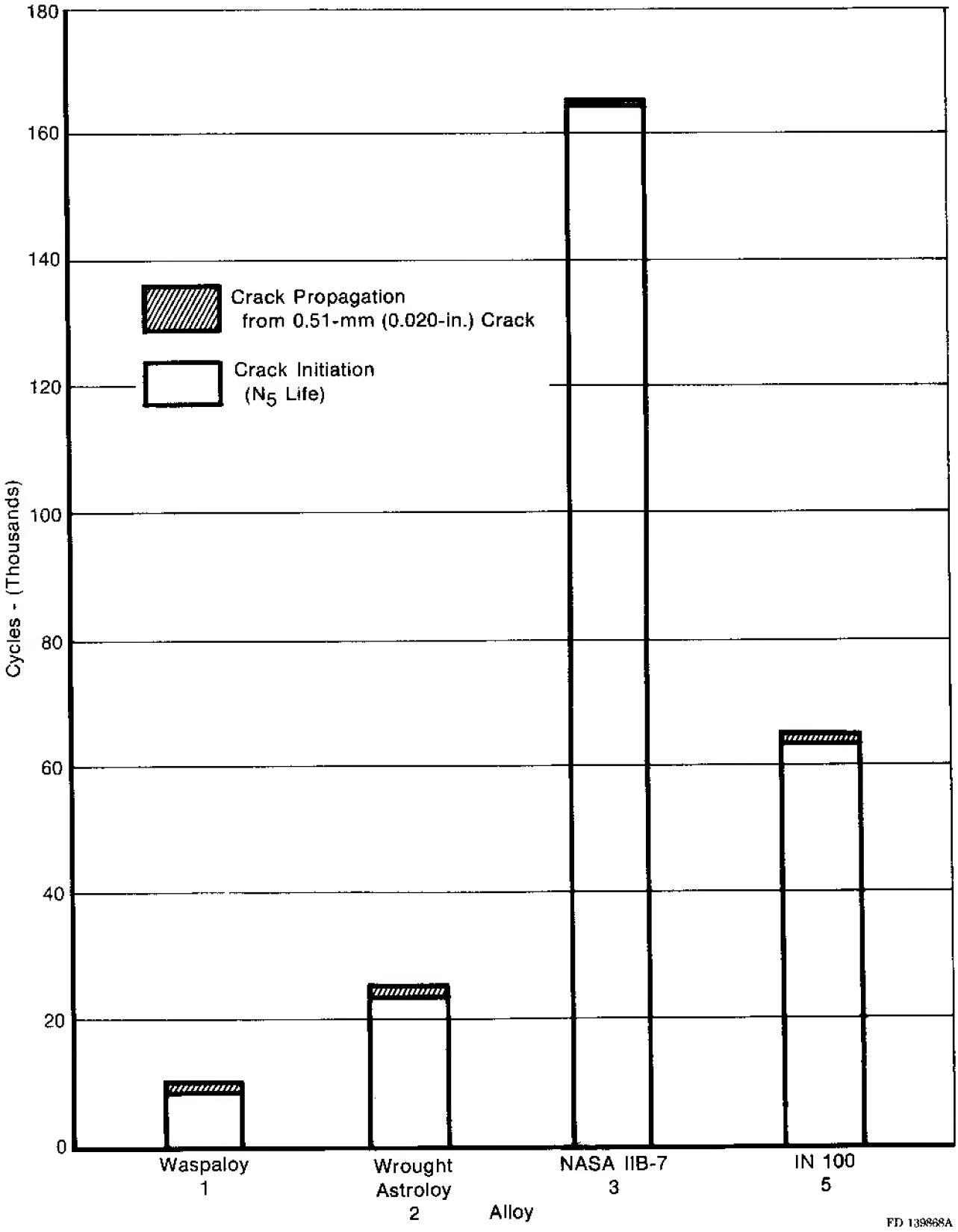

Figure 108. Comparison of Total Predicted Disk LCF Life for Cyclic/Dwell Conditions

TABLE I. CHEMICAL COMPOSITIONS[1] AND HEAT TREATMENTS OF AIRCRAFT TURBINE DISK ALLOYS EVALUATED FOR CYCLIC BEHAVIOR

Element	*Alloy 1 Waspaloy*	*Alloy 2 Wrought Astroloy*	*Alloy 3[2] NASA IIB-7*	*Alloy 4 HIP Astroloy*	*Alloy 5 GATORIZED® IN100*
Carbon	0.06	0.04	0.10	0.03	0.07
Manganese	0.75 max	0.15 max	-	0.15 max	0.020 max
Sulfur	0.02 max	0.015 max	-	0.015 max	0.010 max
Phosphorus	-	0.015 max	-	0.015 max	0.010 max
Silicon	0.75 max	0.20 max	-	0.20 max	0.10 max
Chromium	19.5	15.0	9.0	15.0	12.40
Cobalt	13.5	17.0	9.0	17.0	18.50
Molybdenum	4.0	5.0	2.0	5.0	3.20
Titanium	3.0	3.5	0.70	3.5	4.32
Aluminum	1.4	4.0	3.35	4.0	4.97
Boron	0.065	0.025	0.02	0.02	0.02
Zirconium	0.07	0.06 max	0.10	0.045	0.06
Tungsten	-	0.05 max	7.6	0.05 max	0.05 max
Iron	2.0 max	0.50 max	-	0.50 max	0.30 max
Copper	0.10 max	0.10 max	-	0.10 max	0.07 max
Lead	10 ppm max	10 ppm max	-	10 ppm max	0.0002 max
Tantalum[3]	-	-	10.0	-	0.04 max
Vanadium	-	-	0.5	-	0.78
Hafnium	-	-	1.0	-	-
Nickel	Balance	Balance	Balance	Balance	Balance
Heat Treatment[4]					
Solution, Stabilization, and Age	1024/4/OQ	1108/4/AC	899/16/to	1108/3/AC	1121/2/OQ
	843/4/AC	871/8/AC	1094/1/OQ	871/8/AC	871/40 min/AC
		982/4/AC		982/4/AC	
	760/4/AC	649/24/AC	760/16/AC	649/24/AC	649/24/AC
		760/8/AC		760/8/AC	760/4/AC

[1]Nominal Composition — Percent by Weight
[2]Universal-Cyclops, NAS3-14309, (Reference 1)
[3]Tantalum and Columbium for Alloy 5
[4]Heat Treat Conditions — Nominal Temperature — °C/Time-hr/Air Cool — AC, Oil Quench — OQ

TABLE II. QUALIFICATION TEST RESULTS — ALLOY 1, WROUGHT WASPALOY PRODUCED FROM INGOT

Producer: Ladish Company
Heat Code: LRKB 2017

	Required	*Actual*
Chemical Composition:*		
Carbon	0.02 to 0.10	0.04
Manganese	0.75 max	0.01
Sulfur	0.020 max	0.005
Silicon	0.75 max	0.03
Chromium	18.0 to 21.0	19.25
Cobalt	12.0 to 15.0	13.58
Molybdenum	3.5 to 5.0	4.22
Titanium	2.75 to 3.25	3.09
Aluminium	1.20 to 1.60	1.29
Zirconium	0.02 to 0.12	0.048
Boron	0.003 to 0.010	0.0051
Iron	2.0 max	0.68
Copper	0.10 max	0.01
Bismuth	0.5 ppm max	0.5 ppm
Lead	10 ppm max	3.0 ppm
Nickel	Balance	57.48
Heat Treatment:	1010°C to 1038°C/4/OQ 843°C/4/AC 760°C/16/AC	1016°C/4/OQ 843°C/4/AC 760°C/16/AC

	Ultimate	*0.2% Yield*	*%EL*	*%RA*
Tensile Properties:				
Room Temperature				
Required Minimum	1241 MPa	862 MPa	15	18
Actual	1377 MPa	1060 MPa	21	31
538°C				
Required Minimum	1103 MPa	758 MPa	15	18
Actual	1240 MPa	935 MPa	22	28

	Required Minimum		*Actual*	
	Time	*% EL*	*Time*	*% EL*
Stress Rupture Strength:				
732°C, 552 MPa	23 hr	12	56.8 hr	18
816°C, 293 MPa	23 hr	12	42.5 hr	26

*Percent by weight unless noted.

TABLE III. QUALIFICATION TEST RESULTS — ALLOY 2, WROUGHT ASTROLOY PRODUCED FROM PRE-ALLOYED POWDER

Powder Source: Special Metals, Forging Vendor: Wyman Gordon, Heat Code: XNOE-5

	Required		
Chemical Composition	*Minimum*	*Maximum*	*Actual*
Carbon	0.02	0.06	0.024
Manganese	-	0.15	-
Sulfur	-	0.015	-
Phosphorus	-	0.015	-
Silicon	-	0.20	-
Chromium	14.0	16.00	14.71
Cobalt	16.00	18.00	17.15
Molybdenum	4.50	5.50	4.98
Titanium	3.35	3.65	3.56
Aluminum	3.85	4.15	4.06
Boron	0.020	0.030	0.027
Zirconium	-	0.06	0.002
Tungsten	-	0.05	-
Iron	-	0.50	-
Copper	-	0.10	-
Lead	-	0.0010 (10 ppm)	-
Bismuth	-	0.00005 (0.5 ppm)	-
Oxygen	-	0.010 (100 ppm)	0.0078
Nitrogen	-	0.0050 (50 ppm)	-
Nickel	Remainder		Balance
Heat Treatment:		1079°C to 1135°C/4 hr/AC 871°C/8 hr/AC to RT 982°C/4 hr/AC 649°C/24 hr/AC to RT 760°C/8 hr/AC	1107°C/4 hr/AC 871°C/8 hr/AC to RT 982°C/4 hr/AC 649°C/24 hr/AC to RT 760°C/8 hr/AC

	Ultimate	*0.2% Yield*	*%EL*	*%RA*
Tensile Properties:				
Room Temperature				
Required Minimum	1345 MPa	965 MPa	16	18
Actual	1517 MPa	1055 MPa	23	27
760°C				
Required Minimum	1134 MPa	862 MPa	20	30
Actual	1069 MPa	951 MPa	25	38

	Required Minimum		*Actual*	
	Time	*% EL*	*Time*	*%EL*
Stress Rupture Strength: 760°C, 586 MPa	15 hr	12	62 hr	12

	Required Minimum Time to 0.1% Offset	*Actual*
Creep Strength: 704.4°C, 510 MPa	110 hr	110 hr

TABLE IV. QUALIFICATION TEST RESULTS — ALLOY 3, NASA IIB-7 PRODUCED FROM PREALLOYED POWDER

Producer: Universal Cyclops
Heat: KR 376-8

	Nominal	*Actual*
Chemical Composition:*		
Carbon	0.10	0.12
Manganese	-	<0.05
Sulfur	-	0.003
Phosphorus	-	0.004
Silicon	-	<0.10
Chromium	9.0	8.93
Cobalt	9.0	9.09
Molybdenum	2.0	1.95
Titanium	0.70	0.75
Aluminium	3.35	3.43
Boron	0.02	0.023
Zirconium	0.10	0.08
Tungsten	7.6	7.64
Iron	-	0.19
Copper	-	<0.10
Lead	-	< 1 ppm
Bismuth	-	<0.2 ppm
Oxygen	-	8 ppm
Tantalum	10.0	10.1
Vanadium	0.5	0.51
Hafnium	1.0	1.03
Selenium	-	<0.5 ppm
Thallium	-	<1 ppm
Tellurium	-	<0.5 ppm
Nickel	Balance	Balance
Heat Treatment:	899/16 hr to 1094°C/1 hr/OQ 760°C/16 hr/AC	899°C/16 hr to 1094°C/1 hr/OQ 760°C/16 hr/AC

	Ultimate	*0.2% Yield*	*%EL*	*%RA*
Tensile Properties:				
Room Temperature				
Actual	1770 MPa	1439 MPa	10.1	10.9
Actual	1775 MPa	1438 MPa	9.9	11.4
650°C				
Actual	1537 MPa	1327 MPa	5.3	10.3
Actual	1556 MPa	1328 MPa	6.9	9.5

	Actual		
	Time	*%EL*	*%RA*
Stress Rupture Strength:			
650°C/120/MPa	58.4 hr	2.8	3.3
	51.2 hr	1.8	1.4

*Percent by weight unless noted.

TABLE V. QUALIFICATION TEST RESULTS — ALLOY 4, ASTROLOY PRODUCED AS A HIP FORM FROM PREALLOYED POWDER

Producer: Udimet Powder
KBI Industries for HIP
Heat Code: PUVK-4

	Required	*Actual*
Chemical Composition:*		
Carbon	0.02 to 0.06	0.023
Manganese	0.15 max	0.001
Sulfur	0.015 max	0.003
Phosphorus	0.015 max	<0.005
Silicon	0.20 max	0.06
Chromium	14.0 to 16.0	15.1
Cobalt	16.0 to 18.0	17.0
Molybdenum	4.5 to 5.5	5.2
Titanium	3.35 to 3.65	3.5
Aluminum	3.85 to 4.15	4.0
Boron	0.02 to 0.03	0.024
Zirconium	0.06 max	<0.01
Tungsten	0.05 max	<0.05
Iron	0.5 max	0.09
Copper	0.1 max	<0.05
Lead	10 ppm max	<1 ppm
Bismuth	0.5 ppm max	<0.3 ppm
Oxygen	100 ppm max	80 ppm
Nitrogen	50 ppm max	23 ppm
Nickel	Balance	Balance
Heat Treatment:	1079°C to 1135°C/2 to 4/AC 871°C/8/AC 982°C/4/AC 648°C/24/AC 760°C/8/AC	1107°C/3/AC 871°C/8/AC 982°C/4/AC 648°C/24/AC 760°C/8/AC

	Ultimate	*0.2% Yield*	*%EL*	*%RA*
Tensile Properties:				
Room Temperature				
Required Minimum	1241 MPa	862 MPa	15	18
Actual	1393 MPa	936 MPa	26	31
538°C				
Required Minimum	1103 MPa	758 MPa	15	18
Actual	1287 MPa	869 MPa	26	28

	Required Minimum		*Actual*	
	Time	*%EL*	*Time*	*%EL*
Stress Rupture Strength:				
732°C, 552 MPa	23 hr	8	151 hr	16.7

*Percent by weight unless noted.

TABLE VI. QUALIFICATION TEST RESULTS — ALLOY 5, GATORIZED® IN 100 PRODUCED FROM PREALLOYED POWDER

Powder Source: Homogenous Metals, Forging Vendor: P&WA, Heat Code: BAKY H45-A5

	Required		
Chemical Composition	*Minimum*	*Maximum*	*Actual*
Carbon	0.05	0.09	<0.090
Manganese	-	0.020	0.01
Sulfur	-	0.010	0.004
Phosphorus	-	0.010	0.004
Silicon	-	0.10	0.018
Chromium	11.90	12.90	12.02
Cobalt	18.00	19.00	18.36
Molybdenum	2.80	3.60	3.10
Titanium	4.15	4.50	4.50
Aluminum	4.80	5.15	4.95
Vanadium	0.58	0.98	0.76
Boron	0.016	0.024	0.019
Zirconium	0.04	0.08	0.063
Tungsten	-	0.05	<0.01
Iron	-	0.30	0.14
Copper	-	0.07	<0.005
Columbium and Tantalum	-	0.04	<0.01
Lead*	-	0.0002 (2 ppm)	<1 ppm
Bismuth*	-	0.00005 (0.5 ppm)	<0.5 ppm
Oxygen	-	0.010 (100 ppm)	<89 ppm
Nickel	Remainder		Balance

*If determined.

Heat Treatment:		1121°C/2 hr/OQ 871°C/40 min/AC to below 371°C 649°C/24 hr/AC to below 371°C 760°C/4 hr/AC to below 371°C	1121°C/2 hr/OQ 871°C/40 min/AC to below 371°C 649°C/24 hr/AC to below 371°C 760°C/4 hr/AC to below 371°C

	Ultimate	*0.2% Yield*	*%EL*	*%RA*
Tensile Properties:				
704°C				
Required Minimum	1172 MPa	1014 MPa	12	12
Actual	1220 MPa	1091 MPa	21	25.9

	Required Minimum		*Actual*	
	Time	*% EL*	*Time*	*% EL*
Stress Rupture Strength:				
732°C, 638 MPa	23 hr	5	33.3 hr	8.5

	Required Minimum Time to 0.2% Offset	*Actual*
Creep Strength:		
704°C, 552 MPa	100 hr	0.029 after 75 hr*

*Creep on integral rings may be discontinued after 75 hr if 0.08% extension has not been exceeded.

TABLE VII. ELEVATED TEMPERATURE TENSILE PROPERTIES FOR ALL ALLOYS

Material	*Heat Code*	*Specimen Number*	*Temperature (°C)*	*Ultimate Strength (MPa)*	*0.2% Yield (MPa)*	*EL (%)*	*RA (%)*
Waspaloy	LRKB-2017	A4	650	1259	967	22.5	28.7
		A8	650	1266	947	20.5	25.2
Wrought Astroloy	XNOE-5	A15	650	1366	1006	23.0	27.8
		A18	650	1348	970	23.0	30.8
NASA IIB-7	KR376-8	12A	650	1532	1285	8.0	11.5
		14A	650	1521	1270	7.0	10.1
HIP Astroloy	PUVK-4	CA4	650	1215	871	31.0	36.3
		DA3	650	1253	891	30.0	36.8
IN 100	BAKY-H45-A5	19	650	1359	1113	22.5	25.3
		20	650	1341	1107	21.0	24.6

TABLE VIII. CONTROLLED STRAIN LCF RESULTS FOR TURBINE DISK ALLOY 1, WASPALOY. TESTING CONDUCTED IN AIR AT 650°C (1200°F), 0.33 Hz (20 cpm) RAMP FREQUENCY, MEAN STRAIN = 0

Spec. S/N	*Type Test*	*Strain (m/m at $N_f/2$)*				*Mean Stress at $N_f/2$*		*Stress Range*		*Cyclic Stability*	*Cycles to Failure*	
		Range	*Elastic*	*Inelastic*	*Creep*	*MPa*	*ksi*	*Cycle 1*	*$N_f/2$*		*N_s%*	*N_f*
A-2	Cyclic	0.0143	0.0109	0.0034	0	−32	− 4.7	1975 MPa (286.5 ksi)	1832 MPa (265.6 ksi)	Soften	730	810
A-3	Cyclic	0.0104	0.0097	0.0007	0	−28	− 4.1	1724 MPa (250.1 ksi)	1688 MPa (244.9 ksi)	Soften	2,900	3,375
A-6	Cyclic	0.0081	0.0080	0.0001	0	+13	+ 1.9	1469 MPa (213.0 ksi)	1469 MPa (213.0 ksi)	Stable	13,150	14,665
A-7	Cyclic	0.0081	0.0080	0.0001	0	0	0	1429 MPa (207.3 ksi)	1394 MPa (202.2 ksi)	Stable	9,130	10,622
A-9	Cyclic	0.0081	0.0080	0.0001	0	0	0	1421 MPa (206.0 ksi)	1416 MPa (205.4 ksi)	Stable	7,067	9,051
A-5	Cyclic	0.0067	0.0067	<0.0001	0	0	0	1167 MPa (169.2 ksi)	1175 MPa (170.4 ksi)	Stable	122,719	128,305
A-10	Cyclic	0.0067	0.0067	<0.0001	0	0	0	1183 MPa (171.5 ksi)	1178 MPa (170.9 ksi)	Stable	141,595	145,630
A-11	Cyclic/ Dwell	0.0113	0.0099	0.0014	0.0002	−61	− 8.8	1906 MPa (276.5 ksi)	1817 MPa (263.5 ksi)	Soften	892	1,061
A-13	Cyclic/ Dwell	0.0112	0.0097	0.0015	0.0002	−77	−11.2	1883 MPa (273.0 ksi)	1804 MPa (261.6 ksi)	Soften	855	976
A-14	Cyclic/ Dwell	0.0081	0.0078	0.0003	0.0001	−28	− 4.0	1535 MPa (222.6 ksi)	1447 MPa (209.8 ksi)	Soften	3,300	3,608
A-15	Cyclic/ Dwell	0.0082	0.0080	0.0002	0.0001	−16	− 2.3	1423 MPa (206.4 ksi)	1405 MPa (203.7 ksi)	Soften	7,930	8,255

Note: Cyclic/Dwell tests have a 900-sec (15 min) hold time at the maximum tensile strain.

TABLE IX. CONTROLLED STRAIN LCF RESULTS FOR TURBINE DISK ALLOY 2, WROUGHT ASTROLOY, TESTING CONDUCTED IN AIR AT 650°C (1200°F), 0.33 Hz (20 cpm) RAMP FREQUENCY, MEAN STRAIN = 0

Spec. S/N	Type Test	Strain (m/m at $N_f/2$)				Mean Stress at $N_f/2$		Stress Range		Cyclic Stability	Cycles to Failure	
		Range	Elastic	Inelastic	Creep	MPa	ksi	Cycle 1	$N_f/2$		N_s%	N_f
1A	Cyclic	0.0150	0.0124	0.0026	0	−41	6.0	2172 MPa (315.0 ksi)	2222 MPa (322.4 ksi)	Stable	365	400
2A	Cyclic	0.0125	0.0114	0.0011	0	−37	−5.4	2003 MPa (290.6 ksi)	2050 MPa (297.4 ksi)	Stable	839	863
3A	Cyclic	0.0100	0.0098	0.0002	0	−57	−8.3	1836 MPa (266.3 ksi)	1818 MPa (263.7 ksi)	Stable	2,214	2,767
6A	Cyclic	0.0100	0.0098	0.0002	0	−23	−3.4	1815 MPa (263.3 ksi)	1787 MPa (259.1 ksi)	Stable	1,490	1,871
4A	Cyclic	0.0085	0.0085	<0.0001	0	−62	−9.0	1552 MPa (225.2 ksi)	1539 MPa (223.2 ksi)	Stable	8,979	9,350
7A	Cyclic	0.0085	0.0085	<0.0001	0	−28	−4.0	1580 MPa (229.2 ksi)	1575 MPa (228.5 ksi)	Stable	6,787	7,840
5A	Cyclic	0.0072	0.0072	<0.0001	0	0	0	1342 MPa (194.7 ksi)	1356 MPa (196.7 ksi)	Stable	226,342	226,820
8A	Cyclic/ Dwell	0.0124	0.0108	0.0016	0.0001	−42	−6.1	2005 MPa (290.7 ksi)	2000 MPa (290.0 ksi)	Stable	388	516
9A	Cyclic/ Dwell	0.0119	0.0106	0.0013	0.0002	−36	−5.2	1930 MPa (279.9 ksi)	1925 MPa (279.2 ksi)	Stable	867	934
10A	Cyclic/ Dwell	0.0084	0.0082	0.0002	0.0001	−28	−4.0	1490 MPa (216.1 ksi)	1484 MPa (215.3 ksi)	Stable	7,724	8,087
12A	Cyclic/ Dwell	0.0103	0.0097	0.0006	0.0001	−26	−3.8	1792 MPa (259.9 ksi)	1782 MPa (258.5 ksi)	Stable	920	1,066

Note: Cyclic/Dwell tests have a 900-sec (15 min) hold time at the maximum tensile strain.

TABLE X. CONTROLLED STRAIN LCF RESULTS FOR TURBINE DISK ALLOY 3, NASA IIB-7. TESTING CONDUCTED IN AIR AT 650°C (1200°F), 0.33 Hz (20 cpm) RAMP FREQUENCY, MEAN STRAIN = 0

Spec. S/N	Type Test	Strain (m/m at $N_f/2$)				Mean Stress at $N_f/2$		Stress Range		Cyclic Stability	Cycles to Failure	
		Range	Elastic	Inelastic	Creep	MPa	ksi	Cycle 1	$N_f/2$		N_p%	N_f
1B	Cyclic	0.0150	0.0131	0.0019	0	−36	− 5.2	2626 MPa (380.8 ksi)	2653 MPa (384.7 ksi)	Stable	356	420
2B	Cyclic	0.0125	0.0117	0.0008	0	−57	− 8.2	2241 MPa (325.0 ksi)	2304 MPa (334.2 ksi)	Stable	955	958
7B	Cyclic	0.0116	0.0113	0.0003	0	−18	− 2.6	2142 MPa (310.7 ksi)	2174 MPa (315.3 ksi)	Stable	1,361	1,385
6B	Cyclic	0.0115	0.0112	0.0003	0	−34	− 4.9	2160 MPa (313.3 ksi)	2178 MPa (315.9 ksi)	Stable	1,660	2,249
3B	Cyclic	0.0100	0.0100	<0.0001	0	0	0	1799 MPa (260.9 ksi)	1839 MPa (266.8 ksi)	Stable	16,390	17,002
4B	Cyclic	0.0100	0.0100	<0.0001	0	0	0	1812 MPa (262.8 ksi)	1880 MPa (272.7 ksi)	Stable	17,849	18,774
5B	Cyclic	0.0085	0.0085	<0.0001	0	− 7	− 1.0	1545 MPa (224.1 ksi)	1595 MPa (231.4 ksi)	Stable	—	211,200[1]
8B	Cyclic/ Dwell	0.0117	0.0113	0.0004	0.0001	−68	− 9.8	2150 MPa (311.7 ksi)	2122 MPa (307.8 ksi)	Stable	927	938
9B	Cyclic/ Dwell	0.0126	0.0118	0.0008	0.0001	−57	− 8.3	2362 MPa (342.5 ksi)	2334 MPa (338.6 ksi)	Stable	223	254
10B	Cyclic/ Dwell	0.0101	0.0099	0.0002	0.0001	−92	−13.3	1858 MPa (269.5 ksi)	1853 MPa (268.7 ksi)	Stable	3,864	3,935
16A	Cyclic/ Dwell	0.0100	0.0098	0.0002	<0.0001	−84	−12.2	1951 MPa (282.9 ksi)	1896 MPa (275.0 ksi)	Stable	4,833	4,888

Note: Cyclic/Dwell tests have a 900-sec (15 min) hold time at the maximum tensile strain.

[1]Test discontinued at 211,200 cycles. No indication of failure.

TABLE XI. CONTROLLED STRAIN LCF RESULTS FOR TURBINE DISK ALLOY 4, HIP-ASTROLOY. TESTING CONDUCTED IN AIR AT 650°C (1200°F), 0.33 Hz (20 cpm) RAMP FREQUENCY, MEAN STRAIN = 0

Spec. S/N	Type Test	Strain (m/m at $N_f/2$)				Mean Stress at $N_f/2$		Stress Range		Cyclic Stability	Cycles to Failure	
		Range	Elastic	Inelastic	Creep	MPa	ksi	Cycle 1	$N_f/2$		N_s%	N_f
DB-1	Cyclic	0.0142	0.0110	0.0032	0	−56	− 8.1	1910 MPa (277.1 ksi)	1920 MPa (278.4 ksi)	Stable	850	961
DB-2	Cyclic	0.0100	0.0096	0.0004	0	- 12	−1.7	1688 MPa (244.8 ksi)	1674 MPa (242.8 ksi)	Stable	3,800	4,025
DB-7	Cyclic	0.0100	0.0096	0.0004	0	−19	−2.8	1708 MPa (247.7 ksi)	1660 MPa (240.8 ksi)	Stable	2,900	3,121
DB-4	Cyclic	0.0081	0.0080	0.0001	0	−12	−1.7	1497 MPa (217.1 ksi)	1478 MPa (214.3 ksi)	Stable	5,110	8,498
DB-5	Cyclic	0.0081	0.0080	0.0001	0	0	0	1476 MPa (214.1 ksi)	1466 MPa (212.7 ksi)	Stable	8,176	8,901
DB-3	Cyclic	0.0067	0.0067	<0.0001	0	0	0	1228 MPa (178.2 ksi)	1170 MPa (170.8 ksi)	Stable	—	220,704[1]
DB-10	Cyclic/ Dwell	0.0123	0.0108	0.0015	0.0006	−30	−4.4	1921 MPa (278.6 ksi)	1943 MPa (281.8 ksi)	Stable	300	335
DB-11	Cyclic/ Dwell	0.0119	0.0104	0.0015	0.0004	- 50	−7.2	1855 MPa (269.0 ksi)	1871 MPa (271.4 ksi)	Stable	605	697
CB-13	Cyclic/ Dwell	0.0076	0.0075	0.0001	0.0001	0	0	1417 MPa (205.5 ksi)	1375 MPa (199.4 ksi)	Stable	7,420	7,780
CB-12	Cyclic/ Dwell	0.0077	0.0074	0.0003	0.0001	−22	−3.2	1328 MPa (192.6 ksi)	1355 MPa (196.5 ksi)	Stable	11,625	11,942

Note: Cyclic/Dwell tests have a 900-sec (15 min) hold time at the maximum tensile strain.

[1] Test discontinued at 220,704 cycles. No indication of failure.

TABLE XII. CONTROLLED STRAIN LCF RESULTS FOR TURBINE DISK ALLOY 5, GATORIZED® IN 100. TESTING CONDUCTED IN AIR AT 650°C (1200°F), 0.33 Hz (20 cpm) RAMP FREQUENCY, MEAN STRAIN = 0

Spec. S/N	Type Test	Strain (m/m at $N_f/2$)				Mean Stress at $N_f/2$		Stress Range		Cyclic Stability	Cycles to Failure	
		Range	Elastic	Inelastic	Creep	MPa	ksi	Cycle 1	$N_f/2$		N_s%	N_f
7	Cyclic	0.0148	0.0133	0.0015	0	0	0	2257 MPa (327.4 ksi)	2376 MPa (344.6 ksi)	Harden	541	561
1	Cyclic	0.0142	0.0127	0.0015	0	−41	−5.9	2196 MPa (318.6 ksi)	2328 MPa (337.7 ksi)	Harden	525	749
8	Cyclic	0.0125	0.0117	0.0008	0	−23	−3.3	2148 MPa (311.5 ksi)	2198 MPa (318.8 ksi)	Slight Hardening	1,125	1,159
5	Cyclic	0.0100	0.0098	0.0002	0	−23	−3.3	1774 MPa (257.3 ksi)	1820 MPa (263.9 ksi)	Slight Hardening	8,843	11,782
2	Cyclic	0.0094	0.0093	≤0.0001	0	−16	−2.3	1687 MPa (244.7 ksi)	1715 MPa (248.7 ksi)	Stable	50,837	57,780
3	Cyclic	0.0094	0.0092	0.0002	0	0	0	1756 MPa (254.6 ksi)	1769 MPa (256.6 ksi)	Stable	12,529	15,774
6	Cyclic	0.0080	0.0080	<0.0001	0	−37	−5.3	1450 MPa (210.3 ksi)	1505 MPa (218.3 ksi)	Stable	—	277,000(1)
9	Cyclic/ Dwell	0.0124	0.0113	0.0011	0.0001	− 7	−1.0	2106 MPa (305.4 ksi)	2106 MPa (305.4 ksi)	Stable	213	285
10	Cyclic/ Dwell	0.0123	0.0111	0.0012	0.0002	−21	−3.0	2138 MPa (310.1 ksi)	2133 MPa (309.4 ksi)	Stable	242	285
11	Cyclic/ Dwell	0.0100	0.0097	0.0003	<0.0001	−30	−4.3	1735 MPa (251.7 ksi)	1722 MPa (249.7 ksi)	Stable	2,361	2,515
12	Cyclic/ Dwell	0.0101	0.0097	0.0004	<0.0001	−30	−4.3	1846 MPa (267.7 ksi)	1850 MPa (268.3 ksi)	Stable	851	1,035

Note: Cyclic/Dwell tests have a 900-sec (15 min) hold time at the maximum tensile strain.

(1) Test discontinued at 277,000 cycles. No indication of failure.

TABLE XIII. TOTAL STRAIN VS LIFE EQUATIONS FOR CYCLIC LCF TESTS

Alloy	Life Term	Total Strain (Y)* vs Life (N)* Equation
Waspaloy	N_s	$Y = 4320\ N^{(-1.41)} + 7.96\ N^{(-0.404)} + 0.603$
	N_f	$Y = 4040\ N^{(-1.38)} + 4.06\ N^{(-0.290)} + 0.540$
Wrought Astroloy	N_s	$Y = 7450\ N^{(-1.70)} + 4.27\ N^{(-0.336)} + 0.648$
	N_f	$Y = 2820\ N^{(-1.53)} + 4.62\ N^{(-0.340)} + 0.648$
NASA IIB-7	N_s	$Y = 597\ N^{(-1.34)} + 1.60\ N^{(-0.125)} + 0.510$
	N_f	$Y = 580\ N^{(-1.33)} + 1.66\ N^{(-0.128)} + 0.510$
HIP Astroloy	N_s	$Y = 40200\ N^{(-1.73)} + 7.35\ N^{(-0.392)} + 0.603$
	N_f	$Y = 15433\ N^{(-1.57)} + 7.96\ N^{(-0.394)} + 0.603$
GATORIZED® IN 100	N_s	$Y = 9.71\ N^{(-0.666)} + 2.66\ N^{(-0.229)} + 0.640$
	N_f	$Y = 9.46\ N^{(-0.660)} + 2.36\ N^{(-0.182)} + 0.560$

*Where Y is given in percent strain, and N in cycles.

TABLE XIV. TOTAL STRAIN VS LIFE EQUATIONS FOR DWELL LCF TESTS

Alloy	*Life Term*	*Total Strain (Y)* vs Life (N)* Equation*
Waspaloy	N_0	$Y = 105.5\ N^{(-0.977)} + 2.33\ N^{(-0.127)}$
	N_f	$Y = 174.5\ N^{(-1.02)} + 2.49\ N^{(-0.134)}$
Wrought Astroloy	N_0	$Y = 17.8\ N^{(-0.778)} + 2.02\ N^{(-0.102)}$
	N_f	$Y = 27.9\ N^{(-0.828)} + 2.14\ N^{(-0.108)}$
NASA IIB-7	N_0	$Y = 0.985\ N^{(-0.466)} + 1.74\ N^{(-0.087)}$
	N_f	$Y = 1.14\ N^{(-0.488)} + 1.77\ N^{(-0.089)}$
HIP Astroloy	N_0	$Y = 26.2\ N^{(-0.822)} + 2.10\ N^{(-0.110)}$
	N_f	$Y = 33.6\ N^{(-0.848)} + 2.18\ N^{(-0.117)}$
GATORIZED® IN 100	N_0	$Y = 3.52\ N^{(-0.634)} + 1.72\ N^{(-0.079)}$
	N_f	$Y = 5.04\ N^{(-0.672)} + 1.80\ N^{(-0.084)}$

*Where Y is given in percent strain, and N in cycles.

TABLE XV. CRACK PROPAGATION TEST SPECIMENS

Alloy Number	*Material Name*	*Specimen Number*	*Temperature* (°C)	*Temperature* (°F)	*Cyclic Frequency*	*Stress Ratio*
1	Waspaloy	730	650	1200	0.33 Hz	0.05
1	Waspaloy	731	650	1200	900-sec Dwell	0.05
1	Waspaloy	735	650	1200	0.33 Hz	0.05
1	Waspaloy	736	650	1200	20 Hz	0.05
1	Waspaloy	737	650	1200	120-sec Dwell	0.05
1	Waspaloy	738	650	1200	0.33 Hz	0.05
1	Waspaloy	739	650	1200	300-sec Dwell	0.05
1	Waspaloy	732	650	1200	900-sec Dwell	0.05
2	Wrought-Astroloy	806	650	1200	0.33 Hz	0.05
2	Wrought-Astroloy	808	650	1200	20 Hz	0.05
2	Wrought-Astroloy	809	650	1200	0.33 Hz	0.05
2	Wrought-Astroloy	812	650	1200	0.33 Hz	0.05
2	Wrought-Astroloy	814	650	1200	900-sec Dwell	0.05
2	Wrought-Astroloy	810	650	1200	900-sec Dwell	0.05
2	Wrought-Astroloy	811	650	1200	900-sec Dwell	0.05
2	Wrought-Astroloy	813	650	1200	900-sec Dwell	0.05
3	NASA IIB-7	797	650	1200	0.33 Hz	0.05
3	NASA IIB-7	800	650	1200	900-sec Dwell	0.05
3	NASA IIB-7	801	650	1200	900-sec Dwell	0.05
3	NASA IIB-7	802	650	1200	0.33 Hz	0.05
3	NASA IIB-7	804	650	1200	0.33 Hz	0.05
3	NASA IIB-7	833	650	1200	900-sec Dwell	0.05
3	NASA IIB-7	799	650	1200	900-sec Dwell	0.05
3	NASA IIB-7	798	650	1200	0.33 Hz	0.05
4	HIP-Astroloy	726	650	1200	0.33 Hz	0.05
4	HIP-Astroloy	727	650	1200	0.33 Hz	0.05
4	HIP-Astroloy	728	650	1200	900-sec Dwell	0.05
4	HIP-Astroloy	742	650	1200	120-sec Dwell	0.05
4	HIP-Astroloy	743	650	1200	20 Hz	0.05
4	HIP-Astroloy	744	650	1200	0.0083 Hz	0.05
4	HIP-Astroloy	746	650	1200	900-sec Dwell	0.05
4	HIP-Astroloy	748	650	1200	300-sec Dwell	0.05
5	IN 100	712	650	1200	900-sec Dwell	0.05
5	IN 100	703	650	1200	20 Hz	0.05
5	IN 100	710	650	1200	0.33 Hz	0.05
5	IN 100	713	650	1200	900-sec Dwell	0.05
5	IN 100	716	650	1200	900-sec Dwell	0.05
5	IN 100	717	650	1200	0.33 Hz	0.05
5	IN 100	729	650	1200	0.0083 Hz	0.05
5	IN 100	715	650	1200	900-sec Dwell	0.05

TABLE XVI. SINH MODEL COEFFICIENTS

Alloy Number	Material Name	Cyclic Frequency	Sinh Model Coefficients			
			C_1	C_2	C_3	C_4
1	Waspaloy	20 Hz	0.500	3.645	−1.616	−6.361
1	Waspaloy	0.33 Hz	0.500	3.169	−1.611	−6.120
1	Waspaloy	120 sec Dwell	0.500	4.771	−1.597	−5.765
1	Waspaloy	300 sec Dwell	0.500	5.398	−1.629	−5.487
1	Waspaloy	900 sec Dwell	0.500	6.149	−1.666	−5.153
2	Wrought-Astroloy	20 Hz	0.500	4.449	−1.423	−6.819
2	Wrought-Astroloy	0.33 Hz	0.500	4.316	−1.497	−6.064
2	Wrought-Astroloy	900 sec Dwell	0.500	5.195	−1.581	−5.027
3	NASA IIB-7	0.33 Hz	0.500	5.351	−1.497	−5.827
3	NASA IIB-7	900 sec Dwell	0.500	6.160	−1.452	−3.595
4	HIP-Astroloy	20 Hz	0.500	4.088	−1.521	−6.416
4	HIP-Astroloy	0.33 Hz	0.500	4.436	−1.531	−6.145
4	HIP-Astroloy	0.0083 Hz	0.500	4.750	−1.540	−5.901
4	HIP-Astroloy	120 sec Dwell	0.500	4.069	−1.661	−5.606
4	HIP-Astroloy	300 sec Dwell	0.500	4.442	−1.670	−5.377
4	HIP-Astroloy	900 sec Dwell	0.500	4.889	−1.681	−5.103
5	IN 100	20 Hz	0.500	4.243	−1.544	−6.178
5	IN 100	0.33 Hz	0.500	4.227	−1.561	−5.780
5	IN 100	0.0083 Hz	0.500	4.212	−1.576	−5.421
5	IN 100	900 sec Dwell	0.500	5.047	−1.581	−4.383

Notes: C_3 has units of log (MPa $\sqrt{m}$)
C_4 has units of log (m/cycle)
C_1 and C_2 are dimensionless

TABLE XVII. DISK LIFE STRESS-STRAIN ANALYSIS RESULTS

Alloy	1st Quarter Cycle (max)		1st Half Cycle Strain, (%) (min)	Total Cyclic Strain Range, (%)
	Peak Strain (%)	Inelastic Offset (%)		
Waspaloy	0.988	0.491	0.235	0.753
Wrought Astroloy	0.849	0.294	0.116	0.733
NASA IIB-7	0.814	0.134	0.037	0.777
IN 100	0.783	0.195	0.061	0.722

TABLE XVIII. PREDICTED MEAN CRACK INITIATION LIFE FROM DISK LIFE ANALYSES AND LCF MATERIAL PROPERTY CURVES.

Alloy	Disk Life Analysis Total Strain Range (%)	Cyclic Life to 5% Load Range Drop (N_5)	
		0.33 Hz Testing	900-sec Dwell Testing
Waspaloy	0.753	19,660	8,460
Wrought Astroloy	0.733	117,200	22,770
NASA IIB-7	0.777	1,614,000	165,600
IN 100	0.722	5,888,000	63,490

TABLE XIX. ALLOY PROPAGATION LIFE COMPARISONS

Alloy	*From 0.25 mm Flaw*		*From 0.51 mm Flaw*	
	0.33 Hz	*900-sec Dwell*	*0.33 Hz*	*900-sec Dwell*
Waspaloy	7,275	1,425	6,650	725
Wrought Astroloy	2,290	440	1,790	265
NASA IIB-7	2,470	125	1,515	75
IN 100	870	<10	550	<10

TABLE XX. TOTAL DISK LIFE

	Alloy	*Cyclic (0.33 Hz)*				*Cyclic/Dwell (900-sec Hold)*			
		CI	+ *CP*	=	N_T	*CI*	+ *CP*	=	N_T
1	Waspaloy	19,660	6,650		26,310	8,460	725		9,185
2	Wrought Astroloy	117,200	1,790		118,990	22,770	265		23,035
3	NASA IIB-7	1,614,000	550		1,614,550	165,600	<10		165,610
5	IN 100	5,888,000	1,515		5,889,515	63,490	75		63,565

Notes: CI — Mean cycles to crack initiation — N_i life
CP — Crack propagation from 0.51-mm (0.020-in.) crack to critical crack length
N_T — Sum of CI and CP

REFERENCES

1. Kent, W. B., "Development Study of Compositions for Advanced Wrought Nickel-Base Superalloys," NASA CR-120934, 1972.

2. deNeeve, P. F., and A. Wuerscher, "Evaluation of the Strain Behavior of an LCF Specimen," Pratt & Whitney Aircraft of Canada internal correspondence, April 23, 1970.

3. Socie, D. F., "Fatigue-Life Prediction Using Local Stress-Strain Concepts," SESA Spring Meeting, 11-16 May 1975, Chicago, Illinois.

4. Nachtigall, A. J., "Cyclic Stress-Strain Curve Determination for D6AC Steel by Three Methods," NASA Technical Memorandum, NASA TM-73815, November 1977.

5. Annis, C. G., R. M. Wallace, and D. L. Sims, "An Interpolative Model for Elevated Temperature Fatigue Crack Propagation," Air Force Materials Laboratory, AFML-TR-76-176, November 1976.

6. Sims, D. L., C. G. Annis, and R. M. Wallace, "Cumulative Damage Fracture Mechanics at Elevated Temperatures," Air Force Materials Laboratory, AFML-TR-76-176, Part III, April 1977.

7. Annis, C. G., M. C. Van Wanderham, and R. M. Wallace, "An Experimental Procedure for the Accurate Prediction of Total LCF Life," Materials Science Seminar, Cincinnati, Ohio, P&WA GP-175, November 1975.

REPORT DOCUMENTATION PAGE

Form Approved
OMB No. 0704-0188

1. AGENCY USE ONLY (*Leave blank*)	2. REPORT DATE	3. REPORT TYPE AND DATES COVERED
	October 1978	Final Contractor Report

4. TITLE AND SUBTITLE

Evaluation of the Cyclic Behavior of Aircraft Turbine Disk Alloys

5. FUNDING NUMBERS

WU–None
NAS3–20367

6. AUTHOR(S)

B.A. Cowles, D.L. Sims, and J.R. Warren

7. PERFORMING ORGANIZATION NAME(S) AND ADDRESS(ES)

United Technologies Corporation
Pratt & Whitney Aircraft Group
Government Products Division
Box 2691
West Palm Beach, Florida 33402

8. PERFORMING ORGANIZATION REPORT NUMBER

E–14587

9. SPONSORING/MONITORING AGENCY NAME(S) AND ADDRESS(ES)

National Aeronautics and Space Administration
Washington, DC 20546–0001

10. SPONSORING/MONITORING AGENCY REPORT NUMBER

NASA CR–159409
FR–10299

11. SUPPLEMENTARY NOTES

Project Manager, F.H. Harf and Research Advisor, R.V. Miner, Jr., NASA Lewis Research Center, Cleveland, Ohio.

12a. DISTRIBUTION/AVAILABILITY STATEMENT

Unclassified - Unlimited
Subject Category: 07

Available electronically at http://gltrs.grc.nasa.gov

This publication is available from the NASA Center for AeroSpace Information, 301–621–0390.

12b. DISTRIBUTION CODE

13. ABSTRACT ***(Maximum 200 words)***

Five aircraft turbine disk alloys representing various strengths and processing histories were evaluated at 650 °C to determine if recent strength advances in powder metallurgy have resulted in corresponding increases in low cycle fatigue (LCF) capability. Controlled strain LCF tests and controlled load crack propagation tests were performed. Results were used for direct material comparisons and in the analysis of an advanced aircraft turbine disk having a fixed design and operating cycle. Generally, crack initiation lives were found to increase with increasing tensile yield strength, while resistance to fatigue crack propagation generally decreased with increasing strength.

14. SUBJECT TERMS

Strain control; Fatigue crack propagation; Low cycle fatigue (LCF); Life prediction; NASA IIB–7; IN 100; Waspaloy; Astroloy; HIP-Astroloy; Turbine disks

15. NUMBER OF PAGES

152

16. PRICE CODE

17. SECURITY CLASSIFICATION OF REPORT	18. SECURITY CLASSIFICATION OF THIS PAGE	19. SECURITY CLASSIFICATION OF ABSTRACT	20. LIMITATION OF ABSTRACT
Unclassified	Unclassified	Unclassified	